Isolation of bioactive compounds from selected plants of South African flora (*Helichrysum* and *Aspalathus* species) for application in the preparation of biocompatible metal nanoparticles

by

OMOLAJA AKEEM, AKINFENWA

Thesis submitted in fulfilment of the requirements for the degree

Doctor of Philosophy: Chemistry

in the

Faculty of Applied Sciences

at the Cape Peninsula University of Technology

Supervisor: Prof Ahmed Mohammed

Co-supervisor: Prof Jeanine Marnewick

Bellville (September 2021)

DECLARATION

I, Omolaja Akeem Akinfenwa, declare that the contents of this thesis represent unaided work and that the thesis has not previously been submitted for academic examination towards any qualification. Furthermore, it represents my own opinions and not necessarily those of the Cape Peninsula University of Technology.

29/09/2021

Signed Date

ABSTRACT

The Cape Floral Region of South Africa is among the world floristic regions. Its rich plant diversity makes it ecologically and economically significant for research in natural products and phyto-mediated nanoparticle synthesis. The endemic *Aspalathus linearis* (Fabaceae) and the *Helichrysum foetidum* (Asteraceae) are well distributed in the western cape of South Africa are used as herbal tea and medicinal plants respectively. Recent studies attributed their medicinal use to high antioxidants from chalcones and flavonoids. Flavonoids are known to play significant roles in natural product drugs, and in phyto-assisted metallic nanoparticles for use in nanomedicine. These functional properties were explored for the isolation of bioactive compounds from *Aspalathus linearis* and *Helichrysum foetidum* and their bio-evaluations for protection of skin cells against UVB-induced oxidative stress, mitigation of prediabetes, and toxicity on cancer cells. Also, their role in the preparation of biocompatible metal nanoparticles was established.

UVB-induced skin diseases and high blood glucose are among increasing global health challenges that may lead to socio-economic disorders. A non-sedentary lifestyle is necessary for balanced glucose metabolism from ingested carbohydrates which in turn exposes the skin to prolong UV radiation from sunlight and inflammations of skin cells. Several chemically synthesized drugs mostly prescribed to counteract or mitigate the development of these disease conditions are associated with some side effects on administration. In the light of this, recent researchers have been motivated to formulate immune cosmetic prototypes and antidiabetic drugs at the nanoscale for effective delivery. Biosynthesised nanodrugs are believed to have near-zero side effects and are effective for targeted drug delivery due to their small sizes and large surface area of metal carriers. Gold metal ranks the highest among the metallic nanoparticles used due to its higher biocompatibility. The silver metal has also been indicated as a diagnostic tool for suspected diseases and therapy. However, their conventional synthesis methods by physical and chemical methods also pose concerns from the use of hazardous chemicals, high experimental cost, and long reaction time. Alternative methods that apply green chemistry for biosynthesis from plant phytochemicals have now been considered.

In this study, *A*. *linearis* and *H. foetidum* were exhaustively extracted to obtain the total extract for each plant. Each extract was separately subjected to serial chromatography using different solvent systems and elution modes to isolate their respective compounds. Successive chromatography of *A. linearis* and chemical investigation of its polar fractions yielded a novel compound **4.1** named linearthin, a dihydrochalcone not previously reported in addition to the known compounds **4.2** (aspalathin), **4.3** (nothofagin). The chromatography of *H. foetidum* afforded and five known compounds, **7.1** (quercetin), **7.2** (helichrysetin), **7.4** (helichrysin), **7.5** (luteolin), **7.6** (Kaur-16-en-19-oic acid, 15-methoxylate), and **7.3** (3-methoxyqurecetin + luteolin mixiture). The structural elucidations of the compounds were confirmed from 1D, 2D NMR, HRMS, UV, and IR spectra data.

Investigations on the protective effects of phytochemicals (chalcones) of *A*. *linearis* against UV-induced oxidative stress on skin cells is limited in the literature. In the same vein, the potentials of phytochemicals from *H*. *foetidum* in the management of diabetes is yet to be fully studied. Furthermore, the involvement of pure compounds isolated from both plants in the nanochemistry of metal nanoparticles has not been reported

before this study. Hence, this study investigated the protection offered by *A*. *linearis* phytochemicals against UV-induced oxidative damage on skin cells of human immortalized keratinocytes (HaCaT) and melanocytes (SKMEL-1) via cell viability, cytotoxicity, and caspase-3 activation using ApoTox-Glo™ Triplex Assay. It also evaluated the phytochemicals of *H. foetidum* for glucose uptake, and inhibition of carbohydrate hydrolyzing enzymes (α-glucosidase and α-amylase enzymes) *in vitro* using HEK293 kidney cell and the application of the plants in the synthesis of metallic nanoparticles for drug discovery.

From the chemical profile of *A*. *linearis*, and its bioassays in skin cells, the total extract (TE), **4.1**, **4.2** and **4.3**, all elicited cytoprotection from oxidative damage which is suggestive of their applications for skincare products. Interestingly, **4.1** was most cytoprotective against UVB irradiation of HaCaT cell line (over 24 hours) with an IC_{50} of 282 µg/mL and in the SK-MEL-1 cell line with IC_{50} values of 248.3 and 142.6 µg/mL over 4 and 24 hours, respectively. On the other hand, HaCaT cells exposed to **4.2** over 4 hours before UVB irradiation showed the highest degree of cytoprotection with an IC_{50} of 398.9 µg/mL among the four studied samples. Glucose uptake activities of HEK293 kidney cells by compounds of *H. foetidum* was significantly improved by the total extract (HF), **7.1** and **7.6** . All tested samples showed higher α-glucosidase inhibition compared to the acarbose standard. HF, **7.2** and **7.4** were most potent with IC_{50} at 16.3± 0.1 µg/mL, 19.4± 0.3 µg/mL, and 48.3 ± 0.1 µg/mL respectively. However, only **7.1** showed higher inhibition of α-amylase than the standard. Nano screening of the phytochemicals of both plants revealed that the total extract of both plants, **4.2**, **7.2**, and **7.4** most nano active. Subsequent biosynthesis with the nano active constituents of each plant led to the synthesis, characterisation, *in vitro* stability, and bio-evaluation of quasi-spherical shapes gold nanoparticles (2 – 12 nm) from *H*. *foetidum*, gold and silver nanoparticles (0.9 – 4.3 nm) from *A*. *linearis*.

Summarily, this is the first scientific report on the biosynthesis of nanoparticles from compounds of *H. foetidum* and *A*. *linearis* with potential application in the management of diabetes and cancer cells. In addition to the *in vitro* evaluation of their respective compounds for glucose utilisation and against UVB-induced oxidative stress.

Keywords: *Aspalathus linearis, helichrysum foetidum*, isolation, nanoparticles, bio-reduction, diabetes, skin cells, cancer cells.

ACKNOWLEDGEMENTS

I wish to thank:

- Allah, the Lord of the worlds for His continuous mercies that endures me before, during and after this project.
- My parents, wife, children and siblings for your emotional support, sacrifices, cooperation, and understanding to allow me to be away from you during this study.
- Prof. A.H. Mohammed and Prof. J.L. Marnewick for their acceptance to supervise my project which re-ignites my passion for quality research studies. Words of appreciation are not enough to thank you for empowering me through your wealth of experience, expertise, psychological support, tutelage, constructive criticism, commitment, and insistence on quality and solid work.
- Alhaji R.A Ebiti and Istabaraqim Nigeria Limited for your financial support and compassion towards me.
- Dr Engr. I.B Adefeso, Dr Sheriffdeen Salisu and Mrs Salisu, Dr Olurode Adam, Dr Andre Spies, Dr Shaheeda Adonis, and the Dua Group of South Africa for your love, concerns, and pieces of advice.
- The Chemistry, and Applied Biotechnology and Microbial Lab technicians; Mrs Zandile Mthembu, Mr Fanine, Mr David, Mrs Gillian Fennessy-yon, Mrs Pumza Stemela and Ms Andiswa Valisa
- Colleagues and lab mates, you have been wonderful to accommodate and make the lab space a free for all. It is a long list, just to mention representatives are Dr Abdurahman, Dr Umar, Dr Abubakar, Dr Ninon, Justine, Eloge, Khady, Selina, Aliwa, Ali, Yolanda, Nkosi, Solafa, Romario, Naledi, Masande, Masi and other lab mates.
- Postdocs fellows; Dr Rajan Sharma, Dr Enas Ismail, Dr Slyvester Omoruyia, Dr Naeem Sheik, Dr Badmus Jelili, and Dr Brendon Pearce.
- The financial supports from Cape Peninsula University through the centre for Postgraduate scholarship awards and the Rooibos Council of South Africa towards this research are acknowledged.

DEDICATION

Dedicated to my late mother, Alhaja Abibatu Abake Moliki Sholuade, the sacrifices of the 5A-AKINFENWA and to all who follow their dreams to accomplishment.

PREFACE

This thesis is divided into **8 chapters** and written in the article-based format based on the university requirements and the guidelines of the respective journals where the articles were either published or submitted to.

Chapters 1 briefly introduces the study by giving relevant information on the rich plant diversity of the western cape and South Africa for natural product chemistry research, extraction and isolation of phytochemicals from the plant. It underscores the green synthesis approach to metallic nanoparticles using plant phytochemicals, their advantages over other methods, characterization techniques, and bio-evaluations of gold and silver nanoparticles. The rationale, hypothesis, aims, and objectives of the study were also stated in this chapter.

Chapter 2 reviews the taxonomy and previous works on *Aspalathus linearis* and *Helichrysum foetidum*. It also identified knowledge gaps and areas that could be further explored. Two review articles "**Recent advances on *Aspalathus linearis* (Rooibos tea): phytochemistry, bioactivities and green biosynthesis of metal nanoparticles"** and "***Helichrysum* genus and compounds in the management of diabetes mellitus"** were developed and in the process of article submission.

Chapter 3 is a short communication that compares the effect of sequential and non-sequential solvent extraction on the total polyphenol content of fermented (red) and unfermented (green) rooibos plant using the Trolox equivalent antioxidant capacity (Teac) and ferric reducing ability of plasma (FRAP) assays. It provided the basis for selection between the fermented and unfermented *A. linearis.* A manuscript titled "**Effect of sequential and non-sequential solvent extraction on the total polyphenol content and antioxidants capacity of green and fermented rooibos tea** (***Aspalathus linearis*)"** was written on this and in the process of article submission.

Chapters 4 and **5** further explains the isolation of novel compounds (linearthin) and some known compounds from the crude extract of the green rooibos plant, the applications in skin-related disorder and nanotechnology. Chapter four was submitted to the Phytochemistry section of ***Plants* journal** ([Plants] Article ID: ***Plants* 2021, 10, 1936**) and has been published with the title; **"Protective Effects of Linearthin and Other Chalcone Derivatives from *Aspalathus linearis* (Rooibos) Against UVB Induced Oxidative Stress and Toxicity in Human Skin Cells".** Chapter five is a article titled **"Cytotoxic effects of phytomediated silver and gold nanoparticles synthesised from rooibos *(Aspalathus linearis*), and aspalathin"**. This manuscript has been accepted for publication by the journal of ***Plants***, under Phytochemistry section. Manuscript ID: **Plants-14337**.

Chapters 6 and **7** focus on the phytochemistry and nanochemistry research on *Helichrysum foetidum,* its involvement in plant-mediated metallic nanoparticles and its potential activities on glucose uptake and metabolism. An article on this was published by the **Journal of Surfaces and Interfaces** titled **"The potential of chalcone-capped gold nanoparticles in the management of diabetes mellitus"** while a draft manuscript is under review.

Chapter 8 is devoted to the general discussion of all the findings in summary, conclusions, and recommendations.

plants

MDPI

Article

Protective Effects of Linearthin and Other Chalcone Derivatives from *Aspalathus linearis* (Rooibos) against UVB Induced Oxidative Stress and Toxicity in Human Skin Cells

Akeem O. Akinfenwa [1], Naeem S. Abdul [2], Jeanine L. Marnewick [2] and Ahmed A. Hussein [1,*]

[1] Department of Chemistry, Cape Peninsula University of Technology, Symphony Rd., Bellville 7535, Cape Town, South Africa; oa.akeemlaja@gmail.com

[2] Applied Microbial and Health Biotechnology Institute, Cape Peninsula University of Technology, Symphony Rd., Bellville 7535, Cape Town, South Africa; sheikabduln@cput.ac.za (N.S.A.); marnewickj@cput.ac.za (J.L.M.)

* Correspondence: Mohammedam@cput.ac.za; Tel.: +27-21-959-6193; Fax: +27-21-959-3055

Citation: Akinfenwa, A.O.; Abdul, N.S.; Marnewick, J.L.; Hussein, A.A. Protective Effects of Linearthin and Other Chalcone Derivatives from *Aspalathus linearis* (Rooibos) against UVB Induced Oxidative Stress and Toxicity in Human Skin Cells. *Plants* **2021**, *10*, 1936. https://doi.org/10.3390/plants10091936

Academic Editor: Takeshi Kanto

Received: 24 July 2021
Accepted: 3 September 2021
Published: 17 September 2021

Abstract: Skin cells suffer continuous damage from chronic exposure to ultraviolet light (UV) that may result in UV-induced oxidative stress and skin thinning. This has necessitated the formulation of cosmeceutical products rich in natural antioxidants and free radical scavengers. *Aspalathus linearis* (rooibos) is an endemic South African fynbos plant growing naturally in the Western Cape region. The plant is rich in phenolics and other bioactives with a wide spectrum of health benefits. The chemical study of an acetonic extract of green *A. linearis* afforded a novel compound named linearthin (**1**) and two known dihydrochalcones, aspalathin (**2**) and nothofagin (**3**). The chemical structure of the novel compound was elucidated based on spectroscopic data analysis. The bio-evaluation of the isolated chalcones in vitro for protection against UVB-induced oxidative stress were systematically assessed by examining cell viability, metabolic activity, apoptosis, and cytotoxicity using HaCaT and SK-MEL-1 skin cells models. It was observed that pre-treatment with tested samples for 4- and 24 h at low concentrations were sufficient to protect skin cells from UVB-induced damage in vitro as evidenced by higher cell viability and improved metabolic activity in both keratinocytes (HaCaT) and melanocytes (SK-MEL-1). The results further show that the pre-treatment regimen employed by this study involved some degree of cellular adaptation as evidenced by higher levels of reduced glutathione with a concomitant decrease in lipid peroxidation and lowered caspase 3 activity. Furthermore, compound **1** was most cytoprotective against UVB irradiation of HaCaT cell line (over 24 h) with an IC_{50} of 282 µg/mL and SK-MEL-1 cell line with IC_{50} values of 248.3 and 142.6 µg/mL over 4 and 24 h, respectively. On the other hand, HaCaT cells exposed to **2** over 4 h before UVB irradiation showed the highest degree of cytoprotection with an IC_{50} of 398.9 µg/mL among the four studied samples. These results show that linearthin (**1**) and the two glycoside dihydrochalcone of *A. linearis* have the potential to be further developed as antioxidant cosmeceutical ingredients that may protect skin against UVB-induced damage.

1. Introduction

The human skin is continuously exposed to environmental stressors, among these, solar UV radiation is considered the most ubiquitous and damaging [1]. The UVB component of solar radiation is strongly linked to its potential to generate excessive reactive oxygen species (ROS) that damage cellular macromolecules and is recognised as an initiator of photocarcinogenesis and mutagenesis [2]. Although the skin is equipped with an intricate defence system, encompassing both enzymatic and non-enzymatic components to protect it from these adverse biological effects, excessive exposure to UV radiation can

Keywords: skin cells; UV light-exposure; *Aspalathus linearis*; linearthin; aspalathin derivatives; isolation; characterization

RESEARCH ARTICLE 2

Surfaces and Interfaces 25 (2021) 101251

Contents lists available at ScienceDirect

Surfaces and Interfaces

journal homepage: www.sciencedirect.com/journal/surfaces-and-

The potential of chalcone-capped gold nanoparticles for the management of diabetes mellitus

Akinfenwa A. Omolaja [a], Brendon Pearce [b], Sylvester I. Omoruyia [a], Jelili A. Badmus [c], Enas Ismail [a,f], Jeanine Marnewick [c], Subelia Botha [d], Mongi Benjeddou [b], Okobi E. Ekpob [e], Ahmed A. Hussein [a,*]

[a] Department of Chemistry, Cape Peninsula University of Technology, Symphony Rd. Bellville 7535, South Africa

[b] Precision Medicine Laboratory, Department of Biotechnology, 2nd Floor, Life Science Building, University of the Western Cape, Cape Town 7530, South Africa [c] Applied Microbial and Health Biotechnology Institute, Cape Peninsula University of Technology, Symphony Rd. Bellville, 7535, South Africa [d] Electron Microscope Unit, University of the Western Cape, Bellville, 7535, South Africa [e] Department of Anatomy and Cellular Biology, College of Medicine and Health Sciences, Khalifa University, Abu Dhabi P.O. Box 127788, United Arab Emirates [f] Physics department, Faculty of Science (Girl's Branch), Al Azhar University, Cairo, Egypt

ARTICLEINFO ABSTRACT

Keywords:
Helichrysum foetidum Chalcones
Gold nanoparticles Bio-reduction α-glucosidase Toxicity
Glucose uptake

Searching for new natural bioactive capping agents represent an urgent priority in the green synthesis of metal nanoparticles. Additionally, the biosafety of metal nanoparticles is a major concern, especially in medical applications. Recently, the use of pharmacologically active natural products as capping agents has been deployed to avoid toxic effects during the preparation of the nanoparticles and to enhance their drugability compared with conventional drugs. *Helichrysum foetidum* is a South African medicinal plant used in folk medicine for the treatment of different human pathologies, and it is known to contain a variety of bioactive compounds. Herein, the total extract and two pure chalcones, helichrysetin and helichrysin, isolated from the same plant were successfully used to synthesize quasi-monodispersed gold nanoparticles in the size range of 2–12 nm. The bio-evaluation of samples indicated that the AuNP/capping agent conjugates are biostable, and have different biological profiles from the total extract/pure compounds. The enzymatic inhibition assays showed significant inhibition by the total extract, helichrysetin and their gold nanoparticles. Interestingly, a similar activity was observed for glucose uptake in HEK293 treated cells. On the other hand, all the tested samples relatively demonstrated no cytotoxicity when tested against the HaCaT keratinocytes. In conclusion, the study demonstrated potential enhancement of glucose uptake in mammalian kidney cells, and inhibition of carbohydrate-hydrolysing enzymes by green synthesized gold nanoparticles of *H. foetidum*. It also provides a therapeutic appraisal of AuNPs/chalcones conjugate towards the development of antidiabetes drugs derived from *H. foetidum* and its gold nanoparticles.

TABLE OF CONTENTS

LISTS OF TABLES

LISTS OF FIGURES

LISTS OF SCHEMES

LISTS OF APPENDICES

LIST OF SUPPLEMENTARY

GLOSSARY

ABTS	2, 2’-Azino-bis (3-ethylbenzo thiazoline-6-sulfonic acid)
$AgNO_3$	Silver nitrate
AgNPs	Silver nanoparticles
AAE/g	Ascorbic acid per gram
AuNPs	Gold nanoparticles
ASE	Accelerated solvent extraction
ASP	Aspalathin
ASP-AuNPS	Aspalathin-mediated gold nanoparticles
ASP-AgNPs	Aspalathin-mediated silver nanoparticles
BSA	Bovine serum albumin
^{13}C-NMR	Carbon-13 nuclear magnetic resonance
CYS	Cysteine
1D-NMR	One-dimensional nuclear magnetic resonance
2D-NMR	Two-dimensional nuclear magnetic resonance
DMSO	Dimethyl sulfoxide
DCM	Dichloromethane
DPP-4	Dipeptidyl peptidase-IV
DI	Deionized water
DLS	Dynamic light scattering
DEPT 135	Distortionless enhancement by polarization transfer
DNS	3,5-dinitro salicylic acid
EDX	Energy dispersive x-ray spectroscopy
EtOAc	Ethyl acetate
FCC	Face-centred cubic
FRAP	Ferric Reducing Antioxidant Power
FTIR	Fourier transforms infrared spectroscopy
FC	Folin–Ciocalteu’s phenol reagent
FR	Fermented rooibos
GA	Gallic acid
G	Gram
GLY	Glycine
GR	Green rooibos
GR-AuNPs	Green rooibos extract- mediated gold nanoparticles
GR-AgNPs	Green rooibos extract- mediated silver nanoparticles
HA	Helichrysin

HB	Helichrysetin
HCl	Hydrochloric acid
HepG2	Hepatocellular carcinoma
Hex	Hexane
HDS	Hydrodynamic size
HF	*Helichrysum foetidum*
HF-AuNPs	*Helichrysum foetidum* extract-mediated gold nanoparticles
HPLC	High-performance liquid chromatography
HR-TEM	High-Resolution Transmission Electron Microscopy
HR-MS	High-Resolution Mass Spectrometry
H_2SO_4	Sulphuric acid
1H-NMR	Proton nuclear magnetic resonance
IC_{50}	Half maximal inhibitory concentration
JCPDS	Joint Committee on Powder Diffraction Standards
LC–MS	Liquid Chromatography–Mass Spectrometry
LSPR	Localised surface plasmon resonance
µL	Microlitre
MAE	Microwave assisted extraction
MS	Mass spectrometry
MNPs	Metallic nanoparticles
MeOH	Methanol
mg	Milligram
mL	Millilitre
min	Minutes
$NaAuCl_4.2H_2O$	Sodiumtetrachloroaurate dihydrate salt
NaCl	Sodium Chloride
Na_2CO_3	Sodium carbonate
NaH_2PO_4	Sodium dihydrogen phosphate
Na_2HPO_4	Disodium hydrogen phosphate
NA	Not active at the tested concentration
NMR	Nuclear magnetic resonance
NPs	Nanoparticles
PBS	Phosphate buffered saline
PDI	Polydispersity index

PDT	Photodynamic therapy
p-NPG	P-nitrophenyl-α-D-glucopyranoside
ROS	Reactive oxygen specie
SAED	Selected area electron diffraction
SE	Soxhlet extraction
SD	Standard deviation
SPR	Surface plasmon resonance
TEM	Transmission electron microscopy
TE/g	Trolox equivalent per gram
TLC	Thin-layer chromatography
TBARS	Thiobarbituric acid assay
TPC	Total Phenolic Content
T2DM	Type II diabetes mellitus
TMS	Tetramethylsilane
UAE	Ultrasonic assisted extraction
UV-VIS	Ultra-Violet Visible spectroscopy
UHPLC	Ultra-high-performance liquid chromatography
v/v	Volume by volume
WHO	World Health Organization
XRD	X-ray diffraction
ZP	Zeta potential

Chapter one

1.1. Introduction

1.1.1. South African flora, natural product chemistry and nanoscience

There has been a global increase in research on medicinal plants due to the continuous claims from traditional healers on the use of extracts from some plants to cure diseases. The World Health Organization in 2008 reported that up to 80% of the world population still use medicinal plants as drugs for therapeutic purposes (Mabona a, 2013). Traditional medicine is reported with a significant role in South Africa health care as evident in the large numbers of practitioners of traditional medicine (Puckree et al., 2002). The rich plant diversity of South Africa makes it ecologically and economically significant for natural products chemistry and plant-mediated nanotechnology research (Myers et al., 2000). Being home for Cape Flora, one of the important world floristic regions, it contains medicinal herbs from plants families including Asteraceae, Fabaceae, Lamiaceae etc used in folk medicine for the treatment of fever, wound dressing, cough, stomach damage, weight losses and stress-related diseases among others (Butler, 2004). There are records of approximately 600 species of genus *Helichrysum* from the Asteraceae family distributed in Australia, Southern Europe, South-west Asia and Southern Africa in which over 240 species are endemic to SA (Lourens et al., 2008). Similarly, the Fabaceae family is also known with over 700 general, 20,000 species including *Aspalathus linearis* which is endemic to *the* mountainous region of Clan William Cederberg, Western Cape of South Africa. The Lamiaceae is also known with about 233 genera consisting of 6900 species and approximately 308 species from 41 genera of this family are native to SA (Le Roux et al., 2011). This remarkable plant diversity of South African medicinal plants has increased the numbers of traditional healers and herbal medicine available because they are believed to be a cheaper and better alternative to chemically synthesized drugs. Medicinal plants are known to contain bioactive phytochemicals that can be isolated and formulated as drugs in replacement for chemically synthesized drugs for drug discovery (Cheuka *et al.*, 2016; Saeed *et al*. 2016). In addition to drug discovery, these phytochemicals when functionalized with biocompatible metals-oxide are also found to have application in nanomedicine for diagnosis, treatment and prevention of various diseases. (Dowling et al., 2004; Luisa & Duncan, 2013).

1.1.2. Cape Floral Region of South Africa

The Cape flora region (CFR) of South Africa remains in the list of revised 35 regions of the world hot spot of global biodiversity with an estimated 980 plant genera, 9000 species and 5682 endemics (Coetzee et al., 1999; Myers et al., 2000; Mittermeier et al., 2011). This statistic represents nearly 3% of total world plants species and 1.9% endemic of global plants species respectively. This is despite the relatively small land size of (90 000 km^2 equivalent to 3.4%) compared to the total land size of Southern Africa floristic region (Goldblatt & Manning, 2002). The richness in plant endemism of CFR is also notable when compared with other regions with a similar Mediterranean climate. Central Chile and Southwestern Australia regions occupying larger land sizes which would be expected to have higher diversity have much lower plant genera and species respectively (Goldblatt, Peter 1997). The vegetation of CFR is categorized into three distinctive biomes based on soil types, shrubs, and rainfall per annum as Fynbos, renosterveld, and Forest and thicket (Cowlings *et al*., 1996). Fynbos biome has a sandstone soil type consisting of short shrubs with tiny leaves and fire-prone. The vegetation is known with dominant species from Asteraceae, Proteae, Ericaceae, Fabaceae, Iridaceae, among others. The renosterveld shrubland is a dense semi-arid land rich in herbaceous plants with succulent leaves, rainfall below 200 mm per annum and less prone to fire ravage although share some species with Fynbos. The third biome, Forest is an evergreen forest and consists of broad-leaved, evergreen trees and shrubs (Cowlings *et al*., 1996; Goldblatt, Peter 1997). Given the plant richness of the Cape floral region and a large number of traditional healers, more than 60% of South Africans prefer the use of traditional medicine (Steenkamp, 2003). This account for the current boost in the exploration of South African medicinal plants and scientific research of their bioactive compounds. *Aspalathus linearis* (*Fabaceae*) and *Helichrysum foetidum* (*Asteraceae*) from the fynbos vegetation are among strong medicinal plants of CFR that have been studied and still need reassessment for updated chemical and biological reports.

1.2. Why the study of Aspalathus linearis and Helichrysum foetidum?

Aspalathus linearis is an indigenous medicinal herbal tea plant of South African endemism with international recognition for health-promoting traits of its phytochemical constituents. As a rich source of dietary flavonoids, isolation of these compounds is somewhat complex and often required combinations of techniques. Also, nearly every successful re-investigation of the plant presents a new compound or derivatives of its known compounds. Despite being

well studied, the literature is limited on its potential application in cosmetic formulations, protection of skin from UVB-induced oxidative stress and nanomedicine. Also, the South African species of *Helichrysum foetidum* which has distribution in the eastern and western cape was reportedly used in folk medicine to treat dysmenorrhea, wound, eye infections, influenza, among others. However, its phytochemical constituents and application in nanomedicine are yet to be extensively studied. Chapter two documents the details of these plants' species and the knowledge gap.

1.2.1. Roles of *Aspalathus* linearis and compounds against UV-induced skin diseases and anticancer promotion.

The human skin is ubiquitous and the largest tissue which describes the apparent beauty in a human population of all ages. It serves as a sense organ and as an interface that maintains metabolic equilibrium between the body and the environment. The skin is composed of the inner layers (dermal) and the outer layer (epidermal) which is continually exposed to UV radiation from sunlight from human mobility and daily activities. The prolonged exposure to UV radiation leads to the generation of free radicals and oxidative stress which are the main causes of skin ageing, cutaneous damages, and diseases as skin cancer (Zillich et al., 2015). This accounts for the importance given to skincare products by people of all levels and the cosmetic industries that focus on skincare produce from natural ingredients (Ribeiro et al., 2015). In light of this, Afoalayan et al., (2014), discovered that the remote people of Amanthole district in the eastern cape of South Africa use plant extract in the management of skin disorders. Among 161 plant families reportedly used, the Fabaceae from which *Aspalathus linearis* belong was third of the list of the most frequently used plant (Afolayan et al., 2014). Hence, the interest to discover natural raw materials for skin care products is increasing due to the potential side-effect of free radical generation on exposure to UV light by synthetic cosmetics products and the effect of continuous climate changes on skin cells such as inflammation of melanocyte cells and pigmentation disorder. Worthy of note is the enormous literature studies on the anti-inflammatory and antioxidants properties of rooibos against the over-production of reactive oxygen species in skin cells. The in vitro studies by Marnewick et al. (2005) and Tandeka et al. (2016) showed that the antioxidant potentials of cape herbal teas including *A. linearis* could be responsible for the viability of skin cells exposed to UV light (Marnewick et al., 2005; T. Magcwebeba et al., 2016; Unathi et al., 2016). These reports are complementary to the cosmetic formulation by Cosmetochem International Ltd. Switzerland of rooibos tea for hair growth and skincare (Tiedtke & Marks, 2002). However, it

is clear from the literature that vacuum still exists in the identification of bioactive compounds of *A. linearis* that are responsible for these bioactivities. Scientific validation of the involvement of these compounds will justify the incorporation of *Aspalathus linearis* in cosmetic products. This is of interest to this study.

1.2.2. *Helichrysum foetidum* and compounds potentials against oxidative stress-induced diabetes

Several *helichrysum* species are documented with inhibitory activities against the development of diabetes from induced oxidative stress in organs associated with glucose metabolism (Odeyemi & Bradley, 2018; Nyakudya et al., 2020). The occurrence of oxidative stress in the liver, pancreas, adipose and muscle cells could lead to high blood glucose (Chinsembu, 2019). High blood glucose is estimated as the third-highest risk factor for premature death after high blood pressure and the use of tobacco by the World Health Organization (WHO, 2009). Hyperglycaemia in type 2 diabetes (T2D) is associated with high postprandial glucose due to imbalance and dysfunction in insulin produced by the pancreas to inhibit excessive hydrolysis of starch from the small intestine by alpha-glucosidase and alpha-amylase enzymes. The result is an increased risk of obesity, kidney failure and cardiovascular diseases (Loo *et al*., 2019). Acarbose, voglibose and miglitol are alpha-glucosidase inhibitors that function by inhibiting hepatic glucose production and weight losses are conventional drugs commonly prescribed for antidiabetic (Aoki *et al*. 2019). The reported adverse effect of liver impairment, flatulence, and abdominal pain (Dong *et* al., 2019) on prolong usage is a drawback. Also, despite the documented reports of *Helichrysum* species with antidiabetic potential, isolation of the bioactive compound and *Helichrysum foetidum* is still lacking. These necessitated the exploration of the South African *Helichrysum foetidum* for antidiabetic potentials and its formulation with biocompatible metal nanoparticles for nanomedicine.

1.3. Extraction and isolation of phytochemicals from plant materials

The development of modern medicinal and pharmaceutical chemistry is stimulated by phytochemicals derived from natural products such as plants. Plant-derived drugs are known with high potencies and negligible toxicity that makes them suitable over the chemically synthesised drugs (Peter *et al.*, 2016). The plant material is chemically and biologically profiled through extraction and assessment (*in vitro* and *in vivo*) of its bioactivity. Extraction and

isolation of bioactive compounds is a multi-step procedure that involves; selection and collection of plant materials, collection of ethnobotanical data, extraction, and purification of compounds, and lastly characterisation and identification of the compounds isolated in sequential order. The first stage begins with guided extraction of the total or crude extract from plant material (roots, stem, leaves, flowers, and seed) with a selected (conventional or non-conventional) method (Brusotti et al., 2014; Akinfenwa et al., 2020). The common extraction methods use decoction, infusion, maceration, hydrodistillation or Soxhlet extraction with organic solvents at a regulated temperature. In non-conventional methods, extraction requires the use of advanced techniques that improve the efficiency and extraction time such as supercritical fluid extraction, microwave-assisted extraction, pressurized liquid extraction etc. In the Soxhlet/solvent extraction, the plant material in a flask is submerged in suitable organic solvents as the mobile phase, the set-up is connected to a heating mantle. The solute from the sample is extracted by the solvent used which vaporises through distillation and is condensed back to the flask via a water inlet and outlet system. The same procedure with modification is involved in the non-conventional methods (Azmir *et al.*, 2013). In general, methods selection for extraction depends on the plant matrix under investigation, nature of targeted bioactive compound for isolation, process efficiency and cost of extraction. After extraction, the dried crude extract can then be subjected to fractionation of its constituents through different chromatographic techniques and further purifications process on the fractions lead to the isolation of pure compounds.

1.3.1. Chromatography

Chromatography is an important analytical technique in which constituents of analyte (plant extract) are separated by differences in the rate of migration through a packed column with stationary and mobile phases. It relies on solvent polarity, hydrophilic, and the lipophilic character of the targeted constituents. Typical chromatographic methods include column chromatography (CC), thin-layer chromatography (TLC), high-performance liquid chromatography (HPLC) and liquid chromatography-mass spectrometry (LC-MS) (M. Aslam et al., 2016).

The CC set-up consists of the glass column, stationary phase, mobile phase, and the analyte sample through which separation and elution of compounds from the plant extract are achieved. The column is the warehouse for the analyte sample, the stationary phase, and the mobile phase loading during chromatography. The stationary phase refers to the solid material of known mesh size (silica gel, Sephadex, resins etc) packed into the column through which

analytes are separated by the difference in the rate of migration. The mobile phase also called the eluent is usually liquid (solvent) in column chromatography that provides the gravitational push for migration of analytes through the column for elution based on analyte affinity for the mobile phase. Solvent systems used during chromatography are often varied between nonpolar to mid-polar and polar solvent (hexane < chloroform < dichloromethane < ethyl acetate < acetone < methanol < water) for isolation of targeted compounds.

The TLC is a simple and fast chromatographic technique that is used to identify the number of possible compounds in a mixture and to determine the right solvent system necessary for the separation of compounds. The separation of compounds using TLC is similar to the CC. A small portion of the mixture can be spotted on a line drawn 1 cm from the TLC plate measuring 5 cm x 6.7 cm and developed over the mobile phase in a TLC tank. The analyte moves through the stationary phase (silica impregnated on an aluminium plate) in bands through elution against gravity. The different bands/spots developed on the plate is then observed under UV light with the short (254 nm) and long (366 nm) wavelength for fluorescent compounds. Compounds that do not fluoresce under UV short wavelength require dipping the TLC plate in specific colour detection reagents follow by a spray with the hot-gun. These reagents such as dragendorff's reagent (detection of alkaloids) vanillin-sulphuric acid, and anisaldehyde-sulphuric acid reagents (detection of flavonoids, chalcones and terpenes) produce colour changes to blue, red, orange, brown depending on the compound (Diego Vinueza et al, 2018).

In addition to the separation of components of a mixture provided by the CC and TLC, the HPLC is useful in the quantification and identification of compounds through parameters like peak retention time and peak areas or height that are compared to the known standards. This is achieved with a high-pressure pump that forces the mobile phase through a column densely packed and uniform microsphere. The high sensitivity of HPLC set-up provides an immense surface for adsorption, greatly improved column efficiency and result validation. The HPLC equipment (figure 1.1) is commonly connected to an ultraviolet/visible (UV/Vis) detector (LC-UV) which scans the eluents through UV wavelength and displays the chromatogram showing each compound in the mixture based on their wavelength maxima and times of elution. The equipment can also be hyphenated to high-level detectors which use either a thermal conductivity or flame ionization of the carrier gas such as diode array detector (DAD), mass spectrometer (MS) etc. The LC coupled with MS (LC-MS) is useful in the identification of compounds by providing molecular masses of compounds in the total extract through mass analysis of the different fragments (Tanmay Kumar et al., 2020).

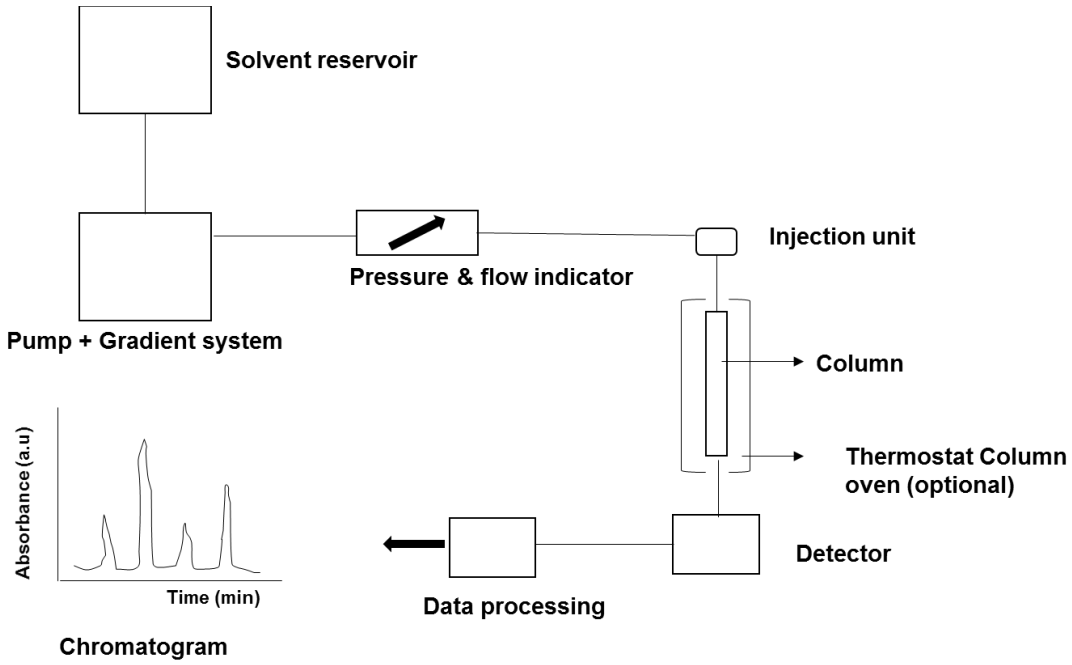

Figure 1.1: Block diagram of HPLC

1.4. Characterisation of isolated compounds by spectroscopy

The pure compounds (molecules) isolated consist of different atoms mostly carbon, hydrogen, oxygen, and a few electronegative elements that are chemically characterised through spectroscopic methods before biological screening as drug candidates. The spectroscopic methods used for the characterisation of compounds depend largely on the region of the EMR used, the chemical bond types (i.e., σ or π bonds) and types of orbitals present in the molecule. These include the application of UV/Vis, infrared (IR), nuclear magnetic resonance (NMR) spectroscopy and mass spectrometry (MS). The molecular orbital of isolates is made up of bonding (σ, π) and antibonding (σ^*, π^*) and non-bonding (n) orbitals of the constituents' atomic orbitals. Spectroscopy involves the study of the interactions between atomic, and molecular orbitals exposed to electromagnetic radiations (EMR). The electromagnetic spectrum (figure 1.1) consists of light of different frequencies (energies) and wavelengths that are absorbed/reflected by molecules. The spectrum which ranges from radio waves, microwaves, infrared rays, ultraviolet light, visible light, x-rays, gamma rays and cosmic rays in increasing order of frequencies passes through organic compounds and molecules in discrete amounts of energy. Absorption occurs when radiation of exact energy quantum interact with the

molecule at a specific wavelength. The magnitude of the energies involved in spectroscopy and the relationship between frequency and wavelength is represented mathematically in equations 1-3.

Equation 1.1

$u = c/l$

Equation 1.2

$\Delta E = h\upsilon$

Equation 1.3

$\Delta E = hc/\lambda$

(h = Planck's constant (6.626×10^{-34} Js), c = speed of light (2.99×10^{10} cm/sec, λ = wavelength in cm and υ = frequency in Hz)

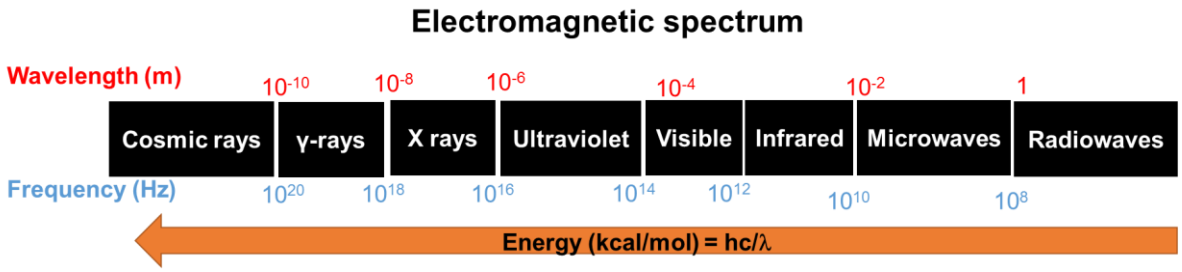

Figure 1.2: Electromagnetic spectrum

1.4.1. UV-vis spectroscopy

In the UV-vis spectroscopy also known as electronic spectroscopy, visible and ultraviolet regions (within the wavelength of 200 - 800 nm) of EM is selected for use in UV/Vis spectrometer. The spectrometer consists of a radiation source, a monochromator that transmits light of specific wavelength, a photomultiplier that slit the UV light to reference beam and incident beam, a sample holder and a detector connected to output data (figure 1.3). Information obtained from UV/Vis analysis is useful in determining the optical activity, maximum wavelength of absorption, the extent of conjugation and substituents in organic and inorganic molecules. The incident light absorbed by the sample compound causes electronic excitation between the highest occupied molecular orbital (HOMO) and the lowest unoccupied molecular orbital (LUMO) energy level in molecular orbital (figure 4). Absorption of energies

in this region leads to four major types of transitions: n → σ^*, n → π^*, π → π^*, and σ → σ^*. n → σ^* transition occurs when atoms in molecules possess lone pairs of electrons that are not involved in internal bonding, for example in compounds of alcohols, amine, and alkyl halides. In n → π^*, Molecules such as aldehyde and ketones containing carbonyl groups have atoms that are involved in π-bonding. Interaction of UV/Vis radiation result in the transition of n from HOMO to π^* (LUMO). Molecules with conjugated systems of double bonds such as alkenes and aromatic compounds have π-orbital as the HOMO and π^*-level as LUMO and require the lowest energy (the longest wavelength) for transition to occur. Hence, the electronic transition is the π → π^* type. The σ → σ^* is common in saturated compounds. These compounds have hybridized atomic orbitals (e.g., carbon-hydrogen bond) which requires the highest energy for transition (very low wavelength) due to the large HOMO-LUMO energy gap.

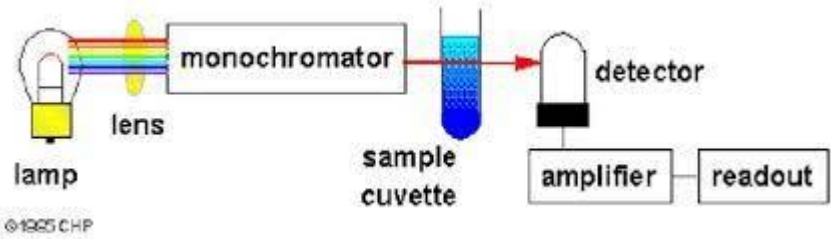

Figure 1.3: Schematic diagram of single UV/Vis spectrometer

(* Source: https://www.ncbi.nlm.nih.gov/books/NBK92014/figure/assayequip.F15/)

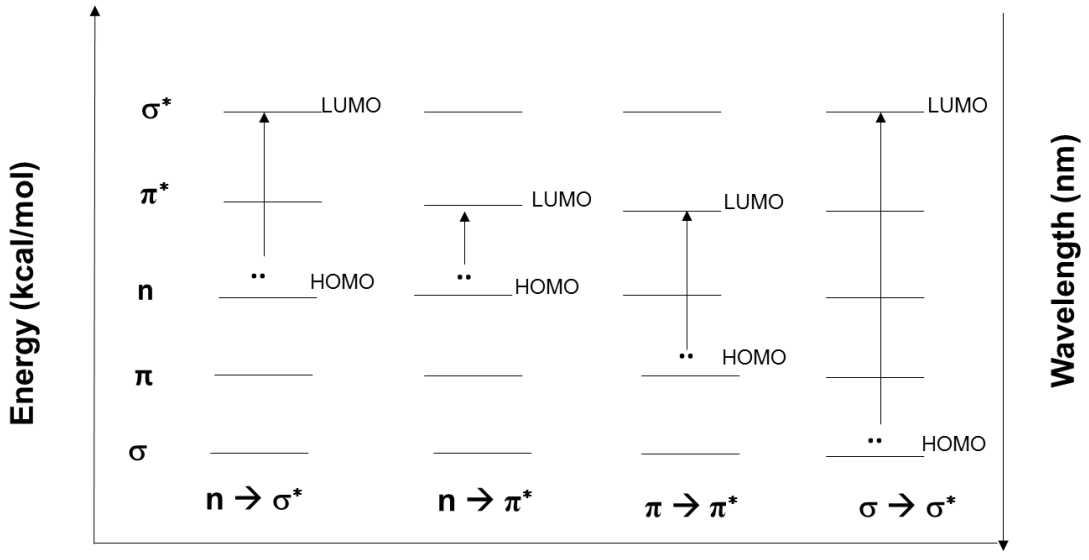

Figure 1.4: HOMO-LUMO energy transition

1.4.2. Infrared spectroscopy

The is referred to as vibrational spectroscopy due to the vibration of bonds at specific frequencies. It is quantitatively similar to UV/Vis spectroscopy for characterisation organic compounds but uses infrared radiation. The IR region is classified as near (approximately 4000 – 14000 cm^{-1}), mid (approximately 400 – 4000 cm^{-1}), and far (approximately 10 – 400 cm^{-1}) IR based on energy and closeness to the UV/Vis region of the EMR. The mid and near-infrared sources are commonly used to characterise chemical bonds (functional groups) in organic molecules. Chemical bonds are thought of as springs connected to atoms at both ends and vibrating at a certain frequency due to atomic masses from both ends. When molecules are exposed to infrared radiations, functional groups with dipole moment molecular vibrations (stretching and bending) with varying frequencies band intensities. In the process, chemical bonds absorbed and transmit quantized light equal to the frequencies of the excited bond that are measured as wavenumbers (cm^{-1}). An advanced form of the infrared spectrometer is the Fourier transform-infrared (FTIR) which scans and transform infrared data at high resolution to IR spectrum. Table 1.2 show characteristic IR absorptions ranges of some functional groups subject to changes due to factors such as bond strength and conjugation.

Table 1.1: Characteristics IR frequencies of selected bonds

Bonds	**Functional group**	**Frequencies (cm^{-1})**	**Intensity**
C-H	Alkane	3000-2850	medium
C=O	ketone	1715	strong
C-C	Aromatics	1600-1580	medium
O-H	Alcohols (H-bonded)	3500-3200	Strong, broad
NO_2	Nitro	1540	Strong
N-H	Amine, Amide	3400-3250	medium
H-C=O	Aldehyde	2830-2695	medium
C=C	Alkene	1680-1640	medium

1.4.3. Nuclear magnetic resonance (NMR)

The nuclear magnetic resonance spectroscopy gives the most valuable information needed for structural elucidation of compounds based on the interaction of radio waves energies of EMR on the nuclear spin (*I*) of atoms in compounds. The spin (nonzero) values due to effective nuclear charge from proton and neutron are responsible for NMR activity of ^{1}H, ^{13}C, ^{15}N, ^{19}F

etc. In principle, an external magnetic field (B_o) supplied by a magnet at a controlled constant frequency by magnet controller is applied through a sample in a sample tube (equation 4, fig. 1.5). The applied field which is usually within frequency ranges of 60 – 1000 MHz causes perturbation of nuclear spin of atoms to either align opposite or in the direction of the applied magnetic field. Equilibrium of the perturbed nuclear spin is then restored when it absorbed the required amount of energy. With this alignment, the spinning nucleus generates electromagnetic signals which resonate at the characteristic frequency of the nucleus that is measured as chemical shift (δ) in part per million (ppm). Figure 1.5 shows the schematic diagram of the major components of an NMR spectrometer.

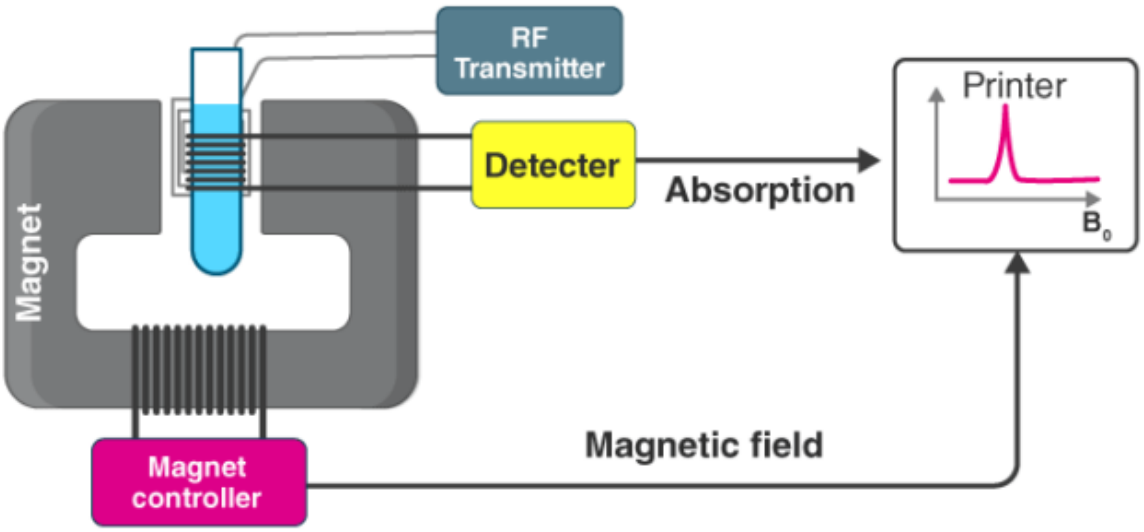

Figure 1.5: Schematic diagram of a typical NMR spectrometer

(https://byjus.com/chemistry/nmr-spectroscopy/**)**

In the NMR spectrometer, the resonance frequency of atoms is referenced to the chemical shift of tetramethylsilane (TMS) standard whose signal has zero interference with signals of most organic compounds. NMR spectra are mostly recorded as ^{1}H and ^{13}C because most compounds contain these atomic nuclei. The chemical shift for the ^{1}H (proton) NMR spectrum ranges from 0 – 5 ppm (upfield/weak field) and then from 6 -14 ppm (downfield/strong field) while the ^{13}C spectrum ranges from 0 – 220 ppm. These spectra which are recorded as intensity on the y-axis versus chemical shift (x-axis) are referred to as one-dimensional (1D).

In addition to 1D-NMR, the two-dimensional (2D) NMR spectrum (figure 1.6) plotted on three axes provides complete confidence for structural elucidation of isolated compounds by providing coupling correlations between homo and heteronuclear atoms as ^{1}H-^{1}H (COSY), and ^{1}H-^{13}C (HMBC and HSQC). Summarily, the NMR spectroscopy provides details of the type of proton and carbon-13 environment, the chemical shifts and the numbers of proton and carbon-13 in the studied compounds.

Equation 1.4

$$\upsilon = \gamma B_o/2\pi$$

Equation 1.5

$$\Delta E = h\,\gamma B_o/2\pi$$

(h = Planck's constant (9.5 x 10^{-14} kcal/mol.s), γ = gyromagnetic ratio (2.7 x 10^{8} rad/T/s, υ = frequency in s^{-1} and π = 3.142).

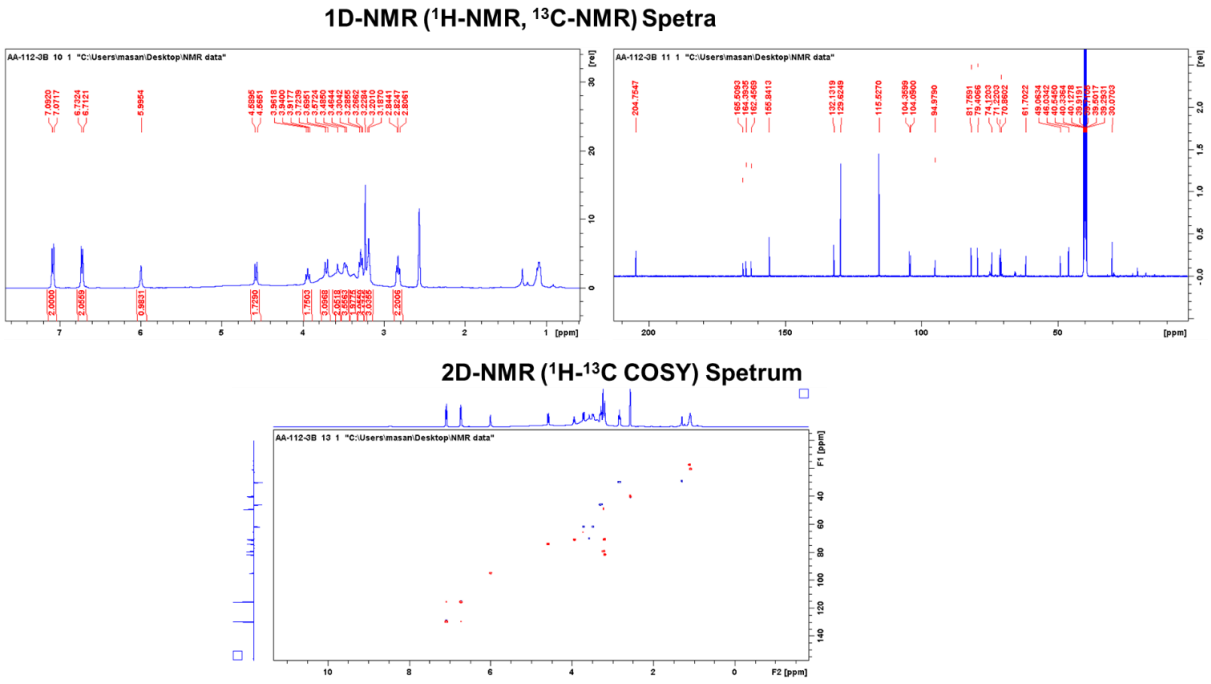

Figure 1.6: Typical 1D and 2D NMR spectra for compound, Nothofagin

1.5. Nanoscience

Nanoscience is a relatively new area of study with active researchers due to its promising potentials in drug delivery systems, electrochemical cells, biotechnology, and agriculture. It is

interdisciplinary that cut across physical sciences, life sciences, material sciences, and engineering. Closely related to nanoscience is nanotechnology which involves the study of processes and manipulation of shapes and dimensions of matters at atomic, molecular and macromolecular levels for functional applications at the nanoscale (1-100 nm) (Dowling et al., 2004). Matters and particles can be described in positions by three dimensions; length (x), breadth (y), and height, (z). A nanomaterial such as nanoparticles has at least a dimension in the nano range (Table 1.0) and the focus here will be on nanoparticles. Nanoparticles have length, breadth, and height all in less than 100 nm. One nanometer is equivalent to one-millionth of a millimetre and materials in this range are known to exhibit quantum phenomenon which makes them remarkable with better functional properties for application in chemistry and physics, imaging, biotechnology, and medicine. An example of the application of nanoparticles is the DNA silicon chip used in nanomedicine (Kricka, 2001). Synthesised nanomaterials (nanoparticles, nanotubes, nanocrystals, nanoshells, nanorods, thin films, nanofibres etc) may have different morphologies and surface properties for different applications. Nanoparticles, because of their 'small size' show unique characteristics different and mostly opposite to the bulk materials of the same substance. Gold metal nanoparticles for example is observed to have optical, strength, colour, electrical and mechanical properties different from that at micron-scale (Luisa & Duncan, 2013). Another importance of nanomaterials is the high surface-to-volume ratio due to their "small sizes", which makes them suitable for the fabrication of devices and processes that requires detections at the surfaces of materials.

1.5.1. Classification of nanoparticles

Nanoparticles are broadly classified in the literature based on the sources, shapes and dimensions of the nanoparticle (Diana Sannino 2021; Firdos Alam Khan, 2020).

i. Natural and modified nanoparticles:

Natural NPs are biomolecules from plants, microbial species and animal origin without modification. Typical examples can be found in the nanostructure and water-resistant properties of leaves of the lotus plant, in the nanoscale arrangement of cellulose fibre in cotton flowers, scattering of light by milk and blood are due to nano composition of the colloids and so on (Luisa & Duncan, 2013; Sakka, Yoshio et al., 2017). Modified NPs are intentionally fabricated through two synthetic methods (Top-down and Bottom-up) using organic and inorganic materials. Among modified NPs are metallic NPs, plant-assisted NPs,

semiconductor NPs, lipid-based NPs, fullerenes, ceramic NPs, polymer NPs, carbon nanotubes etc.

ii. Inorganic and organic nanoparticles.

Inorganic NPs are synthesized by precipitation of inorganic salt on a well-defined metal surface through a top-down and a bottom-down approach. In a top-down approach, a nanostructure can be generated by milling larger size particles into nanoscales through mechanical abrasion of bulk materials. Whereas in the bottom-up method nanosized particles are built up from molecules through synthetic self-assembly and aggregation. Gold, silver, superparamagnetic iron oxide, titanium oxide, zinc oxide nanoparticles, quantum dots, are common examples of inorganic nanoparticles with application in food, drugs, and medicine. Organic nanoparticles such as proteins, liposomes, micelles, dendrimers are also prepared in a bottom-top and top-down method from natural (microbes, plants and animal origin) or synthetic organic (Fuente, 2012). Liposomes for example are phospholipids and natural organic molecules formed by self-aggregation and organization into bilayers from smaller lipids. They have a size range between 50 -100 nm and internal bilayer membrane layers make them suitable for transport and diffusion of encapsulated hydrophobic and hydrophilic drugs (Mordy Nishi et al., 2014). Dendrimer on the other hand is a synthetic organic nanoparticle closest to inorganic nano due to its small size (<10 nm) (Wakaskar, 2018). Like haemoglobin, it has a central atom (nitrogen) through which other atoms aggregate to form a spherical branching structure.

Figure 1.7: Examples of organic and inorganic nanoparticles.

iii Dimensions of nanoparticles

The values of particles sizes in length x, breath, y and height, z dimensions were first used to describe the type of the particles by Pokropivny and Skorokhod (2007) as zero-, one-, two- and three-dimension NPs. Zero-dimension NPs are mostly in single unit nanometer scale in each of the spatial dimensions. In one-dimension NPs such as thin films, nanolayers and nano coatings, particle size in one dimension only is less than 100 nm. Nanowires, nanotubes and nanofibres are two-dimensional NPs having two of the three dimensions in sizes less than

100 nm while three-dimension materials such as nanoparticles, microcapsules, quantum dots, nanoshells, nanorods have sizes in all dimensions less than 100 nm.

1.5.2. Metal NPs Synthesis and green chemistry

Metallic (e.g., gold) nanoparticles are traditionally synthesised by the Turkevich method of chemical reduction and the Anasta and Warmer guidelines (Voliani, Valerio, 2013; Anastas, P. & Eghbali, N. 2010). Other methods commonly used are physical and mechanical methods involving bottom-up (aggregation) and top-down (disintegrations) approaches. The bottom-up aggregation involves assembling MNPs at atomic and molecular levels through synthesis such as chemical reduction and condensation, flame synthesis, laser pyrolysis, ultrasonic method, green synthesis method etc. In the top-down approach, bulky materials are disintegrated to smaller sizes and shapes via physical and mechanical methods such as thermal decomposition, milling, surface-irradiation, laser ablation etc. The major demerits of physical and mechanical methods are the high cost, energy and time requirements for the process (Badeggi et al., 2020). The chemical method was based on the reduction of the bulk metal precursor to its zerovalent state ($M^{n+} + ne^- \rightarrow M^0$) by reducing agents and stabilizers is less expensive but requires the use of hazardous chemicals and are considered not eco-friendly. However, with the application of Anasta and Warmer guidelines which stipulate the use of benign solvent, safe reducing, and stabilizing/capping agent, the procedures have continuously been modified through 12 principles of green chemistry.

Green chemistry according to the American Chemical Society is defined as the design, development and implementation of chemical products and processes that reduces or eliminate the generation of hazardous substances. It is based on the principles that establish the sustainable safety of humans and the environment and emphasises the use of biodegradable and eco-friendly materials that improve process efficiency. These principles and the main objectives are summarised under twelve scopes (Table 1.2)

Table 1.2: Principles of Green chemistry

S/N	Principles	Focus
1	Prevent waste	To minimise waste generation in a chemical process to near-zero level.
2	Atom economy	To ensure an effective mass balance of materials from the start to the end product in the reaction design.
3	Less hazardous synthesis	To reduce the negative effects and impacts of synthetic methods and products on human health and the environment

4	Design benign chemicals	A careful selection of chemicals used in synthesis be considered for safety
5	Benign solvent and auxiliaries	Where necessary to use solvent and auxiliaries in synthesis, they should be harmless
6	Design of energy efficiency	Environmental and economic impacts of energy required for efficient synthesis should be considered.
7	Use of renewable feedstocks	Requires the use of renewable and biodegradable materials which do persist in the environment.
8	Reduce derivatives	To reduce unnecessary derivatization (blocking group, protection/deprotection, temporary modification of physical/chemical processes) whenever possible.
9	Catalysis/stoichiometry	The use of catalytic reagents at ambient temperature and pressure should be considered over their stoichiometry ratio.
10	Design for degradation	To design synthetic process to improve degradation of its end products which are innocuous and do not persist in the environment
11	Real-time analysis for pollution prevention	To develop analytical techniques that allow for real-time monitoring and control of pollutants before their formation.
12	Inherently benign chemistry to prevent accidents	To strategically design experimental pathways that prevent accidents including chemical, mechanical and fire accidents

1.5.3. Synthesis of gold and silver nanoparticles (NPs)

Gold metal is a noble transition metal in the same group as copper and silver a golden yellow colour and the oxidation state of +3. Synthesis of gold nanoparticles using the Turkevich method involves reduction of gold ions in solution with the aid of reducing agents like sodium borohydride ($NaBH_2$) and sodium citrate ($Na_3C_6H_5O_7$) (Jiaqi Dong et al., 2020). In the process, tetrachloroaurate solution of $HAuCl_4$/$NaAuCl_4$ used as the gold precursor reacts with an aqueous solution of either sodium citrate or sodium borohydride which act as both reducing and capping agents under experiment conditions like controlled temperature, pH and time. An important characteristic of synthesized MNPs is local surface plasmon resonance absorption (SPR) under UV-visible wavelengths due to absorption and emission of UV/Vis light by oscillating surface electrons at a specific frequency. Absorption at the required frequency gives rise to intensely coloured solutions in the visible region observed during synthesis. The formation of AuNPs is usually monitored with the appearance of ruby-red colour and SPR on UV/Vis spectrometer which is observed within 500 - 600 nm. Gold nanoparticles are considered better functional materials for use in medicine due to properties like biocompatibility, low toxicity, strong light absorption and scattering, and high turnable surface plasmon resonance (Sumit and Nayak, 2012; Srikar et al., 2016; Ali et al., 2016; Oyagi et al., 2014). These properties of synthesized Au-NPs are reportedly used in photothermal therapy of cancer cells, bacteria, and viruses due to their ability to absorb light and convert to heat that damages targeted cells (Homberger & Simon, 2010). Spampinato *et al.* (2016) reported

functionalised Au-NPs used as a biosensor for specific recognition of maltose-binding protein. Silver NPs are closely related to gold NPs in synthesis and characterisation and have also been well studied. The silver nitrate ($AgNO_3$) salt is used as the metal precursor during chemical synthesis where sodium citrate acts as both a reducing and buffering agent. The appearance of yellowish colour solution LSPR absorption peak within 400 – 500 nm is characteristic of AgNPs formation. It finds excellent usage in cancer, antibacterial and fungicide drugs due to its ability to induce oxidative stress on the living cell wall which reduces activity and final death of the cell (Honary *et al.*, 2012).

However, the green method of synthesis based on the use of plant constituents and microorganisms as reducing and capping agents is gradually taking over the chemical method as it addresses the challenge of pollution of the environment from the release of hazardous and toxic substances and its relatively cheaper. In this method, phytochemicals from plant materials such as phenolic compounds act as reducing/capping in place of sodium citrate used in the Turkevich method which gives it huge applications in target drug delivery (Swilam and Nematallah, 2020). Hence, several articles detailed green synthesised AuNPs and AgNPs from plant phytochemicals having wider application than those from the conventional chemical methods (Peralta-Videa et al., 2016). The results from these articles showed that bioactive compounds from phytochemicals acted as reducing/capping agents. South Africa and Cape Town is rich in plant diversity and offers a good source of medicinal plant for green synthesis of nanostructured materials.

1.5.4. Phyto-assisted nanoparticles

Phytochemical constituents of plants such as phenolics acids, flavonoids, chalcones, aurones and other polyphenolics are known to have high electron affinity and conjugated double bonds to support their reducing and stabilizing abilities in the green synthesis of metallic NPs for biomedical applications (Noha Swilam and Khaled Nematallah 2020; Alaqad and Saleh, 2016). *Helichrysum foetidum* was reported to consist mainly of flavonoids and a few terpenoids class of compounds while *Aspalathus linearis* phytochemicals are polyphenolics (Malolo et al., 2015; Bond et. al., 2020*)*. The chemical profile of these plants makes them suitable to be functionalised to nanoscales for improve biomedical applications.

Phyto-assisted nanoparticles synthesis involves the use of plant and isolated compounds as reducing and stabilizing agents in place of hazardous chemicals in synthesis. This is a green chemistry response to the drawbacks of the conventional chemical and physical methods for

the synthesis of nanoparticles (Noruzi, 2014). It is fast, cheap, and eco-friendly as it removes the use of hazardous chemicals and harsh reaction conditions (Srikar *et al*., 2016; Yuilizar *et al*., 2017). Several studies and review papers that summarised the use of plant extract, bacteria and fungi extracts for the synthesis of nanoparticles have been reported (Anu *et al*., 2020; Sapana et al., 2021). Representative bands for phyto-assisted-metallic nanoparticles in the visible wavelength reported are shown in Table 1.3.

Table 1.3: Plant-based metal nanoparticles and Surface Plasmon Resonance Absorption bands

Plants/compounds	Nanoparticle	Color	Absorption (nm)	Applications	Reference
Leucosidea sericea extract and procyanidin fractions	LSTE-AuNPs, F1-AuNPs, and F2-AuNPs	Ruby red	528-532	Antidiabetic	(Badeggi *et al*., 2020)
Curcuma longa extract	Cu, CuNPs	Brick-brown	524	antimicrobial activity	Jayarambabu et al., 2020
Leucosidea sericea extract and procyanidin fractions	LSTE-AgNPs, F1-AgNPs, and F2-AgNPs	Yellowish-brown	424-426	Antibacterial	Badeggi *et al*., 2020
Resveratrol compound	Res-AuNPs	Ruby-red	535	Anticancer	Thipe et al., 2019
Date fruit extracts	Platinum, Pt	Yellowish	321-329	Anticancer	Al-radadi, Najlaa S., 2019
Taraxacum laevigatum extract	Platinum, PtNPs	Brown	283	Antibacterial	Tahir et. al., 2017
Fermented grape juices	Gold, AuNPS		536-562		Dzimitrowicz et. al., 2018
Phyllanthus niruri leaf extract	Zinc, ZnO-NPs	Dark yellow	349-359	Photocatalysis	(Anbuvannan *et al*., 2015)

1.5.5. Characterisation of nanoparticles

The formation of metallic nanoparticles from plant extract is reported to depend largely on experimental designs such as the plant species, the concentration of metallic precursor used, the stoichiometric ratio of plant extract/ precursor, pH, temperature and reaction time (Peralta-Videa *et al*., 2016). These factors in turn control the properties observed during the characterisation of the nanoparticles. Characterisation of biogenic synthesised metallic nanoparticles employs the Physico-chemical properties of the metal precursor and the

capping/reducing agents involved in the synthesis. Properties such as sizes, shapes, crystallinity, and stability of the nanoparticles are commonly measured with electromagnetic radiation involving imaging by microscopy and spectroscopic analysis. The sizes and shapes of nanoparticles are characterised using a High-Resolution Transmission Electron Microscope (HRTEM) and Selected Area Electron Diffraction (SAED). The microscope provides electron beams which are used to illuminate the particles and images of the particles are recorded. The occurrence of UV-Vis plasmon absorption at a specific range of wavelengths and colours are characteristic of the solution of metals in nano and picomolar concentrations. This absorption band due to oscillation of surface electron by UV-Vis region of the electromagnetic radiation is used for optical characterisation of metallic nanoparticles. Gold and silver are reported to exhibit surface plasmon resonance at 500 – 600 nm and 400 – 500 nm respectively. The Fourier-transform infrared spectroscopy uses infrared radiation on a sample, the absorbance and transmittance of light to determine the involvement of functional group via bond vibration and frequencies in the synthesis. Furthermore, NPs synthesised for biomedical application needs to be quantified for cellular uptake of the metal ions. This is carryout out using an inductively coupled plasma-mass spectrometer (ICP-MS) which can quantitatively determine an element's concentration in the physiological media. Similarly, the potential stability and interparticle interactions of nanoparticles are characterised using zetasizer equipment. The equipment works based on dynamic light scattering of an incident laser beam on hydrodynamic nanoparticles. A third technique seldomly used is the non-radiative and the non-electron method. This method includes thermogravimetric analysis to determine thermal stability, melting point, and mass determination by mass spectrometry.

Presently there is a need to expand previous studies on drug discovery and nanomedicine with phytochemicals of South African flora. In this study, bioactive compounds from selected species of *Helichrysum* and *Aspalathus* were isolated and used in the preparation of green nanoparticles for biomedical applications. We utilize reports from scientific literature and other relevant documents for the method used to isolate some compounds responsible for biological activities on screening and functionalized with metals for nanoparticles synthesis.

1.6. Problem statement and rationale

It is interesting to note that there are over 600 species of *Helichrysum* throughout the world with over 250 species distributed in South Africa. Also, the *Aspalathus* genus commonly known as rooibos tea is endemic to South Africa with over 270 species. *Helichrysum* species is reportedly used in folk medicine (Lourens et al., 2008) while *Aspalathus* species due to its

economic value is generally consumed as beverages and tea to relieve stress and maintain health (Joubert and Beer, 2011). A comprehensive literature review of *Helichrysum* and *Aspalathus* species shows studies of isolations and screening of bioactive compounds have been done on some species of these plants (Koeppen *et al.*, 1962; Malolo *et al.*, 2015). However, limited works on the phytochemical constituents of *Helichrysum foetidum* as a potential antidiabetic drug are available. Also, the applications of *Aspalathus linearis* in the cosmetic formulation are still scanty and the role of these plant species in the green synthesis of metallic nanoparticles. In addition, the isolation of new compounds from the plants was underrated. Therefore, there is a need to expand studies on the phytochemical constituents of these plant species for assessment in diabetes, skin performance under exposure to UVB and their application in green synthesis of metallic nanoparticles. Hence it was thought of interest to study *Helichrysum foetidum L. and Aspalathus linearis* and their phyto-mediated metallic nanoparticles in biomedical applications.

1.7. Research aim

The aim of this study focussed on the isolation and characterisation of bioactive compounds from South African *Helichrysum* and *Aspalathus* species for the green synthesis of gold nanoparticles. Compounds isolated, and the nanoparticles synthesized will be tested in vitro for efficacy as antidiabetic and modulation of glucose uptake potentials.

1.8. Objectives of this study

The main objectives of this study are:

- ✓ Collection of plant samples
- ✓ Retrieval of ethnobotanical classification
- ✓ Extraction, isolation, and purification of pure compounds
- ✓ Identification and characterisation of compounds by spectroscopy
- ✓ Synthesis of biocompatible metallic nanoparticles from isolated pure compounds
- ✓ Bio-evaluations of isolated compounds and the synthesized metal nanoparticles.

REFERENCES

1. Alaqad, K. and Saleh, T.A., 2016. Gold and silver nanoparticles: synthesis methods, characterization routes and applications towards drugs. *J. Environ. Anal. Toxicol*, *6*(4), pp.525-2161.
2. Afolayan, A.J., Grierson, D.S. and Mbeng, W.O., 2014. Ethnobotanical survey of medicinal plants used in the management of skin disorders among the Xhosa communities of the

Amathole District, Eastern Cape, South Africa. *Journal of ethnopharmacology*, *153*(1), pp.220-232.
3. Akinfenwa, A.O., Cheikhyoussef, A., Cheikhyoussef, N. and Hussein, A.A., 2020. Cold pressed chia (*Salvia hispanica L*.) seed oil. In *Cold Pressed Oils* (pp. 181-190). Academic Press.
4. Anastas, P. and Eghbali, N., 2010. Green chemistry: principles and practice. *Chemical Society Reviews*, *39*(1), pp.301-312.
5. Anbuvannan, M., Ramesh, M., Viruthagiri, G., Shanmugam, N. and Kannadasan, N., 2015. *Anisochilus carnosus* leaf extract mediated synthesis of zinc oxide nanoparticles for antibacterial and photocatalytic activities. *Materials Science in Semiconductor Processing*, *39*, pp.621-628.
6. Rana, A., Yadav, K. and Jagadevan, S., 2020. A comprehensive review on green synthesis of nature-inspired metal nanoparticles: Mechanism, application and toxicity. *Journal of Cleaner Production*, p.122880.
7. Aoki, K., Sato, H. and Terauchi, Y., 2019. Usefulness of antidiabetic alpha-glucosidase inhibitors: a review on the timing of administration and effects on gut hormones. *Endocrine journal*, pp.EJ19-0041.
8. Aslam, M.S., Ahmad, M.S. and Mamat, A.S., 2016. Phytochemical evaluation of polyherbal formulation of *Clinacanthus nutans* and *Elephantopus scaber* to identify flavonoids. *Pharmacognosy Journal*, *8*(6).
9. Azmir, J., Zaidul, I.S.M., Rahman, M.M., Sharif, K.M., Mohamed, A., Sahena, F., Jahurul, M.H.A., Ghafoor, K., Norulaini, N.A.N. and Omar, A.K.M., 2013. Techniques for extraction of bioactive compounds from plant materials: A review. *Journal of food engineering*, *117*(4), pp.426-436.
10. Badeggi, U.M., Badmus, J.A., Botha, S.S., Ismail, E., Marnewick, J.L., Africa, C.W. and Hussein, A.A., 2020. Biosynthesis, Characterization, and Biological Activities of Procyanidin Capped Silver Nanoparticles. *Journal of functional biomaterials*, *11*(3), p.66.
11. Bar, H., Bhui, D.K., Sahoo, G.P., Sarkar, P., Pyne, S. and Misra, A., 2009. Green synthesis of silver nanoparticles using seed extract of *Jatropha curcas*. *Colloids and Surfaces A: Physicochemical and Engineering Aspects*, *348*(1-3), pp.212-216.
12. Bond, T. J. and Emma, D. J., 2020. Rooibos Tea and Health: A Systematic Review of the Evidence from the Last Two Decades. *Nutrition and Food Technology* 6 (1) pp. 1- 11.
13. Brusotti, G., Cesari, I., Dentamaro, A., Caccialanza, G. and Massolini, G., 2014. Isolation and characterization of bioactive compounds from plant resources: The role of analysis in the ethnopharmacological approach. *Journal of pharmaceutical and biomedical analysis*, *87*, pp.218-228.
14. Butler, M.S., 2004. The role of natural product chemistry in drug discovery. *Journal of natural products*, *67*(12), pp.2141-2153.
15. Coetzee, C., Jefthas, E. and Reinten, E., 1999. Indigenous plant genetic resources of South Africa.
16. Cheuka, P.M., Mayoka, G., Mutai, P. and Chibale, K., 2017. The role of natural products in drug discovery and development against neglected tropical diseases. *Molecules*, *22*(1), p.58.
17. Chinsembu, K.C., 2019. Diabetes mellitus and nature's pharmacy of putative antidiabetic plants. *Journal of herbal medicine*, *15*, p.100230.
18. Cowling, R.M., MacDonald, I.A.W. and Simmons, M.T., 1996. The Cape Peninsula, South Africa: physiographical, biological and historical background to an extraordinary hot-spot of biodiversity. *Biodiversity & Conservation*, *5*(5), pp.527-550.
19. Diana, S., 2021. Types and Classification of Nanomaterials. *Nanotechnology*. Springer Singapore Pte Ltd. 2021 M. B. Tahir et al. (eds.). ISBN: 9789811594373. pp 15 – 38.
20. Diego, V., Santiago, P., Gisela, P., Marlene, G., Karene, A. and Susana, A., 2018. In vitro anti-inflammatory and cytotoxicity of *Crinum x amabile* grown in Ecuador. *Asian J. Pharm. Clin. Res.*, 11(10) pp.99 -103.
21. Dong, Y., Zhang, B., Sun, W. and Xing, Y., 2019. Intervention of prediabetes by flavonoids from *Oroxylum indicum*. In *Bioactive Food as Dietary Interventions for Diabetes* (pp. 559-575). Academic Press.
22. Dowling, A., Clift, R., Grobert, N., Hutton, D., Oliver, R., O'neill, O., Pethica, J., Pidgeon, N., Porritt, J., Ryan, J., Seaton, A., Tendler, S., Welland, M. and Whatmore, R., 2004.

Nanoscience and nanotechnologies: opportunities and uncertainties, *The Royal Society & The Royal Academy of Engineering Report*. London
23. Drewes S.E, Madau K.S, van Vuuren S.F and Viljoen A.M., 2006. Antimicrobial monomeric and dimeric diterpenes from the leaves of *Helichrysum tenax var tenax*. *Phytochemistry,* 67 (2006) pp. 716-722.
24. Ferreira D., Marais C., and Steenkamp J.A.,1995. Rooibos tea as a likely healthy food supplement. *Fundamental Foods for Health*, pp. 73-88
25. Khan, F.A., 2020. Nanomaterials: types, classifications, and sources. In *Applications of Nanomaterials in Human Health* (pp. 1-13). Springer, Singapore.
26. Fuente, J., Wilde, A., Mayne, G., Dujardin, J, Wilcoxon, J. P., Roy, L. A. and Grazu, V., 2012. Frontiers of Nanoscience. 4, pp. 1-509. DOI: 10.1016/B978-0-12-415769-9.00001-7. Elsevier Ltd. ISBN: 978-0-12-415769-9.
27. Goldblatt P., 1997. Floristic diversity in the Cape Flora of South Africa. *Biodiversity and Conservation*, 6, pp. 359-377.
28. Goldblatt, P. and Manning, J.C., 2002. Plant Diversity of The Cape Region of the South Africa. *Annals of the Missouri Botanical Garden*, 89,(2 Spring, 2002), pp. 281-302.
29. Homberger, M. and Simon, U., 2010. On the application potential of gold nanoparticles in nanoelectronics and biomedicine. *Philosophical Transactions of the Royal Society A: Mathematical, Physical and Engineering Sciences*, *368*(1915), pp.1405-1453.
30. Honary, S., Gharaei-fathabad, E. and Paji, Z., 2012. A Novel Biological Synthesis of Gold Nanoparticle by Enterobacteriaceae Family. *Tropical Journal of Pharmaceutical Research,* 11(6), pp. 887-891.
31. International Diabetes Federation Atlas, 9th edition 2019. Available online version: www.diabetesatlas.org. ISBN: 9782930229874. (Accessed, 11-03-2020).
32. Jae Y.S., Eun-Yeong K. and Beom S.K., 2010. Biological synthesis of platinum nanoparticles using *Diopyros kaki* leaf extract. *Bioprocess Biosyst Eng* (2010) 33, pp.159–164.
33. Jiaqi, D., Carpinone, P., Pyrgiotakis, G., Demokritou, P. and Moudgil, B. M., 2020. Synthesis of Precision Gold Nanoparticles Using Turkevich Method. *KONA Powder and Particle Journal* 37 (2020) pp. 224 – 232.
34. Joubert, E.D.B.D. and de Beer, D., 2011. Rooibos (*Aspalathus linearis*) beyond the farm gate: From herbal tea to potential phytopharmaceutical. *South African Journal of Botany*, *77*(4), pp.869-886.
35. Koeppen, B. H, Smith, C. J. and Roux, D. G., 1962. The flavone C-glycosides and flavonol O-glycosides of *Aspalathus acuminatus* (rooibos tea). *Biochemical Journal* 83, pp. 507 – 511.
36. Kricka, L. J., 2001. Microchips, microarrays, biochips and nanochips: Personal laboratories for the 21st century. *Clinica Chimica Acta* 307 (1-2) pp. 219 – 223.
37. Kumar, T., Khan, Z., Oulkar, D., Singh, B. K., Maurya, A., Singh, B. & Banerjee, K. 2020 'Hig resolution LC-MS characterization of phenolic compounds and the evaluation of antioxidant properties of a tropical purple radish genotype' *Arabian Journal of Chemistry,* 13(1), pp. 1355 – 1366.
38. Lal, S.S. and Nayak, P.L., 2012. Green synthesis of gold nanoparticles using various extract of plants and spices. *International journal of science innovations and discoveries*, *2*(23), pp.325-350.
39. Loo, K.Y., Leong, K.H., Sivasothy, Y., Ibrahim, H. and Awang, K., 2019. Molecular Insight and Mode of Inhibition of α-Glucosidase and α-Amylase by Pahangensin A from Alpinia pahangensis Ridl. *Chemistry & biodiversity*, *16*(6), p.e1900032.
40. Lourens, A., Viljoen, A. and Heerden, F., 2008. South African *Helichrysum* species: A review of the traditional uses, biological activity and phytochemistry. *Journal of Ethnopharmacology* 119, pp. 630–652.
41. Luisa, F. and Duncan, S., 2013. Nanotechnologies: Principles, Applications, Implications and Hands-on Activities. Publications Office of the European Union, Directorate-General for

Research, and Innovation Industrial technologies (NMP) Unit G.4 — Nano Sciences and Nano Technologies 2012.

42. Mabona, U. and Van Vuuren, S.F., 2013. Southern African medicinal plants used to treat skin diseases. *South African Journal of Botany*, *87*, pp.175-193.

43. Magcwebeba, T., Swart, P., Swanevelder, S., Joubert, E. and Gelderblom, W., 2016. Anti-inflammatory effects of *Aspalathus linearis* and *Cyclopia* spp. extracts in a UVB/keratinocyte (HaCaT) model utilising interleukin-1α accumulation as biomarker. *Molecules*, *21*(10), p.1323.

44. Marnewick, J., Joubert, E., Joseph, S., Swanevelder, S., Swart, P. and Gelderblom, W., 2005. Inhibition of tumour promotion in mouse skin by extracts of rooibos (*Aspalathus linearis*) and honeybush (*Cyclopia intermedia*), unique South African herbal teas. *Cancer letters*, *224*(2), pp.193-202.

45. Malolo, F.A.E., Nouga, A.B., Kakam, A., Franke, K., Ngah, L., Flausino, O., Mpondo, E.M., Ntie-Kang, F., Ndom, J.C., da Silva Bolzani, V. and Wessjohann, L., 2015. Protease-inhibiting, molecular modeling and antimicrobial activities of extracts and constituents from *Helichrysum foetidum* and *Helichrysum mechowianum* (Compositae). *Chemistry Central Journal*, *9*(1), pp.1-11.
46. Mittermeier, R.A, Turner, W.R., Larsen, F.W., Brooks, T.M. and Gascon, C., 2011. Global Biodiversity Conservation: The Critical Role of Hotspots. ISBN 9783642209925. Springer-Verlag Berlin Heidelberg.
47. Mody, N., Tekade, R. K., Mehra, N. K., Chopdey, P. and Jain, N. K., 2014. Dendrimer, Liposomes, Carbon Nanotubes and PLGA Nanoparticles: One Platform Assessment of Drug Delivery Potential. *American Association of Pharmaceutical Scientists* 15(2), pp. 388 – 399.

48. Myers, N., Mittermeier, R. A., Mittermeier, C. G., Fonseca, G. and Kent, J., 2000. Biodiversity hotspots for conservation priorities. *Nature,* 403(24), pp. 853-858.
49. Noha, S., and Khaled N., 2020. Polyphenols profile of pomegranate leaves and their role in green synthesis of silver nanoparticles. *Scientific Reports,* 10(14851), pp. 1 – 11.

50. Noruzi, M., 2015. Biosynthesis of gold nanoparticles using plant extracts. *Bioprocess Biosyst Eng,* 38, 1–14.

51. Nyakudya, T. T., Tshabalala, T., Dangarembizi, R., Erlwanger, K. H. and Ndhlala, A.R., 2020. The Potential Therapeutic Value of Medicinal Plants in the Management of Metabolic Disorders. *Molecules*, 25, pp. 1-20.

52. Odeyemi, S. and Bradley, G., 2018. Medicinal Plants Used for the Traditional Management of Diabetes in the Eastern Cape, South Africa: Pharmacology and Toxicology. *Molecules*, 23, pp. 2759.

53. Peralta-Videa, J., Haung, J., Parsons, G., Zhao, L., Lopez-Moreno, L., Hernandez-Viezcas, J. A. and Gardea-Torresdey, J. L., 2016. Plant-based green synthesis of metallic nanoparticles: scientific curiosity or a realistic alternative to chemical synthesis? *Nanotechnology for Environmental Engineering,* 1(4), pp. 1- 29.

54. Peter M., Godfrey M., Peggoty M. and Kelly C., 2016. Review the Role of Natural Products in Drug Discovery and Development against Neglected Tropical Diseases. *Journal Molecules,* 22(58), pp. 1-41.

55. Pokropivny, V. and Skorokhod, V., 2007. Classification of nanostructures by dimensionality and concept of surface forms engineering in nanomaterial science. *Materials Science and Engineering,* C27(2007), pp. 990 – 993.

56. Puckree, T., Mkhize, M., Mgobhozi, Z. and Lin, J., 2002. African traditional healers: what health care professionals need to know. *International Journal of Rehabilitation Research*, *25*(4), pp.247-251.

57. Ribeiro, A. S., Marilene E., Beatriz, M. O. and José Manuel, S. L., 2015. Main Benefits and Applicability of Plant Extracts in Skin Care Products. *Cosmetics*, 2, 48-65.

58. Roux, M., Wyk, B., Boatwright, J. and Tilney, P., 2011. The systematic significance of morphological and anatomical variation in fruits of Crotalaria and related genera of tribe Crotalarieae (Fabaceae). *Botanical Journal of the Linnean Society*, 165(1), pp. 84–106.

59. Saeed, M.E., Meyer, M., Hussein, A. and Efferth, T., 2016. Cytotoxicity of South-African medicinal plants towards sensitive and multidrug-resistant cancer cells. *Journal of ethnopharmacology*, *186*, pp.209-223.

60. Sakka, Y., Chauhan, A., and Chauhan, C., 2017. A review on the classification, characterisation, synthesis of nanoparticles and their application. *IOP Conf. Series: Materials Science and Engineering,* 236(032019), pp. 1-15.

61. Sapana, J., Rizwan A., Nirmala, K. J., and Rajesh, K. M., 2021. Green synthesis of nanoparticles using plant extracts: a review. *Environmental Chemistry Letters,* 19(2021), pp. 355–374.

62. Spampinato, V., Parracino, M.A., La Spina, R., Rossi, F. and Ceccone, G., 2016. Surface analysis of gold nanoparticles functionalized with thiol-modified glucose SAMs for biosensor applications. *Frontiers in chemistry*, *4*, pp. 8.

63. Steenkamp, V., 2003. Traditional herbal remedies used by South African women for gynaecological complaints. *Journal of Ethnopharmacology,* 86(2003), pp.97–108.
64. Sumit, S. L. & Nayak, P. L 2012 'Green synthesis of gold nanoparticles using various extract of plants and spices' *International Journal of Science Innovation and Discoveries* 2 93) pp. 325 – 350.
65. Srikar, S.K., Giri, D.D., Pal, D.B., Mishra, P.K. and Upadhyay, S.N., 2016. Green synthesis of silver nanoparticles: a review. *Green and Sustainable Chemistry*, *6*(1), pp.34-56.
66. Swilam, N. and Nematallah, K.A., 2020. Polyphenols profile of pomegranate leaves and their role in green synthesis of silver nanoparticles. *Scientific Reports*, *10*(1), pp.1-11.

67. Tandeka U. M., Sylvia R., Sonja S., Pieter S., Dalene D. B., Elizabeth J. and Wentzel C. A. G., 2016. The potential role of polyphenols in the modulation of skin cell viability by Aspalathus linearis and Cyclopia spp. herbal tea extracts in vitro. *Journal of Pharmacy and Pharmacology*, 68(2016), pp. 1440–1453.

68. Tiedtke, J. and Marks, O., 2002. Rooibos – The new "WHITE TEA" for hair and skin care. *Cosmetochem International Ltd.*, Sennweidstrasse 44/46, CH-6312, Steinhausen/Zug, Switzerland.
69. Voliani, V., 2013. Update on Gold Nanoparticles: From Cathedral Windows to nanomedicine Smithers Group Company, Shawbury, Shrewsbury, Shropshire, SY4 4NR, United Kingdom.

70. Wakaskar, R.R., 2018. General overview of lipid–polymer hybrid nanoparticles, dendrimers, micelles, liposomes, spongosomes and cubosomes. *Journal of drug targeting*, *26*(4), pp.311-318.

71. World Health Organization, editor 2009. Global health risks: mortality and burden of disease attributable to selected major risks. Geneva, Switzerland: World Health Organization; 2009, (Accessed, 11-03-2020).

72. Dong, Y., Zhang, B., Sun, W. and Xing, Y., 2019. Intervention of prediabetes by flavonoids from *Oroxylum indicum*. In *Bioactive Food as Dietary Interventions for Diabetes* (pp. 559-575). Academic Press.

73. Yulizar, Y., Utari, T., Ariyanta, H.A. and Maulina, D., 2017. Green method for synthesis of gold nanoparticles using Polyscias scutellaria leaf extract under UV light and their catalytic activity to reduce methylene blue. *Journal of Nanomaterials*, *2017*.

74. Zillich, O.V., Schweiggert-Weisz, U., Eisner, P. and Kerscher, M., 2015. Polyphenols as active ingredients for cosmetic products. *International journal of cosmetic science*, *37*(5), pp.455-464.

Chapter two

2.1. Literature review

Aim of this chapter

This chapter is divided into two sections (Chapter Two A, and B). It reviews existing data on the biology and chemistry of *Helichrysum foetidum*, *green Aspalathus linearis*, and their constituents as natural products. Their ethnomedicinal uses, biological studies as drug candidates and green synthesis of metal nanoparticles using these plants are briefly described as applicable to this study.

2.1.1. Asteraceae family and *Helichrysum foetidum*

Asteraceae family is reported as the world largest and most diverse family of a typical flowering plant with 10 subfamilies, approximately 2000 genera and 23,600 species (Peter Goldblatt and Manning John, 2002). In the CFR, the family is also the largest family with attributed 30 endemic genera from 107 genera and 806 endemic species from 986 species of the family (Peter Goldblatt, 1997). It consists of annual, biannual, and perennial herbaceous plants, trees and shrubs and has important pharmaceutical genera. Asteroideae is a subfamily of Asteraceae made up of seven taxa including Astereae, Tagateae, Eupatorieae, Haliantheae, Calenduleae, Senecioneae and Gnaphalieae tribe which has *Helichrysum* genus as a member (Nie et al., 2016; Sharafzadeh, Shahram 2011). The genus is adapted to flourish in arid to semi-arid regions of the Mediterranean with a major concentration in Southern Africa. *Helichrysum Milliganii*. belongs to the family *Asteraceae*, subfamily *Asteroideae* and tribe *Gnaphalieae* (Galbany-casal & Romo, 2008). It is a complex genus showing difficult distinctions among species due to great similarities in leaves, stems, and flowers. Hillard 1983 reported 30 morphological classifications of the *Helichrysum* genus based on the shape and size of flowers for easy identification (Claudia et al., 2016). They all possess glossy and papery

flowers of mostly golden-yellow colour, other colours are silver, red, purple etc. The name *Helichrysum* was reported to originate from helio and chrysum; Greek words for sun and gold respectively due to the shiny golden-yellow colours of its flowers (Hilliard, O.M. & Burtt, 1981). The genus is known with a strong curry-like smell with common names in South Africa as iMphepo (Zulu), phefu and isicwe (Xhosa), kooigoed, sewejartjie (Africans) and phefo-ea-loti, toanae-moru (Southern Sotho) (Grierson and Afolayan, 1999; Masika and Afolayan, 2003). The taxonomical records of the *Helichrysum* genus reveal over 500 species of *Helichrysum* worldwide with approximately 250 species endemic to South Africa. Also, some species are found in areas of Madagascar, Australia, Southern Europe, India, and Southwestern Asia. Several scientific reports on South Africa *Helichrysum* species elucidated their traditional uses for the treatment of common ailments such as gastrointestinal pains, wounds, eye infections (Lourens et al., 2004; Lourens et al., 2008). Accordingly, the South African species of *Helichrysum foetidum* will be studied.

2.1.2. *Helichrysum foetidum* L.

The *Helichrysum foetidum* (HF) species is native to southern Africa (Cape Provinces of South Africa, Mozambique, Zambia, Madagascar), eastern Africa (Ethiopia, Kenya, Eritrea, Uganda, Burundi, Cameroon) and in the naturalised form in Madeira, Spain and Portugal and recently recorded from two localities in Brazil (Barcelos, Laísa & Heiden, 2007; Mercè, Galbany-casals & Àngel M. Romo, 2008; Riveiro et al., 2019). The taxonomy of *H. foetidum* (Table 2.5) is often known with common names in South Africa as isicwe (Zulu), mulshondblaar (Afr.) and yellow everlasting (Eng). The name *foetidum* is derived from the Latin word ‘evil smell’, which describes the strong and persistent aromatic smell of the plant. It is a biennial herb that grows approximately 0.5 -1.5 m high with inflorescence yellow flowerhead and branch stem from the base. The leaves are tiny tomentose with white wool underneath the stem and classified by the South African Biodiversity Institute (SANBI) and *Southern African plant Red Data List* as a safe and unthreatened plant (Swelankomo, N., 2005). *H. foetidum* is traditionally valued for its medicinal effects of the leaves in wound healing, relief from menstrual pains in young girls by drinking of its extract, eye infection, and its ability to induce trances by inhalation (Akinyede et al., 2021). HF is among the less scientifically studied species with few published reports. Malolo et al. (2015) reported the antimicrobial and inhibition of protease enzymes by the methanolic extract and its phytochemicals while Tirillini et al. (2012) studied the antioxidant activities of the methanolic extract. In addition, are the phytochemical constituents previously reported from *H. foetidum* including diterpenoid; kaur-16-en-18-oic and flavonoids;

helichrysetin and its glycoside helichrysin, apigenin and its glycoside and 7,4'-dihydroxy-5-methoxy-flavanone acid (Kakam et al., 2012; Malolo et al., 2015). However, bioactive compounds of the plant and their antihyperglycemic activities are yet to be extensively studied. Also, before this study, the capping ability of crude extract and isolates for green synthesis metallic nanoparticles and their biomedical application has not been reported.

Table 2.1: Taxonomy H. foetidum

Domain	Eukaryota
Kingdom	Plantae
Phylum	Spermatophyta
Subphylum	Angiospermae
Class	Dicotyledonae
Order	Asterales
Family	Asteraceae
Genus	Helichrysum
Species	Helichrysum foetidum

Figure 2.1: Air-dried Helichrysum foetidum

2.2. Fabaceae family and *Aspalathus* genus

Fabaceae is from the order Fabales and like Asteraceae is a family of flowering and seed-producing plants widely distributed worldwide. It is the third-largest family of the angiosperms after Orchidaceae and Asteraceae with over 700 general and 20,000 species (Hawkins et al., 2011) The family also known as leguminous plants are either annual, biennial, and perennial trees, shrubs, and herbs and produce seedpods from which seed are released. Further classification of Fabaceae by most taxonomists leads to six subfamilies including Fabiodeae (Papilionoideae). From the major tribes of Fabiodeae is Crotalarieae flowering plants comprising of eleven genera with division into three clades; Cape, Lotonolis and Crotolaria clades (Boatwright et al., 2008). Cape clade consists of six genera including *Aspalathus*, *Wiborgia* and *Rafnia* which are subendemic to South Africa and *Lebeckia*, *Calebota,* and *Wiborgiella* (Le Roux et al., 2011). The genus *Aspalathus* consists of 281 species endemic to the western cape of South Africa. The *Aspalathus* L. genus includes the *Aspalathus linearis* species used for the production of rooibos tea makes this genus most popular among the *Aspalathus* genus (Boatwright and Cupido, 2011).

2.2.1. Aspalathus linearis

Aspalathus linearis (Burm. F) Dahlg. also known as rooibos tea, is a leguminous shrub of the Cape clade from the *Aspalathus* genus (Table 2.1). Its natural habitat is the mountainous region of the Clan William Cederberg, the western cape of South Africa (Hawkin et al., 2011). It grows on low nutrient soils with yellow flowers and green leaves like tiny spins like broomsticks which turns red after a fermentation process. The species is adapted to grow on deep, acidic, and poor nutrient soil of the fynbos region (Maseko & Dakora 2013; Brink 2016). An important characteristic of *A. linearis* in its is its ecological role in nodulation, nitrogen fixation of soil and resistance to bush fire through regeneration by seed re-sprouting. It is also an economic plant used for the manufacture of the popular beverage rooibos tea, a national and international tea that is currently being exported to over 30 countries in the world (Joubert & Beer, 2011). The chemistry of *A*. *linearis* is well studied in the literature. Rabe et *al.,* 1994 reported the isolation of phenolics; quercetin, cinnamic acids, Protocatechuic acid among other compounds (Table 2.2) most of which are phenolic compounds. In a review by McKay & Blumberg 2007, the bioactivity and medicinal potential were reported for antioxidants, anti-allergenic and immune-modulating actions among others (Mckay & Blumberg, 2007). However, studies on the potential of *A*. *linearis* for use in the management of skin disorders, the synthesis of nanoparticles from *A*. *linearis* as drug candidates are limited.

Figure 2.2: Unfermented (green) and fermented (red) rooibos

Table 2.2: Taxonomy of *Aspalathus linearis*

Domain	Eukaryota
Kingdom	Plantae
Phylum	Spermatophyta
Subphylum	Angiospermae
Class	Dicotyledonae
Order	Fabales
Family	Fabaceae
Genus	Aspalathus

References

1. Akinyede, K.A., Cupido, C.N., Hughes, G.D., Oguntibeju, O.O. and Ekpo, O.E., 2021. Medicinal Properties and In Vitro Biological Activities of Selected *Helichrysum* Species from South Africa: A Review. *Plants*, *10*(8), p.1566.
2. Barcelos, L. and Heiden, G., 2017. First record of *Helichrysum foetidum* (L.) Moench. (Asteraceae, Gnaphalieae) for South America. *Check List*, *13*, p.331.
3. Boatwright, J.S. and Cupido, C.N., 2011. *Aspalathus crewiana* sp. nov.(Crotalarieae, Fabaceae) from the Western Cape Province, South Africa. *Nordic Journal of Botany*, *29*(5), pp.513-517.
4. Brink, C., Postma, A. and Jacobs, K., 2017. Rhizobial diversity and function in rooibos (*Aspalathus linearis*) and honeybush (*Cyclopia spp*.) plants: A review. *South African Journal of Botany*, *110*, pp.80-86.
5. Giuliani, C., Lazzaro, L., Calamassi, R., Calamai, L., Romoli, R., Fico, G., Foggi, B. and Lippi, M.M., 2016. A volatolomic approach for studying plant variability: the case of selected *Helichrysum* species (Asteraceae). *Phytochemistry*, *130*, pp.128-143.
6. Galbany-Casals, M. and Romo, A.M., 2008. Polyploidy and new chromosome counts in Helichrysum (Asteraceae, Gnaphalieae). *Botanical Journal of the Linnean Society*, 158, 511 – 528.
7. Goldblatt, P., 1997. Floristic diversity in the Cape flora of South Africa. *Biodiversity & Conservation*, *6*(3), pp.359-377.

8. Goldblatt, P. and Manning, J.C., 2002. Plant diversity of the Cape region of southern Africa. *Annals of the Missouri Botanical Garden*, pp.281-302.
9. Grierson, D.S. and Afolayan, A.J., 1999. An ethnobotanical study of plants used for the treatment of wounds in the Eastern Cape, South Africa. *Journal of ethnopharmacology*, *67*(3), pp.327-332.
10. Hawkins, H.J., Malgas, R. and Biénabe, E., 2011. Ecotypes of wild rooibos (*Aspalathus linearis* (Burm. F) Dahlg., Fabaceae) are ecologically distinct. *South African Journal of Botany*, *77*(2), pp.360-370.
11. Hilliard, O.M. and Burtt, B.L., 1981. Some generic concepts in Compositae–Gnaphaliinae. *Botanical Journal of the Linnean Society*, *82*(3), pp.181-232.
12. Joubert, E.D.B.D. and de Beer, D., 2011. Rooibos (*Aspalathus linearis*) beyond the farm gate: From herbal tea to potential phytopharmaceutical. *South African Journal of Botany*, *77*(4), pp.869-886.
13. Kakam, A.M.Z., Franke, K., Ndom, J.C., Dongo, E., Mpondo, T.N. and Wessjohann, L.A., 2011. Secondary metabolites from *Helichrysum foetidum* and their chemotaxonomic significance. *Biochemical Systematics and Ecology*, *2*(39), pp.166-167.
14. Lourens, A.C.U., Reddy, D., Başer, K.H.C., Viljoen, A.M. and Van Vuuren, S.F., 2004. In vitro biological activity and essential oil composition of four indigenous South African *Helichrysum* species. *Journal of ethnopharmacology*, *95*(2-3), pp.253-258.
15. Malolo, F.A.E., Nouga, A.B., Kakam, A., Franke, K., Ngah, L., Flausino, O., Mpondo, E.M., Ntie-Kang, F., Ndom, J.C., da Silva Bolzani, V. and Wessjohann, L., 2015. Protease-inhibiting, molecular modeling and antimicrobial activities of extracts and constituents from *Helichrysum foetidum* and *Helichrysum mechowianum* (Compositae). *Chemistry Central Journal*, *9*(1), pp.1-11.
16. Masika, P.J. and Afolayan, A.J., 2003. An ethnobotanical study of plants used for the treatment of livestock diseases in the Eastern Cape Province, South Africa. *Pharmaceutical Biology*, *41*(1), pp.16-21.
17. Masika, P.J. and Afolayan, A.J., 2003. An ethnobotanical study of plants used for the treatment of livestock diseases in the Eastern Cape Province, South Africa. *Pharmaceutical Biology*, *41*(1), pp.16-21.
18. McKay, D.L. and Blumberg, J.B., 2007. A review of the bioactivity of South African herbal teas: rooibos (Aspalathus linearis) and honeybush (Cyclopia intermedia). Phytotherapy Research: An International Journal Devoted to Pharmacological and Toxicological Evaluation of Natural Product Derivatives, 21(1), pp.1-16.
19. Nie, Z.L., Funk, V.A., Meng, Y., Deng, T., Sun, H. and Wen, J., 2016. Recent assembly of the global herbaceous flora: evidence from the paper daisies (Asteraceae: Gnaphalieae). *New Phytologist*, *209*(4), pp.1795-1806.
20. Rabe, C., Steenkamp, J.A., Joubert, E., Burger, J.F. and Ferreira, D., 1994. Phenolic metabolites from rooibos tea (*Aspalathus linearis*). *Phytochemistry*, *35*(6), pp.1559-1565.
21. Riveiro, S.F., García-Duro, J., Cruz, Ó., Casal, M. and Reyes, O., 2019. Fire effects on germination response of the native species Daucus carota and the invasive alien species *Helichrysum foetidum* and *Oenothera glazioviana*. *Global Ecology and Conservation*, *20*, p.e00730.
22. Sharafzadeh, S., 2011. Pyrethrum, coltsfoot and dandelion: important medicinal plants from Asteraceae family. *Australian Journal of Basic and Applied Sciences*, *5*(12), pp.1787-1791.
23. Swelankomo, N., 2005. *Helichrysum foetidum* (L.) Moench (Asteraceae). (accessed on 22 August 2021)
24. Tirillini, B., Menghini, L., Leporini, L., Scanu, N., Marino, S. and Pintore, G., 2013. Antioxidant activity of methanol extract of *Helichrysum foetidum* Moench. *Natural product research*, *27*(16), pp.1484-1487.

2.3. Chapter 2A

Recent advances on *Aspalathus linearis* (Rooibos tea): phytochemistry, bioactivities and green biosynthesis of metal nanoparticles

Akeem O. Akinfenwa [1], Jeanin L. Marnewick [2], Ahmed H. Mohammed [1]

[1] Chemistry Department, Cape Peninsula University of Technology, Bellville campus, Symphony Road, Bellville, Western Cape, South Africa. PO Box 7535 Bellville, South Africa. 217305296@mycput.ac.za (A.O.A), mohammedam@cput.ac.za (A.A.H)

[2] Applied Microbial and Health Biotechnology Institute, Cape Peninsula University of Technology, Symphony Rd. Bellville, 7535, South Africa; sheikabduln@cput.ac.za (A.N.S); marnewickj@cput.ac.za (J.L.M).

Abstract

Aspalathus linearis (Rooibos tea) is an endemic plant that is widely cultivated in South Africa for its bioactivity as herbal tea and health-promoting characteristics due to the high content of phenolic compounds. Emerging studies on the plant have been cross-disciplinary including chemistry, foods, biomedicals and nanosized applications of its constituents. A systematic methodology was used to search for published articles on the chemistry, bioactivities and nanotechnological applications of Aspalathus *linearis* through Google scholar, SciFinder, Medline, Springer and ScienceDirect databases. The mark of this review is to present harmonized and updated published reports on the chemistry of rooibos, structure-function

relationship, bioactivities of compounds and the application in the biosynthesis of metal nanoparticles. This will provide updated knowledge to assist in future research on the plant.

Keywords: *Aspalathus linearis*, phenolic compounds, bioactivity, nanoparticles, biosynthesis.

Corresponding author: Ahmed A. Hussein. mohammedam@cput.ac.za. Tel: +27 76 583 4877.

Content:

2.3.1. Introduction

Aspalathus linearis (Burm, f.) R. Dahlgren popularly known as Rooibos tea is a leguminous shrub from the family of Fabaceae, the tribe of Crotalarieae and the *Aspalathus* genus of Cape clade. Other common names include rooibosch tea, rooitea and red tea. Two types of *A. linearis* exist as Nortier and Cederberg types which can be differentiated by their leaves (Morton, 1983; Hawkins *et al*., 2011). The Nortier type is a cultivated type with needle-like leaves while the Cederberg type is wild-growing with broad leaves (Joubert & Beer, 2011). A special feature of its endemism is its localised distribution around the mountainous region of Clanwilliam Cederberg and Wupperthal, both in the Western Cape and in the Nieuwoudtville areas of the Northern Cape of South Africa *(Malgas et al., 2010; Rabe et al*., 1994). As an

economic plant for the beverage market, it is harvested as green rooibos (unfermented) and exposed to oxidative fermentation where it becomes reddish-brown rooibos (fermented) that is used for tea production (Cheney & Elizabeth, 1963; Cullere et al., 2013). Hence, it is valued for its economic importance as a nationally and internationally accepted beverage drink being exported to over 30 countries in the world (Joubert & Beer, 2011). *A. linearis* arguably has attracted the highest research interests among South African indigenous plants. Published data shows historical studies of the plant since the early 20th century time by chemists, biotechnologists, food scientists and recently by nano chemists and biophysicists till the present time (Koeppen *et al*., 1962; Rabe *et al*., 1994; Marnewick *et al*., 2011; Joubert & Beer, 2012; Ismail *et al.*, 2016; Ferreira *et al*., 1995). Research findings from in vivo and in vitro of rooibos tea over the decades have promoted the plant from just being a tea to a versatile herbal plant with functional application in foods, biotechnology and nanotechnology (Villaño *et al*., 2010; Marnewick *et al*., 2011; Ismail *et al*., 2016; Smith & Swart, 2018). The vitality of rooibos is attributed to the unique chemical constituents as the only source of a dihydrochalcone aspalathin, absence of caffeine, low tannin and high content of phenolic compounds (Koeppen et al., 1962; Heerden et al., 2003; Viljoen et al., 2016).

The different reviews by authors (Joubert & Schulz, 2006; Mckay & Blumberg, 2007; Joubert et al., 2008; Joubert & Beer, 2011; Kanu et al., 2013; Dludla, Joubert, et al., 2017; Johnson et al., 2018; Timothy & Derbyshire, 2020) gave accounts of the bioactivities and health implications of the plant, its cultivation and fermentation process, and usage in the decontamination of aluminium from acidic soil. Despite being the most studied endemic plant of South Africa, there are yet a limited number of published review articles that provide an updated record of non-phenolic metabolites, new phenolics isolated and the versatile application of rooibos as a bio-reducing and capping agents for green synthesis of metal nanoparticles. Hence, this review aimed to discuss published scientific data on the diverse applications of the rooibos plant between chemistry and nanotechnology.

2.3.2. Chemistry of *Aspalathus linearis*

The chemistry of rooibos is well studied in the literature with a long history of over 5 decades and still with ongoing studies. The pioneering work of Koeppen and his co-workers (1962) on flavone *C*-glycosides and flavonol *O*-glycosides of rooibos laid the foundation for subsequent phytochemical research on the plant. Several reports from rooibos discussed the isolation and chemical elucidation of its secondary metabolites. These reports revealed a complex mix of potent antioxidant compounds due to the abundance of polyphenols (Stander *et al*., 2017; Joubert & Beer,

2012) which explains many of its interesting physiological and therapeutic properties (Dludla *et al*., 2014; Ajuwon *et al*., 2014). The present review shows newly isolated compounds not reported in the previous reviews in addition to the known compounds. The chemical investigations of the rooibos plant depend on whether the fermented (red), unfermented (green) or the process green type of rooibos was used. It was reported that significant variation exists between the major compounds obtained from fermented and unfermented rooibos due to oxidative transformation that occurs during the fermentation process. The processed green type (is usually cut, mixed, moisturized, bruised and sun-dried) is also prone to unintended enzymatic fermentation which could account for the difference in the type of compound present in it (Stander et al., 2017; Ferreira et al., 1995). From the literature, compounds identification from rooibos involves two methods: the traditional isolation and characterisation with spectroscopic evidence, and the detection by liquid chromatography-mass spectrometry (LC-MS) or gas chromatography-mass spectrometry (GC-MS) through comparison of their retention times, UV and MS spectra with those of known standards in the library (Bramati et al., 2002). The identification of compounds by LC-MS/GC-MS is plausible only for tentative discussion because several compounds may present the same nominal mass. Therefore, it cannot be completely relied upon for discussion and structural elucidation of compounds. Chemical elucidation of compounds through isolation and identification with full spectral analyses is confirmatory and independent of LC-MS for validation of the occurrence of compounds. Hence, it is important to make the distinction between reports of tentatively identified and structurally conclusive compounds from *A. linearis* (Table 1).

Among the less reported isolated compounds with structural elucidations are linearthin (**1**), aspalalinin (**4**), aspalathin dimer 5 (**5**), aspalathin dimer 14 (**6)**, aspalathin dimer 15 (**7**), 3-hydroxy-1-(4-hydroxy-3-methoxyphenyl)-2-[4-(3-hydroxy-1-(*E*)-propenyl)-2,6 dimethoxyphenoxy]propyl-*β*-*D*-glucopyranoside (**41**), quinoxaline 10 (**52**), quinoxaline 11 (**53**) and uridine (**48**) (Joubert & Beer, 2014; Heinrich et al., 2012; Krafczyk & Glomb, 2008; Krafczyk, Heinrich, et al., 2009; Shimamura et al., 2006). Also, aspalathin dimers 1, 2, 3 and 4 were reported isolated with low yield and were

unstable for full characterization. Generally, the compounds of rooibos comprise majorly phenolic acids, flavonoids with strong antioxidants activities (Manley *et al*., 2006) and a few tannins and lignans (Ferreira et al., 1995). In addition to these compounds are non-phenolic compounds and the volatile components tentatively identified (Kawakami *et al*., 1993; Habu *et al*., 1985; Wyk & Verdoorn, 2000). Table 1 and figure 1 summarize structures of compounds from rooibos.

A lead compound among the polyphenols of rooibos is 2',3,4,4',6'-pentahydroxy-3'-C-*β-D*-glucopyranosyl dihydrochalcone named aspalathin (**2**) by Koeppen in 1961 (Koeppen et al., 1962; Koeppen & Roux, 1966; Baranska et al., 2006). The compound is characteristic of rooibos and is believed to be responsible for the sweet aroma of the tea. Compound **2** was first isolated by Koeppen et al (1962) from unfermented *Aspalathus linearis* and later by other researchers (Beer et al., 2015). The compound represents a typical dihydrochalcone skeleton with a glucose moiety at C-3' of the A-ring. A closely related compound and rarely occurring natural dihydrochalcone is compound **1** which was recently isolated from the unfermented type of the plant and reported by Akinfenwa et al. (2021). Following successive chromatography and HPLC purification of a polar fraction from acetonic extract, the structural elucidation of **1** by the author confirms that, unlike the hexose sugar in **2**, the sugar moiety of **1** is a dioxysugar of fructose-furanoside configuration (Akinfenwa et al., 2021). In addition to compound **2**, Ferreira *et al*. (1995) also isolated nothofagin (**3**), a dehydroxylated aspalathin at position C-3 of the B-ring, as its isomer from the unfermented rooibos (Ferreira et al., 1995). **3** is also a rare acyclic dihydrochalcone like **2** that has only been reported isolated from *Nothofagus fusca* and *Schoepfia chinensis* (Hillis & Inoue, 1967; Joubert, 1996; Huang *et al*., 2008; Beer *et al*., 2015). As noted by Stander et al. (2017) and Ferreira et al. (1995), the unfermented type of *A. linearis* is a better choice than the fermented type for targeted isolation of dihydrochalcone compounds (Ferreira et al., 1995; Stander et al., 2017). The fourth dihydrochalcone reported is aspalalinin (**4**). The cyclic dihydrochalcone was isolated also from unfermented *A. linearis* for the first time by Shimamura *et al*., (2006) among other 24 known compounds from the methanolic (Shimamura *et al*., 2006). The skeletal structure of **4** is similar to

aspalathin and nothofagin except that ring A and B in the acyclic dihydrochalcone are connected by a closed ether bond, figure 1.

Remarkably, the unfermented and fermented rooibos present similar compositions of flavones and flavonols, however, a significant difference exists in the dihydrochalcone content due to derivatization brought about by both enzymatic and non-enzymatic fermentation processes. The non-enzymatic fermentation of green rooibos is reported to account for the browning of green (unfermented) rooibos and the transformation of its dihydrochalcone to derivative compounds (Heinrich et al., 2012). An example of such derivatives is aspalathin dimer 5 (**5**) which was formed by the oxidative degradation/coupling of **2** previously isolated from unfermented rooibos. Under incubation of **2** for 6 hours at room temperature followed by multilayer counter-current chromatography, and preparative HPLC. The mechanism of formation was proposed to be by a 2-fold coupling of **2**. During the formation of **5**, **2** is believed to be auto-oxidized at the B-ring to *O*-quinone in the first step and followed by further oxidation at the A-ring, and re-aromatisation which yielded compound **5** (Heinrich et al., 2012). Other unstable intermediate products from the coupling of **2** such as dimers 8, and 9 were reported derivatised by reacting these intermediates with *O*-phenylenediamine. These yielded their corresponding quinoxaline compounds **52** and **53** reported based on ^{1}H and ^{13}C NMR data. Also, further degradation of **5** on incubation under aerated and deaerated conditions for a period of 10 h was reported to yield the atropisomers named aspalathin dimer 14 (**6**) and dimer 15 (**7**) at equilibrium (Krafczyk, Heinrich, et al., 2009). Phloridzin and sieboldin are new dihydrochalcones identified by LC-MS from the unfermented type collected from the Wupperthal area of the Western Cape (Stander *et al*., 2017). Further study will be needed for targeted isolation of these chalcone compounds. Apart from the aspalathin (chalcone) derivatives discussed, flavones and flavonols compounds have been reported from both fermented and unfermented types. The flavone and its glycosides such as chrysoeriol (**10**), orientin (**13**), vitexin (**11**), quercetin (**15**), rutin (**19**), iso-vitexin (**12**), iso-orientin (**14**) and isoquercitrin (**18**) were reported isolated (Koeppen et al., 1962; Snyckers & Salemi, 1974; Joubert, 1996; Rabe et al., 1994;

Shimamura et al., 2006). In addition to the known **2**, **3**, **12**, **13**, **14**, **18** and **19**, compounds, Krafczyk & Glomb, 2008 successfully isolated a diastereomeric mixture of (*R*)/(*S*) eriodictyol-8-glucopyranosyl (dihydro-orientin) (**20**) and (*R*)/(*S*) eriodictyol-6-glucopyranosyl dihydro-iso-orientin (**21**) as intermediate compounds from **2**, and hyperoside (**16**) for the first time from *A. linearis*. reported (Krafczyk & Glomb, 2008). Furthermore, phenolic acids of hydroxybenzoic and hydroxycinnamic constituents have been reportedly isolated and quantified from *A. linearis*. Although these compounds are well known and were previously reported, Rabe et al. (1994) reported the isolation of *p*-hydroxybenzoic acid (**23**), protocatechuic acid (**24**), vanillic acid (**29**), *p*-coumaric (**32**), caffeic (**33**), ferulic (**34**) and 3,4,5-trihydroxycinnamic (**36**) from unfermented rooibos. While Krafczyk & Glomb, 2008 identified from HPLC-DAD chromatograms and isolated from fermented or unfermented rooibos (**24**), gallic acid **(25)**, salicylic acid **(26)**, gentisic acid **(27)**, 3,5-dihydroxybenzoic acid (**28**), (**29**), syringic (**30**), sinapinic acid (**33**), **(35)** and chlorogenic acid (**37**) (Krafczyk & Glomb, 2008). Other phenolic acid constituents isolated from rooibos are compound **41** known with strong antioxidant activity and was only previously isolated from *Kokuto* cane sugar, and *Z*-2-(*β*-*D*-glucopyranosyloxy)-3-phenylpropenoic (**49**) acid (Ferreira et al., 1995; Takara et al., 2002; Shimamura et al., 2006). Polyphenolic compounds of the class of condensed tannins and lignans have also been isolated from rooibos. Published data shows (+)-catechin (**38**), procyanidin B3 (**39**) and profisetinidin triflavonoid (**40**) (Ferreira *et al*., 1995). Vladinol (**42**), secoisolariciresinol (**43**) and secoisolariciresinol-*β*-*D*-glucoside (**44**) are rare phenolics compounds reported from rooibos (Shimamura *et al*., 2006). 7-dihydroxy-6-C-D-glucopyranosyl chromone (**45**) also a rare phenolic from rooibos was believed to be by-product of oxidation of (**21**) **(**Ferreira *et al*. 1995). The rich constituents of the plant contain non-phenolic metabolites as minor compounds. (+)-Pinitol **(47)**, uridine (**48**) and phenylpyruvic acid-*O*-β-D-pyranosyl (**49**) were isolated and characterised from unfermented green rooibos by Joubert et al., (2013) and Ferreira *et al*. (1995). In a review on the quantitative characterization of flavonoid compounds in *A*. *linearis* using by LC-UV/DAD, Joubert and Schulz (2006) identified **49** as an unknown peak from HPLC chromatogram

with a similar abundance as **2** (Joubert & Schulz, 2006). Shimamura *et al*. (2006) isolated vanylglycol (**50**), esculetin (**46**) and *p*-hydroxyphenyl ethanol (**51**) among other twenty-four known compounds. In an experiment to determine the effect of extraction process on volatile constituents of rooibos of dichloromethane brewed and the simultaneous steam distillation extracts using gas chromatograph-mass spectrometry, Kawakami *et al*. (1993) identified 50 and 123 volatile constituents from rooibos of GC-MS of brewed extract, and steam distillation extract respectively (Kawakami et al., 1993).

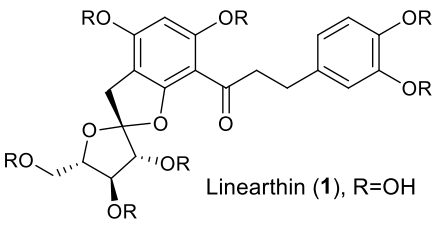

Linearthin (**1**), R=OH

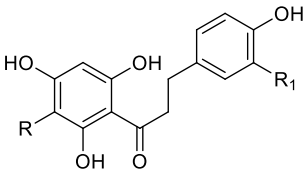

Aspalathin (**2**), R=Glc, R_1=OH
Nothofagin (**3**), R=Glc, R_1=H

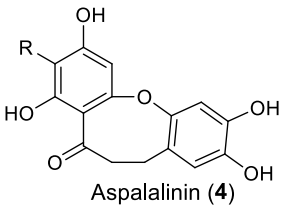

Aspalalinin (**4**)

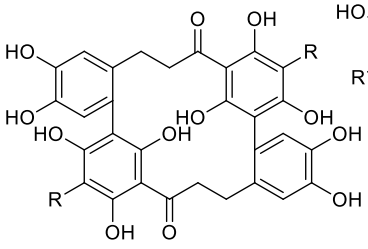

Aspalathin dimer 5 (**5**), R=Glc

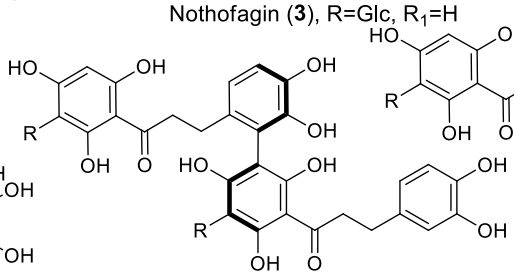

Aspalathin dimer 14 (**6**), R=Glc

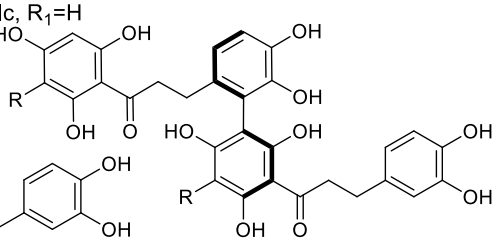

Aspalathin dimer 15 (**7**), R=Glc

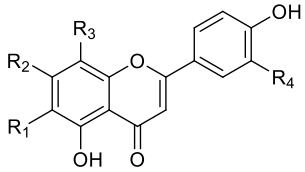

Luteolin (**8**), R_1= R_3=H, R_2= R_4=OH. Luteolin-7-O-β-*D*-glucopyranoside (**9**), R_1=R_3=H, R_2= O-β-*D*-glucopyranosyl, R_4=OH. Chrysoeriol (**10**), R_1= R_3=H, R_2= OH, R_4=OMe. Vitexin (**11**), R_1=R_4=H, R_3= C-β-*D*-glucopyranosyl, R_2=OH. Iso-vitexin (**12**), R_3=R_4=H, R_1= C-β-*D*-glucopyranosyl, R_2=OH. Orientin (**13**), R_1=H, R_3= C-β-*D*-glucopyranosyl, R_2=R_4=OH. Iso-orientin (**14**), R_3=H, R_1= C-β-*D*-glucopyranosyl, R_2=R_4=OH.

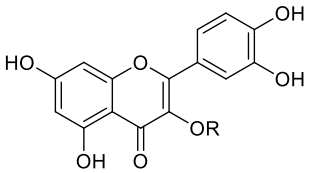

Quercetin (**15**), R=H. Hyperoside (**16**), R= O-β-*D*-galactosyl. Quercetin-3-robinobioside (**17**), R= O-β-*D*-robinobiosyl. Isoquercitrin(**18**), R= O-β-*D*-glucosyl. Rutin (**19**), R= O-β-*D*-rutinosyl.

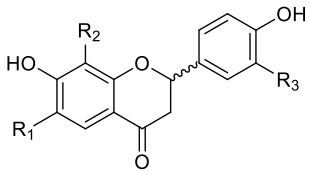

Dihydro-orientin (**20**), R_1=H, R_2=C-β-*D*-glucopyranosyl, R_3=OH.
Dihydro-iso-orientin (**21**), R_1= C-β-*D*-glucopyranosyl, R_2=H, R_3=OH.
Hemiphlorin (**22**), R_1= C-β-*D*-glucopyranosyl, R_2= R_3=H.

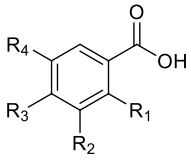

p-hydroxybenzoic acid (**23**), R_1=R_2=R_4=H, R_3=OH. Protocatechuic acid (**24**), R_1= R_4 =H, R_2= R_3=OH. Gallic acid (**25**), R_1=H, R_2= R_3=R_4=OH. Salicylic acid (**26**), R_1=OH, R_2=R_3=R_4=H. Gentisic (**27**), R_1=R_4=OH, R_2=R_3=H. 3,5-dihydroxybenzoic acid (**28**), R_2=R_4=OH, R_1=R_3=H. Vanillic acid (**29**), R_1= R_4 =H, R_2=OMe, R_3=OH. Syringic acid (**30**), R_1=H, R_2=OH, R_2=R_4=OMe.

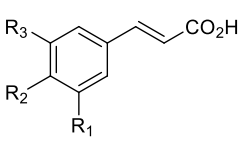

4-hydroxy-3,5-dimethoxy-cinnamic acid (**31**), R_1=R_3=OMe R_2=OH. *p*-Coumaric acid (**32**), R_1= R_3=H, R_2=OH. Caffeic acid (**33**), R_1= R_2=OH, R_3=H. Ferulic acid (**34**), R_3=OMe, R_2=OH, R_1=H. Sinapic acid (**35**), R_1= R_3=OMe, R_2=OH. 3,4,5-trihydroxycinnamic acid (**36**), R_1= R_2=R_3=OH

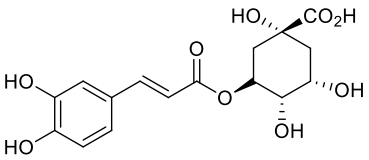

Chlorogenic acid (**37**)

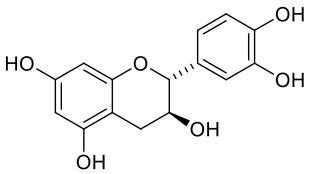

Catechin (**38**)

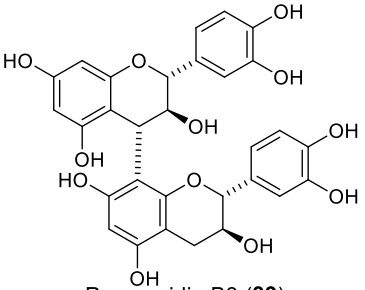

Procyanidin B3 (**39**)

Figure 2.3: Compounds isolated and identified from *A. linearis*

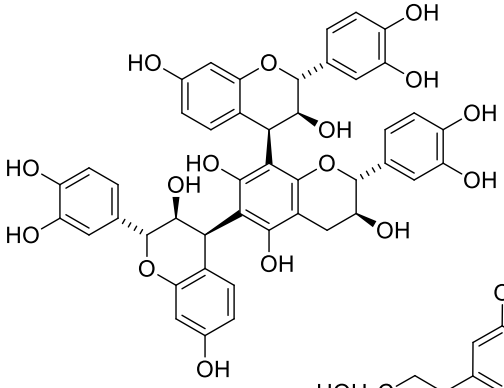

Profisetinidin triflavonoid (**40**)

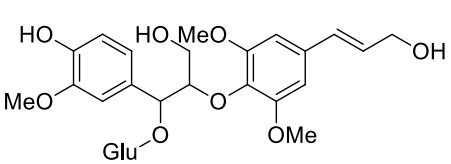

3-hydroxy-1-(4-hydroxy-3-methoxyphenyl)-2-[4-(3-hydroxy-1-(E)-propenyl)-2,6-dimethoxyphenoxy] propyl-β-*D*-glucopyranoside (**41**)

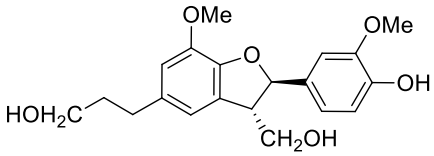

Vladinol (**42**)

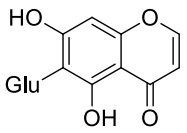

5,7-dihydroxy-6-C-*D*-glucopyranosyl chromone, (**45**)

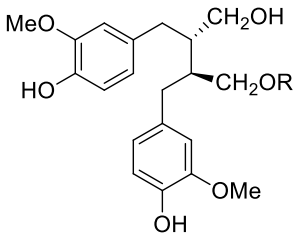

Secoisolariciresinol (**43**), R=H
Secoisolariciresinol-β-*D*-glucoside (**44**), R=Glu

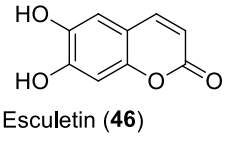

Esculetin (**46**)

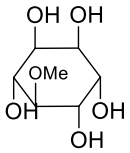

(+)-Pinitol (**47**)

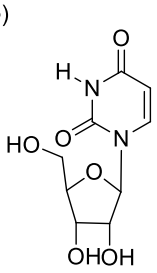

Uridin (**48**)

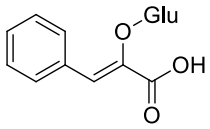

Z-2-(β-*D*-glucopyranosyloxy)-3-phenylpropenoic acid (**49**)

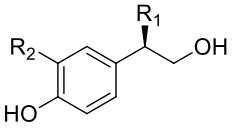

Vanylglycol (**50**), R_1=OH, R_2=OH
p-hydroxyphenyl ethanol (**51**), R1=R2= OH

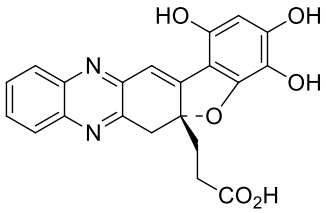

Quinoxaline 10 (**52**)

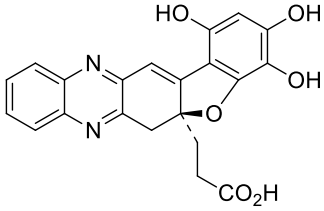

Quinoxaline 11(**53**)

Figure 2.4: Compounds isolated and identified from *A. linearis cont.*

Compounds	Rooibos type	Method	Reference
1	UFG	CC+ HPLC+ SE	Akinfenwa et al., 2021.
2 and 3	UFG	HPCCC + SE	De Beer et al., 2015.
49	UFG	HPLC + SE	Joubert et al., 2013
52 and 53	UFG and FER	MLCCC + HPLC + SE	Glomb et al., 2012.
6, 7	UFG and FER	MLCCC + HPLC + SE	Krafczyk et al., 2009
2, 3, 8, 10, 11, 12, 13, 14, 16, 18, 19, 20, 21, 23, 24, 25, 26, 27, 28, 29, 30, 32, 33, 34, 35, 15 and 38.	UFG and FER	MLCCC + HPLC + I	Krafczyk & Glomb, 2008
8, 10, 15,23, 24, 25, 26, 27, 28, 29, 30, 32, 33, 34, 35, and 38.	UFG and FER	MLCC + HPLC + SE	Krafczyk & Glomb, 2008
2, 3, 4, 8, 9, 11, 12, 15, 16, 17, 18, 20, 21, 22, 23, 30, 32, 42, 43, 44, 46, 50 and 51.	FER	PC + HPLC + SE	Shimamura *et al*., 2006
2, 3, 11, 18, 19, 20, 23, 24, 32, and 34.	UFG, FER, and GRP	Q + HPLC	Joubert, 1996
2, 8, 10, 11, 12, 15, 18, 29, 32, 33, 34 and 36.	GRP	TI + SE	Rabe et al., 1994
2, 3, 8, 9, 10, 11, 12, 13, 14, 15, 18, 19, 20, 21, 24, 29, 30, 31, 32, 33, 34, 36, 45, 38, 39, 40, 45, 47, 48 and 49.	UFG	CC + SE	Ferreira et al., 1995

8 and 15.	FER	CC + SE	Snyckers & Salemi, 1974
14, 29 and 33.	UFG	CC + SE	Koeppen & Roux, 1966
2.	UFG	CC + SE	Koeppen et al., 1962

Table 3.1: Compounds from Aspalathus linearis (Rooibos)

CC = Column chromatography, PC = partition chromatography, SE = Spectra evidence, Q = Quantification, I = Identified, FER = fermented (red), UFG = Unfermented (green), GRP = Green (processed). MLCCC = Multilayer counter current chromatography, HPLC = preparative high-performance liquid chromatography.

2.3.3. Structure-related bioactivities of Rooibos Compounds

Flavonoids and phenolic acids are known to play vital roles in the body as an immune booster, in metabolic activities and drug pharmacokinetics via interaction with enzymes (Rodriguez *et al*., 2014). Their interactions with physiological systems in-vitro and in-vivo have been reported to reflect a strong relationship with their chemical structures. The skeletal structures of flavonoids which include flavones, flavanol, isoflavones, flavanone, dihydroflavonols, chalcones and aurones, fig. 1 and table 1 are based on the C_{15} (C_6- C_3- C_6) system with a central ring C and sides ring A and B. Also, rooibos present a central C_6 (hydroxybenzoic acid) and C_6-C_3 (hydroxycinnamic acids) systems for phenolic acids and a similar C_6-C_3 for its rarely occurring glycoside of phenyl pyruvic acid respectively (Martins *et al*., 2011). These skeletons allow for possible *O*-methylation, acetylation, glycosylation, hydroxylation, deoxygenation and dehydroxylation of the ring protons that enhance its hydrophilicity or lipophilicity. Also, is their metal-chelating ability and the potential to quench singlet oxygen as primary antioxidants. Hence, polyphenols present multiple binding sites for interaction and modification of physiological membranes involving enzymes, metalloenzymes, proteins, polysaccharides, and lipids metabolism and correlate with their bioactivities (Tsukuba, 2000; Tsuchiya, 2010).

Dietary flavonoids are plant-derived flavonoids obtained from vegetables, fruits, and herbal tea such as rooibos tea. Extensive reports revealed that rooibos tea is a rich source of dietary flavonoids with functional activities that promote healthy living (Corcoran *et al*., 2012; Tsukuba, 2000; Oteiza *et al*., 2005; Santos *et al.*, 2016). The structure-function-relation of dietary flavonoids and phenolic acids of rooibos has been reported due to dihydroxylation of the ring B, linking conjugated system and a keto group of C ring which reflect their roles as antioxidants, cardioprotective agents, antimicrobials, antiviral, phytoestrogens, anti-inflammation and suppression of metabolic syndrome (Tsuchiya, 2010; Liu *et al*., 2010; Joubert & Beer, 2012; Joubert & Beer, 2014; Dong *et al*., 2019; Krafczyk, Woyand, *et al*., 2009). Table 2 indicates the bioactivities of **2**, **3**, **8**, **9**, **10**, **11**, **12**, **13**, **14**, **15**, **16**, **18**, **19**, **23**, **24**, **29**, **30**, **32**, **33**, **34**, **38**, **39** and **49** as health promoters.

2.3.4. Nutraceutical and Health-promoting traits of Rooibos tea and compounds

Rooibos is generally consumed as a herbal tea for its health vitality and has recently become a value-added product in the food and drug industries (Da Silva Pinto, 2013). As a value-added product, it has functional applications in cosmetics, beverages, and drugs alongside other cape herbal teas such as honeybush (*Cyclopia spp.*), cancer bush (*Sutherlandia frutescens*) and green tea (*Camellia sinensis*) (Wyk & Gorelik, 2016). The functional applications are attributed to the high bioavailability of its bioactive compounds which makes it suitable for use as both intermediate and final products (Breiter *et al*., 2011). Numerous studies have reported the versatility of rooibos extracts with potential applications as a drug candidate in the intervention of life-threatening diseases (Waisundara & Yian, 2015; Muller et al., 2018). For instance, extensive reports (*in vivo* and *in vitro* studies) on fermented and unfermented rooibos extracts and their major flavonoids have been reported on their potentials as an antidiabetic drug (Sasaki et al., 2018). The high polyphenol content is also unique to its disease-preventing properties resulting from the overproduction of reactive oxygen species (ROS). Although ROS are useful to the body system in cell apoptosis and defence against foreign bodies, negative effects of the excess result in oxidative stress, protein and nucleic acid damage, lipid oxidation, blood glucose level resulting from metabolic activities (Awoniyi *et al*., 2012; Smith & Swart, 2018; Diallo *et al*., 2018). ROS are linked to the major cause of cell inflammation, viral diseases, cancer growth, and cardiovascular diseases such as hypertension (Ajuwon *et al.*, 2015). ROS produced from the electron transport chain of the oxygen atom in the mitochondrial and in phagocytic cells possess unpaired electrons that make them very reactive, thus serving as a defence against pathogens (Parasuraman & Maithili, 2014). However, the uncontrolled production of ROS inflicts damages on cell biomolecules that result in oxidative stress. A necessary step to prevent or slow down oxidation is the activation of free radical scavenging agents (Mekni *et al*., 2013). Enzymatic antioxidants; catalase (CAT), serum superoxide dismutase (SOD) and glutathione peroxidase (GSH) and plant-derived antioxidants (vitamin C, tocopherols and polyphenols) play significant roles in protecting cell damages from oxidant stress (Gadow *et al*., 1997; Pieme *et al*., 2017). The rooibos tea presents a plethora of antioxidants such as dihydrochalcones, flavanols, flavanones, flavones, flavonols, isoflavones and tannins as polyphenols (Krafczyk & Glomb, 2008; Damiani et al., 2019). The antioxidant activities, free radical scavenging and the prevention of DNA strands scission by rooibos are well documented in the literature (Shimoi *et al*., 1994; Lee & Jang, 2004; Hong *et al*., 2014; Waisundara & Yian, 2015; Santos *et al*., 2018; Villaño *et al*., 2010).

2.3.5. DNA and hepatoprotection

Cumulative data from research studies unequivocally affirm the rich antioxidant property of rooibos tea in managing oxidative stress. Dietary constituents of rooibos have been attributed to its ability to modulate metabolizing enzymes to either prevent or delay oxidative stress of cells that could lead to chronic diseases (Orzel *et al*., 2014). Cullere *et* al. (2013) demonstrated the antioxidant effect of green and fermented rooibos against lipid oxidation in meat products to effectively prolong the shelf-life (Cullere et al., 2013). Among the effects of oxidative stress is the DNA damage by ROS that causes scission of the double-strands or reaction with DNA bases that produce 8-hydroxydeoxyguanosine (8-OHdG), a signal of DNA damage. Lee & Jang (2004) studied the prevention of DNA scission by peroxyl radicals due to aqueous and 75% ethanolic extract of rooibos. The authors attributed the antioxidant activity of rooibos phenolics to the scavenging of hydrogen peroxide of peroxyl radical-induced DNA (Lee & Jang, 2004). Baba *et* al. (2009) reported animal studies of Wistar rats fed with rooibos tea. The result parameters revealed that the DNA damage and inflammation were prevented via the antioxidants property of rooibos tea against the observed result of the control group (Baba *et al*., 2009). Marnewick *et al.* (2003) found that consumption of processed rooibos tea and honeybush tea by Wistar rats had no adverse effect on the liver and the kidney. Also, there was an enhanced activity of metabolizing enzymes which increase the antioxidant status of the rat liver. Further studies on Fischer rats by Marnewick *et al.* (2004) on liver cells mutation induced by aflatoxin B_1 and 2-acetylaminofluoren toxins show that green and fermented rooibos ameliorated mutagenesis by aflatoxin B_1 but no response on 2-acetylaminofluoren (Marnewick et al., 2003; Marnewick et al., 2004). According to Ajuwon *et al*., (2014), administration of aqueous rooibos extract on male Wistar rats with lipopolysaccharide-induced acute liver injury was attenuated (Ajuwon et al., 2014). Similarly, the counter-effect of rooibos on oxidative stress was highlighted to facilitate the regeneration of Coenzymes Q_9 and inhibited oxidative stress from Wistar rats with tetrachloromethane (CCl_4) induced liver damage (Kucharská et al., 2004; Uličná et al., 2008). The ameliorative effect of rooibos consumption on hepatic injury induced by ter-butyl hydroperoxide also confirmed that rooibos could be a potential hepatic drug for the treatment of liver diseases (Canda *et al*., 2014). Furthermore, a histological study of the effect of commercial green rooibos extract on the hepatoprotection from diet-induced obesity was carried out by Layman *et al*. (2019) within four groups of seven Wistar rats each. The result demonstrated a significant reduction in body mass, liver mass, and volume density of liver steatosis for the group co-treated with green rooibos extract (Layman et al., 2019). The observed result was indicated green rooibos extract rich in aspalathin in amelioration of liver dysfunction.

2.3.6. Cardiac and Neuroprotection

The protection of the cardiac and the neuro cavities are major concerns with chronic diseases that are related to stress and ageing. The reviews by Smith & Swart 2018 and by Gerald J. Maarman (2019) on rooibos as a functional food targeting cardiovascular diseases and the mechanism of action described a series of research studies that bring to light, the cardioprotective effect of aqueous extract of rooibos (Smith & Swart, 2018; Maarman, 2019). Cardiotoxicity is a common side-effect experienced during chemotherapy of cancer cells treated with Doxorubicine. A necessary procedure taken in the clinicals is to protect the cardiac of Doxorubicine toxicity which involves co-treatment with Dexrazoxane. The protective effect of Dexrazoxane is related to its ability to regulate overproduction of reactive oxygen species through chelation and although poses some resistance to treatment. In a similar study, Johnson *et al*., (2017) showed that co-treatment of **2** with Doxorubicine affect apoptosis of cancer cells while also shielding the cardiac cavity of toxicity from Doxorubicine. A similar study by the group also potentiates **2** for myocardial protection from lipid toxicity resulting from lipid metabolism (Johnson, Shabalala, et al., 2017; Johnson, Dludla, et al., 2017). In addition, Dlulda *et al*., (2017) reported **2** to exhibit cardioprotection against hyperglycaemia-induced oxidative damage in H9c2 cardiomyocytes and diabetic (db/db) mice, respectively. The result showed that daily treatment of mice with **2** at a dose of 130 mg/kg for six weeks effectively rectify complications resulting from the induced damage compare to metformin drug via up-regulation of the nuclear factor Nrf2 (Dludla, Muller, et al., 2017). A more recent study by P.V. Dludla *et al* (2020) supports the evidence by Pantsi *et* al. (2011) that consumption of fermented rooibos offers cardiac protection against ischaemia and glucose-induced cardiac damage *(Pantsi et al*., 2011; Dludla *et al*., 2020). Pyrzanowska, *et al*. (2019) showed that intake of fermented rooibos tea by experimental rats exhibited neuroprotection and cranial activities by improving long term memory and also reducing blood glucose levels in adult Sprague-Dawley male rats (Pyrzanowska et al., 2019; Dludla et al., 2020; Pyrzanowska et al., 2021). Hong *et* al. (2014) evaluated the effect of rooibos consumption on the brains of experimental rats exposed to neurodegenerative stress. The measured stress-induced characters (body weight, lipid peroxidation, SOD, CAT, GSH and protein degradation) of the rat brain revealed that rooibos tea attenuated the induce-oxidative stress (Hong *et al*., 2014). Cardiovascular and microvascular damages are often underlined by complications from hypertension, diabetes and obesity brought about by the imbalanced metabolic breakdown of glycerides and lipids and their utilization (Chen *et al*., 2013). This metabolic syndrome is controlled by abnormal insulin secretion or receptor for glucose uptake from the bloodstream which may lead to any of hyperglycemic, hypoglycemic, hyperglycemic or hypolipidemic condition. In vitro experiment with C2C12 skeletal muscle cells by Mazibuko *et* al. (2013) established that rooibos extract attenuates palmitate-induced insulin

resistance via inhibition of the primary antibodies such as protein kinase C theta (PKC θ) and the activation of 5' adenosine monophosphate-activated protein kinase (AMPK) and protein kinase B (AKT) (Mazibuko et al., 2013). Different animal studies with Wistar rats fed with rooibos tea proved the nutraceutical value of the herbal tea. Green rooibos tea was observed to suppress high blood glucose in type 2 diabetic model in-vitro and in-vivo (Kamakura *et al*., 2015). Dludla *et al*. (2014) reported that cardiomyocytes cultured from streptomycin-induced diabetic rats were improved on exposure to aqueous extract of fermented rooibos tea than those exposed to antioxidant vitamin E (Dludla et al., 2014). Obesity is the build-up of body fat (adipose tissue) in which cell sizes increase during adipogenesis. An obsessed person is at a greater risk of a metabolic syndrome triggered by stressed cells. Sanderson *et al*. (2014) study the effect of hot water soluble solid of fermented rooibos on adipose tissue for the prevention of obesity. The result reflects the inhibition of adipogenesis and adipocyte metabolism via decrease lipid accumulation and increases glucose uptake (Sanderson *et al.*, 2014). Furthermore, in an herb-drug interaction experiment of hypoglycemic and hypolipidemic drugs and their metabolisms with cytochrome P450 enzymes, Patel *et al.* (2016) separately co-administered green and fermented rooibos with thiazolidinediones, sulfonylureas and atorvastatin drugs. Both green and fermented rooibos exhibited potent inhibition against these enzymes suggesting an improved performance of the drugs (Patel *et al*., 2016).

2.3.7. Anti-inflammation and anti-viral potential

Oxidative stress and inflammation are interdependent as the root causes of cell damages (Beltrán-Debón *et al*., 2011). Inflammation occurs when the immune system is triggered by any of the physical factors that cause pain, heat, redness, loss of function, or swelling in a part of the body. This condition is marked by an increase in the biomarker of inflammation such as C-reactive protein (CRP). Sometimes the defence mechanism randomly attacks normal cells in an autoimmune reaction. Steroidal and nonsteroidal anti-inflammatory drugs are prescribed to counter the activity of cytokines enzymes causing inflammation. Inflammation of skin cells is mostly due to exposure of the epidermal layer to ultraviolet radiation, a major cause of skin cancer. This condition is marked by increase inflammation of biomarkers such as C-reactive protein (CRP), TNF- α, interleukin-1, IL-1, IL-6, IL-10 etc. Studies of the anti-inflammatory activities of herbal tea show that rooibos ameliorates pro-inflammatory enzymes. Magcwebeba and co-workers (2016) evaluated the anti-inflammatory effects of methanol and aqueous extracts of rooibos tea and honeybush with a UVB/HaCaT keratinocyte model using extract of green tea as a benchmark. The removal of interleukin-1α as the inflammatory marker was correlated with the anti-inflammatory activities of the herbal teas. It was noted that extract of rooibos and honeybush increased inhibition of UVB-induced cell viability, proliferation and induction of apoptosis (Magcwebeba et al., 2016). Smith & Swart 2016 reported the enhanced anti-inflammatory effect of rooibos to reduce glucocorticoid and

inflammatory cytokine levels in vivo and in vitro studies with Wistar rats and H295R cell mode, respectively. This result gives credence to previous work of these authors that rooibos has a positive impact on the glucocorticoid levels and biosynthesis of stress hormones (Smith & Swart, 2016; Schloms *et al*., 2012). Furthermore, investigation of the biological activity of rooibos extract has indicated its antiviral activity against human influenza virus and human immunodeficiency virus (HIV), protective property against cancer promotion, promoting skin cell viability, muscle cell growth and antimicrobial effects. Nakano *et al*. (2014) demonstrated that the alkaline extract of rooibos leaves inhibited the binding of HIV-1 to MT-4 cells in vitro. The alkaline extract was also reported by Rahmasari *et al.* (2017) to inhibit the replication of influenza A virus while the ethanol, ethyl acetate and n-hexane extract did not (Nakano *et al*., 1997; Rahmasari *et al*., 2017). Prevention of cancer growth by rooibos and other herbal teas was demonstrated by Marnewick *et al*. (2009). The result shows that rooibos tea significantly reduced kidney and liver cancers that may occur from fumonisin B_1 in induced-diethylnitrosamine Fischer rats (Marnewick *et al*., 2009). Similarly, Unathi *et al*. (2016) finding showed that methanol extract of rooibos was effective as a cytoprotective agent for skin cells survival (Unathi *et al*., 2016).

2.3.8. Glucose modulation and associated diseases

Control of blood glucose is a major step in the management of diabetes resulting from insulin dysfunction and the activity of carbohydrate-hydrolyzing enzymes. The onset of diabetes is often associated with induced metabolic stress leading to some cardiovascular diseases, including obesity and hypertension. Bioactive phenolic glycones from rooibos have shown promising potential as antidiabetic drugs (Johnson *et al*., 2018). Yamasaki *et al*. (2011) demonstrated that glucose moieties of flavonoids at C-3 positions are responsible for the activity of glucose uptake in a cell culture line (Yamasaki *et al*., 2011). This gives credence to the increasing reports of the major flavonoid of rooibos, **2** with C-C linked glycone at position C-3 in the modulation of blood glucose and insulin secretion. An *in vitro* and *in vivo* study by Kawano *et al*. (2009) revealed that **2** accelerates glucose uptake in muscle tissues and insulin secretion from pancreatic β-cells. Several experimental findings show that compounds **2** and **49** are the most potent for diabetes-related complications that require protection of the liver and β-cells of the pancreas from induced cell death. Smit et al., (2017) presented that co-treatment of **2** at 10 μM for 90 minutes with insulin on insulin-sensitive cardiomyocytes isolated from diet-induced obese, young and, matured Wistar rats significantly improve glucose clearance in all control rats except in the aged rat (Smit et al., 2017). This indicates that ageing is a limiting factor. The cytoprotective effect of **49** on β-cells of the pancreas from induced acute diabetogenic cell death was reported by Himpe et al., (2016). The in vitro studies showed that **49** prevented β-cells apoptotic cell death from oxidative stress induced by hydrogen peroxide and streptozotocin after 30 hours of treatment (Himpe et al., 2016). Similar

findings were reported by W. Chen *et al*. 2013, and by Mazibuko-Mbeje *et al*. 2019. Their results showed that **2** ameliorated hepatic insulin resistance in liver cells and reduce oxidative stress *in vivo* via an insulin signalling pathway (Kawano et al., 2009; Chen et al., 2013; Mazibuko-Mbeje et al., 2019; Mazibuko-mbeje et al., 2019). Also, the uncontrolled hydrolysis of carbohydrates by α-glucosidase and α-amylase enzymes has been linked to increasing postprandial blood glucose and the development of type 2 diabetes. Nana *et al*. demonstrated that **2** inhibited α-glucosidase and α-amylase enzymes and suppressed the elevation of blood glucose *in vivo* (Nana *et al*., 2015). The antidiabetic potentials of **2** and **19** were accessed as single glycone flavonoid by Muller *et al*. (2012) and as a mixture of streptozotocin-induced diabetic rats. The result reflects the synergistic effect of the mixture was relatively higher in the streptozotocin-induced rats than for single compounds (Muller *et al*., 2012). In addition to the above flavonoids, **49** a major non-phenolic glycone at C-2 position possess a C_6-C_3 skeleton was also reported to enhance glucose uptake *in vitro* and *in vivo* with an obese insulin-resistant Wistar rat (Christo *et al*., 2013).

2.3.9. Anti-inflammatory and endothelial protein C receptor (EPCR)

Endothelial inflammation of the blood vessels is an important precursor of hypertension and corona artery diseases. Inflammation of the arteries caused by defects in thrombin production and conversion of plasma protein to fibrin may lead to dilation of blood walls, blood coagulation and stroke. The endothelial cell surface is regulated by the protein-C complex (including thrombomodulin, EPCR and protein S) that deactivate activated coagulation factors V and VIII. There has been an increasing number of research on the potential dermal wound healing of rooibos, and its compounds. compounds **2**, **3**, and **49** have indicated to downregulate coagulation of platelets and shedding of activated EPCR from an endothelial surface(Kwak *et al*., 2015). Lee and co-workers (2015) investigated the responses of **2** and **3** to suppress lipopolysaccharide (LPS)-mediated vascular inflammation and high mobility group box 1 protein (HMGB1)-mediated septic *in vitro* and *in vivo*. Each compound was found to inhibit induced-vascular hyperpermeability, leukocytes migration in vivo and suppression of build-up of tumour necrosis factors that could result in leukocyte proliferation in the vascular cells. Their results are in agreement with Ku *et al*. 2015 for the inhibition of glucose-induced inflammation by **2** and **2** (Lee & Bae, 2015; Lee *et al*., 2015; Ku *et al*., 2015). Pingle et al., (2018) highlighted that the fermented and unfermented rooibos exhibit proinflammatory activities that could protect protein fibroblast from ROS damage and regulate cyclo-oxygenase-2 level which are biomarkers for the severity of inflammation and wound healing (Pingle et al., 2018).

2.3.10. Oestrogenic and exocrine gland activity

Sex hormones are naturally secreted from the ovaries which are important factors in female reproductive health and strengthening of bones. Phytoestrogens are mimics of oestrogens obtained from plants like legumes, vegetables and fruits mostly isoflavones, prenylflavonoids, coumestans and lignans (Rietjens *et al*., 2017). Shimamura *et al*. (2006) investigated the flavonoids of rooibos for phytoestrogen activity compared to flavonoids genistein and resveratrol known for phytoestrogen activity (Sirotkin & Halim, 2014). The report shows that **3**, **9** and **12** exhibit high oestrogenic activity probably due to glycosylation in ring A and hydroxylation in ring B while **22** show moderate activity and **2** and **4** show less activity compared to **3** (Shimamura *et al*., 2006). The sweat, tear, and salivary exocrine glands are essential for protecting the skin, eyes and mouth from diseases related to dryness and regulating the moisture content. Secretions of these glands are known to be activated by different classes of muscarinic acetylcholine receptors (M1R – M5R) by eliciting parasympathetic reactions in these organs. Nishimachi, et al., (2019) evaluated rooibos extract among other samples for the activation of M3R using a cellular assay system and human trials against commercial compound **21** as standard. The studies showed that rooibos extract was effective in stimulating M3R involves in lowering dryness of the skin, eyes, and mouth in humans. The efficacy of rooibos extract was attributed to **21** constituents only due to no effect from structurally related compounds **13**, **14** and **20** the major compound **2** (Nishimachi et al., 2019).

2.3.11. Anti-mutagenic activity

The abilities of fermented and unfermented extracts of rooibos, and some flavonoid compounds of the tea to counteract mutagens has been validated *in vitro*. 4-(methylnitrosamino)-1-(3-pyridyl)-1-butanone (NNK) and N-oxide, 4 (methyl-nitrosamino)-1-(3-pyridyl)-1-butanol (NNAL) are specific tobacco mutagens produced from catalytic oxidation of nicotine in tobacco smokes that are connected to lung tumour. Gelderblom, W.C.A. et al., (2016) assessed the potency of hot aqueous herbal teas (honeybush; *Cyclopia intermedia*, cancer bush; *Sutherlandia frutescens*) including fermented and unfermented rooibos extract in the prevention of mutagenicity against *Salmonella typhimurium* tester strain (TA1535). Using green and black tea (*Camellia sinensis*) as positive controls, the authors reported that black tea and rooibos extract demonstrated the highest inhibition in NNK-induced mutagenesis while for NNAL, the black tea, green tea, and fermented rooibos exhibited the highest antimutagenic effects (Gelderblom et al., 2016). A similar study on the compounds of rooibos using *Salmonella typhimurium* tester strain TA98 and TA100 as antimutagenicity assay was accessed for 2-acetamido-fluorene (2-AAF) and aflatoxin B1 (AFB_1) mutagens relative to green tea flavonoid (epigallocatechin gallate EGCG) as positive control by Snijman e*t al*., 2007. The study showed activities of **2**, **3**, **8**, **10**, **11**, **12**, **13**, **14**, **15**, **16**, **18**, **19** and **38** in

a range of responses; antimutagenic by lowering mutagenic effect as displayed by EGCG, comutagenic by improving the mutagenic response of a mutagen, promutagenic and directly mutagenic which required metabolic activation to promote responses. It also indicated the dependence of the degree of hydroxylation, *O*-methylation and glycosylation on rings A and B as well as the presence of the C_4-keto group and the C_2–C_3 double bond on flavonoid-mutagen interactions. It was noted that **2**, **3**, **11**, **12**, **13**, **14** showed antimutagenic (against 2-AAF and AFB_1), **8** and **10** exhibited comutagenic (against 2-AAF) while, **15** and **18** displayed both promutagenic and direct mutagenic activities. Similar structure-related activities for oestrogenic activities of **3**, **9** and **12** have been earlier reported by Shimamura *et al*., 2006. Dose-response effects of the flavonoids on mutagens were also reported to reflect **2** and **3** with no dose-response (against 2-AAF) at different concentrations tested. **15** and EGCG exhibited a direct relationship with concentration tested in a typical dose-response effect while **10** (against 2-AAF), **19** and **38** (against AFB_1) effects were atypical. The last dose-response effect observed on mutagens was a combination of other dose-responses displayed by **8**, **10**, **19** and **38** (against 2-AAF) and **18** (against AFB_1). In all, higher antimutagenic protection against mutagenesis by rooibos flavonoids was found to be higher in AFB_1-induced than in 2-AAF and **8** portrayed the highest activity similar to (-) EGCG at 0.8mM and greater activity at a concentration less than 0.4 mM (Snijman *et al*., 2007).

Table 2: Bioactivities of Rooibos flavonoids with references

Compounds	Experiments	Activities	Reference
Aspalathin, Nothofagin	In vivo & In vitro.	Anti-inflammatory.	Lee & Bae 2015.
	In vivo & In vitro.	Inhibition of glucose-induced inflammation.	Ku, Kwak, Kim, and
	In vivo & In vitro.	Antiseptic effect against high mobility group box 1 (HMGB1).	2015. Lee, Kim & Bae 2015.
Aspalathin	In vivo.	Hypoglycaemic.	Kawano *et al*. 2009.
	In vivo.	Reduce oxidative stress and promote longevity.	W. Chen *et al*. 2013.
	In vivo.	Suppression of blood glucose.	Nana *et al*. 2015.
	In vivo.	α-glucosidase and α-amylase inhibition.	
	In vivo.	Reverse hepatic insulin resistance.	Mazibuko-Mbeje *et*
	In vivo.	Regress Doxorubicin-induced cardiotoxicity.	2019.
	In vivo.	Cardiomyocytes protection from induced-lipid toxicity.	Johnson *et al*., 2017.
	In vitro and In vivo	Cardio-protection against induced-oxidative damage.	Johnson *et al*., 2017. Dludla *et al*., 2017.
Z-2-(*β-D*-glucopyranosyloxy)-3-phenylpropenoic acid	In vivo.	Hypoglycaemic activity.	Muller *et al*. 2013.
	In vivo.	Cytoprotective effect of beta cells	Himpe et al., 2016.
Aspalathin, Z-2-(β-D-glucopyranosyloxy)-3-phenylpropenoic acid	In vivo.	Hypoglycaemic and hypolipidemic activity.	Oelfah *et al.* 2016
Aspalthin-Rutin mixture	In vitro and In vivo.	Hypoglycaemic activity.	Muller *et al*. 2012
Aspalathin, Nothofagin, Z-2-(*β-D*-glucopyranosyloxy)-3-phenylpropenoic acid	In vitro and In vivo.	Anti-endothelial cell protein C receptor EPCR.	Kwak *et al*. 2015
Isovitexin, nothofagin, luteolin-7-glycoside	In vivo.	Phytoestrogen.	Shimamura *et al*. 2006

Aspalathin, quercetin, vitexin, (+)-catechin, rutin, luteolin, isoquercitrin, protocatechuic acid, caffeic acid, *p*-benzoic acid, *p*-coumaric acid, ferulic acid, syringic acid, and vanillic acid	In vivo.	Antioxidants	von Gadow *et al.* 1997
Chrysoeriol	In vivo.	Cardioprotection	Arif-ullah *et al*. 2006
Aspalathin, nothofagin, luteolin, chrysoeriol, quercetin, orientin, iso-orientin, vitexin, isovitexin, (+)-catechin, isoquercitrin, hyperoside and, rutin	In vivo.	Anti-mutagenic	Snijman *et al*. 2007.

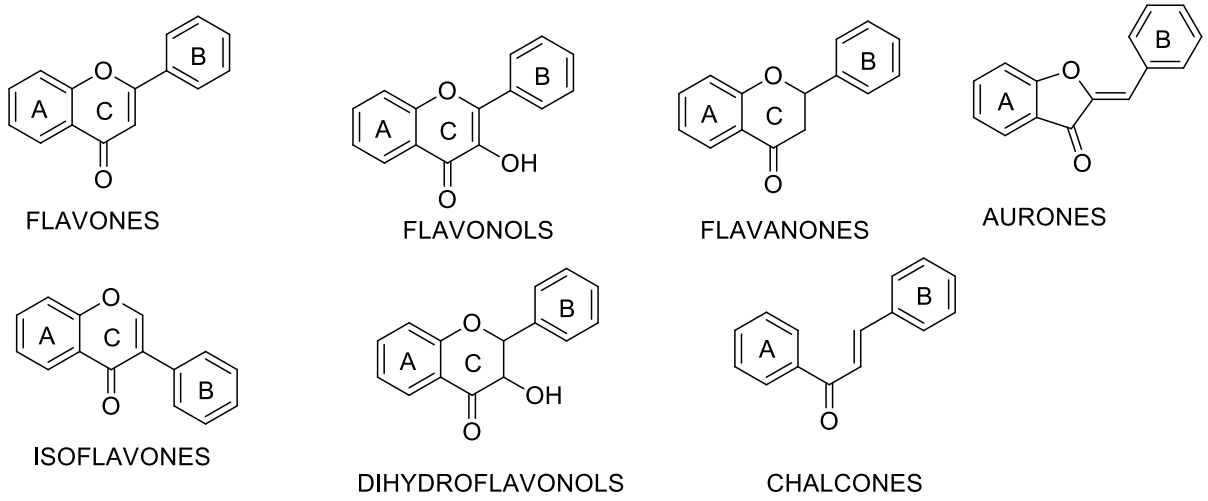

Figure 3.1: Chemical skeleton of naturally occurring flavonoids

2.3.12. Metal-nanoparticles synthesis via *Aspalathus linearis*

The chemical profile of phytochemicals from *Aspalathus linearis* revealed they are secondary metabolites of phenolics and flavonoids and a few non-phenolics compounds with tremendous therapeutic and health benefits (Maria *et al*., 2017) as discussed in section. An essential property of rooibos tea like other teas is the antioxidant ability of its polyphenolics to reduce free reactive ions by scavenging. Polyphenolics have been elucidated to have high electron affinity and conjugated double bonds which contribute to their reducing and stabilizing potential for phyto-assisted nano synthesis (Nune *et al*., 2009). These properties challenged emerging researchers in nanotechnology for possible application as both reducing and stabilizing agents for the green synthesis of nanomaterials (Santhoshkumar *et al*., 2017; Santos *et al*., 2018). Phyto-assisted nanoparticles involve the use of biodegradable plant materials and benign solvents for less hazardous synthesis. It is generally accepted to be environmentally friendly,

cheap, reduce the use of hazardous compounds and harsh reaction conditions (Srikar *et al*., 2016; Yulizar *et al*., 2017). Several publications that summarised the use of leaf extract, bacteria and fungi extracts for the synthesis of nanoparticles have been reported (Mata *et al*., 2016; Peralta-Videa *et al*., 2016; Ahmed *et al*., 2017).

Recent curiosity on *Aspalathus linearis* in the last decade confirmed its reducing and stabilizing potential for nano-enabled materials. Hence, an increasing number of reports have demonstrated the green synthesis of metal nanoparticles using the rooibos plant and its compounds. Table 4 summarizes the present research on the biosynthesis of metal nanoparticles via the rooibos plant. It shows the relevant information on the size, crystallinity, shapes and activity of the nanoparticles. Oyagi *et al*. (2014) described the effect of varying temperatures on the extraction of polyphenols from leaves of rooibos tea used for silver nanoparticle synthesis from silver nitrate ($AgNO_3$) and the physicochemical character. The result suggested a linear relationship between increasing extraction temperature (25°C, 30°C, 50°C, 70°C and 90°C) and the yield of silver nanoparticle as demonstrated by increasing absorbance wavelength. The UV-Vis monitoring of synthesis reported yellow to dark brown colour changes at the absorbance range of 440-489 nm. The crystallinity of the particles above 30° was reported to be face centred cubic on XRD, SEM images showed spherical shapes with average sizes of 4.5 - 4.8 nm (Oyagi *et a*l., 2014). Similarly, zinc(II), cobalt (II) and nickel (II) metals were reduced to their respective zero valences by rooibos extract for nanoparticles synthesis (Diallo *et al*., 2015a; Diallo *et al*., 2015b; Diallo *et al*., 2018). Measurement of their optical and physical properties using zinc nitrate hexahydrate [$Zn(NO_3)_2.6H_2O$] and cobalt nitrate hexahydrate [$Co(NO_3)_2.6H_2O$] respectively as precursor agents were reported. Morphology and size distribution measurement by HRTEM reflected a quasi-spherical image of sizes 3.57±0.05 nm (cobalt oxide) and 4.08±0.08 nm (zinc oxide) nanoparticles. The amorphous nature and purity of three metal oxides nanoparticles synthesized were also determined by XRD, EDS and XPS techniques while crystallinity was induced by annealing at 300°C (Diallo *et al*., 2015a; Diallo *et al*., 2015b). The authors also successfully synthesized spherical crystalline cobalt oxide nanoparticles which showed magnetic properties dependent on the mean size of the particles, photocatalytic nanocrystal nickel and tin oxide nanoparticles that decolourised methylene Congo red and Eosin Y as well as luminescent europium nanoparticles from *Aspalathus linearis*. Structural and morphological characteristics of the cobalt, nickel and europium nanoparticles reported show non-crystalline nature without thermal treatment, spherical shapes with average particle sizes of 11.6 nm, quasi-spherical shapes of 7 nm and cubic-like shapes of 16.5 nm respectively. While shapes and crystallinity of tin oxide nanoparticles varied with thermal treatment from 400°C - 900°C (A Diallo *et al*., 2016; Abdoulaye Diallo *et al*., 2016; Dialloa *et al*., 2017; Diallo *et al*., 2018). Furthermore, recent works by Ismail *et al*., *Aspalathus linearis* was used as both reducing and capping agents for

the biosynthesis of some platinum group metals nanoparticles including rhodium, palladium and ruthenium metal. Their studies confirmed the reduction of rhodium (III) and palladium (II) to respective zero oxidation state nanoparticles by chelation with phytochemicals in *Aspalathus linearis* at absorbance maxima monitored by UV-Visible spectroscopy. The report indicated a variety of shapes for palladium while rhodium was observed to exhibit a nearly homogeneous shape. Noteworthy is that the synthesized ruthenium nanoparticles (2-5 nm sizes) were functionalised as superconductors and solar water photo-splitters (Ismail, Diallo, et al., 2016; Ismail, Khamlich, et al., 2016; Ismail, 2017; Ismail et al., 2017). More recently is the contribution by Noluthando *et al*., (2018) for the biosynthesis of polycrystalline palladium, nickel and binary metal oxide (zinc-tin) nanoparticles from *Aspalathus linearis* confirmed by several characterisation techniques. The result of cyclic voltammetry experiment for palladium and nickel nanoparticles confirmed their electrochemical conductivities, although palladium nanoparticle was more conductive. In addition to cyclic voltammetry, electrochemical impedance spectroscopy qualifies $ZnSnO_3$ nanoparticles as both semiconductors and electrolytes (Noluthando *et al*., 2018a; Noluthando *et al*., 2018b). Lately, Akinfenwa et al. (2021) indicated that the reducing and stabilizing ability of the rooibos plant used for the synthesis of nanoparticles was due to the antioxidant activity of the major compound, aspalathin. This was following a successful biosynthesis of gold, and silver nanoparticles from the isolated compound and the natural extract of rooibos. The result of their study is the first report of the efficacy of the major compound of rooibos in the green synthesis of gold and silver nanoparticles. Also, it potentiates silver nanoparticles of both aspalathin and rooibos as anticancer drugs (Akeem et al., 2021).

Table 3.2: Rooibos-assisted metal nanoparticles

S/n	Meta-oxide	λ_{max} (nm)	Size (nm)	Crystallinity	Application	Reference
1	Silver	440-489	4.4-5.8	Crystalline	*	Oyagi *et al*., 2014
2	Zinc	400-700	4.08±0.08	Amorphous	*	Diallo *et al*., 2015
3	Cobalt	*	3.57±0.05	Amorphous	*	Diallo *et al*., 2015
4	Tin	*	2-11.4	Amorphous/polycrystalline	Photocatalyst	Diallo *et al*., 2016
5	Ruthenium	*	<5	Amorphous	Supercapacitor	Ismail *et al*., 2016

6	Ruthenium	428	2.25	Amorphous	Water photo-splitting	Ismail *et al*., 2016
7	Europium	614.8	16.6	Amorphous	Luminescence	Diallo *et al*., 2016
8	Cobalt		11.6	Crystalline	Magnetization	Diallo *et al*., 2017
9	Palladium	225-700	12.7	Amorphous	*	Ismail *et al*., 2017
10	Rhodium	225-600	1.2±0.3	Amorphous	*	Ismail *et al*., 2017
11	Nickel	519.8	7	Crystalline	Photocatalyst	Diallo *et al*., 2018
12	Palladium Nickel	* *	22.7±4.3 31.8±5	Polycrystalline Polycrystalline	Semiconductor	Noluthando *et al*., 2018
13	Zinc-tin	354	18±2	Polycrystalline	Electrolyte	Noluthando *et al*., 2018
14	Gold Silver	530 440	0.9 – 1.7 4.2 – 4.3	Crystalline	Anticancer	Akinfenwa et al., 2021

2.3.13. Conclusion

Numerous studies on the bioactivities of *Aspalathus linearis* and its phytochemicals exist in the research community. Smith and Swart (2018) in their report dissected the functional application of the tea to ameliorate the risk of cardiovascular diseases which was attributed mainly to its antioxidants, modulation of biochemical activities and anti-inflammatory potential ((Smith & Swart, 2018). Also, growing evidence confirm its involvement in the green synthesis of plant-mediated metal nanoparticles for diagnostic and catalytic purposes. Going forward, novel research will be clinical trials on human studies as a double assurance of its health-promoting traits and possible application of its compounds for the biosynthesis of both single and mixed metal nanoparticles.

Conflict of interest

The authors declare no conflict of interest

Acknowledgement

The authors would like to appreciate the financial support by the National Research Foundation of South Africa and the Cape Peninsula University of Technology, South Africa.

References

Ahmed, S., Ali, S. & Ikram, S. 2017. A review on biogenic synthesis of ZnO nanoparticles using plant extracts and microbes: A prospect towards green chemistry. *Journal of Photochemistry & Photobiology, B: Biology*, 166(2017): 272–284.

Ajuwon, O.R., Marnewick, J.L. & Davids, L.M. 2015. Rooibos (*Aspalathus linearis*) and its Major Flavonoids — Potential Against Oxidative Stress-Induced Conditions. In S. T. Growder, ed. *Basic Principles and Clinical Significance of Oxidative Stress*. IntechOpen: 171–218. https://www.intechopen.com/books/basic-principles-and-clinical-significance-of-oxidative-stress/rooibos-aspalathus-linearis-and-its-major-flavonoids-potential-against-oxidative-stress-induced-cond.

Ajuwon, O.R., Oguntibeju, O.O. & Marnewick, J.L. 2014. Amelioration of lipopolysaccharide-induced liver injury by aqueous rooibos (*Aspalathus linearis*) extract via inhibition of pro-inflammatory cytokines and oxidative stress. c*omplementary and Alternative Medicine*, 14(392): 1–12.

Akeem, A.O., B, A.N.S., Fathima, D.T., Marnewick, J. & Hussein, A.A. 2021. Anticancer potency of phytomediated silver and gold nanoparticles synthesised from rooibos (*Aspalathus linearis*), and its major dihydrochalcone compound. *Plants-14337*.

Akinfenwa, A.O., Abdul, N.S., Marnewick, J.L. & Hussein, A.A. 2021. Protective Effects of Linearthin and Other Chalcone Derivatives from *Aspalathus linearis* (Rooibos) against UVB Induced Oxidative Stress and Toxicity in Human Skin Cells. *Plants*, 10(1936): 1–21.

Ali, Z.A., Yahya, R., Sekaran, S.D. & Puteh, R. 2016. Green synthesis of silver nanoparticles using apple extract and its antibacterial properties. *Advances in Materials Science and Engineering*, 2016.

Anbuvannan, M., Ramesh, M., Viruthagiri, G. & Shanmugam, N. 2015. *Anisochilus carnosus* leaf extract mediated synthesis of zinc oxide nanoparticles for antibacterial and photocatalytic activities. *Materials Science in Semiconductor Processing*, 39(2015): 621–628. http://dx.doi.org/10.1016/j.mssp.2015.06.005.

Awoniyi, D.O., Aboua, Y.G., Marnewick, J. & Brooks, N. 2012. The Effects of Rooibos (*Aspalathus linearis*), Green Tea (*Camellia sinensis*) and Commercial Rooibos and Green Tea Supplements on Epididymal Sperm in Oxidative Stress-induced Rats. *Phytotherapy Research*, 26: 1231–1239.

Baba, H., Ohtsuka, Y., Haruna, H., Lee, T., Nagata, S., Maeda, M. & Yamashiro, Y. 2009.

Studies of anti-inflammatory effects of Rooibos tea in rats. *Pediatrics International*, 51: 700–704.

Badeggi, U.M., Ismail, E., Adeloye, A.O., Botha, S. & Hussein, A.A. 2020. Green Synthesis of Gold Nanoparticles Capped with Procyanidins from *Leucosidea sericea* as Potential Antidiabetic and Antioxidant Agents. *Biomolecules*, 10(452).

Baranska, M., Schulz, H., Joubert, E. & Manley, M. 2006. In Situ Flavonoid Analysis by FT-Raman Spectroscopy: Identification, Distribution, and Quantification of Aspalathin in Green Rooibos (*Aspalathus linearis*). *Analytical Chemistry*, 78(22): 7716–7721.

Beer, D. De, Malherbe, C.J., Beelders, T., Willenburg, E.L., Brand, D.J. & Joubert, E. 2015. Isolation of aspalathin and nothofagin from rooibos (*Aspalathus linearis*) using high-performance countercurrent chromatography: Sample loading and compound stability considerations. *Journal of Chromatography A*, 1381: 29–36. http://dx.doi.org/10.1016/j.chroma.2014.12.078.

Beltrán-Debón, R., Rull, A., Rodríguez-Sanabria, F., Iswaldi, I., Herranz-López, M., Aragonès, G., Camps, J., Alonso-Villaverde, C., Menéndez, J.A., Micol, V., Segura-Carretero, A. & Joven, J. 2011. Continuous administration of polyphenols from aqueous rooibos (*Aspalathus linearis*) extract ameliorates dietary-induced metabolic disturbances in hyperlipidemic mice. *Phytomedicine*, 18(5): 414–424.

Bramati, L., Minoggio, M., Gardana, C., Simonetti, P., Mauri, P. & Pietta, P. 2002. Quantitative characterization of flavonoid compounds in Rooibos tea (*Aspalathus linearis*) by LC-UV/DAD. *Journal of Agricultural and Food Chemistry*, 50(20): 5513–5519.

Breiter, T., Laue, C., Kressel, G., Gröll, S., Engelhardt, U.H. & Hahn, A. 2011. Bioavailability and antioxidant potential of rooibos flavonoids in humans following the consumption of different rooibos formulations. *Food Chemistry*, 128(2): 338–347. http://dx.doi.org/10.1016/j.foodchem.2011.03.029.

Canda, B.D., Oguntibeju, O.O. & Marnewick, J.L. 2014. Effects of Consumption of Rooibos (*Aspalathus linearis*) and a Rooibos-Derived Commercial Supplement on Hepatic Tissue Injury by tert-Butyl Hydroperoxide in Wistar Rats. *Oxidative Medicine and Cellular Longevity*, 2014: 1–9.

Chen, W., Resmala, I., Wang, E., Joubert, E., Wyk, B. Van & Wink, M. 2013. Ameliorative effect of aspalathin from rooibos (*Aspalathus linearis*) on acute oxidative stress in Caenorhabditis elegans. *Phytomedicine*, 20: 380–386. http://dx.doi.org/10.1016/j.phymed.2012.10.006.

Cheney, R.H. & Elizabeth, S. 1963. Rooibos Tea, a South African Contribution to World

Beverages. *Economic Botany*, 17(3): 186–194.

Christo, J.F., Joubert, E., Pheiffer, C. & Ghoor, S. 2013. Z-2-(*β-D*-glucopyranosyloxy)-3-phenylpropenoic acid, an α-hydroxy acid from rooibos (*Aspalathus linearis*) with hypoglycemic activity. *Mol. Nutr. Food Res.*, 57: 2216–2222.

Corcoran, M.P., Mckay, D.L., Blumberg, J.B., Corcoran, M.P., Mckay, D.L. & Blumberg, J.B. 2012. Flavonoid Basics: Chemistry, Sources, Mechanisms of Action, and Safety. *Journal of Nutrition in Gerontology and Geriatrics*, 31: 176–189.

Cullere, M., Hoffman, L.C. & Zotte, A.D. 2013. First evaluation of unfermented and fermented rooibos (*Aspalathus linearis*) in preventing lipid oxidation in meat products. *Meat Science*, 95: 72–77. http://dx.doi.org/10.1016/j.meatsci.2013.04.018.

Damiani, E., Carloni, P., Rocchetti, G., Senizza, B., Tiano, L., Joubert, E., Beer, D. De & Lucini, L. 2019. Impact of Cold versus Hot Brewing on the Phenolic Profile and Antioxidant Capacity of Rooibos (*Aspalathus linearis*) Herbal Tea. *Antioxidants*, 8(499): 1–19.

Diallo, A, Beye, A.C., Doyle, T.B., Park, E., Maaza, M., Beye, A.C., Doyle, T.B., Park, E. & Green, M.M. 2015. Green synthesis of Co 3 O 4 nanoparticles via *Aspalathus linearis*: Physical properties. *GREEN CHEMISTRY LETTERS AND REVIEWS*, 8(3–4): 30–36.

Diallo, A., Kaviyarasu, K., Ndiaye, S., Mothudi, B.M., Ishaq, A. & Rajendran, V. 2018. Structural, optical and photocatalytic applications of biosynthesized NiO nanocrystals. *GREEN CHEMISTRY LETTERS AND REVIEWS*, 11(2): 166–175.

Diallo, A, Manikandan, E., Rajendran, V. & Maaza, M. 2016. Physical & enhanced photocatalytic properties of green synthesized SnO 2 nanoparticles via *Aspalathus linearis*. *Journal of Alloys and Compounds*, 681: 561–570. http://dx.doi.org/10.1016/j.jallcom.2016.04.200.

Diallo, Abdoulaye, Mothudi, B.M., ElayaperumalManikandan & Maaza, M. 2016. Luminescent Eu2O3 nanocrystals by *Aspalathus linearis*' extract: structural and optical properties. *Journal of Nanophotonics*, 10(2): 026010-1-026010–12.

Diallo, A., Ngom, B.D., Park, E. & Maaza, M. 2015. Green synthesis of ZnO nanoparticles by *Aspalathus linearis*: Structural & optical properties. *Journal of Alloys and Compounds*, 646: 425–430. http://dx.doi.org/10.1016/j.jallcom.2015.05.242.

Dialloa, A., Doyle, T.B., Mothudi, B.M., Manikandan, E., Rajendran, V. & Maaza, M. 2017. Magnetic behaviour of biosynthesized Co_3O_4 nanoparticles. *Journal of Magnetism and Magnetic Materials*, 424 (October 2016): 251–255. http://dx.doi.org/10.1016/j.jmmm.2016.10.063.

Dludla, P. V., Muller, C.J.F., Louw, J., Joubert, E., Salie, R., Opoku, A.R. & Johnson, R. 2014. The cardioprotective effect of an aqueous extract of fermented rooibos (*Aspalathus linearis*) on cultured cardiomyocytes derived from diabetic rats. *Phytomedicine*, 21: 595–601. http://dx.doi.org/10.1016/j.phymed.2013.10.029.

Dludla, P. V, Johnson, R., Mazibuko-mbeje, S.E., Muller, C.J.F., Louw, J., Joubert, E., Orlando, P., Silvestri, S., Chellan, N., Nkambule, B.B., Essop, M.F. & Tiano, L. 2020. Fermented rooibos extract attenuates hyperglycemia-induced myocardial oxidative damage by improving mitochondrial energetics and intracellular antioxidant capacity. *South African Journal of Botany*, 131: 143–150. https://doi.org/10.1016/j.sajb.2020.02.003.

Dludla, P. V, Joubert, E., Muller, C.J.F., Louw, J. & Johnson, R. 2017. Hyperglycemia-induced oxidative stress and heart disease-cardioprotective effects of rooibos flavonoids and phenylpyruvic acid-2- *O* - *β* -*D*-glucoside. *Nutrition & Metabolism*, 14(45): 1–18.

Dludla, P. V, Muller, C.J.F., Joubert, E., Louw, J., Essop, M.F., Gabuza, K.B., Ghoor, S. & Huisamen, B. 2017. Aspalathin Protects the Heart against Hyperglycemia-Induced Oxidative Damage by Up-Regulating Nrf2 Expression. *Molecules*, 22(129): 1–16.

Dong, Y., Zhang, B., Sun, W. & Xing, Y. 2019. Intervention of Prediabetes by Flavonoids From *Oroxylum indicum*. In *Bioactive Food as Dietary Interventions for Diabetes*. Elsevier Inc.: 559–575. http://dx.doi.org/10.1016/B978-0-12-813822-9.00036-9.

Ferreira, D., Marais, C., Steenkamp, J.A. & Joubert, E. 1995. Rooibos tea as a likely health food supplement. In *Proceedings of Recent Development of Technologies on Fundamental Foods for Health*. 73–88.

Freund, H.-J., Nilius, N., Menzel, D. & Watanabe, K. 2006. Photochemistry on Metal Nanoparticles. *Chemical Reviews*, 106(10): 4301–4320.

Gadow, A. Von, Joubert, E. & Hansmann, C.F. 1997. Comparison of the Antioxidant Activity of Aspalathin with That of Other Plant Phenols of Rooibos Tea (*Aspalathus linearis*), γ - Tocopherol, BHT, and BHA. *J. Agric. Food Chem.*, 45: 632–638.

Gangadoo, S., Taylor-Robinson, A. & Chapman, J. 2015. Nanoparticle and biomaterial characterisation techniques. *Materials Technology*, 30(B1): B44–B56.

Gelderblom, W.C.A., Joubert, E., Gamieldien, K., Sissing, L., Malherbe, C.J. & Maritz, G. 2016. Rooibos (*Aspalathus linearis*), honeybush (*Cyclopia intermedia*) and cancer bush (*Sutherlandia frutescens* subsp. microphylla) protect against tobacco-specific mutagenesis in vitro. *South African Journal of Botany*. http://dx.doi.org/10.1016/j.sajb.2016.06.004.

Habu, T., Flath, R.A., Mon, T.R. & Morton, J.F. 1985. Volatile Components of Rooibos Tea (*Aspalathus linearis*). *Journal of Agricultural and Food Chemistry*, 33(2): 249–254.

Hawkins, H.J., Malgas, R. & Biénabe, E. 2011. Ecotypes of wild rooibos (*Aspalathus linearis* (Burm. F) Dahlg., Fabaceae) are ecologically distinct. *South African Journal of Botany*, 77(2): 360–370.

Heerden, F.R. Van, Wyk, B. Van & Viljoen, A.M. 2003. Phenolic variation in wild populations of *Aspalathus linearis* (rooibos tea). *Biochemical Systematics and Ecology*, 31(2003): 885–895.

Heinrich, T., Willenberg, I. & Glomb, M.A. 2012. Chemistry of Color Formation during Rooibos Fermentation. *Journal of Agricultural and Food Chemistry*, 60: 5221−5228.

Hillis, W.E. & Inoue, T. 1967. The polyphenols of NOTHOFAGUS SPECIES-II. THE HEARTWOOD OF NOTHOFAGUS FUSCA. *phytochemistry*, 6: 59–67.

Himpe, E., Cunha, D.A., Song, I., Bugliani, M., Marchetti, P., Cnop, M. & Bouwens, L. 2016. Phenylpropenoic Acid Glucoside from Rooibos Protects Pancreatic Beta Cells against Cell Death Induced by Acute Injury. *PLoS ONE*, 11(6): 1–13.

Hong, I.-S., Lee, H.-Y. & Kim, H.-P. 2014. Anti-Oxidative Effects of Rooibos Tea (Aspalathus linearis) on Immobilization-Induced Oxidative Stress in Rat Brain. *PL0S ONE*, 9(1): 1–9.

Huang, C.F., Gan, X.W., Bai, H.Y., Ma, L. & Hu, L.H. 2008. Schoepfin A, B, C: three new chalcone C-glycosides from *Schoepfia chinensis*. *Natural Product Research*, 22(7): 623–627.

Ismail, E. 2017. Molecular Nanotechnology Green Biosynthesis of Rhodium Nanoparticles Via *Aspalathus linearis*. : 2–8.

Ismail, E., Diallo, A., Khenfouch, M., Dhlamini, S.M. & Maaza, M. 2016. RuO 2 nanoparticles by a novel green process via *Aspalathus linearis* natural extract & their water-splitting response. *Journal of Alloys and Compounds*, 662: 283–289.

Ismail, E., Khamlich, S., Dhlamini, M. & Maaza, M. 2016. Green biosynthesis of ruthenium oxide nanoparticles on nickel foam as electrode material for supercapacitor applications. *Royal Society of Chemistry*, 6(1): 86843–86850.

Ismail, E., Khenfouch, M., Dhlamini, M., Dube, S. & Maaza, M. 2017. Green palladium and palladium oxide nanoparticles synthesized via *Aspalathus linearis* natural extract. *Journal of Alloys and Compounds*, 695: 3632–3638.

Johnson, R., Beer, D. De, Dludla, P. V, Ferreira, D., Muller, C.J.F. & Joubert, E. 2018. Aspalathin from Rooibos (*Aspalathus linearis*): A Bioactive C -glucosyl Dihydrochalcone

with Potential to Target the Metabolic Syndrome Natural source. *Planta Med*, 84: 568–583.

Johnson, R., Dludla, P. V, Muller, C.J.F., Huisamen, B., Essop, M.F. & Louw, J. 2017. The Transcription Profile Unveils the Cardio-Protective Effect of Aspalathin against Lipid Toxicity in an In Vitro H9c2 Model. *Molecules*, 22(219): 1–17.

Johnson, R., Shabalala, S., Louw, J., Kappo, A.P. & Muller, C.J.F. 2017. Aspalathin Reverts Doxorubicin-Induced. *Molecules*, 22(1589).

Joubert, E. 1996. HPLC quantification of the dihydrochalcones, aspalathin and nothofagin in rooibos tea (*Aspalathus linearis*) as affected by processing. *Food Chemistry*, 55(4): 403–411.

Joubert, E. & Beer, D. De. 2014. *Antioxidants of Rooibos Beverages : Role of Plant Composition and Processing*. Elsevier.

Joubert, E. & Beer, D. De. 2012. Phenolic content and antioxidant activity of rooibos food ingredient extracts. *Journal of Food Composition and Analysis*, 27(1): 45–51.

Joubert, E. & Beer, D. De. 2011. Rooibos (*Aspalathus linearis*) beyond the farm gate: From herbal tea to potential phytopharmaceutical. *South African Journal of Botany*, 77(4):

Joubert, E., Gelderblom, W.C.A., Louw, A. & de Beer, D. 2008. South African herbal teas: *Aspalathus linearis*, *Cyclopia* spp. and *Athrixia phylicoides*-A review. *Journal of Ethnopharmacology*, 119: 376–412.

Joubert, E. & Schulz, H. 2006. Production and quality aspects of rooibos tea and related products. A review. *Journal of Applied Botany and Food Quality*, 80: 138–144.

Kamakura, R., Jin Son, M., Beer, D. de, Elizabeth, J., Miura, Y. & Kazumi, Y. 2015. Antidiabetic effect of green rooibos (*Aspalathus linearis*) extract in cultured cells and type 2 diabetic model KK-Ay mice. *Cytotechnology*, 67: 699–710. http://dx.doi.org/10.1007/s10616-014-9816-y.

Kanu, S.A., Okonkwo, J.O. & Dakora, F.D. 2013. *Aspalathus linearis* (Rooibos tea) as potential phytoremediation agent : a review on tolerance mechanisms for aluminium uptake. *Environ. Rev*, 92(March): 85–92.

Kawakami, M., Kobayashi, A. & Kator, K. 1993. Volatile constituents of rooibos tea (*Aspalathus linearis*) as affected by extraction process. *J. Agric. Food Chem.*, 41: 633–636.

Kawano, A., Nakamura, H., Hata, S., Minakawa, M., Miura, Y. & Yagasaki, K. 2009. Hypoglycemic effect of aspalathin, a rooibos tea component from *Aspalathus linearis*, in type 2 diabetic model db/db mice. *Phytomedicine*, 16: 437–443.

Khan, Ibrahim, Saeed, K. & Khan, Idrees. 2017. Nanoparticles: Properties, applications and toxicities. *Arabian Journal of Chemistry*.

Koeppen, B.H. & Roux, D.. 1966. C-Glycosylflavonoids the chemistry of aspalathin. *Biochemical Journal*, 99: 604–609.

Koeppen, B.H., Smit, J.B. & Roux, D.G. 1962. The flavone C-glycosides and flavonol O-glycosides of *Aspalathus acuminatus* (rooibos tea). *Biochemical Journal*, 83: 507–511.

Krafczyk, N. & Glomb, M.A. 2008. Characterization of Phenolic Compounds in Rooibos tea. *Journal of Agricultural and Food Chemistry*, 56: 3368–3376.

Krafczyk, N., Heinrich, T., Porzel, A. & Glomb, M. 2009. Oxidation of the dihydrochalcone Aspalathin leads to dimerization. *J. Agric. Food Chem.*, 57: 6838–6843.

Krafczyk, N., Woyand, F. & Glomb, M.A. 2009. Structure–antioxidant relationship of flavonoids from fermented rooibos. *Mol. Nutr. Food Res.*, 53: 635–642.

Ku, S., Kwak, S., Kim, Y. & Bae, J. 2015. Aspalathin and Nothofagin from Rooibos (*Aspalathus linearis*) Inhibit High Glucose-Induced Inflammation In Vitro and In Vivo. *Inflammation*, 38(1): 445–455.

Kucharská, J., Ná, O.U.L.I.Č., Gvozdjáková, A., Sumbalová, Z., Ová, O.V.A.N.Č., Božek, P., Nakano, M. & Greksák, M. 2004. Regeneration of Coenzyme Q 9 Redox State and Inhibition of Oxidative Stress by Rooibos Tea (*Aspalathus linearis*) Administration in Carbon Tetrachloride Liver Damage. : 515–521.

Kwak, S., Han, M.S. & Bae, J.S. 2015. Aspalathin and nothofagin from rooibos (*Aspalathus linearis*) inhibit endothelial protein C receptor shedding in vitro and in vivo. *Fitoterapia*, 100: 179–186.

Layman, J.I., Pereira, D.L., Chellan, N., Huisamen, B. & Kotzé, S.H. 2019. A histomorphometric study on the hepatoprotective effects of a green rooibos extract in a diet-induced obese rat model. *Acta Histochemica*, 121(5): 646–656. https://doi.org/10.1016/j.acthis.2019.05.008.

Lee, E.-J. & Jang, H.-D. 2004. Antioxidant activity and protective effect on DNA strand scission of Rooibos tea (*Aspalathus linearis*). *BioFactors*, 21: 285–292.

Lee, W. & Bae, J. 2015. Anti-inflammatory Effects of Aspalathin and Nothofagin from Rooibos (*Aspalathus linearis*) In Vitro and In Vivo. *Inflammation*, 38(4): 1502–1516.

Lee, W., Kim, K. & Bae, J. 2015. Ameliorative Effect of Aspalathin and Nothofagin from Rooibos (*Aspalathus linearis*) on HMGB1-Induced Septic Responses In Vitro and In Vivo. *The American Journal of Chinese Medicine*, 43(5): 1–22.

Liu, H., Mou, Y., Zhao, J., Wang, J., Zhou, L., Wang, M., Wang, D., Han, J., Yu, Z. & Yang, F. 2010. Flavonoids from Halostachys caspica and Their Antimicrobial and Antioxidant Activities. *Molecules 2*, 15: 7933–7945.

Luisa, F. & Duncan, S. 2013. *Nanotechnologies: Principles, Applications, Implications and Hands-on Activities.* First. M. Bonazzi, ed. Luxembourg: Luxembourg: Publications Office of the European Union, 2012.

Maarman, G. 2019. Cardioprotection conferred by rooibos (*Aspalathus linearis*): A mini review to highlight a potential mechanism of action. *South African Journal of Science*, 115(7/8): 1–4.

Magcwebeba, T., Swart, P., Swanevelder, S., Joubert, E. & Gelderblom, W. 2016. Anti-Inflammatory Effects of *Aspalathus linearis* and Cyclopia spp. Extracts in a UVB/Keratinocyte (HaCaT) Model Utilising Interleukin-1 Accumulation as Biomarker. *Molecules*, 21(1323): 1–21.

Malgas, R.R., Potts, A.J., Oettlé, N.M., Koelle, B., Todd, S.W., Verboom, G.A. & Hoffman, M.T. 2010. Distribution, quantitative morphological variation and preliminary molecular analysis of different growth forms of wild rooibos (*Aspalathus linearis*) in the northern Cederberg and on the Bokkeveld Plateau. *South African Journal of Botany*, 76(2010):

Manley, M., Joubert, E. & Botha, M. 2006. Quantification of the major phenolic compounds, soluble solid content and total antioxidant activity of green rooibos (*Aspalathus linearis*) by means of near infrared spectroscopy. , 222: 213–222.

Maria A, S., Wyk, B. Van, Taylor, M.J.C. & Long, H.S. 2017. Analysis of Phenolic Compounds in Rooibos Tea (*Aspalathus linearis*) with a Comparison of Flavonoid-Based Compounds in Natural Populations of Plants from Different Regions. *J. Agric. Food Chem*, 65: 10270–10281.

Marnewick, J., Joubert, E., Swart, P. & Westhuizen, F. van der. 2003. Modulation of Hepatic Drug Metabolizing Enzymes and Oxidative Status by Rooibos (*Aspalathus linearis*) and Honeybush (*Cyclopia intermedia*), Green and Black (*Camellia sinensis*) Teas in Rats. *Journal of Agricultural and Food Chemistry 2003*, 51: 8113−8119.

Marnewick, J.L., Batenburg, W., Swart, P., Joubert, E., Swanevelder, S. & Gelderblom, W.C.A. 2004. Ex vivo modulation of chemical-induced mutagenesis by subcellular liver fractions of rats treated with rooibos (*Aspalathus linearis*) tea, honeybush (*Cyclopia intermedia*) tea, as well as green and black (*Camellia sinensis*) teas. *Mutation Research*, 558: 145–154.

Marnewick, J.L., Rautenbach, F., Venter, I., Neethling, H., Blackhurst, D.M., Wolmarans, P. &

MacHaria, M. 2011. Effects of rooibos (*Aspalathus linearis*) on oxidative stress and biochemical parameters in adults at risk for cardiovascular disease. *Journal of Ethnopharmacology*, 133(1): 46–52.

Marnewick, J.L., Westhuizen, F.H. Van Der, Joubert, E., Swanevelder, S., Swart, P. & Gelderblom, W.C.A. 2009. Chemoprotective properties of rooibos (*Aspalathus linearis*), honeybush (*Cyclopia intermedia*) herbal and green and black (*Camellia sinensis*) teas against cancer promotion induced by fumonisin B_1 in rat liver. *Food and Chemical Toxicology*, 47(1): 220–229.

Martins, S., Mussatto, S.I., Martínez-Avila, G., Montañez-Saenz, J., Aguilar, C.N. & Teixeira, J.A. 2011. Bioactive phenolic compounds: Production and extraction by solid-state fermentation. A review. *Biotechnology Advances*, 29(3): 365–373.

Mata, R., Nakkala, J.R. & Sadras, S.R. 2016. Polyphenol stabilized colloidal gold nanoparticles from *Abutilon indicum* leaf extract induce apoptosis in HT-29 colon cancer cells. *Colloids and Surfaces B: Biointerfaces*, 143: 499–510.

Mazibuko-mbeje, S.E., Dludla, P. V, Roux, C., Johnson, R., Ghoor, S., Joubert, E., Louw, J., Opoku, A.R. & Muller, C.J.F. 2019. Aspalathin-Enriched Green Rooibos Extract Reduces Hepatic Insulin Resistance by Modulating PI3K/AKT and AMPK Pathways. *International Journal of Molecular Science*, 20(633): 1–16.

Mazibuko-Mbeje, S.E., DludlaI, P. V., Johnson, R., Joubert, E., Louw, J., Ziqubu, K., Tiano, L., Silvestri, S., Orlando, P., Opoku, A.R. & Muller, C.J.F. 2019. Aspalathin, a natural product with the potential to reverse hepatic insulin resistance by improving energy metabolism and mitochondrial respiration. *PLoS ONE*, 14(5): 1–16.

Mazibuko, S.E., Muller, C.J.F., Joubert, E., Beer, D. De, Johnson, R., Opoku, A.R. & Louw, J. 2013. Amelioration of palmitate-induced insulin resistance in C2C12 muscle cells by rooibos (*Aspalathus linearis*). *Phytomedicine*, 20: 813–819. http://dx.doi.org/10.1016/j.phymed.2013.03.018.

Mckay, D.L. & Blumberg, J.B. 2007. A Review of the Bioactivity of South African Herbal Teas: Rooibos (*Aspalathus linearis*) and Honeybush (*Cyclopia intermedia*). *Phytotherapy Research*, 16(July 2006): 1–16.

Mekni, M., Azez, R., Tekaya, M., Mechri, B. & Hammami, M. 2013. Phenolic, non-phenolic compounds and antioxidant activity of pomegranate flower, leaf and bark extracts of four Tunisian cultivars. *Journal of Medicinal Plants Research*, 7(17): 1100–1107.

Morton, J.F. 1983. Rooibos Tea, *Aspalathus linearis*, a Caffeineless, Low-Tannin Beverage. *Economic Botany*, 37(2): 164–173.

Muller, C.J.F., Joubert, E., Beer, D. De, Sanderson, M., Malherbe, C.J., Fey, S.J. & Louw, J. 2012. Acute assessment of an aspalathin-enriched green rooibos (*Aspalathus linearis*) extracts with hypoglycemic potential. *Phytomedicine*, 20: 32–39.

Muller, C.J.F., Malherbe, C.J., Chellan, N., Miura, Y. & Joubert, E. 2018. Potential of rooibos, its major C-glucosyl phenylpropenoic acid in the prevention of metabolic syndrome. *Critical Reviews in Food Science and Nutrition.*, 58(2).

Nakano, M., Itoh, Y., Mizuno, T. & Nakashima, H. 1997. Polysaccharide from Aspalathus linearis with Strong Anti-HIV Activity Polysaccharide from Aspalathus linearis with Strong Anti-HIV Activity. *Biosci. Biotech. Biochem.*, 61(2): 267--271.

Nana, M., Junko, T., Ayumi, S., Akiko, N., Mayumi, S., Motoshi, K., Shuichi, H. & Eri, H. 2015. Green Rooibos Extract from *Aspalathus linearis*, and its Component, Aspalathin, Suppress Elevation of Blood Glucose Levels in Mice and Inhibit α-amylase and α-glucosidase Activities in vitro. *Food Science and Technology Research*, 21(2): 231–240.

Nishimachi, S., Iwai, T., Nakamura, Y., Yuyama-masuda, K., Tsutsui, T., Monoi, N., Uchiyama, A. & Nakamura, S. 2019. Rooibos (*Aspalathus linearis*) extract, containing eriodictyol-6-C-β-D-glucoside as the active component, stimulates exocrine glands via the M3 muscarinic acetylcholine receptor. *Journal of Functional Foods*, 55(January): 248–254.

Noluthando, M., Mongwaketsi, N., Khamlich, S., Kaviyarasu, K., Matinise, Nolubalbao & Maaza, M. 2018. Green synthesis of nickel oxide, palladium and palladium oxide synthesized via *Aspalathus linearis* natural extracts : physical properties & mechanism of formation. *Applied Surface Science*, 446: 266–272. https://doi.org/10.1016/j.apsusc.2017.12.116.

Noluthando, M., Mongwaketsi, N., Khamlich, S., Kaviyarasu, K., Matinise, Nolubabalo & Malik, M. 2018. Green synthesis of zin tin oxide ($ZnSnO_3$) nanoparticles using *Aspalathus Linearis* natural extracts : Structural, morphological, optical and electrochemistry study. *Applied Surface Science*, 446: 250–257.

Noruzi, M. 2014. Biosynthesis of gold nanoparticles using plant extracts. *Bioprocess Biosyst Eng*, (August 2014).

Nune, S.K., Chanda, N., Shukla, R., Katti, Kavita, Kulkarni, R.R., Thilakavathy, S., Mekapothula, S. & Katti, Kattesh V. 2009. Green nanotechnology from tea: phytochemicals in tea as building blocks for production of biocompatible gold nanoparticles. *Journal of Materials Chemistry*, 19: 2912–2920.

Orzel, J., Daszykowski, M., Kazura, M., Beer, D. De, Joubert, E., Schulze, A.E., Beelders, T., Villiers, A. De, Malherbe, C.J. & Walczak, B. 2014. Modeling of the total antioxidant

capacity of rooibos (*Aspalathus linearis*) tea infusions from chromatographic fingerprints and identification of potential antioxidant markers. *Journal of Chromatography A*, 1366: 101–109.

Oteiza, P.I., Erlejman, A.G., Verstraeten, S. V & Keen, C.L. 2005. Flavonoid-membrane interactions : A protective role of flavonoids at the membrane surface ? *Clinical & Developmental Immunology*, 12(1): 19–25.

Oyagi, M.O., Michira, I.N., Guto, P., Baker, P.G.L. & Kamau, G. 2014. Polydisperse Low Diameter 'Non-toxic' Silver Nanoparticles Encapsulated by Rooibos Tea Templates. *Nano Hybrids*, 8(2014): 57–72.

Pantsi, W.G., Marnewick, J.L., Esterhuyse, A.J., Rautenbach, F. & Van Rooyen, J. 2011. Rooibos (*Aspalathus linearis*) offers cardiac protection against ischaemia/reperfusion in the isolated perfused rat heart. *Phytomedicine*, 18(14): 1220–1228.

Parasuraman, S. & Maithili, K.. 2014. Antioxidant and drug metabolism. *Free Radicals and Antioxidants*, 4(1): 1–2.

Patel, O., Muller, C., Joubert, E., Louw, J. & Rosenkranz, B. 2016. Inhibitory Interactions of *Aspalathus linearis* (Rooibos) Extracts and Compounds, Aspalathin and Z-2-(β-D-Glucopyranosyloxy)-3-phenylpropenoic Acid, on Cytochromes Metabolizing Hypoglycemic and Hypolipidemic Drugs. *Molecules*, 21(1515): 1–13.

Peralta-Videa, J.R., Huang, Y., Parsons, J.G., Zhao, L., Lopez-Moreno, L., Hernandez-Viezcas, J.A. & Gardea-Torresdey, J.L. 2016. Plant-based green synthesis of metallic nanoparticles: scientific curiosity or a realistic alternative to chemical synthesis? *Nanotechnology for Environmental Engineering*, 1(4): 1–29.

Pieme, C.A., Tatangmo, J.A., Simo, G., Cabral, P., Nya, B., Jocelyne, V., Moor, A., Moukette, B.M., Nzufo, F.T., Legrand, B., Nono, N. & Sobngwi, E. 2017. Relationship between hyperglycemia, antioxidant capacity and some enzymatic and non-enzymatic antioxidants in African patients with type 2 diabetes. *BMC Research Notes*, 10(141): 1–7.

Pingle, N.A., Koekemoer, T.C., Holzer, A., Young, C., Venables, L. & Venter, M. van de. 2018. Potential Therapeutic Benefits of Green and Fermented Rooibos (*Aspalathus linearis*) in Dermal Wound Healing. *Planta Medica*.

Pyrzanowska, J., Fecka, I., Mirowska-Guzel, D., Joniec-Maciejak, I., Blecharz-Klin, K., Piechal, A., Wojnar, E. & Widy-Tyszkiewicz, E. 2019. Long-term administration of *Aspalathus linearis* infusion affects spatial memory of adult Sprague-Dawley male rats as well as increases their striatal dopamine content. *Journal of Ethnopharmacology*, 238(March): 111881.

Pyrzanowska, J., Joniec-maciejak, I., Blecharz-klin, K., Piechal, A., Mirowska-Guzel, D., Fecka, I. & Widy-Tyszkiewicz, E. 2021. *Aspalathus linearis* infusion affects hole-board test behaviour and amino acid concentration in the brain. *Neuroscience Letters*, 747(135680): 1–7.

Rabe, C., Steenkamp, J.A., Joubert, E., Burger, J.F.W. & Ferreira, D. 1994. Phenolic metabolites from rooibos tea (*Aspalathus linearis*). *Phytochemistry*, 35(6): 1559–1565.

Rahmasari, R., Haruyama, T., Charyasriwong, S., Nishida, T. & Kobayashi, N. 2017. Antiviral Activity of *Aspalathus linearis* against Human Influenza Virus. *Natural Product Communications*, 12(4): 1–4.

Rietjens, I.M.C.M., Louisse, J. & Beekmann, K. 2017. The potential health effects of dietary phytoestrogens. *British Journal of Pharmacology*, 174: 1263–1280.

Rodriguez, A., David, M., Christian, V., Shanmuganayagam, D., Reed, J., Calani, L., Mena, P., Del, D. & Alan, R. 2014. Bioavailability, bioactivity and impact on health of dietary flavonoids and related compounds : an update. *Arch Toxicol*, 88: 1803–1853.

Sanderson, M., Mazibuko, S.E., Joubert, E., Beer, D. De, Johnson, R., Pheiffer, C., Louw, J. & Muller, C.J.F. 2014. Effects of fermented rooibos (*Aspalathus linearis*) on adipocyte differentiation. *Phytomedicine*, 21: 109–117.

Santhoshkumar, J., Rajeshkumar, S. & Venkat Kumar, S. 2017. Phyto-assisted synthesis, characterization and applications of gold nanoparticles – A review. *Biochemistry and Biophysics Reports*, 11(May): 46–57. http://dx.doi.org/10.1016/j.bbrep.2017.06.004.

Santos, J.S., Deolindo, C.T.P., Esmerino, L.A., Genovese, M.I., Fujita, A., Marques, M.B., Rosso, N.D., Daguer, H., Valese, A.C. & Granato, D. 2016. Effects of time and extraction temperature on phenolic composition and functional properties of red rooibos (*Aspalathus linearis*). *Food Research International*, 89: 476–487.

Santos, J.S., Deolindo, C.T.P., Ho, J.F., Chaves, F.C., Prado-silva, L., Sant, A.S., Azevedo, L., Araújo, M. & Granato, D. 2018. Optimized *Camellia sinensi*s var. sinensis, *Ilex paraguariensis*, and *Aspalathus linearis* blend present high antioxidant and antiproliferative activities in a beverage model. , 254(February): 348–358.

Sasaki, M., Nishida, N. & Shimada, M. 2018. A Beneficial Role of Rooibos in Diabetes Mellitus : A Systematic Review and Meta-Analysis. *Molecules*, 23(89): 1–15.

Schloms, L., Storbeck, K.H., Swart, P., Gelderblom, W.C.A. & Swart, A.C. 2012. The influence of *Aspalathus linearis* (Rooibos) and dihydrochalcones on adrenal steroidogenesis: Quantification of steroid intermediates and end products in H295R cells. *Journal of Steroid Biochemistry and Molecular Biology*, 128(3–5): 128–138.

Sengani, M., Grumezescu, A.M. & Rajeswari, V.D. 2017. Recent trends and methodologies in gold nanoparticle synthesis – A prospective review on drug delivery aspect. *OpenNano*, 2(July): 37–46.

Shimamura, N., Miyase, T., Umehara, K., Warashina, T. & Fujii, S. 2006. Phytoestrogens from *Aspalathus linearis*. *Biol. Pharm. Bull.*, 29(June): 1271–1274.

Shimoi, K., Hokabe, Y., Sasaki, Y.F., Yamada, H. & Kator, K. 1994. Inhibitory Effect of Rooibos Tea (*Aspalathus linearis*) on the Induction of Chromosome Aberrations In Vivo and In Vitro. In *FOOD PHYTOCHEMICALS II: TEAS, SPICES, AND HERBS*. ACS Symposium Series; American Chemical Society: Washington, DC, 1994.: 105–113.

Da Silva Pinto, M. 2013. Tea: A new perspective on health benefits. *Food Research International*, 53(2): 558–567.

Sirotkin, A. V & Halim, A. 2014. Phytoestrogens and their effects. *European Journal of Pharmacology*, 741: 230–236.

Smit, S.E., Johnson, R., Vuuren, M.A. Van & Huisamen, B. 2017. Myocardial Glucose Clearance by Aspalathin Treatment in Young, Mature, and Obese Insulin-Resistant Rats Authors. *Planta Med*: 1–8.

Smith, C. & Swart, A. 2018. *Aspalathus linearis* (Rooibos) – a functional food targeting cardiovascular disease. *Royal Society of Chemistry Food and Function*, 9(1).

Smith, C. & Swart, A.C. 2016. Rooibos (*Aspalathus linearis*) facilitates an anti-inflammatory state, modulating IL-6 and IL-10 while not inhibiting the acute glucocorticoid response to a mild novel stressor in vivo. *Journal of Functional Foods*, 27: 42–54.

Snijman, P.W., Swanevelder, S., Joubert, E., Green, I.R. & Gelderblom, W.C.A. 2007. The antimutagenic activity of the major flavonoids of rooibos (*Aspalathus linearis*): Some dose-response effects on mutagen activation-flavonoid interactions. *Mutation Research - Genetic Toxicology and Environmental Mutagenesis*, 631(2): 111–123.

Snyckers, F.. & Salemi, G. 1974. Studies of South African medicinal plants. Part 1 quercetin as the major in vitro active component of rooibos tea. *Journal of the South African Chemical Institute*, XXVII: 5–7.

Srikar, S.K., Giri, D.D., Pal, D.B., Mishra, P.K. & Upadhyay, S.N. 2016. Green Synthesis of Silver Nanoparticles: A Review. *Green and Sustainable Chemistry*, 6(February): 34–56.

Stander, M.A., Van Wyk, B.E., Taylor, M.J.C. & Long, H.S. 2017. Analysis of Phenolic Compounds in Rooibos Tea (*Aspalathus linearis*) with a Comparison of Flavonoid-Based Compounds in Natural Populations of Plants from Different Regions. *Journal of*

Agricultural and Food Chemistry, 65(47): 10270–10281.

Tahir, K., Nazir, S., Ahmad, A., Li, B., Ullah, A., Ul, Z., Khan, H., Ullah, F., Ullah, Q., Khan, A. & Ur, A. 2017. Facile and green synthesis of phytochemicals capped platinum nanoparticles and in vitro their superior antibacterial activity. *Journal of Photochemistry & Photobiology, B: Biology*, 166(2017): 246–251.

Takara, K., Matsui, D., Wada, K., Ichiba, T. & Nakasone, Y. 2002. New antioxidative phenolic glycosides isolated from *kokuto* non-centrifuged cane sugar. *Bioscience, Biotechnology and Biochemistry*, 66(1): 29–35.

Timothy, B.J. & Derbyshire, E.J. 2020. Rooibos Tea and Health: A Systematic Review of the Evidence from the Last Two Decades. *Nutrition and Food Technology*, 6(1): 1–11.

Tsuchiya, H. 2010. Structure-dependent membrane interaction of flavonoids associated with their bioactivity. *Food Chemistry*, 120(4): 1089–1096.

Tsukuba, I. 2000. The Structure and Distribution of the Flavonoids in Plants. *Journal of Plant Research.*, 113: 287–299.

Uličná, O., Vančová, O., Waczulíková, I., Božek, P., Janega, P., Babál, P. & Líšková, S. 2008. intoxication by carbon tetrachloride ? Does rooibos tea (*Aspalathus linearis*) support regeneration of rat liver after intoxication by carbon tetrachloride ? *General Physiology and Biophysics ·*, 27: 179–186.

Unathi, T., Riedel, S., Swanevelder, S., Swart, P. & Beer, D. De. 2016. The potential role of polyphenols in the modulation of skin cell viability by *Aspalathus linearis* and Cyclopia spp. herbal tea extracts in vitro. *Journal of Pharmacy and Pharmacology*, 68: 1440–1453.

Viljoen, M., Muller, M., Beer, D. De & Joubert, E. 2016. Identification of broad-based sensory attributes driving consumer preference of ready-to-drink rooibos iced tea with increased aspalathin content. *South African Journal of Botany*. http://dx.doi.org/10.1016/j.sajb.2016.07.019.

Villaño, D., Pecorari, M., Testa, M.F., Raguzzini, A., Stalmach, A., Crozier, A., Tubili, C. & Serafini, M. 2010. Unfermented and fermented rooibos teas (*Aspalathus linearis*) increase plasma total antioxidant capacity in healthy humans. *Food Chemistry*, 123(3): 679–683.

Voliani, V. 2013. *Update on Gold Nanoparticles From Cathedral Windows to Nanomedicine*. First. Smithers Rapra Technology Ltd, 2013. www.polymer-books.com.

Waisundara, V.Y. & Yian, L. 2015. Free radical scavenging ability of *Aspalathus linearis* in two in vitro models of diabetes and cancer. *Journal of Traditional Complementary Medicine*, 5: 174–178. http://dx.doi.org/10.1016/j.jtcme.2014.11.009.

Wyk, B. Van & Gorelik, B. 2016. The history and ethnobotany of Cape herbal teas. *South African Journal of Botany*. http://dx.doi.org/10.1016/j.sajb.2016.11.011.

Wyk, B. Van & Verdoorn, G.H. 2000. Alkaloids of the genera *Aspalathus*, *Rafnia* and *Wiborgia* (Fabaceae - Crotalarieae). *South African Journal of Botany*, 55(5): 520–522.

Yamasaki, K., Hishiki, R., Kato, E. & Kawabata, J. 2011. Study of kaempferol glycoside as an insulin mimic reveals glycon to be the key active structure. *ACS Medicinal Chemistry Letters*, 2(1): 17–21.

Yulizar, Y., Utari, T., Ariyanta, H.A. & Maulina, D. 2017. Green Method for Synthesis of Gold Nanoparticles Using *Polyscias scutellaria* Leaf Extract under UV Light and Their Catalytic Activity to Reduce Methylene Blue. *Journal of Nanomaterials*, 2017.

2.4. Chapter 2B

Helichrysum genus and compounds activities in the management of diabetes mellitus

Akeem O. Akinfenwa [1], Ahmed A. Hussein [1]

[1] Chemistry Department, Cape Peninsula University of Technology, Bellville campus, Symphony Road, Bellville, Western Cape, South Africa. PO Box 7535 Bellville, South Africa. 217305296@mycput.ac.za (A.O.A), mohammedam@cput.ac.za (A.A.H)

Abstract

The global management of diabetes mellitus involves the administration of recommended drugs in addition to a non-sedentary lifestyle upon diagnosis. Despite the success recorded from these synthetic drugs, the traditional method of treatment using medicinal plants is increasingly accepted by the locals due to low cost and the perceived no side effects. *Helichrysum* species are used in folk medicine and are documented for the treatment of DM in different regions of the world. This review focuses on recent advances in *Helichrysum* species used for the treatment of type 2 diabetes mellitus with emphasis on its compounds and the mechanism of action. An extensive literature search via scientific databases including Science

Direct, Google Scholar, PubMed, SciFinder, JSTOR, Web of Science, and Z-library revealed the previous and current studies on the antidiabetic potential of the *Helichrysum* genus.

2.4.1. Introduction

Diabetes mellitus (DM) is a metabolic syndrome marked by increase glycogenosis and impaired glucose uptake by insulin from the bloodstream, thus, becoming a socio-economic problem. Concerted efforts by the International Diabetes Federation (IDF) and the American Diabetes Association (ADA) to reduce the spike in global diabetes and related mortality has witnessed different advocacies over the past years. The IDF (2019) report shows that 463 million (9.3%) adults worldwide are diabetes individuals and is projected to increase by 51% in 2030 (578 million) and 2045 (700 million) (Silvia Gorban et al., 2019; American Diabetes Association, 2020). During the digestion of carbohydrates, insulin secretion by β-cells of the pancreas is vital to the activity of carbohydrate hydrolysing enzymes and glucose metabolism. Glucose metabolism begins with the intake of foods, hydrolysis of carbohydrates from the to glucose through α-1,4-glycosidic bonds, and absorption of glucose in the bloodstream for energy production and utilisation. A continuous fluctuation in blood glucose occurs due to glucose utilisation from dietary intake. Excess blood glucose is taken up by β-cells of the pancreas and stored as glycogen in the liver for release when it is deficient. The β-cells of the pancreas release insulin to stimulate muscles cells and adipose tissue for uptake (IfedibaluChukwu *et a*l., 2020). Therefore, an equilibrium state of glucose release from polymeric glucose and insulin utilisation in the body cells is required for a diabetes-free life. Two types of diabetes are recorded based on heredity history, lifestyle and dietary intake of individuals are insulin-dependent (type 1) and non-insulin-dependent (type 2). The type 1 is reported to be common in children and is controlled by an autoimmune disorder resulting in a lack of insulin production. Type 2 diabetes (T2D) prevalent among adults is characterised by insufficient insulin production and or sensitivity to glucose uptake (Mahmood, 2016). T2D patients have been reported with symptoms including one or a combination of frequent urination, dehydration, fatigue, and weight loss which are indicative of abnormal glucose metabolism (Cock et al., 2020). The onset of T2D leads to prediabetes in which blood glucose level is higher than normal but within the accepted range and may lead to T2D if not timely managed. Therefore, a prolonged condition of T2D in patients is reported to be accompanied by life-threatening diseases such as vision impairment or loss, cardiovascular diseases, kidney damage and stroke (Pieme *et al*., 2017). At this stage, interventions usually require chemotherapy on patients in addition to a non-sedentary lifestyle and controlled dietary intake that lowers the blood glucose level. The conventional treatment of T2D requires oral administration of synthetic hypoglycaemic agents such as acarbose, voglibose, miglitol and metformin among others that ultimately suppress increasing plasma glucose. These drugs are known to function in two ways; during glucose synthesis via enzyme inhibition of glycopolymers

breakdown and in insulin bioavailability via repair of β-cells of the pancreas. Thus, improving insulin release and sensitivity for glucose uptake (Bedekar et al., 2010). However, these drugs present growing concerns over some negative side-effects such as abdominal pain, diarrhoea and flatulence as well as high cost limit their usage (Akinfenwa et al., 2021). Hence, the increasing research in recent that focuses on the discovery of cheaper and efficient drugs through the application of natural products from medicinal plants with near-zero side-effect (Hung et al., 2012).

Many lines of research have reported the use of natural products as an alternative in the treatment of DM (Rout et al., 2008; Brusotti et al., 2014; Chinsembu, 2019). Duarte *et al*., (2020) discussed naturally occurring compounds from different plant samples that portend inhibition of α-amylase, α-glucosidase and related enzymes in the management of T2D (Duarte et al., 2020). Similarly, Nana *et al*., (2015), Etsassala et al., (2019) and IfedibaluChukwu *et al*., (2020) reported *in vitro* and *in vivo* antidiabetic properties of plants species and isolates from *Fabaceae*, *Lamiaceae* and *Asteraceae*. Phytochemicals of these plants demonstrated strong inhibition of α-amylase and α-glucosidase enzymes with reduction of glucose levels. The inhibitory activities were attributed to phytochemicals constituents like diterpenes, flavonoids, chalcones, dihydrochalcone glycosides (Nana et al., 2015; Etsassala et al., 2019; IfedibaluChukwu et al., 2020). Previously, Mollica et al. (2017), showed that aqua-methanolic extract of *Capparis spinosa* L. was active in both *in vivo* and *in vitro* studies. In a similar report, Hassan *et al.,* (2018) and El-Manawaty and Gohar (2018) gave a list of medicinal plants and compounds with proven antidiabetic activities *in vivo* and *in vitro* (Mollica *et al*., 2017; Hasan *et al*., 2018; El-Manawaty & Gohar, 2018). Interestingly, the phytochemicals of the plant genera reportedly used as antidiabetic agents are well distributed in the *Helichrysum* genus. This probably supports the traditional uses of the *Helichrysum* species documented for antidiabetes in many parts of the world.

2.4.2. An overview of Ethnobotanical and pharmacological relevance of *Helichrysum* genus

The early survey of the Southern Africa *Helichrysum* genus by Hilliard & Burtt (1981) described it as an everlasting and *daisi papery* plant with shiny golden-yellow flowers and woolly leaves from *Asteraceae* (Composite) family (Hilliard, O.M. & Burtt, 1981). The taxonomical records of the family show that it is the world largest and most diverse family of a typical angiosperm with 10 subfamilies, approximately 2000 genera and 23,600 species (Goldblatt, 1997). A subfamily of Asteraceae is *Asteroideae*, made up of seven taxa including Astereae, Tagateae, Eupatorieae, Haliantheae, Calenduleae, Senecioneae, and Gnaphalieae tribe which has the *Helichrysum* genus as a member (Sharafzadeh, 2011). Over 500 species of *Helichrysum* exist which are mostly used in folk medicine, as food flavours, and for ornamental and industrial uses (Antunes Viegas et al., 2014; Vanessa et al., 2017). The genus has a worldwide distribution, adapted to flourish in arid to semi-arid regions of the Mediterranean and a major

concentration in Southern Africa. Common names used for it in Turkey are ölmez çiçek or altınotu (Albayrak, Aksoy, Sağdiç, et al., 2010). In South Africa it is known with different names; imphepo, phefu and isicwe, kooigoed, sewejartjie and phefo-ea-loti, toanae-moru (Lourens et al., 2008; Albayrak, Aksoy, Sagdic, et al., 2010). Other areas of distribution are Australia, India and south-western Asia (Nie *et al*., 2016). According to several reports of the literature, *Helichrysum* species are known with strong aromatic smell used as food and herbs in folk medicine in different parts of the world with little or no empirical knowledge (Akaberi *et al*., 2019). However, with the emergence of scientific data on the bio-evaluation of the *Helichrysum* genus in the last few decades, some of the traditional claims have recently been supported. To mention a few, are the antioxidants activity of methanol extract of *H. foetidum* from east Africa (Tirillini et al., 2012), the antitumor potential of *Helichrysum zivojinii* extract and the antimicrobial actions of flavonoids of *Helichrysum chasmolycicum* both from south-eastern Europe (Süzgeç-Selçuk & Birteksöz, 2011; Mati et al., 2013), antiplasmodial effects of extract and flavonoids of *Helichrysum gymnocephalum Humbert* from southern Africa (Ranaivoarisoa *et al*., 2020), anti-inflammatory *Helichrysum stoechas* (L.) *Moench* extracts from north Africa (Kherbache et al., 2020) and among others. *Helichrysum* has been more extensively researched for these bioactivities than its role as an antidiabetic agent. Interestingly, the recent review by Nyakudya *et al*., (2020) on medicinal plants for the management of metabolic disorders included some *Helichrysum* species used locally for the treatment of DM (Nyakudya et al., 2020). Still, there is a need to document the scientific evaluation of phytochemicals from the genus with antidiabetic potentials.

2.4.3. Antidiabetic potentials of *Helichrysum* species and metabolites in folk medicine.

Plant genera from the Asteraceae family together with Asclepiadaceae, Asphodelaceae, Cucurbitaceae, Fabaceae and Myrtacea*e* have been reported to display antidiabetic properties perhaps because of the large size of the family (Hung et al., 2012; Panda et al., 2019) The large size of the family includes different species of *Helichrysum* reported from the ethnobotanical survey used for treating diabetes. To this end, several reviews have been published from Europe and Africa to reflect the antidiabetic potential of *Helichrysum* species (Nyakudya et al., 2020). In Europe, Turkey is known for a wealth of medicinal plants including *Helichrysum* used in folk (Altundag & Ozturk, 2011). According to an ethnobotanical survey, *H*. *plicatum* DC was reportedly used by local people of Solhan, Sivrice, Yazıkonak and Yurtbaşı district in the Eastern Anatolia of Turkey to treat DM (Polat et al., 2013; Cakilcioglu & Turkoglu, 2010; Çakılcıoğlu et al., 2010; Mükemre et al., 2015). Savych *et al*., (2020;2021) reported the use of a herbal mixture consisting of *H*. *arenarium* flowers in Ukraine as an antidiabetic drug. Although it remains unclear which of the component mixtures presented the highest effect, the antidiabetic potential was attributed to the synergistic effect of polyalcohol in the mixtures (Savych A, Marchyshyn S, 2020; Savych et al., 2021). are used in com Also, in the Eastern

Cape of South Africa, traditional healers and herbalists were reported to prescribed boiled leaves, roots and sometimes the whole plant of *H*. *odorratissiumi* L.*, H*. *petiolare* H. & B.L, *H*. *gymnocomum* and *H*. *nudifolium* L. to be taken orally for the treatment of DM (Erasto et al., 2005; Oyedemi et al., 2009; Odeyemi & Bradley, 2018). A similar report of the ethnobotanical survey conducted in Kannaland of the Western Cape, the Basotho Tribe of Eastern Free State and five municipalities in Limpopo provinces showed that native doctors use *H*. *caespititium* (DC) *Har* H. *aureum* and *H*. *crispum* D. Don for treatment of diabetes among plants used as herbal medicine (Semenya et al., 2012; Balogun et al., 2016; Hulley & Wyk, 2019; Mogale et al., 2019).

2.4.4. *In vitro* evaluation of *Helichrysum* species as hypoglycaemic agents.

A generally accepted model for *in vitro* studies of bioassay includes the use of enzymes extracted from mammalian cell lines, plants, and microorganisms. α-amylase and α-glucosidase obtained from a porcine pancreas or *Aspergillus oryz*ae and *Saccharomyces cerevisiae* respectively and phytochemicals from plants are actively being used for enzymatic studies (Badeggi et al., 2020). In the brush border membrane and lumen of the small intestine are carbohydrate hydrolysing enzymes majorly α-glucosidase and α-amylase respectively that complete the digestion of saccharides to glucose. Also important is dipeptidyl peptidase-IV (DPP-4), a protease enzyme involved in glucose metabolism and insulin secretion as needed by the body. The DPP-4 through rapid activation of the hormone incretin helps in the interconversion of glucagon to glucose (Hung et al., 2012). Activities of these enzymes may increase the glucose level in the blood and insulin resistance to glucose uptake. Extracts and compounds of *Helichrysum* have also been shown to mimic the hypoglycaemic activity of the commonly used synthetic drugs. These drugs have the effects to decrease the level of blood glucose through inhibitory activities on α-amylase and α-glucosidase and increasing the glucose uptake by cells. Table 2.6 & 2.7 and Fig. 2.4 summarise recent *in vitro* antidiabetic studies with extract and compounds of *Helichrysum*.

The development of *in vitro* experiments to potentiate the efficacy of *Helichrysum* species as hypoglycaemic agents are evident by research between 2016 – 2021. For instance, a recent study on the potentials of South African species of *H. foetidum* and its major compounds in the management of diabetes mellitus reported inhibitory effects on α-glucosidase enzymes with no activity against α-amylase (Akinfenwa et al., 2021). The aerial parts of *H*. *stoechas* extract collected from Spain was evaluated for α-glucosidase and DPP-4 inhibitions by Les et al., 2017. The author showed that the activity of *H*. *stoechas* against enzymes were similar to acarbose at IC_{50} of 481.01 and 378.92 μgmL^{-1} for α-glucosidase and DPP-4 respectively. Although, inhibition of DPP-4 was recorded at higher doses (Les et al., 2017). The Turkey species of this plant was extracted via conventional and non-conventional methods such as maceration, soxhlet extraction (SE), accelerated solvent extraction (ASE), microwave-assisted

extraction (MAE), and ultrasonication-assisted extraction (UAE). The result of α-glucosidase enzyme inhibition demonstrated that ASE extract (1.66 mmol acarbose equivalent [ACAE]/g) effectively inhibited α-glucosidase (Zengin et al., 2020). Also, Spínola et al., (2016) reported that the inhibition of the enzyme of methanolic extracts of different parts of *H*. *melaleucum* Rchb. ex. Holl, *H*. o*bconicum* DC, *H*. *devium* Johns and *H*. *monizii* Lowe endemic to Madeira of Portugal and other Asteraceae studied could be correlated to the polyphenolic contents, especially the caffeoylquinic acids derivative. It was observed that the species selectively exhibited high inhibition for α-glucosidase over low α-amylase inhibition. This was suggested to help prevent the accumulation of undigested carbohydrates that may result from the inhibition of both enzymes (Spínola et al., 2016). A similar experiment by the authors showed that all *H.* species demonstrated higher inhibition of α-glucosidase than acarbose positive control (2.06 ± 0.04 mg/mL DE) except *H*. *monizii* Lowe (Spínola & Castilho, 2017). Also, the ability of the aqueous extract of *H*. *sanguineum* (L.) Kostel of Palestinian origin to inhibit α-amylase at IC_{50} higher (28.18 μgmL^{-1} ± 1.04) than acarbose, the positive control (31.6 μgmL^{-1} ± 1.22) is interesting when compared to the hexane, acetone and methanolic extracts and may suggest that inhibition of carbohydrate hydrolysing enzyme in *Helichrysum* is due to aqueous fraction rich in polyphenols (Jaradat et al., 2020). This could be supported by Aladejana *et al*., (2020) report of relatively higher inhibitory activities of (boiled and cold) aqueous extract of *H*. *petiolare Hilliard & B.L. Burtt* on α-amylase and α-glucosidase over the ethanolic extract which was significantly toxic over L6 myocytes and HepG2 hepatocytes cell lines. The authors also showed that improved glucose uptake was observed in L6 myocytes and HepG2 hepatocytes treated with *H*. *petiolare* aqueous extracts, and the cold aqueous extract demonstrated stronger activity in the L6 myocytes than in the HepG2 hepatocytes cell line. While the cold aqueous extract was dose-dependent, the boiled extract was concentration-dependent and no significant effect by ethanol extract on treated cells (Aladejana et al., 2020). Similarly, aqueous extract of the flowers, vegetative and the root part (by infusion and by decoction) of Portuguese *H*. *italicum subsp. picardii* also demonstrated a moderate inhibition of α-glucosidase, the flower and the root extract having the highest and the least activities respectively (Guerreiro et al., 2017). Investigation of its methanolic leaves-extract among three other aromatic plants by Gonclaves *et al*., (2017) for effect on carbohydrate hydrolysing enzymes also support the previous report of its antihyperglycemic potential (Gonc¸alves et al., 2017). Furthermore, the antidiabetic potential of Turkish *H*. *plicatum* DC. subsp. *Plicatum* and *H. chionophilum* extracts from the flowers, and stem with ethanol, ethyl acetate and methanol solvents were evaluated by Acet *et al*., (2020). From the result, the highest inhibitory effect of α-amylase was noted for the ethanolic (stem) extract of *H. chionophilum* while for α-glucosidase, ethyl acetate (flower) extract of *H*. *plicatum* DC. subsp. *Plicatum* was strongest (Acet *et al*., 2020). Earlier in the same year, Aydin report

showed that the methanolic extract of *H*. *plicatum* DC. subsp. *plicatum* and its isolates demonstrated strong inhibition of α-glucosidase although, the compounds demonstrated higher activity than the extract (Aydin, 2020). A comparative study of aqueous and hydro-ethanolic extracts of *H*. *plicatum ssp. plicatum* and *H*. *graveolens* among other plant species by Orhan *et al* (2014) support the potentials of the two species to lower blood glucose. *H*. *plicatum ssp. plicatum* exhibited a low and dose-dependent effect on α-glucosidase and α-amylase. *H*. *graveolens* on the other hand displayed a strong highest inhibitory effect on α-amylase dosed at 3000 µg/mL but a lower effect on α-glucosidase (Orhan et al., 2014). The selective enzymes inhibition by *H*. *graveolens* could be favourable to prevent excessive accumulation of carbohydrates in the body that might lead to an obese condition due to delay in carbohydrate digestion. In a similar study by Garza *et al*., (2013) with *H*. *italicum* and *Citrus* × *paradisi*, both extracts showed strong inhibitory activities. Interestingly, a higher and dual activity for α-amylase and α-glucosidase was demonstrated by *H*. *italicum* (Garza et al., 2013).

Until the time of this review, all the *helichrysum* species discussed above demonstrated moderate to strong inhibition for either α-amylase or α-glucosidase or both enzymes. However, it was noted that flowers of *H. arenarium L. Moench* showed no inhibitory effect to both α-amylase and α-glucosidase except DDP-4. The investigation of its methanolic extract by Morikawa *et al*., (2015) on α-glucosidase gave a negative result. Other than that, all authors who studied the *in vitro* inhibition of α-amylase and α-glucosidase enzymes using *Helichrysum* species proposed that the species might be useful in the formulation of products that ameliorate T2D.

Table 3.3: α-Amylase and α-Glucosidase IC50 values of *Helichrysum* species

Samples	**IC_{50}**	**Acarbose standard**	**Experiment**	**Samples**
H. foetidum	27.5±0.301 µg/mL	610.4 ± 1.0 µg/mL	α-Glucosidase	Akinfenwa et al., 2021
H. foetidum	NA	10.2 ± 0.6 µg/mL	α-Amylase	Akinfenwa et al., 2021
H. stoechas	481.01 µg/mL	378.92 µg/mL	α-Glucosidase	Zengin et al., 2020
H. stoechas	1.59	mmol ACAE	α-Glucosidase	Les et al., 2017
H. devium Johns	1.44 ± 0.03 mg/mL DE	2.06±0.04 mg/mL DE	α-Glucosidase	(Spínola & Castilho, 2017)
H. melaleucum Rchb. ex. Holl (L)	0.99 ± 0.03 mg mL DE	2.06±0.04 mg/mL DE	α-Glucosidase	(Spínola & Castilho, 2017)
H. melaleucum Rchb. ex. Holl (F)	1.25 ± 0.04 mg/mL DE	2.06±0.04 mg/mL DE	α-Glucosidase	(Spínola & Castilho, 2017)
H. obconicum DC (L)	1.35 ± 0.02 mg/mL DE	2.06±0.04 mg/mL DE	α-Glucosidase	(Spínola & Castilho, 2017)
H. *sanguineum* (L.) Kostel	28.18 µgmL^{-1} ± 1.04	31.6 µg/mL ± 1.22	α-Amylase	Jaradat et al., 2020.
H. petiolare Hilliard & B.L. (BA)	0.361 µg/mL ± 0.0210	0.378 µg/mL ±0.0084	α-Amylase	Aladejana et al., 2020.
H. italicum subsp. Picardii (R:I)	22.9%±5.6,	88.3%±0.5	α-Glucosidase	Aladejana et al., 2020.

H. italicum subsp. Picardii (R:D)	31.0%±4.7	88.3%±0.5	α-Glucosidase	Aladejana et al., 2020.
H. italicum subsp. Picardii (V:I)	41.2% ± 3.5	88.3%±0.5	α-Glucosidase	Aladejana et al., 2020.
H. italicum subsp. Picardii (A:D)	45.7% ± 3.9	88.3%±0.5	α-Glucosidase	Aladejana et al., 2020.
H. italicum subsp. Picardii (F:I)	48.3% ± 5.7	88.3%±0.5	α-Glucosidase	Aladejana et al., 2020.
H. italicum subsp. Picardii	6.79% ± 0.57	72.47%	α-Amylase	Gonc¸alves et al., 2017.
H. italicum subsp. Picardii	58.41% ± 1.97	80.71%	α-Glucosidase	Gonc¸alves et al., 2017.
H. plicatum (F: Et)	22.33 ± 0.03	mmol ACAE/g extract	α-Glucosidase	Acet *et al.,* 2020
H. plicatum (F: M)	11.70± 0.05	mmol ACAE/g extract	α-Glucosidase	Acet *et al.,* 2020
H. plicatum (F: E)	17.84± 0.03	mmol ACAE/g extract	α-Glucosidase	Acet *et al.,* 2020
H. plicatum (F: Et)	197.12± 0.94	mmol ACAE/g extract	α-Amylase	Acet *et al.,* 2020
H. plicatum (F: M)	170.02± 0.99	mmol ACAE/g extract	α-Amylase	Acet *et al.,* 2020
H. plicatum (F: E)	105± 0.65	mmol ACAE/g extract	α-Amylase	Acet *et al.,* 2020
H. plicatum (S: Et)	146.18± 0.8	mmol ACAE/g extract	α-Amylase	Acet *et al.,* 2020
H. plicatum (S: M)	162.55± 1.39	mmol ACAE/g extract	α-Amylase	Acet *et al.,* 2020
H. plicatum (S: E)	105.12± 0.95	mmol ACAE/g extract	α-Amylase	Acet *et al.,* 2020
H. plicatum (S: Et)	18.73± 002	mmol ACAE/g extract	α-Glucosidase	Acet *et al.,* 2020
H. plicatum (S: M)	15.25± 0.04	mmol ACAE/g extract	α-Glucosidase	Acet *et al.,* 2020
H. plicatum (S: E)	18.83± 0.05	mmol ACAE/g extract	α-Glucosidase	Acet *et al.,* 2020
H. chionophilum (F: Et)	25.42± 0.09	mmol ACAE/g extract	α-Glucosidase	Acet *et al.,* 2020
H. chionophilum (F: M)	7.43± 0.02	mmol ACAE/g extract	α-Glucosidase	Acet *et al.,* 2020
H. chionophilum (F: E)	7.31± 0.05	mmol ACAE/g extract	α-Glucosidase	Acet *et al.,* 2020
H. chionophilum (F:Et)	158.98± 0.53	mmol ACAE/g extract	α-Amylase	Acet *et al.,* 2020
H. chionophilum (F: M)	173.0± 01.84	mmol ACAE/g extract	α-Amylase	Acet *et al.,* 2020
H. chionophilum (F: E)	156.53± 01.35	mmol ACAE/g extract	α-Amylase	Acet *et al.,* 2020
H. chionophilum (S: Et)	8.92± 0.06	mmol ACAE/g extract	α-Glucosidase	Acet *et al.,* 2020
H. chionophilum (S: M)	3.77± 0.03	mmol ACAE/g extract	α-Glucosidase	Acet *et al.,* 2020
H. chionophilum (S: E)	7.61± 0.04	mmol ACAE/g extract	α-Glucosidase	Acet *et al.,* 2020
H. chionophilum (S: Et)	149.16± 0.91	mmol ACAE/g extract	α-Amylase	Acet *et al.,* 2020
H. chionophilum (S: M)	158.15± 0.82	mmol ACAE/g extract	α-Amylase	Acet *et al.,* 2020
H. chionophilum (S:E)	193.36 ± 0.67	mmol ACAE	α-Amylase	Acet *et al.,* 2020
H. plicatum DC. subsp. Plicatum	81.53 mg/mL	NC	α-Glucosidase	Aydin 2020
H. graveleons (HA)	0.7129 mg/mL	0.0009 mg/mL	α-Glucosidase	Orhan *et al*., 2014
H. graveleons (Aq)	2.1979 mg/mL	0.0009 mg/mL	α-Glucosidase	Orhan *et al*., 2014
H. graveleons (Aq)	3.5 ± 1.8%	73.7±0.6%	α-Amylase	Orhan *et al*., 2014
*H. graveleons (*HA)	55.7 ± 2.2%	73.7±0.6%	α-Amylase	Orhan *et al*., 2014
H. plicatum ssp. *Plicatum* (HA)	0.8570 mg/mL	0.0009 mg/mL	α-Glucosidase	Orhan *et al*., 2014
H. plicatum ssp. *Plicatum* (Aq)	5.0933 mg/mL	0.0009 mg/mL	α-Glucosidase	Orhan *et al*., 2014
H. plicatum ssp. *Plicatum* (Aq)	12.7 ± 2.8%	73.7±0.6%	α-Amylase	Orhan *et al*., 2014
H. plicatum ssp. *Plicatum* (HA)	5.4±2.4%	73.7±0.6%	α-Amylase	Orhan *et al*., 2014
H. italicum	0.19 ± 0.1 mg/mL	6.91 ± 0.01 mg/mL	α-Glucosidase	Garza et al., 2013
H. italicum	0.83 ± 0.05 mg/mL	4.17 ± 0.01 mg/mL	α-Amylase	Garza et al., 2013

* A = Aerial, ACAE = Acarbose equivalent, Aq = Aqueous, BA = Boiled aqueous, D = Decoction, DE = Dry extract, E = Ethanol, Et = Ethyl acetate, F = Flower, HA = Hydro-alcoholic, I = Infusion, L = Leaves, M = Methanol, S = Stem NC = Not calculated = Not active, R = Root, V =Vegetative.

Table 3.4: Documented in vitro and in vivo antidiabetic potentials of *Helichrysum* from different countries

s/n	Species	Part used	Extract/compound	Origin	Model	Reference
1	*H. foetidum*	Plant	Methanolic extract	South Africa	In vitro	(Akinfenwa et al., 2021)
2.	*H. sanguineum* (L.) Kostel.	Aerial parts	Aqueous extract	Palestine	In vitro	(Jaradat et al., 2020)
3.	*H. petiolare* Hilliard & B.L.	Whole plant	Aqueous and ethanolic extracts	South Africa	In vitro	(Aladejana et al., 2020)
4.	*H. plicatum* DC. subsp. plicatum	Flowers	Methanolic extract	Turkey	In vitro	(Aydin, 2020)
5.	*H. chionophilum* and *H. plicatum* subsp. plicatum	Flowers, stem, and root	ethanol, methanol, and ethyl acetate	Turkey	In vitro	(Acet et al., 2020)
6.	*H. stoechas* Moench	Aerial parts	ASE, MAE, UAE, and SE	Turkey	In vitro	(Zengin et al., 2020)
7.	*H. italicum* subsp. picardii	Whole plant	Aqueous extract	Portugal	In vitro	(Guerreiro et al., 2017)
8.	*H. italicum* subsp. picardii	Leaves	Methanolic extract	Portugal	In vitro	(Gonc¸alves et al., 2017)
9.	*H. stoechas* Moench	Flowers	Methanolic extract	Spain	In vitro	(Les et al., 2017)
10.	*H. devium* Johns, *H. melaleucum* Rchb. ex. Holl, *H. monizii* Lowe and *H. obconicum* DC	Leaves Flowers, and aerial part	Methanolic	Portugal	In vitro	(Spínola et al., 2016)
11.	*H. odoratissimum*	Leaves	Aqueous extract	Kenya	In vivo	(Njagi et al., 2015)
12.	*H. arenarium* L. Moench	Flowers	Methanolic extract	Poland	In vitro and in vivo	(Morikawa et al., 2015)
13.	*H. graveolens* and *H. plicatum* ssp. plicatum	Whole plant	Aqueous, Hydro-ethanol	Turkey	In vitro	(Orhan et al., 2014)
14.	*H. italicum* subsp. picardii	Whole plant	ASE	Spain	In vitro	(Garza et al., 2013)
15.	*H. italicum*	Whole plant	ASE	Spain	In vivo	(Garza et al., 2013; Laura et al., 2014)
16.	*H. graveolens*	Flowers	Aqueous and ethanolic	Turkey	In vivo	(Aslan et al., 2007a)
17.	*H. plicatum* ssp. plicatum	Flowers	Aqueous and ethanolic	Turkey	In vivo	(Aslan et al., 2007b)

2.4.5. *Helichrysum* species with documented *in vivo* antidiabetic activities

Insulin secretion by the pancreas, glucose uptake into fat and muscle cells and glucose production by the liver are known to collectively determine the glucose tolerance level of individuals, a key factor to the onset of T2D. This is in addition to uncontrolled hydrolysis of saccharides by intestinal α-amylase and α-glucosidase enzymes. Scientific data on enzyme inhibitory effects of *Helichrysum* species from different regions which lower postprandial hyperglycaemia have been highlighted in the previous session. To further validate the activities of *Helichrysum* species as antidiabetics drug candidates, *in vivo* and clinical trials through laboratory animals and human diabetic patients are necessary. Commonly used laboratory animals for *in vivo* experiments are rodents (Wister rats and mice) for ease and short time of induction of diabetes with chemicals, the low maintenance cost of the rodents and overall experimental budget (Hasan et al., 2018). Among chemicals currently used to induce diabetes are streptozotocin and alloxan (Fig. 1). When administered either through intravenous, subcutaneous, or intraperitoneal injection, these drugs selectively intoxicate the pancreatic β-cells that stimulate insulin secretion and consequently impair the cells. To date, various *in vivo* studies have been published to demonstrate the antidiabetic efficacy of *Helichrysum* species.

In a study by Njagi *et al*., (2015), aqueous leaves extract of *H*. *odoratissimum* collected from Kenya was dose-administered to four groups of alloxan induced-diabetic male Swiss albino mice (2 groups as control) at a different time interval. The dose range of 50 – 150 mg/kg body weight effect was measured for four hours and the blood sugar measurement is taken before and after treatment with *H*. *odoratissimum*. The 150 mg/kg body weight dose was noted to lower blood sugar levels comparable to insulin. This demonstrated a non-dose dependence hypoglycaemic effects of *H*. *odoratissimum* and is suggestive of insulin release improvement from diabetic mice (Njagi et al., 2015). A methanol extract of *H*. *arenarium* flowers from Poland was also reported to suppress blood glucose elevation in sucrose loaded mice at 500 mg/kg p.o (Morikawa et al., 2015). Another therapeutic approach to DM pathogenesis is the regulation of glucose phosphorylation in the liver by glucokinase (GCK). The liver regulates hepatic glucose release (via glycolysis) and peripheral glucose uptake (via glycogenesis) depending on glucose availability and cell requirements. The effect of *H*. *italicum* extract on the postprandial glucose level in Male Wistar rats fed with starch was examined by Garza *et al*., (2013). The effects measured by an oral starch tolerance test showed a significant lowering of induced hyperglycaemia and decreased plasma glucose levels after 30 mins. Supplementation of the species in rats diet for 5-weeks also demonstrated a positive effect of decreased serum glucose, insulin levels, and lowering of homeostasis model of insulin resistance index in insulin-resistant rats (Garza et al., 2013). In addition, Laura et al., (2014) found that livers of diabetic *db/db* mice administered with Spanish *H*. *italicum* showed lower glycaemic level and expressed a high level of GCK, an enzyme that modulates phosphorylation of glucose and a

decreased glucose level possibly through stimulation of peripheral glucose uptake (Laura et al., 2014). The Turkish *H*. *plicatum ssp. plicatum* and *H*. *graveolens* species used for antidiabetic treatments are well documented in published ethnobotanical surveys and *in vitro* studies (Table 1). These studies have been corroborated with animal models for their antihyperglycemic and hypoglycaemic effects as antidiabetic drugs. In different *in vivo* experiments, Orhan *et al*., (2007a; 2007b) determined the antidiabetic effects of aqueous and ethanolic extract of *H. graveolens* on blood glucose levels in normoglycemic and STZ-induced-diabetic rat models for 8 days. The author reported higher activity of the aqueous and ethanol extract over the positive control (Tolbutamide) with significant antidiabetic noted on day 5 (Aslan et al., 2007a) for both models. In a similar study, aqueous and ethanolic extract of *H. plicatum* subsp. *plicatum* assessed for STZ-induced-diabetic and normoglycemic rats resulted in an immediate and significant lowering of blood sugar levels in the two models. The potency of the *H. plicatum ssp. Plicatum* extract was stronger than the reference tolbutamide drug due to excessive hypoglycaemic effect on normoglycemic rats (Aslan et al., 2007b)

A: Helichrysum compounds isolated and documented with in vitro hypoglycaemic potentials

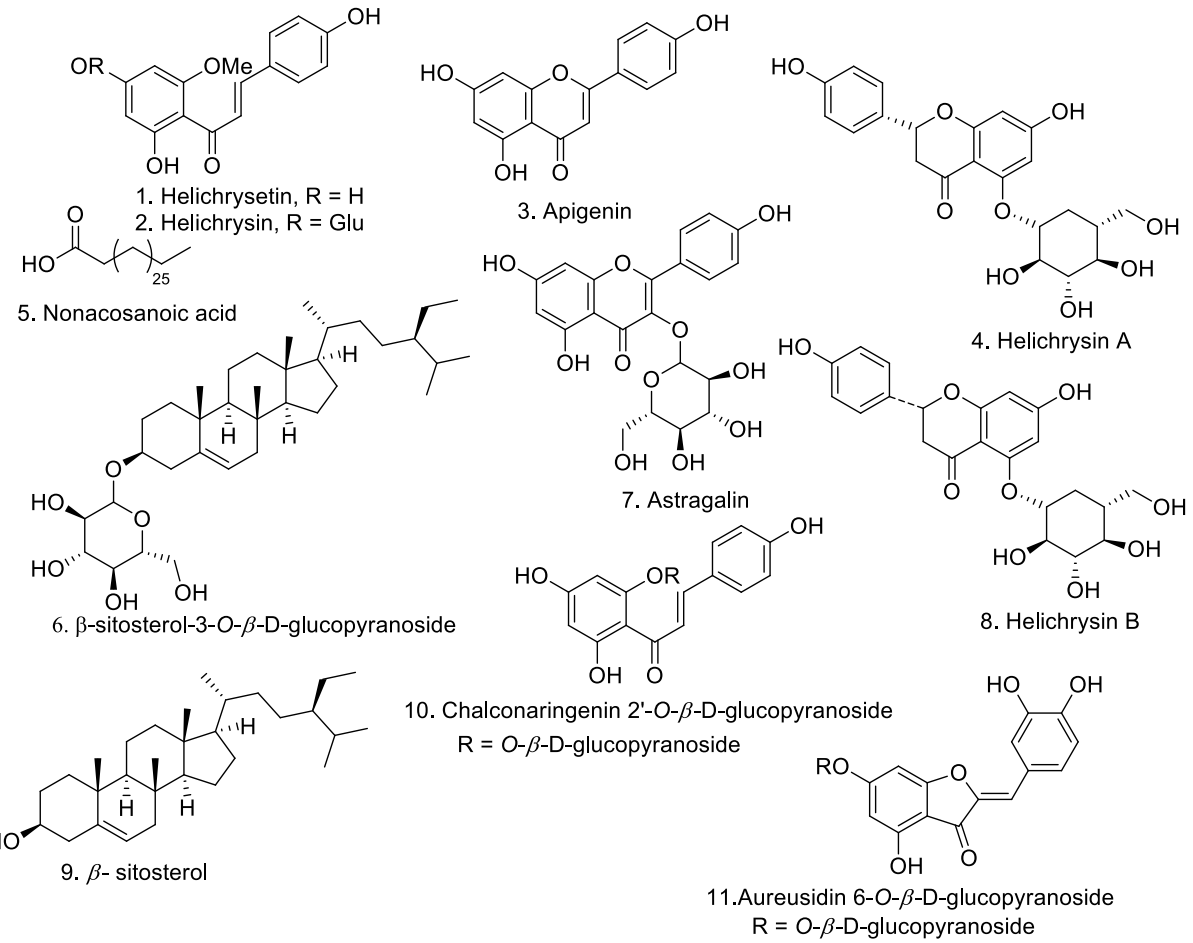

B: Synthetic antidiabetic compounds (standards)

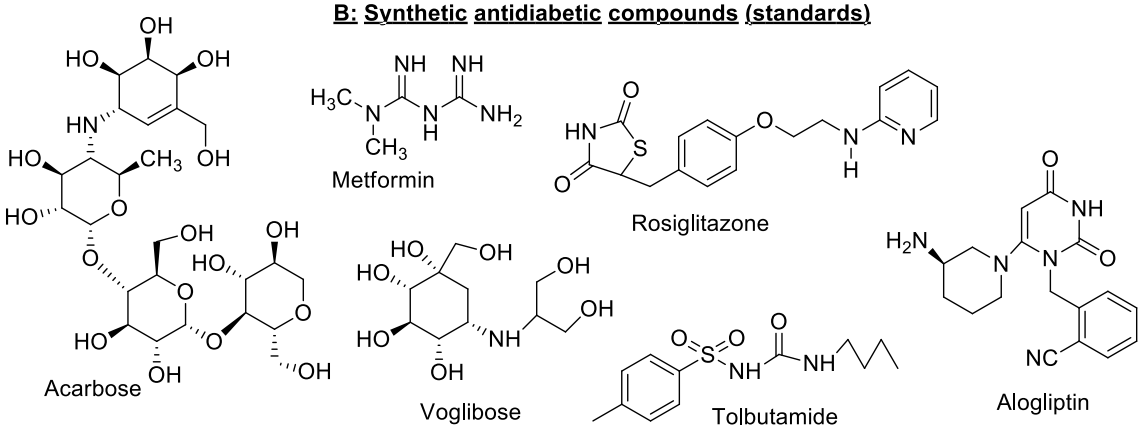

C: Documented chemical drugs to induced diabetes mellitus *in vivo* studies with *Helichrysum* species

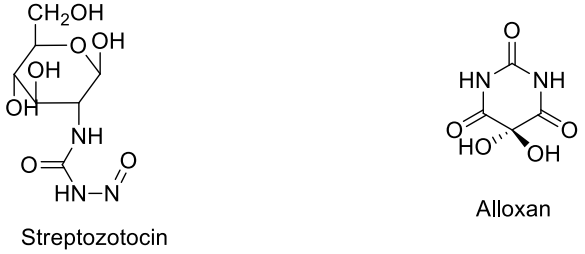

Figure 3.2: Structures of isolated compounds from *Helichrysum* and synthetic drugs documented for antidiabetic experiments

2.4.6. Secondary metabolites of *Helichrysum* as antidiabetic agents

More than 300 secondary metabolites from *Helichrysum* species have been reportedly isolated as naturally occurring bioactive compounds in the last few decades. This includes terpenoids, flavonoids, phloroglucinols, chromones, acetylene derivatives, benzopyrone, coumarins, benzofurans, quinones and other compounds grouped as miscellaneous compounds (Popoola, 2015; Akaberi et al., 2019). Although there are a few scientific reports on specific compounds of *Helichrysum* evaluated for inhibition of carbohydrate hydrolysing enzymes, repair of β-cells, and insulin sensitivity. Several bio-evaluations of the plant species, including antidiabetic activities have been attributed to the bioactivities of these compounds (Khan et al., 2012; Alkhalidy et al., 2018). This suggestion is supported by the report of Aydin Tuba (2020) for evaluation of apigenin, astragalin, helichrysin A, helichrysin B, isosalipurposide, nonacosanoic acid, β-sitosterol and β-sitosterol-3-*O*-β-D-glucopyranoside isolated from flowers methanol extract of *H. plicatum* subsp. *plicatum*. Nonacosanoic (1.61 mg/mL) was noted with the strongest inhibition for α-glucosidase followed by isosalipurposide (1.99 mg/mL), a dihydrochalcone glycoside among tested compounds. Other compounds were reported to show high inhibition relative to the acarbose standard (22.8 mg/mL) except astragalin which shows no activity (Aydin, 2020). In addition, the report of Akinfenwa et al. (2021) revealed that two dihydrochalcones (helichrysin and helichrysetin) isolated from *H. foetidum* were more active against α-glucosidase enzymes than the acarbose standard (Akinfenwa et al., 2021). Going by this report, it appears the carboxylic acid, dihydrochalcone glycosides, stigmastanes and their glycosides, and flavonoids of *helichrysum* are responsible for the antidiabetic potential. To further buttress the involvement of dihydrochalcone glycosides from *helichrysum* as hypoglycaemic phytochemicals, Morikawa *et al*., (2015) that showed the decrease in blood glucose elevation of sucrase loaded mice by methanol extract of *H*. *arenarium* could be attributed to chalcone glycosides of chalconaringenin 2'-*O*-β-D-glucopyranoside (23.1 μM) and aureusidin 6-*O*-β-D-glucopyranoside (24.3 μM). In addition to the inhibitory activity over DDP-4 which act complementarily to α-amylase and α-glucosidase enzymes through interconversion of glucagon to glucose (Morikawa et al., 2015).

2.4.7. Putative mechanism of action of Helichrysum as hypoglycaemic agents

The pathogenesis of T2D is a complex phenomenon involving the small intestine, pancreas, liver, muscle cells and adipose tissues and therefore involves many mechanisms (Brownlee, 2005). The mechanism of action of *helichrysum* constituents could be explained based on the class antidiabetic drugs used as the positive control. Biguanides, α-glucosidase inhibitors, DPP-4 inhibitors, sulfonylureas and thiazolidinediones are common drugs used as controls in experiments. The biguanides (for example, metformin) essentially decrease glucose production from the liver while increasing insulin sensitivity. α-glucosidase inhibitors (e.g., acarbose) and DPP-4 inhibitors (e.g., alogliptin) interfere with glucose metabolising enzymes

in the small intestine and liver, respectively. The sulfonylureas (e.g., tolbutamide) enhance insulin secretion by the pancreas, the thiazolidinediones (e.g., rosiglitazone) sensitize insulin activation for glucose uptake by the muscle and adipose tissues (Hung et al., 2012). The mechanism of action of *H*. species as hypoglycaemic agents in the pathogenesis is yet to be extensively studied. However, several experimental pieces of evidence showed that studied *H*. species affects activities of carbohydrate hydrolysing enzymes and insulin as reported from several *in vitro* and *in vivo* studies. Nearly all the studies in this regard reported a higher inhibition at a lower IC_{50} value of *helichrysum* compared to the acarbose standard used. The is suggestive of a similar mechanism of action to acarbose through interaction with the surface of the enzyme and blocking the reactive sites. The acarbose drug has glucose moiety structurally similar to oligosaccharides chain in amylase and glucosidase enzymes which helps in molecular recognition active sites for interaction This results in delay in carbohydrate digestion and glucose availability (Aoki et al., 2019). This similarity in the glucose moiety is believed to facilitate binding with α-amylase and α-glucosidase enzymes slow down hydrolysis of α-1,4-glycosidic linkage bonds and consequently reduce glucose absorption into the bloodstream (Zengin et al., 2020). The presence of structural similarities of glucose moiety, polyphenols, and keto functional groups in the flavonoid skeleton (Figure 1) of *helichrysum* compounds could be responsible for the recognition of the binding sites of the enzymes by *Helichrysum*. The binding of these reactive groups could lead to blockage of the active sites to limit their activities. Thus, a reduction in the glucose absorbed into the bloodstream. A scientific investigation of the structure-activity relationship of flavonoids and its glycoside on α-glucosidase inhibition revealed that different substitution of -OH on rings A, B and C and the keto group on the centre ring of the flavonoid plays a vital role. The mechanism by which different flavonols inhibit α-glucosidase was studied with molecular docking and kinetic inhibition simulation by Didem *et al*., (2018). He concluded that substitution of -OH at C-3, C-5, C-7 and C-4', C=O at C-4 and substitution of -OH by galloyl moieties at C-3" of the flavonols improve enzyme inhibition while OH substitution at C-3' decrease inhibition (Didem et al., 2018). In addition, the type of glycoside substitution at the C-3 position of ring C was reported to increase or decrease inhibition of α-glucosidase. Notably, substitution by galloyl moieties at C-3 improve inhibition of α-glucosidase. Another plausible mechanism of action could be attributed to the antioxidant effects of *helichrysum* polyphenols to reduce production of reactive oxygen species (ROS) by the mitochondrial (Aryaeian et al., 2017). The mitochondrial through phosphorylation and electron transport chain reactions, convert glucose to adenosine triphosphate (ATP) with the release of ROS in the process. Overproduction of ROS (superoxide, peroxide, hydroxyl radicals etc) in the body cell is a leading cause of oxidative stress, apoptosis and is complimentary to the onset of diabetes associated with cell stress and dysfunction (Burgos-mor et al., 2019; Meo et al., 2018). To show that natural flavone glycoside could downregulate hyperglycaemia resulting from excessive production of ROS, Bi-yu et al.,

(2020) demonstrated from *in vitro*, *in vivo*, and molecular docking experiments that puerarine enhanced insulin activities and glucose uptake into the cytoplasm through modulation of oxidative stress and mitochondrial function via AMPK (Bi-yu et al., 2020). The mechanism of the antidiabetic effect of the compound was described as a two-step. The first step was improvement of the mitochondrial function and followed by attenuation of oxidative stress. Based on these pieces of evidence for the mechanism of antidiabetic plants rich in polyphenols similar to the *helichrysum*, it may be concluded that the potency of *helichrysum* as potential hypoglycaemic drug is related to degree of hydroxylation on aromatic rings, position of glycosylation and its antioxidant property.

2.4.8. Conclusion and future work

Following documented ethnobotanical relevance of *helichrysum* species for the treatment of DM, several species have shown promising potentials as antidiabetic drugs with scientific evidence. Although, extracts from the flowers, leaves and whole plant from a few tens of the plant species have been scientifically evaluated there is a need for evaluation of other species of the plant. In most of the reports, only a few studies involve *in vivo* experiments which is more accurate and quantifiable than *in vitro* experiments reported. Also, limited literature work exists that attributed the potency of *helichrysum* to its compounds and no report of clinical studies to validate the results from enzymatic studies. This opens more research questions for future studies on the potency of *helichrysum* species as antidiabetic agents.

References

1. Acet, T., Ozcan, K. & Zengin, G. 2020. An assessment of phenolic profiles, fatty acid compositions, and biological activities of two *Helichrysum* species : *H . plicatum and H . chionophilum*. *Journal of Food Biochemistry*, 44(e13128.), pp. 1–11.
2. Akaberi, M., Sahebkar, A., Azizi, N. & Emami, S.A. 2019. Everlasting flowers: Phytochemistry and pharmacology of the genus *Helichrysum*. *Industrial Crops and Products*, 138(March), pp. 111471.
3. Akinfenwa, O.A., Pearce, B., Omoruyia, S.I., Badmus, J.A., Ismail, E., Marnewick, J., Botha, S., Benjeddou, M., Ekpob, O.E. and Hussein, A.A., 2021. The potential of chalcone-capped gold nanoparticles for the management of diabetes mellitus. *Surfaces and Interfaces*, *25*, p.101251.
4. Aladejana, A., Bradley, G. & Afolayan, A. 2020. In vitro evaluation of the anti-diabetic potential of *Helichrysum petiolare* Hilliard & B . L . Burtt using HepG2 (C3A) and L6 cell lines. *F1000Research*, 9(1240), pp. 1–12.
5. Albayrak, S., Aksoy, A., Sağdiç, O. & Budak, Ü. 2010. Phenolic compounds and antioxidant and antimicrobial properties of *Helichrysum* species collected from eastern Anatolia, Turkey. *Turkey Journal of Biology*, 34, pp. 463–473.
6. Albayrak, S., Aksoy, A., Sagdic, O. & Hamzaoglu, E. 2010. Compositions, antioxidant and antimicrobial activities of *Helichrysum* (Asteraceae) species collected from Turkey. *Food Chemistry*, 119(2010), pp. 114–122.
7. Alkhalidy, H., Wang, Y. & Liu, D. 2018. Dietary Flavonoids in the Prevention of T2D : An Overview. *Nutrients*, 10(438), pp. 1–33.

8. Altundag, E. & Ozturk, M. 2011. Ethnomedicinal studies on the plant resources of east Anatolia, Turkey Ethnomedicinal studies on the plant resources of east Anatolia, Turkey. *Procedia Social and Behavioral Sciences*, 19(2011), pp. 756–777.
9. Aoki, K., Sato, H. & Terauchi, Y. 2019. Usefulness of antidiabetic alpha-glucosidase inhibitors: A review on the timing of administration and effects on gut hormones. *Endocrine Journal*, 66(5), pp. 395–401.
10. Aryaeian, N., Sedehi, S.K. & Arablou, T. 2017. Polyphenols and their effects on diabetes management : A review, 2017.
11. Aslan, M., Orhan, D., Orhan, N., Sezik, E. & Yesilada, E. 2007. In vivo antidiabetic and antioxidant potential of *Helichrysum plicatum* ssp. *plicatum capitulums* in streptozotocin-induced-diabetic rats. *Journal of Ethnopharmacology*, 109(1), pp. 54–59.
12. Aslan, M., Orhan, D., Orhan, N., Sezik, E. & Yeşilada, E. 2007. A study of antidiabetic and antioxidant effects of *Helichrysum graveolens capitulums* in streptozotocin-induced diabetic rats. *Journal of Medicinal Food*, 10(2), pp. 396–400.
13. American Diabetes Association 2020. Diabetes Advocacy : Standards of Medical Care in Diabetes d 2019. *Diabetes Care*, 43(January), pp. S203–S204.
14. Aydin, T. 2020. Secondary metabolites of *Helichrysum plicatum* DC. *subsp. plicatum* flowers as strong carbonic anhydrase, cholinesterase and α-glycosidase inhibitors. *Zeitschrift für Naturforschung C*, 75(5–6).
15. Badeggi, U.M., Ismail, E., Adeloye, A.O., Botha, S. & Hussein, A.A. 2020. Green Synthesis of Gold Nanoparticles Capped with Procyanidins from Leucosidea sericea as Potential Antidiabetic and Antioxidant Agents. *Biomolecules*, 10(452).
16. Balogun, F.O., Tshabalala, N.T., Omotayo, A. & Ashafa, T. 2016. Antidiabetic Medicinal Plants Used by the Basotho Tribe of Eastern Free State : A Review. *Journal of Diabetes Research*, 2016(4602820), pp. 1–13.
17. Bedekar, A., Shah, K. & Koffas, M. 2010. *Chapter 2 - Natural Products for Type II Diabetes Treatment*. 1st ed. Elsevier Inc.
18. Bi-yu, H.O.U., Yue-rong, Z., Peng, M.A., Chun-yang, X.U., Ping, H.E., Xiu-ying, Y., Li, Z., Gui-fen, Q. & Guan-hua, D.U. 2020. Hypoglycemic activity of puerarin through modulation of oxidative stress and mitochondrial function via AMPK. *Chinese Journal of Natural Medicines*, 18(11), pp. 818–826.
19. Brownlee, M. 2005. The pathobiology of diabetic complications: A unifying mechanism. *Diabetes*, 54(6), pp. 1615–1625.
20. Brusotti, G., Cesari, I., Dentamaro, A., Caccialanza, G. & Massolini, G. 2014. Isolation and characterization of bioactive compounds from plant resources: The role of analysis in the ethnopharmacological approach. *Journal of Pharmaceutical and Biomedical Analysis*, 87, pp. 218–228.
21. Burgos-mor, E., Abad-jim, Z., Mart, A., Marañ, D., Iannantuoni, F., Escribano-l, I., Sandra, L., Salom, C., Jover, A., Mora, V., Roldan, I., Sol, E., Rocha, M. & V, M. 2019. Relationship between Oxidative Stress, ER Stress, and Inflammation in Type 2 Diabetes : The Battle Continues. *Journal of Clinical Medicine*, 8(1385), pp. 1–22.
22. Cakilcioglu, U. and Turkoglu, I., 2010. An ethnobotanical survey of medicinal plants in Sivrice (Elazığ-Turkey). *Journal of Ethnopharmacology*, *132*(1), pp.165-175.
23. Çakılcıoğlu, U., Şengün, M.T. & Türkoğlu, I. 2010. An ethnobotanical survey of medicinal plants of Yazıkonak and Yurtba ş ı districts of Elazığ province, Turkey. *Journal of Medicinal Plants Research*, 4(7), pp. 567–572.
24. Chinsembu, K.C. 2019. Diabetes mellitus and nature's pharmacy of putative antidiabetic plants. *Journal of Herbal Medicine*, 15(100230), pp. 1–12.
25. Cock, I.E., Ndlovu, N. & Vuuren, S.F. Van. 2020. The use of South African botanical species for the control of blood sugar. *Journal of Ethnopharmacology*, 264(113234), pp. 1–21.
26. Decroux, S.G. de L.A.F. de M.C., Duke, L., Hammond, L., Jacobs, E., Kaundal, A., Li, J., Liu, J., Ohlrogge, A.W., Petersohn, I., Piemonte, L., Swansea, U., Riley, P., Gonzalez, M.R., Sung, E., Wilson, M., Jiménez, B.Y., Yang, W. & Ysebaert, M. 2019. *International Diabetes Federation Atlas*. Ninth. S. Karuranga, B. Malanda, P. Saeedi, & P. Salpea, eds. International Diabetes Federation, 2019. www.diabetesatlas.org. (accessed, October 2020)
27. Didem, Ş., Sari, S., Barut, B. & Özel, A. 2018. Bioorganic Chemistry Discovery of potent α-glucosidase inhibitor flavonols: Insights into mechanism of action through inhibition kinetics and docking simulations. *Bioorganic Chemistry*, 79(April), pp. 257–264.
28. Duarte, A.M., Guarino, M.P., Barroso, S. & Gil, M.M. 2020. Phytopharmacological Strategies in the Management of Type 2 Diabetes Mellitus. *Foods*, 9(271), pp. 1–31.

29. El-Manawaty, M.A. & Gohar, L. 2018. In vitro alpha-glucosidase inhibitory activity of Egyptian plant extracts as an indication for their antidiabetic activity. *Asian Journal of Pharmaceutical and Clinical Research*, 11(7), pp. 360–367.
30. Erasto, P., Adebola, P.O., Grierson, D.S. & Afolayan, A.J. 2005. An ethnobotanical study of plants used for the treatment of diabetes in the Eastern Cape Province, South Africa. *African Journal of Biotechnology*, 4(12), pp. 1458–1460.
31. Etsassala, N.G.E.R., Waryo, T., Popoola, O.K., Adeloye, A.O., Iwuoha, E.I. & Hussein, A.A. 2019. Electrochemical screening and evaluation of Lamiaceae plant species from South Africa with potential tyrosinase activity. *Sensors (Switzerland)*, 19(5).
32. Garza AL, Etxeberria U, Lostao MP, San Román B, Barrenetxe J, Martínez JA, Milagro FI. *Helichrysum* and grapefruit extracts inhibit carbohydrate digestion and absorption, improving postprandial glucose levels and hyperinsulinemia in rats. *Journal of Agricultural and Food Chemistry*. 2013.
33. Goldblatt, P. 1997. Floristic diversity in the Cape Flora of South Africa. *Biodiversity and Conservation*, 6(1997), pp. 359–377.
34. Gonçalves, S., Moreira, E., Grosso, C., Andrade, P.B., Valentão, P. and Romano, A., 2017. Phenolic profile, antioxidant activity and enzyme inhibitory activities of extracts from aromatic plants used in Mediterranean diet. *Journal of Food Science and Technology*, *54*(1), pp.219-227.
35. Guerreiro, C., Barreira, L., Bijttebier, S., Pieters, L., Neves, V., João, M., Rivas, R., Varela, J. & Custódio, L. 2017. Chemical profiling of infusions and decoctions of *Helichrysum italicum* subsp. picardii by UHPLC-PDA-MS and in vitro biological activities comparatively with green tea (*Camellia sinensis*) and rooibos tisane (*Aspalathus linearis*). *Journal of Pharmaceutical and Biomedical Analysis*, 145: 593–603.
36. Hasan, M., Uddin, Q., Zaiton, S., Soad, M. & Sarwar, T. 2018. Animal models and natural products to investigate *in vivo* and *in vitro* antidiabetic activity. *Biomedicine & Pharmacotherapy*, 101, pp. 833–841.
37. Hilliard, O.M. & Burtt, L.B. 1981. Some generic concepts in Compositae-Gnaphaliinae. *Botanical Journal of the Linnean Society.*, (82), pp. 181–232.
38. Hulley, I.M. & Wyk, B. Van. 2019. Quantitative medicinal ethnobotany of Kannaland (western Little Karoo, South Africa): Non-homogeneity amongst villages. *South African Journal of Botany*, 122(April 2017), pp. 225–265.
39. Hung, H., Qian, K., Morris-natschke, S.L., Hsu, C. & Lee, K. 2012. Recent discovery of plant-derived anti-diabetic natural products. *Natural Product Reports*, 29, pp. 580–606.
40. IfedibaluChukwu, E.I.M., Aparoop, D. & Kamaruz, Z. 2020. Antidiabetic, anthelmintic and antioxidation properties of novel and new phyto compounds isolated from the methanolic stem-bark of *Vernonia amygdalina Delile* (Asteraceae). *Scientific African*, 10(e00578), pp. 1–17.
41. Jaradat, N., Qneibi, M., Hawash, M., Sawalha, A., Qtaishat, S. & Hussein, F. 2020. Chemical Composition, Antioxidant, Antiobesity, and Antidiabetic Effects of *Helichrysum sanguineum* (L.) Kostel. from Palestine. *Arabian Journal for Science and Engineering*.
42. Khan, V., Najmi, A.K., Akhtar, M., Aqil, M. & Mujeeb, M. 2012. A pharmacological appraisal of medicinal plants with antidiabetic potential. *Journal of Pharmacy and Bioallied Sciences*, 4(1), pp. 27–42.
43. Kherbache, A., Senator, A., Laouicha, S., Al-Zoubi, R.M. and Bouriche, H., 2020. Phytochemical analysis, antioxidant and anti-inflammatory activities of *Helichrysum stoechas* (L.) Moench extracts. *Biocatalysis and Agricultural Biotechnology*, *29*, p.101826.
44. de la Garza, A.L., Etxeberria, U., Palacios-Ortega, S., Haslberger, A.G., Aumueller, E., Milagro, F.I. and Martínez, J.A., 2014. Modulation of hyperglycemia and TNFα-mediated inflammation by helichrysum and grapefruit extracts in diabetic db/db mice. *Food & function*, *5*(9), pp.2120-2128.
45. Les, F., Venditti, A., Cásedas, G., Frezza, C., Guiso, M., Sciubba, F., Serafini, M., Bianco, A., Valero, M.S. & López, V. 2017. Everlasting flower *(Helichrysum stoechas Moench*) as a potential source of bioactive molecules with antiproliferative, antioxidant, antidiabetic and neuroprotective properties. *Industrial Crops and Products*, 108(July), pp. 295–302.
46. Lourens, A.C.U., Viljoen, A.M. & van Heerden, F.R. 2008. South African *Helichrysum* species: A review of the traditional uses, biological activity and phytochemistry. *Journal of Ethnopharmacology*, 119(3), pp. 630–652.
47. Mahmood, N. 2016. A review of α-amylase inhibitors on weight loss and glycemic control in pathological states such as obesity and diabetes. *Comparative Clinical Pathology*, 25, pp. 1253–1264.

48. Malolo, F.A.E., Nouga, A.B., Kakam, A., Franke, K., Ngah, L., Flausino, O., Mpondo, E.M., Ntie-Kang, F., Ndom, J.C., Bolzani, V. & Wessjohann, L. 2015. Protease-inhibiting, molecular modeling and antimicrobial activities of extracts and constituents from *Helichrysum foetidum* and *Helichrysum mechowianum* (Compositae). *Chemistry Central Journal*, 9(1).
49. Mati, I.Z., Aljan, I., Ž, Ž., Vajs, V., Jadranin, M., Milosavljevi, S. & Jurani, Z.D. 2013. In vitro antitumor actions of extracts from endemic plant *Helichrysum zivojinii*. *BMC Complementary and Alternative Medicine*, 13(36), pp. 1–12.
50. Meo, S. Di, Reed, T.T., Venditti, P., Victor, V.M., Biologia, D. & Federico, N. 2018. Harmful and Beneficial Role of ROS 2017. *Oxidative Medicine and Cellular Longevity*, 2018(5943635), pp. 1–2.
51. Mogale, M.M.P., Raimondo, D.C. & Vanwyk, B. 2019. The ethnobotany of Central Sekhukhuneland, South Africa. *South African Journal of Botany*, 122, pp. 90–119.
52. Mollica, A., Zengin, G., Locatelli, M., Stefanucci, A., Mocan, A., Macedonio, G., Carradori, S., Onaolapo, O., Onaolapo, A., Adegoke, J., Olaniyan, M., Aktumsek, A. & Novellino, E. 2017. Antidiabetic and antihyperlipidemic properties of Capparis spinosa L.: In vivo and in vitro evaluation of its nutraceutical potential. *Journal of Functional Foods*, 35, pp. 32–42.
53. Morikawa, T., Ninomiya, K., Akaki, J. & Kakihara, N. 2015. Dipeptidyl peptidase-IV inhibitory activity of dimeric dihydrochalcone glycosides from flowers of *Helichrysum arenarium*. *Journal of Natural Medicines*, 69, pp. 494–506.
54. Mükemre, M., Behçet, L. & Çakılcıoğlu, U. 2015. Ethnobotanical study on medicinal plants in villages of Çatak (Van-Turkey). *Journal of Ethnopharmacology*, 166(2015), pp. 361–374.
55. Nana, M., Junko, T., Ayumi, S., Akiko, N., Mayumi, S., Motoshi, K., Shuichi, H. & Eri, H. 2015. Green Rooibos Extract from *Aspalathus linearis*, and its Component, Aspalathin, Suppress Elevation of Blood Glucose Levels in Mice and Inhibit α-amylase and α-glucosidase Activities in vitro. *Food Science and Technology Research*, 21(2), pp. 231–240.
56. Nie, Z., Funk, V.A., Meng, Y., Deng, T., Sun, H. & Wen, J. 2016. Recent assembly of the global herbaceous flora: evidence from the paper daisies (Asteraceae: Gnaphalieae). : 1795–1806.
57. Njagi, J.M., Ngugi, M.P., Kibiti, C.M., Ngeranwa, J., Njue, W., Gathumbi, P. & Njagi, E. 2015. Hypoglycemic effect of *Helichrysum odoratissimum* in alloxan-induced diabetic mice. *The Journal of Phytopharmacology*, 4(1), pp. 30–33.
58. Nyakudya, T.T., Tshabalala, T., Dangarembizi, R., Erlwanger, K.H. & Ndhlala, A.R. 2020. The Potential Therapeutic Value of Medicinal Plants in the Management of Metabolic Disorders. *Molecules 2*, 25, pp. 1–20.
59. Odeyemi, S. & Bradley, G. 2018. Medicinal Plants Used for the Traditional Management of Diabetes in the Eastern Cape, South Africa: Pharmacology and Toxicology. *Molecules*, 23(2759).
60. Orhan, D.D., Aslan, M. & Ergun, F. 2014. Enzyme inhibitory and radical scavenging effects of some antidiabetic plants of Turkey. *Iranian Journal of Basic Medical Sciences*, 17, pp. 426–432.
61. Oyedemi, S.O., Bradley, G. & Afolayan, A.J. 2009. Ethnobotanical survey of medicinal plants used for the management of diabetes mellitus in the Nkonkobe municipality of South Africa. *Journal of Medicinal Plants Research*, 3(12), pp. 1040–1044.
62. Panda, S.K., Cláudio, L., Sahal, D. & Leonti, M. 2019. Editorial : Ethnopharmacological Studies for the Development of Drugs With Special Reference to Asteraceae. *Frontiers in Pharmacology*, 10(September), pp. 1–2.
63. Pieme, C.A., Tatangmo, J.A., Simo, G., Cabral, P., Nya, B., Jocelyne, V., Moor, A., Moukette, B.M., Nzufo, F.T., Legrand, B., Nono, N. & Sobngwi, E. 2017. Relationship between hyperglycemia, antioxidant capacity and some enzymatic and non - enzymatic antioxidants in African patients with type 2 diabetes. *BMC Research Notes*, 10(141), pp. 1–7.
64. Polat, R., Cakilcioglu, U. & Satıl, F. 2013. Traditional uses of medicinal plants in Solhan (Bingöl-Turkey). *Journal of Ethnopharmacology*, 14830(3), pp. 951–963.
65. Ranaivoarisoa, R.H., Ralambonirina, S.T.R., Randriamialinoro, F., Randrianasolo, R., Ratsimbason, M. & Ranarivelo, L.R. 2020. Antiplasmodial Activity of the Extracts and Flavonoids Isolated from *Helichrysum gymnocephalum Humbert* (Asteraceae) from Madagascar. In *African Natural Plant Products, Volume III: Discoveries and Innovations in Chemistry, Bioactivity, and Applications*. 2020 American Chemical Society, pp. 171–178.
66. Rout, S.P., Chowdary, K.A., Kar, D.M. & Das, L. 2008. Plants as source of novel Anti-Diabetic Drug: Present Scenario and Future Plants as source of novel Anti-Diabetic Drug: Present Scenario. *Current Trends in Biotechnology and Pharmacy*, 3(1), 614–632.
67. Savych A, Marchyshyn S, B.R. 2020. Determination of fatty acid composition content in the herbal antidiabetic collections. *Pharmacia*, 67(3): 153–159.

68. Savych, A., Marchyshyn, S. and Milian, I., 2021. Determination of carbohydrates in the herbal antidiabetic mixtures by GC-MC. *Acta Pharmaceutica*, *71*(3), pp.429-443.
69. Semenya, S., Potgieter, M. & Erasmus, L. 2012. Ethnobotanical survey of medicinal plants used by Bapedi healers to treat diabetes mellitus in the Limpopo Province, South Africa. *Journal of Ethnopharmacology*, 141(1), pp. 440–445.
70. Sharafzadeh, S. 2011. Pyrethrum, Coltsfoot and Dandelion: Important Medicinal Plants from Asteraceae Family. *Australian Journal of Basic and Applied Sciences*, 5(12), pp. 1787–1791.
71. Spínola, V. & Castilho, P.C. 2017. Evaluation of Asteraceae herbal extracts in the management of diabetes and obesity. Contribution of caffeoylquinic acids on the inhibition of digestive enzymes activity and formation of advanced glycation end-products (*in vitro*). *Phytochemistry*, 143(2017), pp. 29–35.
72. Spínola, V., Gouveia-Figueira, S. & Castilho, P. 2016. Endemic Asteraceae from Madeira archipelago: A relation of hypoglycemic activity to their polyphenolic composition. *Planta Medica 2016*, 82(S01), pp. S1–S381.
73. Süzgeç-Selçuk, S. & Birteksöz, A.S. 2011. Flavonoids of *Helichrysum chasmolycicum* and its antioxidant and antimicrobial activities. *South African Journal of Botany*, 77(1), pp. 170–174.
74. Tirillini, B., Menghini, L., Leporini, L., Scanu, N., Marino, S., Pintore, G., Saffi, V.A. & Pu, U. 2012. Antioxidant activity of methanol extract of *Helichrysum foetidum Moench*. *Natural Product Research*, 27(16), pp. 14.
75. Zengin, G., Cvetanović, A., Gašić, U., Tešić, Ž., Stupar, A., Bulut, G., Ibrahime, K., Uysal, S., Carene, M., Picot-allain, N. & Fawzi, M. 2020. A comparative exploration of the phytochemical profiles and bio-pharmaceutical potential of *Helichrysum stoechas* subsp. barrelieri extracts obtained via five extraction techniques. *Process Biochemistry*, 91(2019), pp. 113–125.

Chapter three

Effect of sequential and non-sequential solvent extraction on the total polyphenol content and antioxidants capacity of green and fermented rooibos tea (*Aspalathus linearis*)- Short communication.

Akinfenwa O. Akeem [a], Abdul N. Sheik [b], Jeanine L. Marnewick [b], Ahmed A. Hussein [a]*

[a] Department of Chemistry, Cape Peninsula University of Technology, Symphony Rd. Bellville 7535, South Africa; oa.akeemlaja@gmail.com (A.O.A); mohammedam@cput.ac.za (A.A.H.)

[b] Applied Microbial and Health Biotechnology Institute, Cape Peninsula University of Technology, Symphony Rd. Bellville, 7535, South Africa; sheikabduln@cput.ac.za (A.N.S); marnewickj@cput.ac.za (J.L.M.).

*Correspondence: mohammedam@cput.ac.za; Tel.: +27-21-959-6193; Fax: +27-21-959-3055

Abstract

Rooibos tea (*Aspalathus linearis*) is a functional herbal tea widely consumed for health benefits in South Africa and many countries of the world. In this study, we present the use of sequential (SE) and nonsequential (NSE) solvent extraction of green (GR) and fermented (FR) rooibos tea (*Aspalathus linearis*) with acetone, ethanol and aqueous ethanol, and its effects on total polyphenol and antioxidant capacity. The total polyphenol content (TPC) was determined using Folin Ciocalteu's phenol reagent while the antioxidant capacities (AC) were determined by Trolox equivalent antioxidant capacity (Teac) and ferric reducing ability of plasma (FRAP) assays. This study aimed to demonstrate the polyphenol and antioxidant capacity of GR and FR extracts as influenced by the sequence of extraction and solvent polarity used. From the results, GR is more active and have higher TPC and antioxidant capacity (AC) than FR at 1 mg/mL in all sequence and the solvent used. TPC follows the order; GR; 100% Ethanol (NSE) > GR; 30% hydro ethanol (SE) > GR; 100% Acetone (NSE) > FR; 30% hydro ethanol (SE) > FR; 100% Ethanol (NSE) > FR; 100% Acetone (NSE). The result indicated that a two-step SE with hydroethanolic extract of GR gives a better total polyphenol and antioxidant potential than with acetone. This study contributes to the bioavailability of bioactive constituents of rooibos tea through solvent-polarity specificity.

Keywords: Extraction, solvents, polarity, green rooibos, fermented rooibos, polyphenol content, antioxidant capacity.

3.1. Introduction

Determination of phytochemical constituents of functional plant materials by extraction is essential to achieve the optimum potential of the plant. Solvent extraction remains the most used conventional method over the non-conventional extraction for extraction and isolation of bioactive compounds in phytochemistry. This is attributed to high yield, short process time and a relatively low cost (Akinfenwa et al., 2020). The method requires the selection of appropriate solvent and polarity for the targeted secondary metabolites such as phenolic compounds, alkaloids and terpenoids (Brusotti et al., 2014). The plethora of evidence confirming the

richness of rooibos in antioxidant polyphenols places the tea at a central focus in foods, drugs, and biomedical research (Dludla et al., 2020). Two variants of the tea are the green (unfermented) rooibos tea and the red (fermented) tea. Fermentation of GR to red, FR brought about by enzymes and heat, gives the tea a soothing aroma that is responsible for sensory acceptance result in a slight variation of its constituents. However, it is known that aspalathin, the major compound exist in both GR and FR and the polar fractions represent the phenolic constituent of both type (Viljoen et al., 2016; Joubert et al., 2013). To achieve total extraction of the polar fraction, a solvent polarity-specific is required. Worthy of note is that acetone and methanol have a similar polarity index (5.1) that is less than water (10.2) but greater than ethanol (4.3) on the polarity index scale (Gupta et al., 1997). This probably accounts for why most reports of extraction of the phenolic content of rooibos were done with water. Despite this, we believe that variation of solvent polarity between acetone and ethanol and aqueous ethanol would be best to determine the impact of solvent polarity on the extraction of TPC which can also reflect on the AC. The effects of different extraction parameters have been studied on the extraction of total polyphenol content (TPC). Joubert (1990) reported the effect of extraction temperature, the mass ratio of dry tea leaf and flow rate of water on single-stage batch extraction of TPC (Joubert, 1990). In a comparative study of extraction temperature on TPC of aqueous rooibos extracts, Santos et al., (2016) found that extraction temperature at 85˚C yielded higher TCP, followed by at 75 ˚C and 65 ˚C was least effective (Santos et al., 2016). A similar study by Damiani et al., (2019) evaluated the influence of cold and hot brewing of rooibos which proved that extract from hot brewing demonstrated higher AC and TCP from in vitro experiments. Furthermore, the effect of extraction time from rooibos infusion by Michael D. McAlpine and Wendy E. Ward (2016) suggested that increased TPC and AC of rooibos can be achieved with a longer steep time (10 minutes) (Damiani et al., 2019; McAlpine & Ward, 2016). However, for the isolation of phytochemicals from plant materials, solvent extraction is commonly used to obtain the total extract. Until the time of this study, limited reports exist of the impact of solvent polarity on the SE and NSE extraction of TPC and the AC of rooibos. Hence, this study aimed to demonstrate the influence of sequence and solvent polarity in the extraction of polyphenol and antioxidant capacity of GR and FR extracts.

3.2. Materials

Coarsely ground rooibos tea (GR and FR) was generously donated by the South African Rooibos Council, P.O Box 64, Rooibos Avenue, 8135. Clanwilliam. All reagents are analytical grade. Acetone and ethanol were supplied by KIMIX Chemical and Lab Supplies, Western Cape, South Africa. 2,2'-azinobis-(3-ethylbenzothiazoline-6-sulfonic acid) diammonium salt (ABTS), 6-hydroxy-2,5,7,8-tetramethylchroman-2-carboxylic acid (Trolox), 3,4,5-trihydroxybenzoic acid (gallic acid), Folin-Ciocalteu reagent (2N solution), potassium persulfate

($K_2S_2O_8$), and sodium carbonate (Na_2CO_3) were purchased from Sigma-Aldrich Chemical Co. (Milan, Italy). Deionized water was generated in-house from a Milli-Q system by Merck Millipore (Merck KGaA, Darmstadt, Germany).

3.3. Method

3.3.1. Sequential and non-sequential Extraction

A two-step sequential extraction of GR and FR were carried out separately. 100 grams each of coarsely ground GR and FR respectively were first soaked in 500 mL (100%) acetone respectively overnight. The supernatant solvent was carefully decanted, filtered through Whatman No. 4 filter paper and vacuum concentrated to give two samples. The residue obtained in each case was further extracted with 30% aqueous ethanol respectively which gave the third and fourth samples. The non-sequential extracts were obtained in one step with (100%) ethanol for both GR and FR and resulted in two samples. A total of six samples were collected from the extractions and accessed for total polyphenols content and antioxidants capacities.

3.3.2. Determination of Total polyphenol content

The total polyphenol content of the aqueous rooibos extract was determined using the Folin Ciocalteu's phenol reagent according to the method described by Ajuwon *et al*., (2014) with modification and result expressed as mg gallic acid equivalents (Ajuwon et al., 2014). In brief, Folin & Ciocalteu's phenol reagent was diluted 10 times with distilled water and a 7.5% sodium carbonate (Sigma, South Africa) solution was prepared. In a 96-well plate, 25 µL of the extract was mixed with 125 µL Folin & Ciocalteu's phenol reagent and 100 µL sodium carbonate. The plate was incubated for 2 hours at room temperature. The absorbance was then measured at 765 nm in a Multiskan spectrum plate reader (Thermo Electron Corporation, USA). The samples polyphenol values were calculated using gallic acid (Sigma, South Africa) standard curve with concentrations varying between 0 and 500 mg/L.

3.3.3. Determination of Antioxidants capacities of extracts

The antioxidants capacities were determined by the methods of ABTS and ferric reducing ability of plasma (FRAP). The ABTS and FRAP assays use an oxidation/reduction reaction to measure the ability of a sample to reduce hydrogen peroxide and Fe (III) to Fe (II) respectively. An antioxidant donates electrons in the same manner as a reductant in oxidation/reductions, so it is assumed that the FRAP assay is a method for evaluating antioxidant capacity. Briefly, the free radical of ABTS was prepared by mixing 8 mM ABTS salt with 140 mM potassium peroxodisulfate ($K_2S_2O_8$), and the solution was stored in the dark for 48 hours before the assay was performed. Each sample (25 μL) was mixed with 275 μL $ABTS^+$ solution in a 96-well clear

plate. The plate was read after 30 min incubation at room temperature in a Multiskan Spectrum plate reader (Thermo Fisher Scientific, Waltham, MA, USA). Trolox was used as the standard. To carry out the FRAP assay, 10 µL (in triplicate) of samples and standards were pipetted to microwell plates. The standards comprised various concentrations (0–1000 µM) of ascorbic acid (AA). Thereafter, 300 µL of FRAP reagent was added to the plates. The FRAP reagent was prepared as follows: 300 mM acetate buffer (pH 3.6), 10 mM TPTZ solution, 20 mM $FeCl_3$ solution and distilled water that made up a final volume of 300 µL. The final volume added to the plate was 310 µL. The plate was incubated for 30 min in the dark and read at 593 nm in a Multiskan reader. The results were expressed as µmol Ascorbic Acid Equivalents (AAE)/g.

3.4. Result:

3.4.1. Total polyphenol content

The TPC of GR and FR extracts are presented in Table 3.1 and Fig 3.1. NSE ethanolic extract of GR displayed the highest content of polyphenols (0.372912 mg gallic acid equivalents). This was repeated for other solvent-polarity for GR over FR at 1 mg/mL concentration. However, the amount of TPC in both GR and FR extracts from hydroethanolic (SE) became nearly the same as the concentration decreased to 0.0625 mg/mL. Cumulative results show that GR samples of both sequential and non-sequential extraction are more active and have higher polyphenol content compared to FR extracts. The total polyphenol content of extracts at concentration of 1 mg/mL follows the order; GR; 100% Ethanol (NSE) > GR; 30% hydro ethanol (SE) > GR; 100% Acetone (NSE) > FR; 30% hydro ethanol (SE) > FR; 100% Ethanol (NSE) > FR; 100% Acetone (NSE). This result agrees strongly with earlier reports of Damian *et al*. 2019 on hot and cold brewing of green and fermented rooibos and TCP and AC measurement of *Coronopus didymus* by Noreen *et al*., (2017) (Damiani et al., 2019; Noreen et al., 2017)

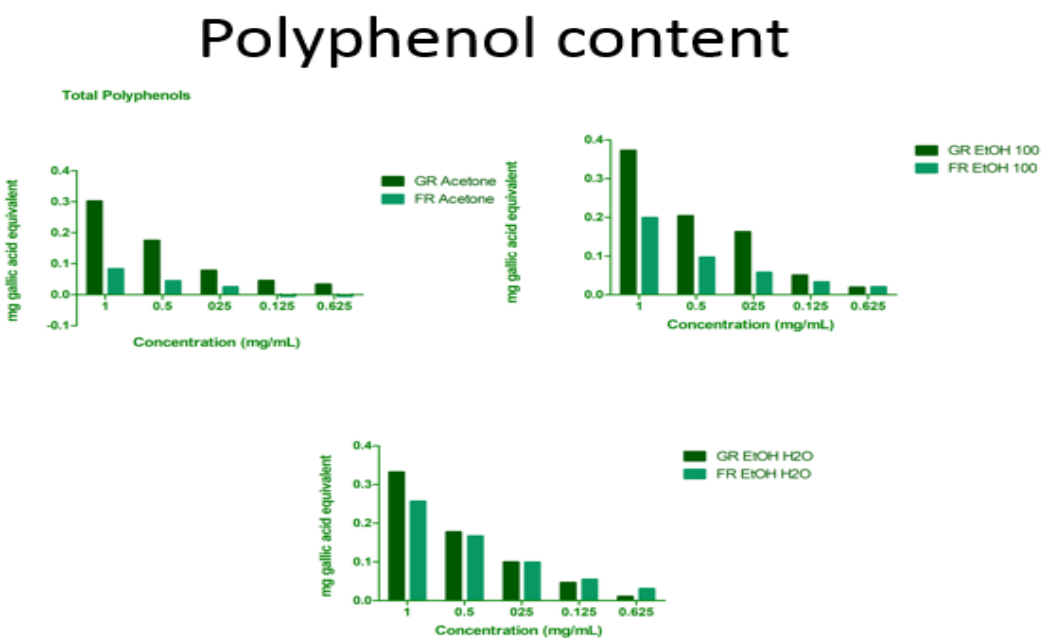

Figure 0.1: Total Polyphenol content of GR and FR extracts

Table 0.1: TPC, FRAC and AC of GR and FR at 1 mg/mL

Samples	**Total polyphenol content**		**ABTS**		**FRAP**	
Solvent Conc. (1 mg/mL)	GR	FR	GR	FR	GR	FR
100% Acetone (NSE)	0.301453	0.082868	0.239997	0.4637	0.848905	0.631696
30% hydro ethanol (SE)	0.331335	0.256111	0.250173	0.293635	1.04207	1.077099
100% Ethanol (NSE)	0.372912	0.199009801	0.321474	0.53132	1.075812	0.662488

3.4.2. Antioxidant capacities

The FRAP assay measures the antioxidant potential in samples while the TEAC assay measures the ability of antioxidants to scavenge the stable radical cation $ABTS^{+}$ (a blue-green chromophore) that decreases in its intensity in the presence of antioxidants. Reduction of Fe (III)/(II) was measured as µmole vitamin C/g sample and $ABTS^{+}$ as µmole Trolox/g sample respectively. As illustrated in Table 3.3, Fig. 3.2 and Fig. 3.3, the scavenging (antioxidant) potential of the extracts revealed higher FRAP values for GR than FR within the same solvent-polarity. A similar trend was recorded for TPC. A higher FRAP and lower ABTS values indicate better antioxidant potential. Hence, GR displayed higher antioxidants potentials as indicated by higher FRAP and lower ABTS values, respectively.

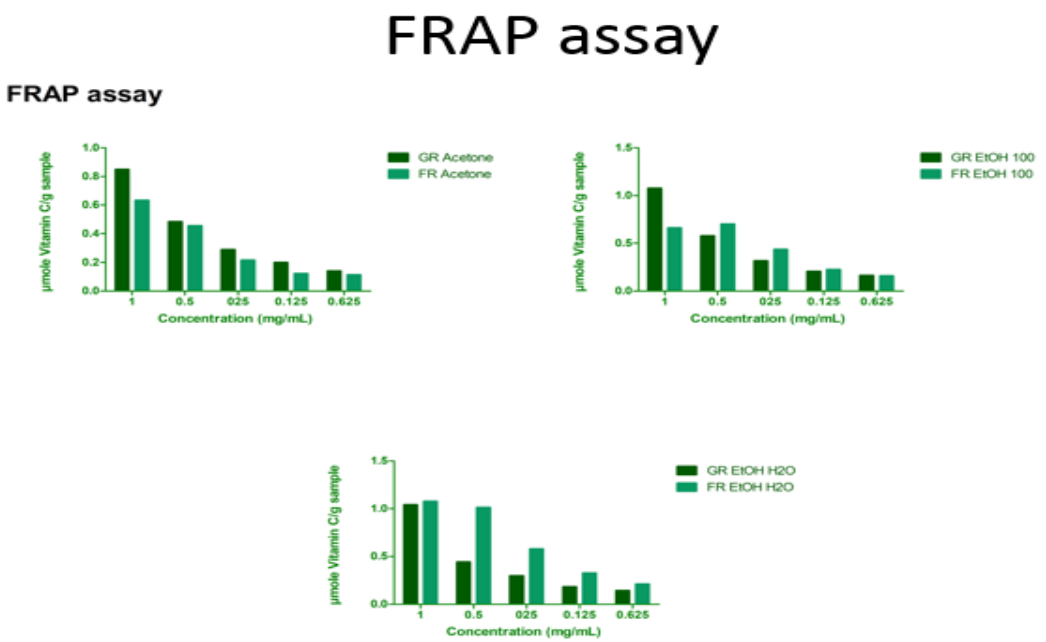

Figure 0.2: Ferric reducing potentials of Gr and FR extracts

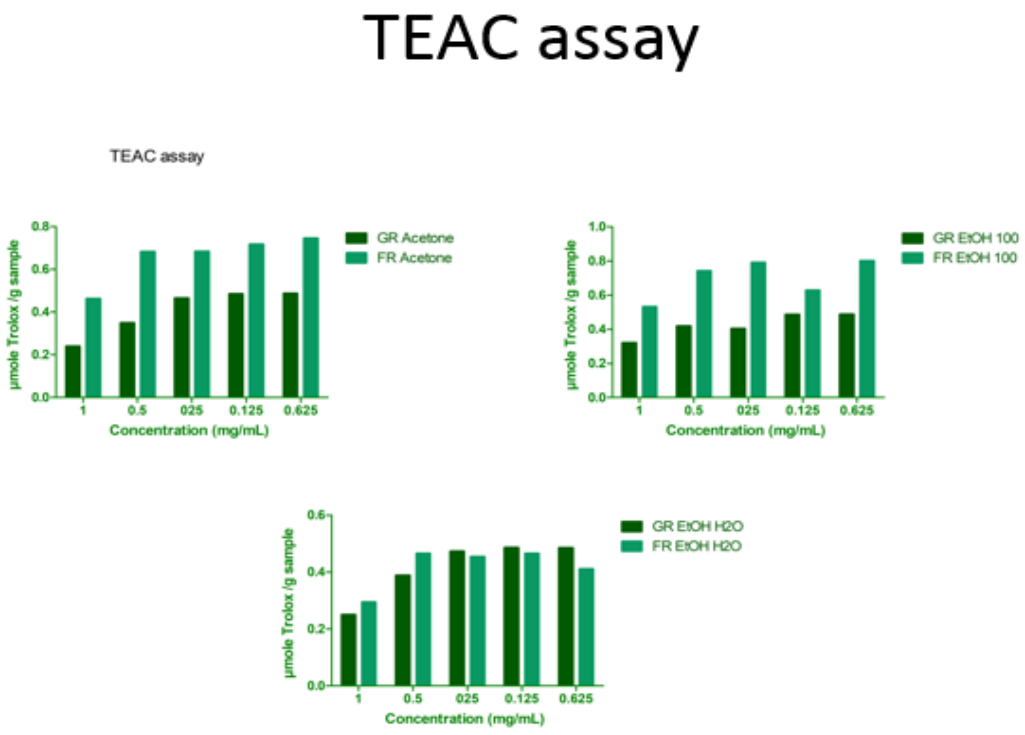

Figure 0.3: Free radical scavenging ability of GR and FR extracts

3.4.3. Conclusion

In the present study, we explored a single and double step solvent extraction of both fermented and unfermented rooibos for evaluation of their phenolic and antioxidant properties. Data from in vitro antioxidant capacity by FRAP and ABTS assays confirmed a higher potency for ethanol and hydro ethanol extracts over acetone extracts for green rooibos and red rooibos. Further studies to fully characterise and compare the bioactive compounds from the three solvents used and their related application is ongoing. Information from this work will be helpful in the background for better utilisation of the green and red *Aspalathus linearis*.

Conflict of interest statement:

The authors declare no conflict of interest.

Acknowledgement:

We wish to acknowledge the South African Rooibos Council (SARC) and Centre for Postgraduate Studies of cape Peninsular university of technology for their financial support towards the completion of this research. In addition, partial funding was provided by the South African Medical Research Council (SAMRC) through its Division of Research Capacity Development under funding received from the South African National Treasury. The content hereof is the sole responsibility of the authors and do not necessarily represent the official views of the SAMRC or the funders.

References

Ajuwon, O.R., Oguntibeju, O.O. & Marnewick, J.L. 2014. Amelioration of lipopolysaccharide-induced liver injury by aqueous rooibos (*Aspalathus linearis*) extract via inhibition of pro-inflammatory cytokines and oxidative stress. C*omplementary and Alternative Medicine*, 14(392), pp. 1–12.

Akinfenwa, A.O., Cheikhyoussef, A., Cheikhyoussef, N. and Hussein, A.A., 2020. Cold pressed chia (Salvia hispanica L.) seed oil. In *Cold Pressed Oils* (pp. 181-190). Academic Press.

Brusotti, G., Cesari, I., Dentamaro, A., Caccialanza, G. & Massolini, G. 2014. Isolation and characterization of bioactive compounds from plant resources: The role of analysis in the ethnopharmacological approach. *Journal of Pharmaceutical and Biomedical Analysis*, 87, pp. 218–228.

Damiani, E., Carloni, P., Rocchetti, G., Senizza, B., Tiano, L., Joubert, E., Beer, D. De & Lucini, L. 2019. Impact of Cold versus Hot Brewing on the Phenolic Profile and Antioxidant Capacity of Rooibos (*Aspalathus linearis*) Herbal Tea. *Antioxidants*, 8(499), pp. 1–19.

Dludla, P. V, Johnson, R., Mazibuko-mbeje, S.E., Muller, C.J.F., Louw, J., Joubert, E., Orlando, P., Silvestri, S., Chellan, N., Nkambule, B.B., Essop, M.F. & Tiano, L. 2020. Fermented rooibos extract attenuates hyperglycemia-induced myocardial oxidative damage by improving mitochondrial energetics and intracellular antioxidant capacity. *South African Journal of Botany*, 131, pp. 143–150.

Gupta, M.N., Batra, R., Tyagi, R. & Sharma, A. 1997. Polarity Index : The Guiding Solvent Parameter for Enzyme Stability in Aqueous-Organic Cosolvent Mixtures. *Biotechnology Progress*, 13(3), pp. 284–288.

Joubert, E. 1990. Effect of batch extraction conditions on extraction of polyphenols from rooibos tea (*Aspalathus linearis*). *International Journal of Food Science and Technology*, 25, pp. 339–343.

Joubert, E., Beer, D. De, Malherbe, C.J., Muller, N., Bonnet, S.L., Westhuizen, J.H. Van Der & Ferreira, D. 2013. Occurrence and sensory perception of Z-2-(*β-D*-glucopyranosyloxy)-3-phenylprop-enoic acid in rooibos (*Aspalathus linearis*). *Food Chemistry*, 136(2), pp. 1078–1085.

McAlpine, M.D. & Ward, W.E. 2016. Influence of steep time on polyphenol content and antioxidant capacity of black, green, rooibos, and herbal teas. *Beverages*, 2(17), pp. 1–12.

Noreen, H., Semmar, N., Farman, M. & McCullagh, J.S.O. 2017. Measurement of total phenolic content and antioxidant activity of aerial parts of medicinal plant *Coronopus didymus*. *Asian Pacific Journal of Tropical Medicine*, 10(8), pp. 792–801.

Santos, J.S., Deolindo, C.T.P., Esmerino, L.A., Genovese, M.I., Fujita, A., Marques, M.B., Rosso, N.D., Daguer, H., Valese, A.C. & Granato, D. 2016. Effects of time and extraction temperature on phenolic composition and functional properties of red rooibos (Aspalathus linearis). *Food Research International*, 89, pp. 476–487.

Viljoen, M., Muller, M., De Beer, D. and Joubert, E., 2017. Identification of broad-based sensory attributes driving consumer preference of ready-to-drink rooibos iced tea with increased aspalathin content. *South African Journal of Botany*, *110*, pp.177-183.

SUPPLEMENTARY DATA

Supplementary 0.1: Total polyphenol and antioxidant capacity of acetone extract of GR

Conc. of GR Acetone (mg/mL)	Total polyphenols (mg gallic acid equivalent)	FRAP assay (µmole vitamin C/g sample)	ABTS (µmole Trolox/g sample)
1	0.301453	0.848905	0.239997
0.5	0.174958	0.484067	0.348451
0.25	0.078261	0.288472	0.465275
0.125	0.044777	0.198773	0.484892
0.65	0.033248	0.139928	0.487226

Supplementary 0.2: Total polyphenol and antioxidant capacity of ethanol (100%) extract of GR

Conc. of GR 100% Ethanol (mg/mL)	Total polyphenols (mg gallic acid equivalent)	FRAP assay (µmole vitamin C/g sample)	ABTS (µmole Trolox/g sample)
1	0.372912	1.075812	0.321474
0.5	0.203958	0.57722	0.417166
0.25	0.161689	0.316426	0.403646
0.125	0.050203	0.20509	0.485839
0.65	0.018976	0.162238	0.487479

Supplementary 0.3: Total polyphenol and antioxidant capacity of hydroethanolic extract of GR

Conc. of GR 30% aqueous ethanol (mg/mL)	Total polyphenols (mg gallic acid equivalent)	FRAP assay (µmole vitamin C/g sample)	ABTS (µmole Trolox/g sample)
1	0.331335	1.04207	0.250173
0.5	0.177147	0.440566	0.387834

0.25	0.099045	0.296245	0.472445
0.125	0.046441	0.181673	0.485502
0.65	0.010161	0.141745	0.484787

Supplementary 0.4: Total polyphenol and antioxidant capacity of acetone extract of FR

Conc. Of FR Acetone (mg/mL)	Total polyphenols (mg gallic acid equivalent)	FRAP assay (µmole vitamin C/g sample)	ABTS (µmole Trolox/g sample)
1	0.082868	0.631696	0.4637
0.5	0.044331	0.456027	0.68284
0.25	0.024739	0.215548	0.68342
0.125	-0.00469	0.121992	0.71738
0.65	-0.0046	0.112822	0.74613

Supplementary 0.5: Total polyphenol and antioxidant capacity of ethanol extract of FR

Conc. Of FR 100% ethanol (mg/mL)	Total polyphenols (mg gallic acid equivalent)	FRAP assay (µmole vitamin C/g sample)	ABTS (µmole Trolox/g sample)
1	0.199009801	0.662488	0.53132
0.5	0.096412	0.700824	0.741578
0.25	0.057626	0.436171	0.790
0.125	0.032818	0.224606	0.62873
0.65	0.019608	0.159712	0.8014

Supplementary 0.6: Total polyphenol and antioxidant capacity of hydroethanolic extract of FR

Conc. Of FR 30% aqueous ethanol (mg/mL	Total polyphenols (mg gallic acid equivalent)	FRAP assay (µmole vitamin C/g sample)	ABST (µmole Trolox/g sample)
1	0.256111	1.077099	0.293635
0.5	0.166961	1.012878	0.46456
0.25	0.098906	0.576757	0.4539
0.125	0.054538	0.325229	0.46479
0.65	0.030414	0.209434	0.411

Chapter four

Protective Effects of Linearthin and Other Chalcone Derivatives from *Aspalathus linearis* (Rooibos) Against UVB Induced Oxidative Stress and Toxicity in Human Skin Cells

Akinfenwa O. Akeem [a], Abdul N. Sheik [b], Jeanine Marnewick [b], Ahmed A. Hussein [a]*

[a] Department of Chemistry, Cape Peninsula University of Technology, Symphony Rd. Bellville 7535, South Africa; oa.akeemlaja@gmail.com (A.O.A); mohammedam@cput.ac.za (A.A.H.)

[b] Applied Microbial and Health Biotechnology Institute, Cape Peninsula University of Technology, Symphony Rd. Bellville, 7535, South Africa; sheikabduln@cput.ac.za (A.N.S); marnewickj@cput.ac.za (J.L.M.).

*Correspondence: mohammedam@cput.ac.za; Tel.: +27-21-959-6193; Fax: +27-21-959-3055

Abstract

Skin cells continuously suffer damages from exposure to ultraviolet light which results in ultraviolet light induced-oxidative stress and skin thinning. This has necessitated the formulation of several cosmetic products rich in antioxidants and free radical scavengers. *Aspalathus linearis* (rooibos) is an endemic South African plant growing naturally in the Cape region. The plant is rich in phenolics with a wide spectrum of health benefits. The chemical study of an acetonic extract of green *A. linearis* afforded a novel compound namely linearthin (**1**) and two known dihydrochalcones, aspalathin (**2**) and nothofagin (**3**). The chemical structure of the novel compound was elucidated based on spectroscopic data analysis. The bio-evaluation of the isolated chalcones *in vitro* for protection against UV-induced oxidative stress via cell viability, metabolic activity, apoptosis, and cytotoxicity using HaCaT and SK-MEL-1 skin cells models. Cell viability, metabolic activity, oxidative status, and apoptotic markers were systematically assessed. It was observed that pre-treatment with isolates for 4- and 24 hours at low concentrations were sufficient to protect skin cells from UVB damage *in vitro* as evidenced by higher cell viability and improved metabolic activity. The results further show that the pre-treatment regimen employed by this study involved some degree of cellular adaptation as evidenced by higher levels of reduced glutathione with a concomitant decrease in lipid peroxidation and lowered caspase 3 activity. Furthermore, compound **1** was most cytoprotective against UVB irradiation of HaCaT cell line (over 24 hours) with an IC_{50} of 282 µg/mL and SK-MEL-1 cell line with IC_{50} values of 248.3 and 142.6 µg/mL over 4 and 24 hours, respectively. On the other hand, HaCaT cells exposed to **2** over 4 hours before UVB irradiation showed the highest degree of cytoprotection with an IC_{50} of 398.9 µg/mL among the four studied samples. These results show that linearthin (**1**) and the two glycoside dihydrochalcone

of *A. linearis* have the potential to be further developed as antioxidant cosmetic ingredients that protect skin against UVB induced damage.

Keywords: Skin cells, UV light exposure, *Aspalathus linearis*, linearthin, aspalathin derivatives, isolation, characterisation.

4.1. Introduction

The human skin is continuously exposed to environmental stressors, among these, solar UV radiation is considered the most ubiquitous and damaging [1]. The UVB component of solar radiation is strongly linked to its potential to generate excessive reactive oxygen species (ROS) that damage cellular macromolecules and is recognised as an initiator of photocarcinogenesis and mutagenesis [2]. Although the skin is equipped with an intricate defence system, encompassing both enzymatic and non-enzymatic components to protect it from these adverse biological effects, excessive exposure to UV radiation can overwhelm and diminish these systems [3-4]. Studies have shown that excessive ROS production and/or its ineffective elimination is implicated in triggering pro-inflammatory and apoptotic signalling cascades that are implicated in many cutaneous pathological processes [2, 5].

With a notion to protect humans against the adverse effects of UV radiation, there is growing interest in the use of naturally occurring plant products, including polyphenols, for the prevention of UV-induced skin photodamage, with ethnobotanical antioxidants showing surmountable promise [6-8]. *Aspalathus linearis* (Brum.f) Dahlg. (Fabaceae) (rooibos) is a fynbos shrub endemic to the Cape Floristic Region of South Africa [9]. It is globally consumed as a herbal tisane but is increasingly being used as an additive to skincare products [10-13]. *A. linearis* commonly exists as a green (unfermented) rooibos with a chemical profile that reflects high chalcone contents including the unique chalcone, aspalathin. The red type (fermented rooibos) has been shown to result from the oxidative/enzymatic fermentation of the green rooibos plant material under certain conditions. The oxidation reactions that occur during the fermentation process change the chemical profile of the plant and showed a decrease in the dihydrochalcone derivatives content especially aspalathin [14-15]. Hence, the green rooibos is a better option for targeted isolation of aspalathin and polyphenolic compounds reported as active ingredients for cosmeceutical products [16-17]. Extracts prepared from green rooibos possess potent antioxidant, anti-inflammatory, and anti-tumour properties [18-21] with evidence supporting its photoprotective effects in the skin [12, 20, 21]. These effects are strongly linked to its unique phytochemical composition and bioactive compounds [23].

The green rooibos is characterized by high aspalathin (ASP) derivatives content. These compounds are known to have a dihydrochalcone skeleton and are connected with a *C*-glycosidic linkage [11, 24]. Several studies have exhibited the potent antioxidant properties of ASP [24-26] with percutaneous permeation studies revealing some degree of absorption through the skin [27] which supports its use in cosmeceutical preparations. However, evidence on the role of ASP in UVB-induced skin damage is still lacking.

This study was designed to assess the effects of a green rooibos total extract and three chalcone-related structures on UVB-irradiated human skin cells. We examined the potential of the extract and tested samples to attenuate UVB-induced oxidative stress and maintain cell viability. This study was designed to assess the possible interactions between a green rooibos total extract and three isolated compounds with chalcone-related structures and UVB radiation using two different human cell lines, i.e., HaCaT, an immortalized human keratinocyte cell line derived from non-tumourigenic epidermal cells representing the pre-malignant state and SK-Mel-1, a melanoma cell line established from patient-derived tumour cells. We examined the potential of the extract and test compounds/ samples to attenuate UVB-induced oxidative stress and maintain cell viability in both cell lines.

4.2. Materials and Methods

4.2.1. Plant

Freshly dried and pulverized green rooibos plant was generously donated by the Rooibos Council of South Africa (P.O Box 64, Rooibos Avenue, 8135. Clanwilliam) in April 2019. The plant was stored at room temperature and protected from light before use.

4.2.2. Chemicals and equipment

Analytical/HPLC grade chemicals supplied by Sigma-Aldrich, Cape Town, South Africa and Merck, Cape Town, South Africa were used in this study. Organic solvents and acids such as dichloromethane (DCM), ethyl acetate, acetone, methanol (HPLC grade), ethanol, formic acid, and acetic acid were supplied by Merck (Cape Town, South Africa). Thin-layer chromatography (TLC) plates of Silica gel 60 PF_{254} pre-coated on aluminium, Silica gel 60 H (0.040–0.063 mm particle size, from Merck and Sephadex LH-20 (Sigma-Aldrich, Cape Town, South Africa) were used. De-ionized water was generated in-house using Merck Millipore (18.2 MΩ·cm at 25°C) water purification system.

Chromatographic fingerprints were conducted on Reverse-phase High-Performance Liquid Chromatography (Shimadzu, Kyoto, Japan) coupled with a photo-diode array detector equipped with a Discovery® C_{18} column (25 x 1.0 cm, SUPELCO, St, Louis, MO, USA). Structural information's of compounds were recorded using nuclear magnetic resonance (NMR) Ascend 400 MHz NMR spectrometer (Bruker, Rheinstetten, Germany) in deuterated

acetone and deuterated dimethyl sulfoxide. HRMS analysis was conducted on an Ultimate 3000 LC (Dionex, Sunnyvale, CA, USA) coupled to a Bruker QTOF with an electrospray ionization (ESI) interface working in the positive ion mode. UV measurement was done with SPECTROstar Nano (BMG LABTECH, Ortenberg, Germany) 2450 UV-vis spectrophotometer. IR spectrum was recorded on PerkinElmer Fourier- Transform Infrared Spectrometer 2000, equipped with a universal ATR-FTIR (PerkinElmer Spectrum 100, Llantrisant, Wales, UK) at transmission mode of 400 – 4000 cm^{-1}. Cell culture reagents were supplied by ThermoFisher (Cape Town, South Africa) unless otherwise stated.

4.2.3. Extraction and isolation of pure linearthin, aspalathin and nothofagin

One kilogram of green *A. linearis* was exhaustively extracted with acetone (4 litres) in the dark for 24h at room temperature and then filtered. After filtration and concentration, the total extract obtained, 30 g (3%) was then transferred to vials and kept dry till further use. The extract was later subjected to silica gel column (75 x 10 cm) on gradient system (1% MeOH/DCM to 100% MeOH). 250 mL fractions were collected. The concentrated fractions were monitored using TLC and resulted in twenty-two main fractions, labelled I – XXII.

Gravity column chromatography of the main polar fraction XI (3 g) on a silica gel column (40 × 8 cm, gradient mode) using EtOAc, acetone and MeOH afforded a semi-pure compound, 1.2 g), which was further purified on Sephadex column (using gradient mode; 100% H_2O to 100% MeOH) to yield the major compound aspalathin (**4.2**, 0.7 g). The same compound was also isolated from the main fractions VIII, X, and XII. The main fraction XV (0.5 g) was subjected to the silica gel and then Sephadex column chromatography to yield nothofagin (**4.3**, 64 mg). Sequential processing of the main fraction XXII (1 g) on a silica gel column afforded three subfractions; A (382 mg), B (207 mg), and C (124 mg). Subfractions A and B were identified as the same as compound **4.2** from TLC and semi-prep HPLC showing similar retention times/factors. The subfraction C was applied to a Sephadex column and further purified with HPLC using 80% aqueous acetonitrile in isocratic mode resulted in a novel compound linearthin (**4.1**, 10 mg, R_t; 30 min) as an amorphous white-yellowish powder. UV λ_{max} 283.6 and 332 nm (MeOH). FTIR: 1050, 1705, 2950 and 3340 cm^{-1}. HRMS *m*/*z* 443.1135 $[M-H]^+$; 311.0, 269.0, 233.0, 221.0, 179.0, 167.0. $[\alpha]_{25}^{D}$: – 13.3 (*C*: 0.04; MeOH). ^1H and ^{13}C NMR see Table 4.1. To prepare the acetate derivative **4.1a**, 5 mg of **4.1** was mixed with pyridine and acetic anhydride (2.0 mL each; 1:1). The resulting mixture was kept at 37 ℃ for 24 h and then partitioned in ethyl acetate, washed thrice with water and finally purified on silica gel column which yielded 2 mg of compound **4.1a**. ^1H- and ^{13}C-NMR see Table 4.1.

4.2.4. Cell culture and cell conditioning

The human epidermal keratinocytes (HaCaT) and the human melanoma cell line (SKMEL-1) cells used in this study were cultured in Roswell Park Memorial Institute (RPMI) 1640 media

supplemented with antibiotics (100 U/mL streptomycins, 100 U/mL penicillin) and fetal calf serum (FCS, 10 %). Cells were maintained at 37℃ in a humidified atmosphere of 5% CO_2.

For experiments, before exposure to UVB, the cells were conditioned with various concentrations of total green rooibos extract and isolated compounds thereof for 4 or 24 hours. These periods were selected based on the half-life of the compounds as well as previous studies [22, 33]. Exposure to UVB was done according to a previous study. Cells were seeded (3×10^4) in 96-well tissue culture microtitre plates. Cell culture media was aspirated, and the cells were overlayed with PBS. The cells were exposed to UVB light ($80mJ/cm^2$) without the plastic lid. A UVIlink UV crosslinker (UVitek Ltd., Aberdeen, UK) was fitted with six 8-Watt UV tubes giving a wavelength of 302 nm (Vilber Lourmat, Collengien, France) [22]. Control plates were not exposed to UVB light.

4.2.5. Cytotoxicity - MTT

The MTT assay has been extensively used for determining the cytoprotective effects of several phytochemicals [45]. To monitor cell viability as a measure of metabolic activity the MTT assay was performed. The conditioned HaCat and SK-MEL-1 cells (15 000 cells per well in 96-well plates) were incubated for 2 hours using 100 µL MTT solution (5 mg/mL) after PBS washing. The MTT formazan crystals were then solubilised by DMSO resuspension. The optical density of the formazan product was read at 570 nm wavelength with a reference wavelength of 690 nm. The half-maximal inhibitory concentration (IC_{50}) was determined.

4.2.6. Cell Viability - ATP assay

The ATP bioluminescent assay was used to quantify cellular ATP. The Cell Titer-Glo® assay (Promega) was carried out according to the manufacturer's instructions. Cells were seeded in a white microtitre plate (20,000 cells per well) to which the ATP Cell Titer-Glo® Reagent was added (50 µL). The plate was incubated for 30 min at room temperature (RT) in the dark. Luminescence was measured on a Multiskan

Spectrum plate reader (Thermo Fisher Scientific, Waltham, MA, USA). Luminescence is proportional to ATP levels and expressed as relative light units (RLU).

4.2.7. Viability, cytotoxicity, and apoptosis

The ApoTox-Glo™ Triplex Assay (Promega) was used to assess cytotoxicity and apoptosis events in the same cell-based assay well according to the manufacturer's instructions with no deviation from standard protocol. Both luminescence and fluorescence were detected using the Multiskan spectrum plate reader (Thermo Fisher Scientific, Waltham, MA, USA).

4.2.8. Antioxidant response

The thiobarbituric acid assay (TBARS) was used to quantify the levels of melandialdehyde (a marker of lipid peroxidation) in the supernatant of UVB irradiated and non-irradiated cells. The

experiments were conducted as previously described [46]. The optical density was measured at 532 nm with a reference wavelength of 600 nm using a Multiskan Spectrum plate reader (Thermo Fisher Scientific, Waltham, MA, USA). The mean optical density of five samples per treatment was calculated and divided by the absorption coefficient (156 mM^{-1}). Results were expressed as MDA concentration (µM).

Reduced glutathione (GSH) was quantified using an in-house protocol with minor modifications [21]. After the addition of reagents, the cells were lysed to allow quantification of GSH colourimetrically using a plate reader (Thermo Fisher Scientific, Waltham, MA, USA).

4.2.9. Statistical analysis

Biological experiments were conducted in triplicate (independently). Statistical data was determined by one way ANOVA and the Bonferroni test for multiple group comparisons unless otherwise stated. The software used for all analyses was GraphPad prism v.5.0 software (GraphPad Software Inc., San Diego, CA, USA). Results were considered statistically significant where $p < 0.05.5$

4.3. Results

4.3.1. Characterization of isolated compounds

Chromatographic purification of an acetone extract of A. linearis using different techniques including semi-prep HPLC yielded three pure chalcone derivatives, isolated and identified as linearthin (**4.1**), aspalathin (**4.2**) nothofagin (**4.3**) (Figure 4.1).

Compounds **4.2** and **4.3**, consist of *C*-glycoside linked to dihydrochalcone structure and are only being reported from rooibos except for [**4.3**] which was previously isolated from *Nothofagus fusca* and *Schoepfia chinensis* [27-29]. Compounds **4.2**, and **4.3** were identified from their NMR spectra as aspalathin, nothofagin by comparison with the literature (Table 4.1) [30-31, 47]. In addition to the known compounds, we report in this study the isolation and full characterisation of compound **4.1** for the first time.

Compound **4.1** (10 mg) was isolated as an amorphous white-yellowish powder. The HRMS of **4.1** showed a peak at *m*/*z* 443.1135 $[M-H]^+$ corresponding to the molecular formula $C_{21}H_{22}O_{10}$. The UV showed absorption at 332 nm and its FTIR spectrum exhibited bands at 1705 and 3340 cm^{-1} representing the carbonyl and hydroxyl functional groups. The NMR spectra (Table 1) demonstrated dihydrochalcone skeleton features with 3,4-disubstituted ring B. ^{1}H-NMR showed a singlet at 5.82 (H-5'), aromatic signals of 1,3,4-trisubstituted benzene ring at 6.49 (H-6); 6.63 (H-5); 6.61 (H-2) and two methylene groups, at 3.18/3.35 (CH_2-a); 2.75 (CH_2-b). In addition to 1-dioxysugar signals at 3.10/2.91 (CH_2-1``); 3.88 (H-3``); 3.83 (H-4``); 3.77 (H-5``) and 3.43/3.54 (H-6``). The protons CH-2`` showed a germinal large coupling of (*d*, *J*=16.4 Hz) and indicated the group exist in a cyclic structure and isolated by two fully substituted carbons from both sides.

The ^{13}C, and DEPT-135 (Figure 4.2) showed 21 carbons, 15 of them belonging to dihydrochalcone skeleton at d_C: 132.4 (C-1); 116.3 (C-2); 143.6 (C-3); 145.4 (C-4); 115.9(C-5); 119.1(C-6); 100.7 (C-1`); 161.2 (C-2`); 103.0 (C-3`); 161.4 (C-4`); 95.9(C-5`); 164.6(C-6`); 43.6 (C-a); 29.1(C-b) and 203.3 of a carbonyl group. The other 6 carbons belong to a deoxy sugar at ◎C: 33.3 (C-1``); 117.8 (C-2``); 80.0 (C-3``); 74. 1(C-4``); 84.2(C-5``); 63.8(C-6``). The chemical shift of C-2`` (117.8) indicated a dioxygenated carbon. The COSY spectrum showed correlations between H3``/H4``; H4``/H5``; H5``/H6`` which support the location of the dioxygenated carbon at the C2``position. The above NMR data showed very close similarity with **4.2**, especially ring A, and B and the 3 C's unit between the two rings. The differences arise only in the signals of the sugar moiety. Table 4.1 showed the presence of a CH_2 group (d_C 33.3) and a dioxygenated carbon (117.8) in the new structure which indicated a deoxy monosaccharide (Figure 4.2). According to the molecular formula as determined by HRMS ($C_{21}H_{22}O_{10}$) and when compared to aspalathin ($C_{21}H_{23}O_{11}$) indicate the presence of extra unsaturation, and it should be cyclic ether. The acetate derivative (linearthin hepta-acetate, **4.1a**) of **4.1** showed 7 acetate groups which indicate further the presence of the extra cyclic ether.

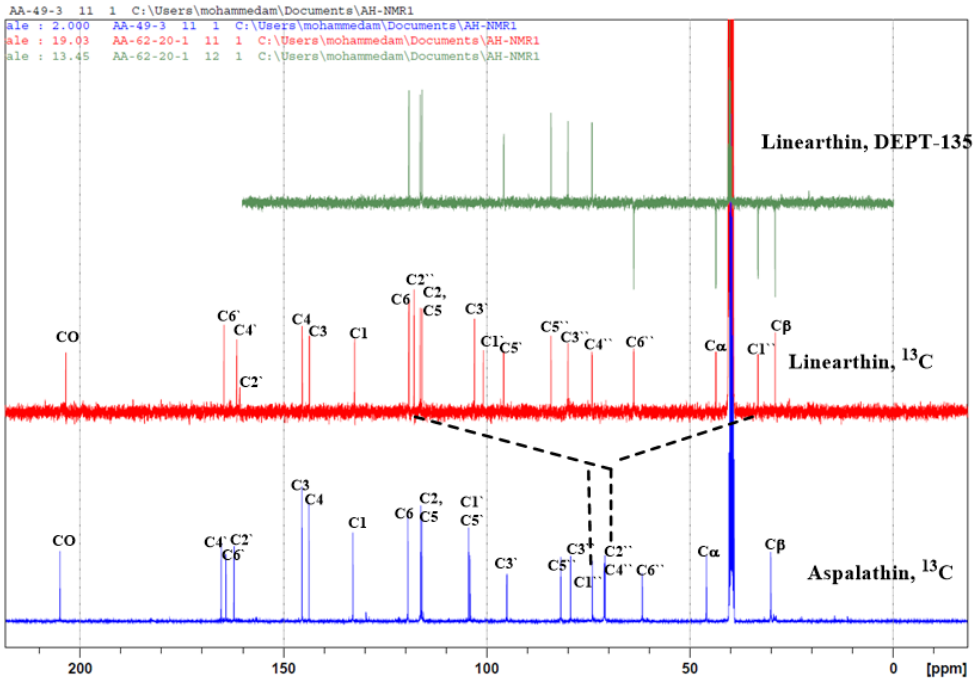

Figure 4.1: Carbon-13 and DEPT-135 comparisons between linearthin (4.1) and aspalathin (4.2)

2D NMR spectra fully established the structure of **4.1**, in particular, the HMBC correlations spectrum (Fig 1) which showed cross-peaks between H-5'/C-1', C-3`, C-6', C-4'; H-1''/C-2`, C-3`, C-4', C-2``, C-3``; H-2``/C-4``; H-4``/C-2``, C-6``; H-5``/C-3``, C-6``; 5`-OH/C-1', C-2', C3' among others and confirmed the structure as shown in Figure 4.1. This compound was given the trivial name linearthin. The relative configuration of the sugar moiety was established from ^{1}H-^{1}H couplings and NOESY spectra of the hepta-acetate derivative (**4.1a**). The spectra from the original compound (**4.1**) could not be used because of the complexity of the sugar protons area. The NOESY spectrum of the hepta-acetate derivative showed a typical fructose-furanoside configuration and showed correlations between H-1``, H-3`` and H-5``; and confirm the *syn*-relationship and the spiral linkage at C-2``, while H-4`` showed correlation with H-6``. Trials to crystalize the acetate derivative to establish the absolute configuration of the isolated compounds were not successful. To the best of our knowledge and according to the SciFinder database, linearthin (**4.1**) has not been isolated before from a natural source, and linearthin represent a very rare skeleton containing *C*-fructofuranoside.

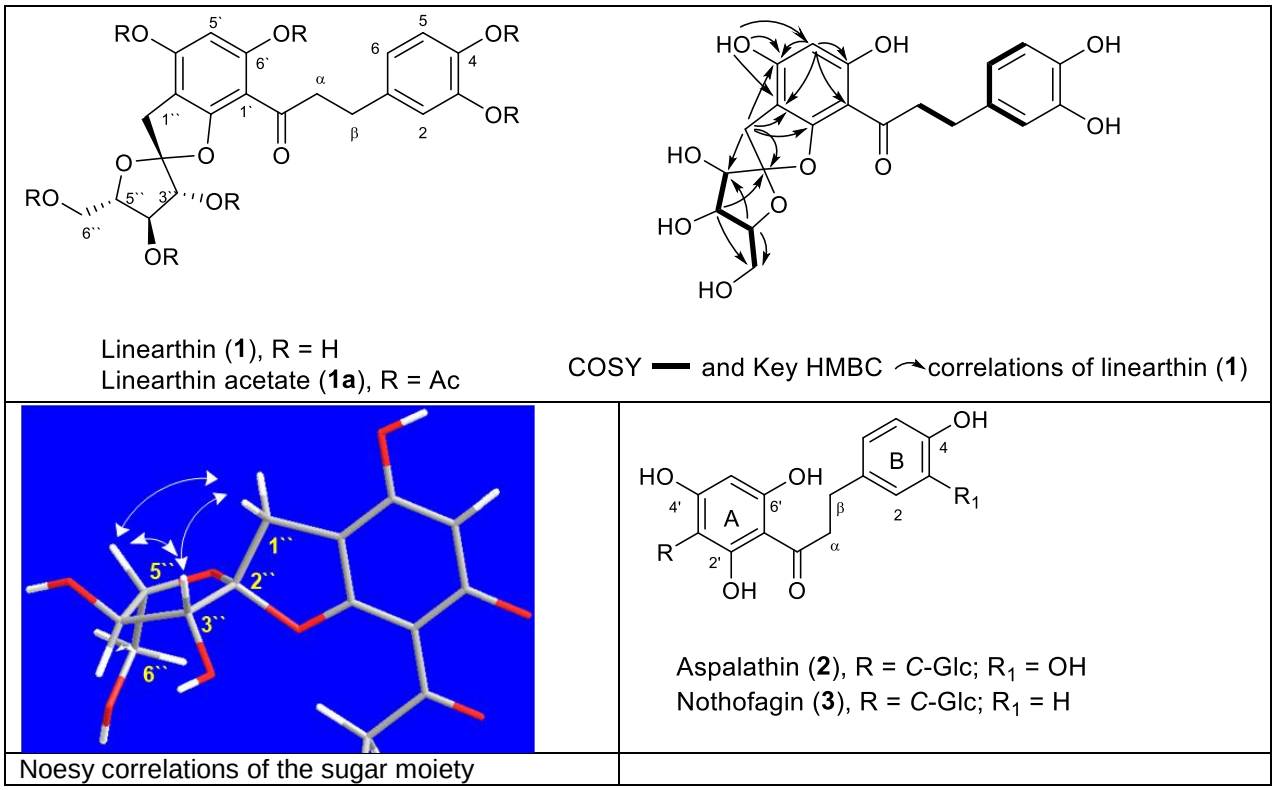

Figure 4.2: Chemical structure of the isolated compounds and COSY, HMBC, and NOESY correlations of 4.1

Table 4.1: ^{1}H and ^{13}C NMR data for compounds 1-3

	Linearthin (4.1) (DMSO-d_6)		Linearthin acetate (4.1a) ($CDCl_3$)		Aspalathin (4.2), (DMSO-d_6)		Nothofagin (4.3), (DMSO-d_6)	
	δ_C	δ_H, (*J*, Hz)	δ_C	δ_H, (*J*, Hz)	δ_C	δ_H, (*J*, Hz)	δ_C	δ_H, (*J*, Hz)
1	132.4		139.2		132.9		132.1	
2	116.3	6.61 (*d*, 1.7)	123.4	7.04†	116.2	6.61 (*br s*)	129.6	7.09 (*d*, 8.1)
3	143.6		141.8		145.4		115.5	6.73 (*d*, 8.1)
4	145.4		141.8		143.7		155.8	
5	115.9	6.63 (*d*, 8.0)	123.4	7.06†	115.9	6.47 (*d*, 8.0)	115.5	6.73 (*d*, 8.1)
6	119.1	6.49 (*br d*, 8.0)	126.5	7.09†	119.4	6.63 (*br d*, 8.0)	129.6	7.09 (*d*, 8.1)
1`	100.7		113.9		104.4		104.4	
2`	161.2		157.6		162.1		165.5	
3`	103.0		115.9		104.1		104.1	
4`	161.4		149.3		164.1		164.4	
5`	95.9	5.82 (*s*)	110.4	6.45 (*s*)	95.0	5.95 (*s*)	95.0	5.99 (*s*)
6`	164.6		149.4		165.3		162.4	
a	43.6t	3.18 (*t*, 7.6) 3.35*	45.0	3.20 (*t*, 7.0)	45.9	3.32 (*m*)	46.0	3.28 (*t*, 8.7)
b	29.1	2.75 (*t*, 7.6)	28.9	2.96. 2.94 (*t*/each, 7.0)	30.1	2.83 (*t*, 7.9)	30.1	2.82 (*t*, 7.8)
CO	203.3		196.9		205.0		204.8	
1``	33.3	3.10 (*d*, 16.4) 2.91 (*d*, 16.4)	35.0	3.15 (*d*, 16.8) 3.29 (*d*, 16.8)	74.0	4.52 (*d*, 9.9)	74.3	4.58 (*d*, 9.8)
2``	117.8		116.2		70.9	3.89 (*t,* 8.7)	71.2	3.94 (*t*, 8.7)
3``	80.0	3.88 (*d*, 8.0)	77.8	5.47 (*d*, 7.0)	79.3	3.22 (*t,* 7.6)	79.4	3.22*
4``	74. 1	3.83 (*br d*, 7.5)	77.8	5.27 (*br t*, 6.2)	71.1	3.14 (*br t,* 7.3)	70.8	3.18*
5``	84.2	3.77 (*m*)	79.5	4.25††	81.7	3.18*	81.7	3.19*
6``	63.8	3.43* 3.54 (*br d*, 12.5)	64.5	4.27†† 4.03 (*br d*, 10.6)	61.7	3.42 (*dd,* 3.6, 11.6) 3.66 (*d*, 11.6)	61.7	3.48 (*br d*, 11.5) 3.70 (*d,* 11.5)

*,†, †† overlapped signals in the same column

4.3.2. Cytoprotective effect of isolates on skin cells exposed to UVB irradiation.

The HaCaT and SK-MEL-1 cells were pre-treated with isolates (TE, **4.2**, **4.1**, and **4.3**) for 4 or 24 hours before exposure to UVB irradiation. The MTT assay was then used to determine the cytoprotective effects of the tested samples. After exposure to UVB the viability of HaCaT cells not pre-treated with isolates decreased to 72% and 63% for the 4- and 24-hour experiments respectively when compared to cells not exposed to UVB or isolates, while the viability of SK-MEL-1 was found to have decreased to 77% and 70 % for the 4- and 24-hour experiments respectively when compared to cells not exposed to UVB or tested samples.

Following the observation that our UVB model was cytotoxic, the two cell lines were incubated with the isolates (0-100 µg/mL) for 4- and 24-hours. The results showed that all the tested samples showed time and dose-dependent cytotoxic effects against the treated cell lines independent of UVB exposure. It was interesting to note that at lower concentrations the

isolates were able to stimulate cell metabolic activity and cell viability (Figure 4.3A-H) in UVB and non-UVB exposed cells. These increases in cell viability indicate a reduction in UVB-induced cytotoxicity. We also noted that the SK-MEL-1 melanocytes showed greater resilience to UVB-induced toxicity when compared to HaCaT and that these protective effects were potentiated by pre-treatment with tested samples.

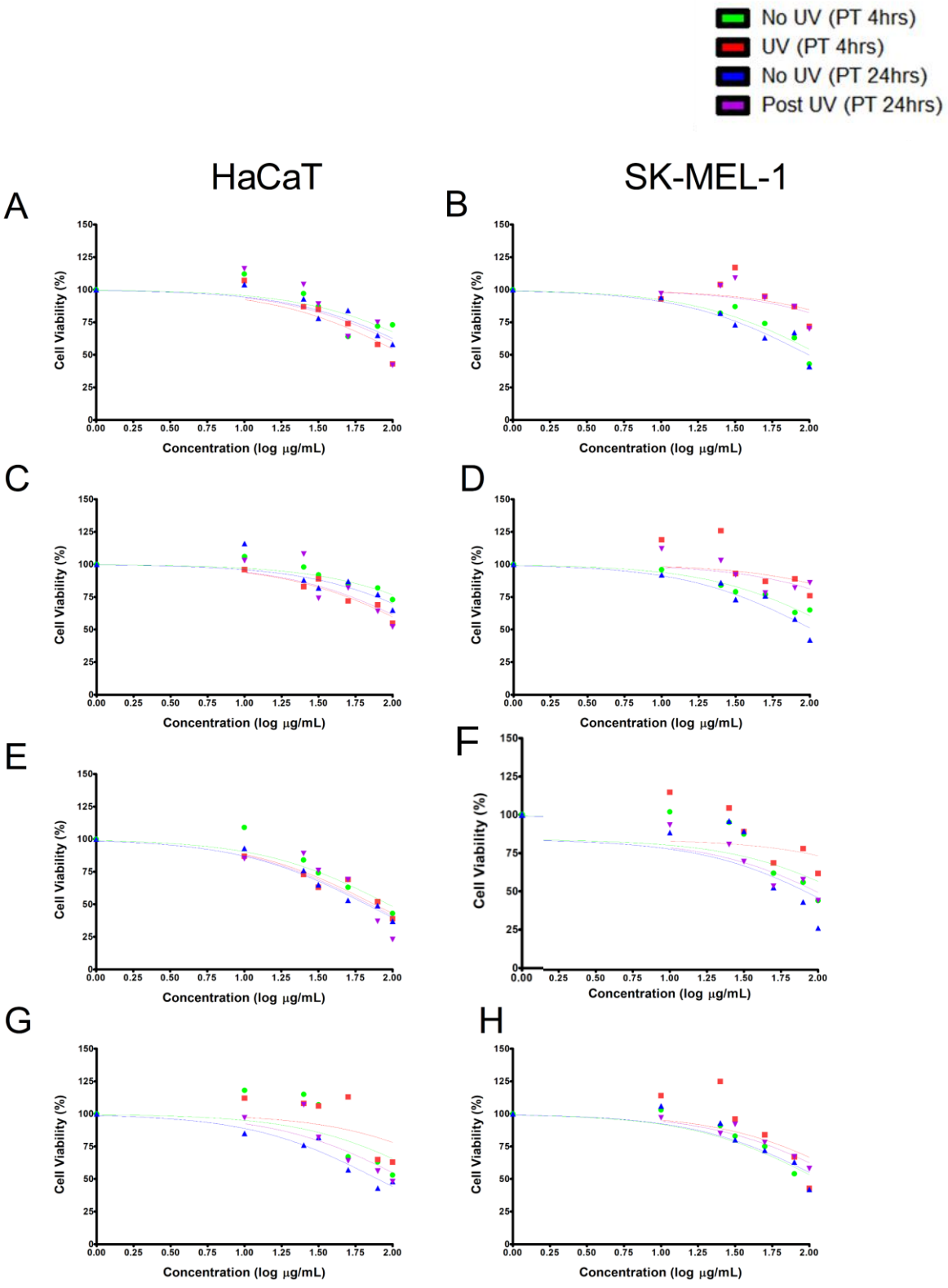

Figure 4.3: Effect of the tested samples pre-exposure [4- and 24-hours; A, B (TE); C, D (compound 4.1); E, F (compound 4.2); G, H (compound 4.3)] on UVB irradiation in HaCaT and SK-MEL-1 cells. The MTT cytotoxicity curve alluded to time and dose-dependent cytotoxic effects by the tested samples at higher concentrations.

4.3.3. Determination of the IC_{50} values of the tested samples under UVB exposure.

To confirm which of the tested samples were the most cytoprotective against UVB irradiation the IC_{50} values were determined. Results confirmed that HaCat cells exposed to **4.2** for 4 hours before UVB irradiation showed the highest degree of cytoprotection among the four studied extracts, with an IC_{50} of 398.9 µg/mL while 24-hour pre-exposure to **4.1** was shown to be the most effective isolate against UVB irradiation with an IC_{50} of 282 µg/mL. In the SK-MEL-1 cell line, we observed **4.1** to be the most effective isolate in protecting cells against UVB irradiation with IC_{50} values of 248.3 and 142.6 µg/mL over 4 and 24 hours, respectively. The IC_{50} values for all tested samples are illustrated in S1. The IC_{50} values reported in Figure 4.4, are defined here as the concentration of isolate required for 50% inhibition of viable cell number *in vitro*, obtained from each cytotoxicity curve (Figure 4.3), these reflect the differences where a higher IC_{50} value is attributed to a higher concentration of isolate being needed to reduce cell viability. Based on these data we selected concentrations of tested samples to be used for all subsequent assays.

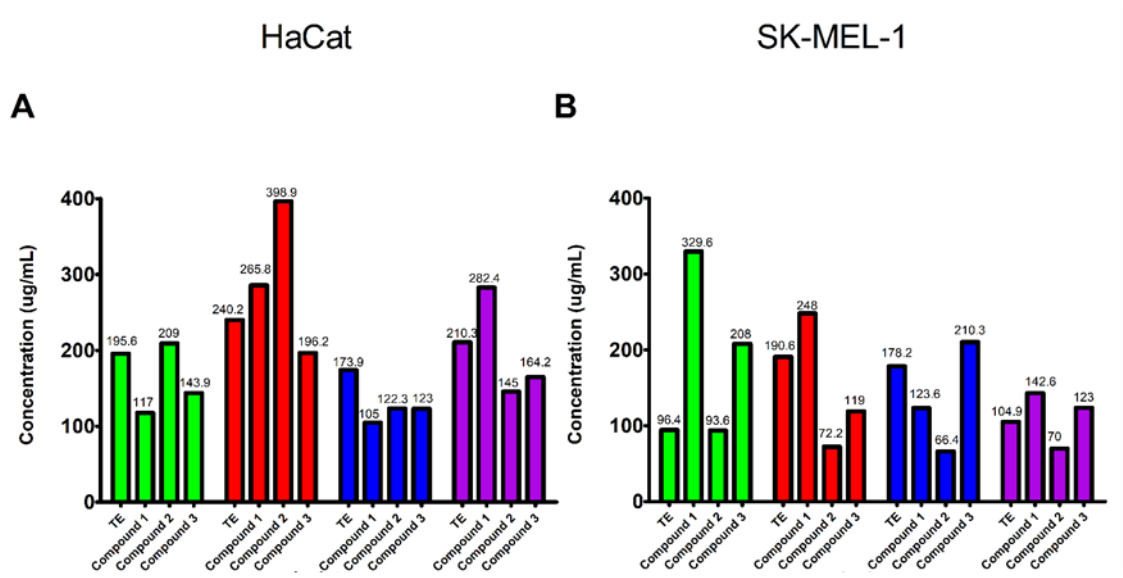

Figure 4.4: The IC_{50} concentrations of studied isolates on the two cell lines after 4- and 24- hour pre-exposure to determine cytoprotection against UVB.

4.3.4. Effect of the tested samples on cell viability.

The ATP bioluminescent assay (PROMEGA) is a reliable method to determine cell viability by quantifying ATP. In HaCaT cells ATP content was significantly increased in cells pre-treated for 4 hours with the lowest concentration (10 µg/mL) of isolates when compared to untreated

cells independent of UVB exposure (Figure 4.5A, C, E, G). However, after 24 hours of pre-exposure to isolates, only compounds **4.1** (Figure 4.5E) and **4.3** (Figure 4.5G) were able to maintain ATP above control cell levels in UVB irradiated cells. Intriguingly, **4.3** was able to increase ATP in UVB irradiated cells to above levels observed in non-irradiated cells at the 100 µg/mL concentration (Figure 4.5G).

The tested samples were less active in the SK-MEL-1 cell pre-treated for 4 hours as evidenced by depleted ATP levels in UVB irradiated cells when compared to non-irradiated cells (Figure 4.5B, D, F, H). In contrast, 24-hour pre-treatment resulted in all isolates increasing ATP levels in UVB-irradiated cells when compared to cells not pre-treated with the isolates (Figure 4.5B, D, F, H). The closer analysis also revealed that **4.2** and **4.3** at 10 µg/mL were able to significantly increase ATP to above levels observed in non-UVB irradiated cells (Figure 4.5D and H).

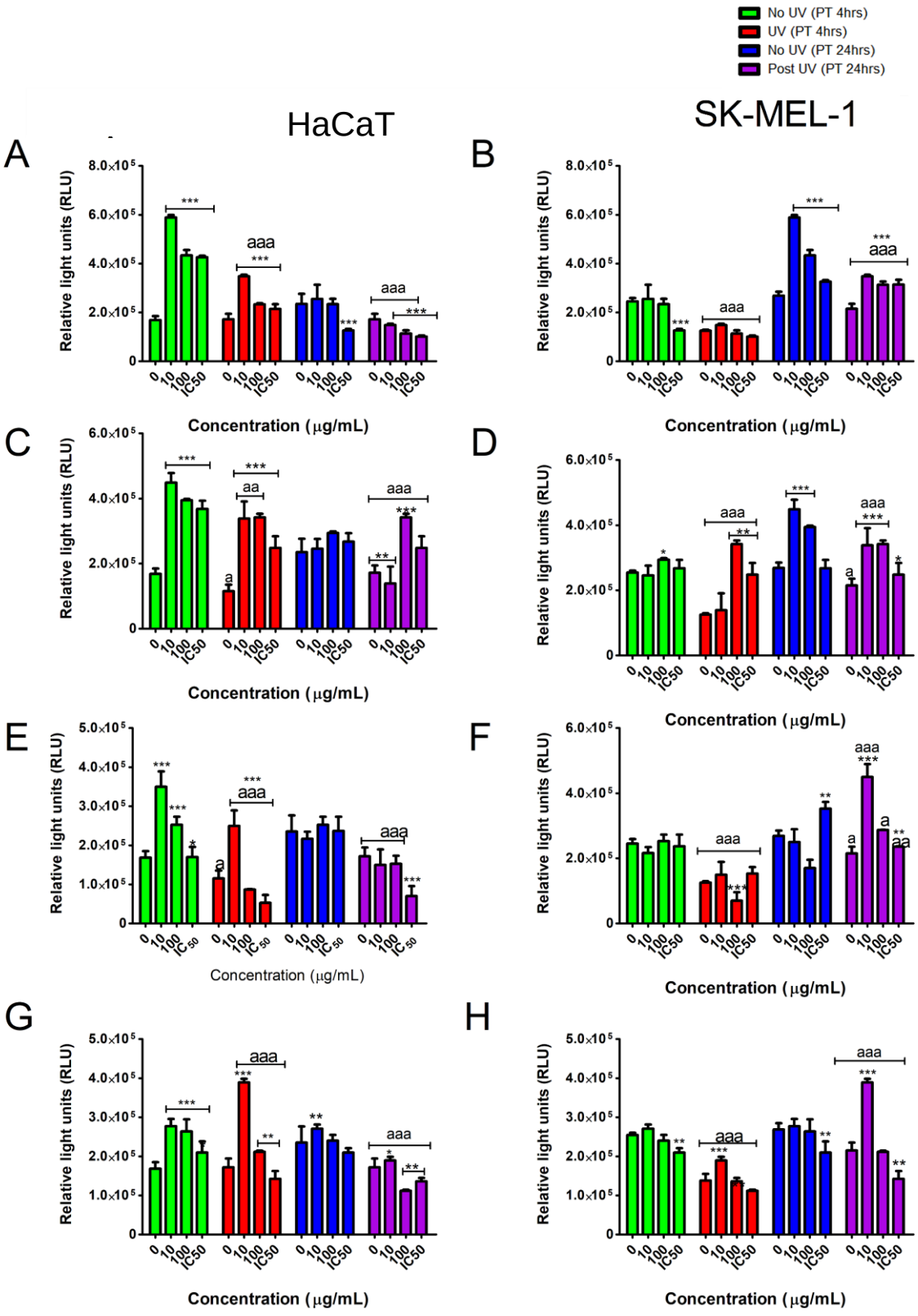

Figure 4.5: Cells were treated with selected concentrations of the tested samples [10, 100 and the IC50 (µg/mL); A, B (TE); C, D (compound 4.1); E, F (compound 4.2); G, H (compound 4.3)] before exposure to UVB and the levels of ATP were detected using luminometry. The error bars express the standard deviation.

* $P < 0.05$, ** $P < 0.01$, *** P< 0.001 control *vs* experimental concentrations

[a] $P < 0.05$, [aa] $P < 0.01$, [aaa] P< 0.001 No UVB irradiation *vs* UVB irradiation for experimental concentrations

4.3.5. Modulation of UVB-induced oxidative damage by the tested samples.

Exposure to UVB light is known to induce oxidative stress and subsequent lipid peroxidation [32]. We, therefore, measured the levels of melondialdehyde (MDA) as a biomarker for lipid peroxidation. From our investigation, it became clear that after a 4-hour pre-treatment with the tested samples, both cell lines exposed to UVB displayed an overall hormetic response in which lower concentrations (10 and 100 µg/mL) significantly (P<0.05) decreased the levels of MDA to below those observed in cells with no isolate intervention (Figure 4.6A-H). An exception to this was observed in HaCaTs pre-exposed to **4.1**, where only the lowest concentration reduced MDA significantly (P<0.05). We further showed that **4.1** at the lowest concentration was able to circumvent MDA formation by UVB to below levels observed in cells not exposed to UVB. This highlights **4.1** as the most protective compound.

In contrast, 24-hour pre-treatment with the tested samples appeared to have a pro-oxidant effect as we show a significant (P<0.05) increase in MDA levels following UVB exposure in the HaCaT and SK-MEL-1 cell lines with only the lowest concentration (10 µg/mL) offering protection (Figure 4.5A-H). However, **4.2** showed a significant (P<0.05) reduction in MDA levels at all tested concentrations in both cell lines after UVB exposure (Figure 4.6C and 4.6D).

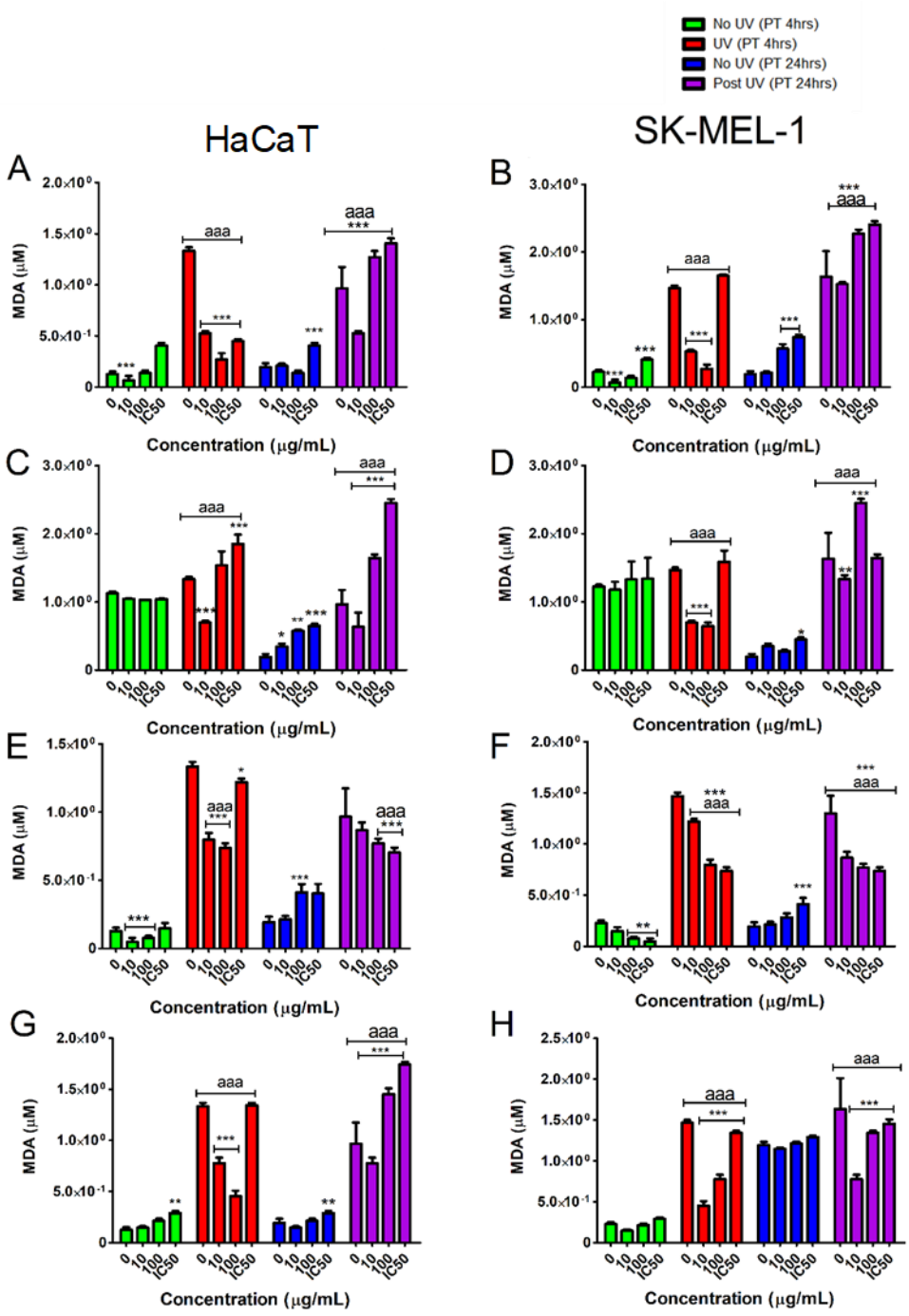

Figure 4.6: Protective effects of the tested samples [A, B (TE); C, D (compound 4.1); E, F (compound 4.2); G, H (compound 4.3)] against lipid peroxidation after 4- and 24-hour treatment before exposure to UVB irradiation. The error bars express the standard deviation.

* $P < 0.05$, ** $P < 0.01$, *** P< 0.001 control *vs* experimental concentrations

[a] $P <$ 0.05, [aa] $P <$ 0.01, [aaa] P< 0.001 No UVB irradiation *vs* UVB irradiation for experimental concentrations.

4.3.6. The tested samples regulate GSH levels in skin cells exposed to UVB.

Changes in GSH levels are important when assessing cell defence responses and are an indicator of oxidative stress. GSH content declined immediately after exposure to UVB in all tested cell models (Fig. 4.7) when no intervention with isolates was applied. Pre-treatment with TE for 4hrs appeared to significantly improve GSH content in both UVB exposed and non-exposed cells. However, 24h pre-treatment with TE did not improve GSH levels. **4.2** was only active at the lowest concentration tested in HaCaT cells when pre-treated for 4 hrs and 24 hrs. In contrast, SKMEL-1 pre-treated cells showed better resistance profiles to UVB irradiation as evidenced by improved GSH. A similar pattern was observed for both **4.1** and **4.3**.

Closer scrutinization of the data showed that the cells pretreated with **4.2**, **4.1**, and **4.3** had higher GSH levels after UVB exposure when compared to cells not exposed to UVB. This suggests that GSH synthesis is boosted in cell stress systems by the tested samples.

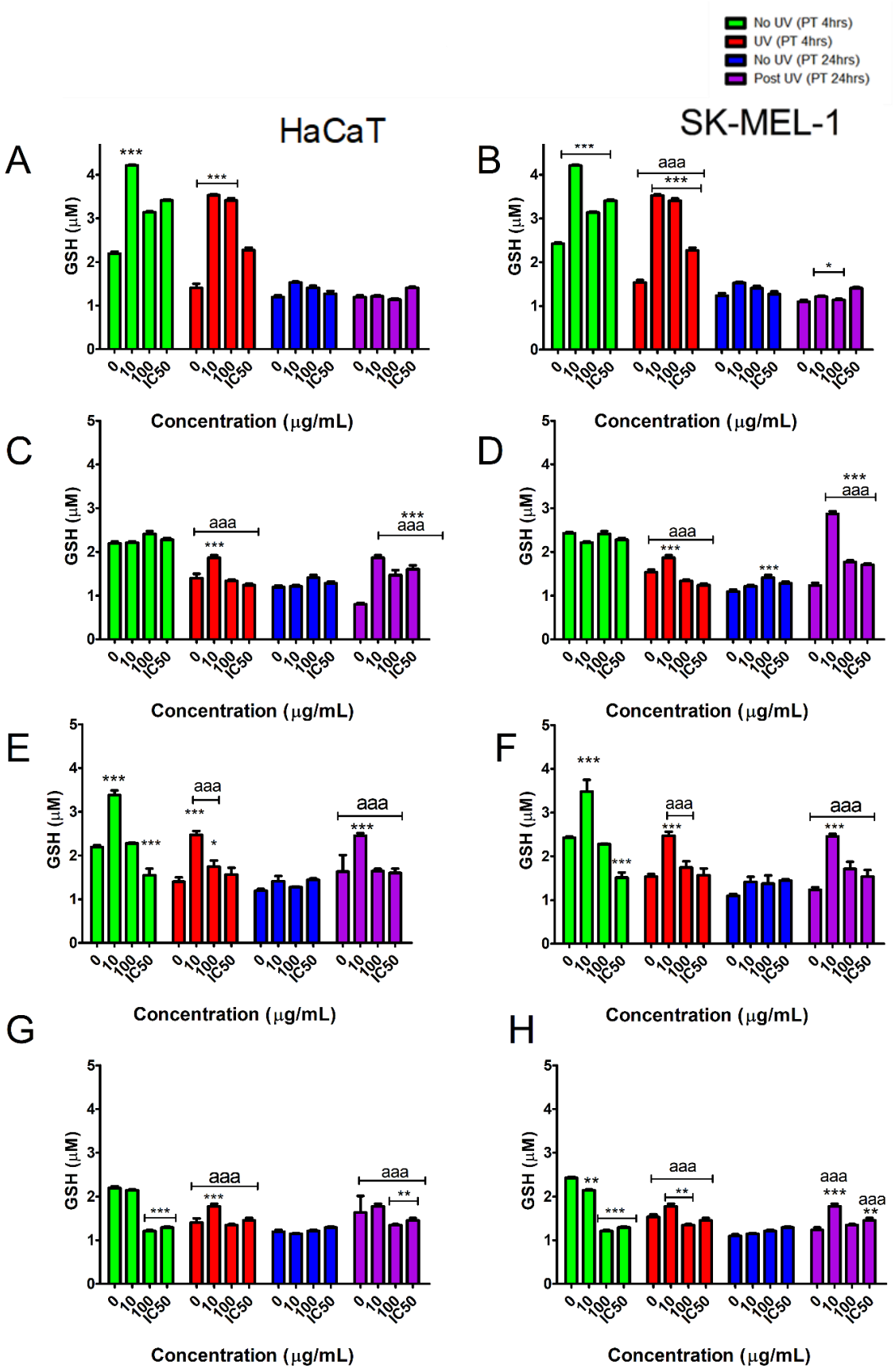

Figure 4.7: Effect of the tested samples [A, B (TE); C, D (compound 4.1); E, F (compound 4.2); G, H (compound 4.3)] on glutathione (GSH) on glutathione concentration in skin cells exposed to UVB irradiation. The error bars express the standard deviation

* $P < 0.05$, ** $P < 0.01$, *** P< 0.001 control *vs* experimental concentrations

[a] $P < 0.05$, [aa] $P < 0.01$, [aaa] P< 0.001 No UVB irradiation *vs* UVB irradiation for experimental concentrations.

4.3.7. The tested samples inhibited caspase 3 activation and were not cytotoxic in UVB irradiated skin cells.

To confirm the anti-apoptotic potential of the isolates the activation of caspases 3/7 was investigated as these are the executioners of cell death via apoptosis. All isolates were able to reduce caspase activation in UVB irradiated cells as can be seen in Fig. 4.8 suggesting a protective effect. It was observed that the lower test concentrations were more effective in significantly reducing apoptosis of UVB irradiated cells. We also show that the anti-apoptotic effects are dependent on the induction of cell damage by UVB as the non-irradiated cells appeared to have a dose-dependent increase in caspase activity and resultant apoptotic cell death.

4.3.8. Cytotoxic potential of tested samples in skin cells exposed to UVB irradiation

Further evaluation of the cytotoxic potential of the test compounds revealed toxicity only at the highest concentrations tested. This was indicated by elevated fluorescence detected in dead cells (Fig. 4.9). In combination with UVB exposure as the non-tested samples induced a marked decrease in cytotoxicity at low concentrations. Thus, the low concentrations of tested samples appear to have a photo-protective ability as they ameliorate UVB induced cell damage.

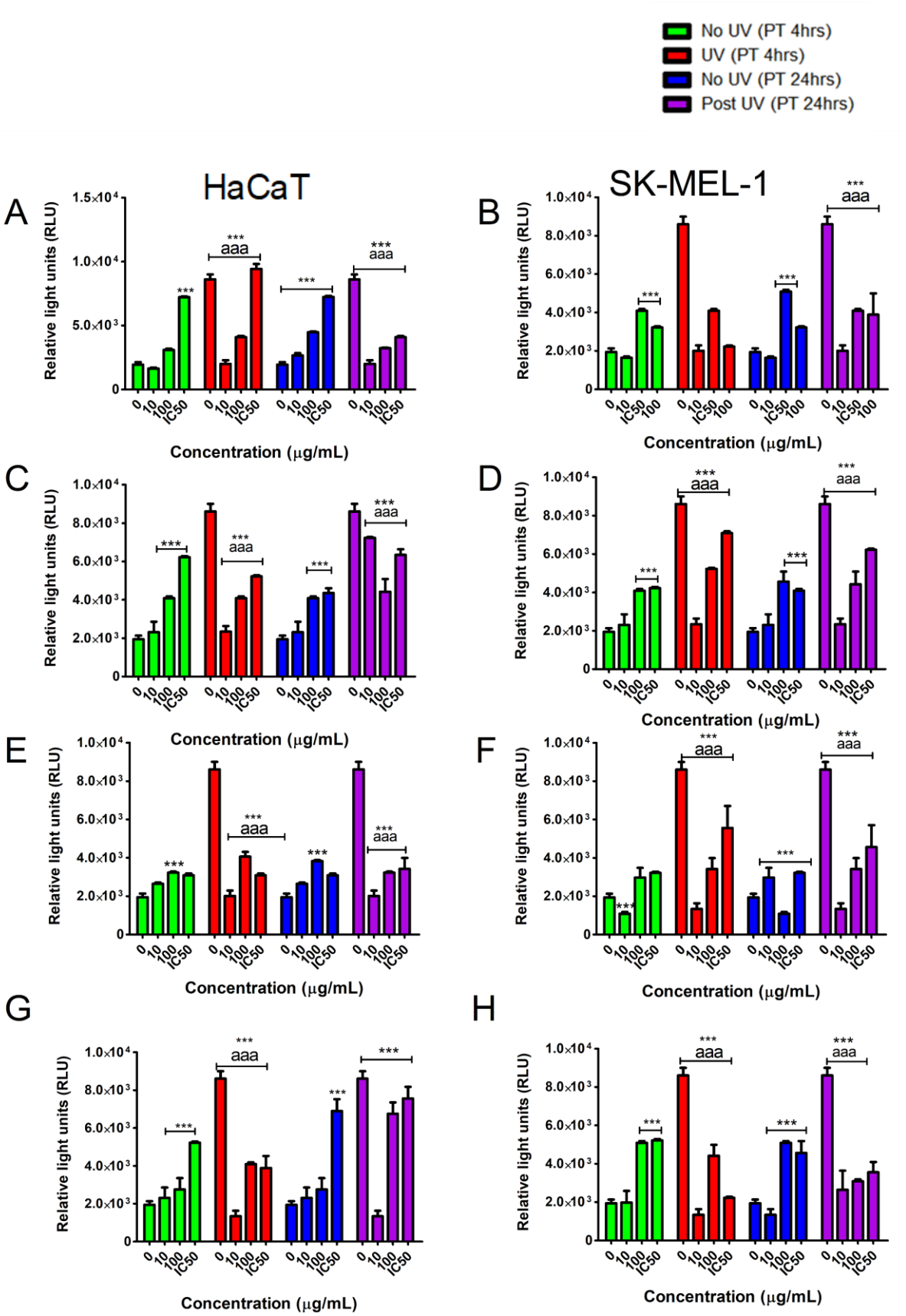
No UV (PT 4hrs)
UV (PT 4hrs)
No UV (PT 24hrs)
Post UV (PT 24hrs)
A
HaCaT
B
SK-MEL-1
C
D
E
F
G
H
Relative light units (RLU)
Concentration (μg/mL)
0
10
100
IC50
***
aaa

Figure 4.8: Pre-treatment with tested samples [A, B (TE); C, D (compound 4.1); E, F (compound 4.2); G, H (compound 4.3)] effects in caspase 3 activation in skin cells exposed to UVB irradiation. The error bars express the standard deviation.

* $P < 0.05$, ** $P < 0.01$, *** P< 0.001 control *vs* experimental concentrations

$^{a}P < 0.05$, $^{aa}P < 0.01$, ^{aaa} P< 0.001 No UVB irradiation *vs* UVB irradiation for experimental concentrations.

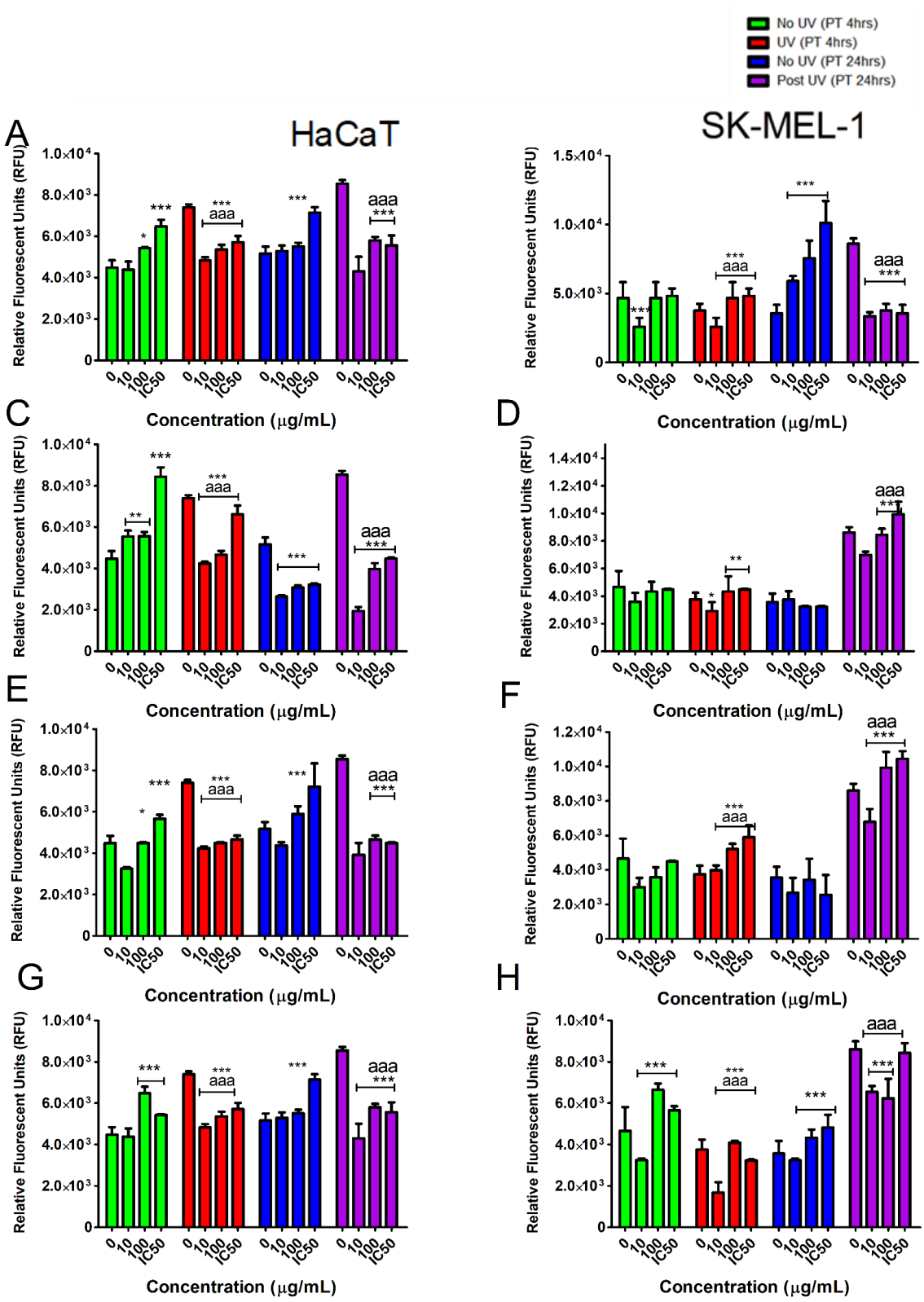

Figure 4.9: Pre-treatment with tested samples [A, B (TE); C, D (compound 4.1); E, F (compound 4.2); G, H (compound 4.3)] and their cytotoxic potential in skin cells exposed to UVB irradiation. The error bars express the standard deviation.

4.4. Discussion

UVB irradiation is seen as the primary extrinsic contributor to damage of the epidermal layer of skin through mechanisms associated with oxidative distress in cells [1]. This is associated with the potential of UVB to disrupt vital enzymatic and non-enzymatic antioxidant systems in cells as well as the execution of apoptosis [2, 3] and makes it important to explore novel and effective antioxidant molecules to protect cells from UVB-induced damage [2].

Previous studies have reported that rooibos total extracts markedly enhanced UVB-induced inhibition of cell viability, proliferation, and induction of apoptosis in a UVB/Keratinocyte model [22, 23]. However, the potential of **4.2** and its derivatives to attenuate oxidative stress in UVB/Keratinocyte models is currently unclear. Its application in skincare is made appealing by its ability to cross physiological barriers [27] while still maintaining pharmacological activity in skin cells [22, 23].

To systemically evaluate the cytoprotective effects of **4.2** and derivatives, we measured cell viability in the UVB/Keratinocyte (HaCaT) and UVB/Melanocyte (SK-MEL-1) models that were pre-exposed to the tested samples for 4 and 24 hours. From this study, **4.1** was the most active in preventing loss of cell viability after exposure to UVB compared to all other tested samples in the UVB/Keratinocyte model, we observed that this protective effect was most evident when cells were pre-treated for 4 hours. This suggests that **4.1** is likely to target and elicit an early defence response against UVB damage. This contrasts with the UVB/Melanocyte model which showed **4.1** to be most effective after 24-hour pre-treatment while **4.2** the best for maintaining cell viability after 4 hours of pre-treatment. This suggests that the protective effects of the tested samples are time and cell type dependent. While this is the first study to evaluate the protective effects of rooibos **4.2** derivatives in a UVB toxicity model it is important to note that this data contrasts with previous studies which elaborate on the synergism of rooibos polyphenolic constituents over rooibos monomeric compounds [22, 33, 34].

The MTT assay used to evaluate cell viability is based on the ability of metabolically active cells to metabolise the salt into a soluble formazan product [35]. To verify that tested samples maintained metabolic activity after UVB exposure we assessed intracellular ATP levels. UVB exposure in the models significantly depleted ATP in cells not pre-treated with tested samples, this may be attributed to UVB directly inhibiting ATP synthesis in the skin [36]. Alternatively, The reduction in cellular ATP seen after irradiation may also reflect increased ATP usage by cells recovering from UV damage [37]. Our data indicate that a 4-hour pretreatment with 10µg/mL with tested samples was sufficient to elevate ATP levels in cells exposed to UVB. This indicates that at the lowest tested concentration, TE along with **4.2** derivatives stimulates ATP production in both models. The higher levels of ATP may contribute to cell survival by

supporting energy-dependent DNA repair processes [37] as well as stimulating pigmentation processes in keratinocytes to directly protect against UV [38]. These findings underscore the potential of the tested samples in reducing the genotoxic effects of UV to maintain genomic stability and to prevent malignant transformation.

It is important to note that at the highest concentrations tested, the experimental samples decreased ATP levels in UVB irradiated and non UVB irradiated cells, suggesting that these compounds have a modulatory role on cell energy pathways that is concentration-dependent. Functional mitochondria and the NAD: NADH ratio are essential to maintaining cellular ATP levels. Strong evidence has found that polyphenols present in total rooibos extracts may inhibit the mitochondrial respiratory chain [39] and may explain the loss of ATP at higher concentrations. This observation is in line with previous studies that highlight the therapeutic potential of rooibos extracts in skin cancer [22, 33, 39].

UVB irradiation is well known to cause skin damage and premature ageing through the excessive production of ROS and induction of oxidative stress [2]. In this study, the suppression of MDA generation indicated that certain concentrations of dihydrochalcone of *A. linearis* can decrease skin damage and protect skin cells from the oxidative stress induced by UVB irradiation. Similarly, previous studies on rooibos and its polyphenols have been shown to possess antioxidant potential. Several mechanisms have been proposed, including direct scavenging of ROS as well as up-regulation of ROS detoxifying enzymes [20-21, 34]. This study demonstrates that **4.2** and its derivatives have a favourable biological effect within a zone of low dose pre-treatment and UVB stress while higher concentrations, above a threshold of 100 µg/mL elicit a high degree of oxidative damage as ROS levels exceed the endogenous antioxidant capacity. The potential of rooibos and its constituents to enhance the Fenton reaction has been established [34] and associated with the metal-chelating properties of rooibos and its polyphenols [33] may contribute to the pro-oxidant effects observed.

Several lines of evidence have indicated that the antioxidant functionality of skin is modulated by the redox status of GSH under UVB stress to maintain homeostasis [40]. The epidermis contains glutathione (GSH), a hydrophilic tripeptide (l-g-glutamyl-l-cysteinyl-glycine), with characteristic sulfhydryl groups readily reacting with ROS and other mediators of oxidative stress. Since glutathione, alone or as a co-factor of several enzymes (GSH peroxidases, reductases, and GSH-S transferase), plays a pivotal role in the biological antioxidant defence systems, it was chosen as the most relevant parameter for the quantification of the UVB/Keratinocyte (HaCaT) and UVB/Melanocyte (SK-MEL-1) redox status. Reduced GSH is naturally present in the skin and its intracellular levels are regulated by several metabolic pathways. Reduced GSH forms oxidised GSH after detoxification of ROS and must be converted to reduced GSH before detoxification of ROS can continue. Therefore, reduced

GSH is indicative of the redox status of skin cells and the effectiveness of regenerating systems [40]. The results showed that the total rooibos extract was biologically more active in inducing an increase in GSH than **4.2** when keratinocytes and melanocytes were exposed to UVB especially at the lowest concentration tested, however, **4.2** and its derivatives were still able to significantly rescue the GSH status in exposed cells. These results indicate that **4.2** and its derivatives may have a role to play in GSH recycling or enhancing GSH production in skin cells exposed to UVB. This suggests a protective, antioxidant effect against UVB damage at low concentrations.

Growth inhibition and apoptosis by rooibos is well documented for pre-malignant and malignant skin cells suggesting its potential as a potent drug candidate against hyperproliferative diseases [20, 22, 35, 41]. However, little work has been done to establish the protective effects of rooibos and its polyphenols against UVB-induced apoptosis. Our work aims to address this knowledge gap. The results of this study clearly indicate that pre-treatment with total extract, **4.1**, **4.2**, and **4.3** inhibited the activation of executioner caspases in a dose-dependent manner with lower concentrations showing the most potent inactivation. It also shows that in agreement with previous studies apoptosis was enhanced by all tested samples when UVB was not used as a stressor [22, 33, 39]. This suggests that the anti-apoptotic effects are UVB dependent and that the tested isolates do not act as a photosensitiser to apoptosis. The tested samples were able to induce photoprotective effects against UVB induced cytotoxicity. The cytotoxicity effects of rooibos extracts have been well established in studies using cancer models [20, 22]. This study shows that the potential of lower concentrations of rooibos extracts show promise as cytoprotective agents.

Apoptosis and the sustained activation of caspase 3 is an energy-dependent process [41]. The decreased caspase activity may be associated with inhibition of ATP producing pathways since UVB irradiation is known to target the mitochondria [42] and inhibit glycolysis due to elevated ROS [43]. The mitochondrial succinate dehydrogenase enzyme activity can be indirectly detected using the MTT assay. Pre-treatment with high concentrations of test compounds before UVB-irradiation resulted in a significant decrease of MTT reduction, indicating a decrease of metabolically active cells compared to non-UVB control. Pre-treatment with low concentrations provided protection to the metabolic activity of cells, as reflected by high conversion of MTT, suggesting that both malignant and premalignant cell types used in this study are susceptible to cell death through pathways that are independent of apoptosis. This is supported by data showing elevated ROS damage biomarkers.

From the structural-activity relationship of the isolated compounds, it was noted from compounds **4.2** and **4.3** are structurally similar dihydrochalcone with *C*-glucose at C-3`. However, they differ due to the presence/absence of 3-OH of ring B (Fig. 4.1). On the other hand, **4.1** and **4.2** are closely related except for the sugar unit, the presence of dioxysugar and the extra ether linkage decrease the polarity than the parent compound **4.2** and may be one reason for the observed differences in activities. This structural-activity relationship of **4.1**, **4.2** and **4.3** is suggestive of the observed activity order of **4.1** > **4.2** > **4.3** in all treated cells at 4 hrs. Keeping these similarities and slight differences among the derivatives in mind, we hypothesised for the observed similar or time-dependent activities of the total extract, **4.1**, **4.2** and **4.3** on skin cells irradiated with UVB irradiation.

The excessive ROS levels associated with UVB exposure downregulates anti-apoptotic proteins and upregulate pro-apoptotic proteins, resulting in interference with the normal release of cytochrome-c, which activates the caspase family proteins, and finally induces cell death [2, 5]. The alterations in UV-induced apoptosis regulation may have an important impact on the induction of skin photoaging and skin cancer. Previous studies have demonstrated that the inhibition of excessive apoptosis and the accelerated elimination of ROS induced by UVB could protect the skin from UVB-induced ageing and carcinogenesis [44]. Our results showed that the tested samples effectively attenuated UVB-induced oxidative stress and apoptosis, thereby protecting the skin from UVB-induced damage. The pre-treatment regimen employed by this study suggests that the protective effects of tested samples involve some degree of cellular adaptation, resulting in enhanced protection against UVB damage.

4.5. Conclusion

Acetonic extract of green rooibos from this study presents a novel dihydrochalcone compound, linearthin with a unique glucose moiety in addition to the previously reported aspalathin, nothofagin, catechin and 3-hydroxyphloretin. These chalcones despite the notable differences in their structures, all prevented skin cells from oxidative damages at lower concentrations. According to scientific reports, little is known of the protective effects of chalcone derivatives from green rooibos. The findings of this study demonstrated for the first time the application of linearthin and other chalcone derivatives from rooibos to protect human-derived skin cells from excessive ROS generated by UVB exposure in vitro. It is clear that structural differences in the glucose moiety and position of hydroxyl among the chalcones may have accounted for the different activities of these chalcones. The chalcones used in this study have the capacity to improve cell viability and inhibit apoptosis induced by UVB exposure by likely exploiting pathways associated with the established antioxidant properties of rooibos. The results also show that the chalcones reduced biomarkers associated with lipid oxidative damage and improved the oxidative status of the cell. Overall, linearthin and other chalcone derivatives can

be beneficial as a therapeutic agent to alleviate the effects of extreme sun exposure and subsequent oxidative stress.

Acknowledgement

We wish to acknowledge the South African Rooibos Council (SARC) and Centre for Postgraduate Studies of cape Peninsular university of technology for their financial support towards the completion of this research. In addition, partial funding was provided by the South African Medical Research Council (SAMRC) through its Division of Research Capacity Development under funding received from the South African National Treasury. Also, we would like to thank Rooibos Ltd for the donation of the plant materials. The content hereof is the sole responsibility of the authors and do not necessarily represent the official views of the SAMRC or the funders.

Conflicts of Interest: The authors declare no conflict of interest.

References

1. Matsumura, Y.; Ananthaswamy, H.N. Toxic effects of ultraviolet radiation on the skin. *Toxicol. Appl. Pharmacol.* **2004**, *195*, 298–308.
2. Afaq, F.; Adhami, V.M.; Mukhtar, H. Photochemoprevention of ultraviolet B signalling and photocarcinogenesis. *Mutat. Res. Fundam. Mol. Mech. Mutagenesis* **2005**, *571*, 153–173.
3. Biniek, K.; Levi, K.; Dauskardt, R.H. Solar UV radiation reduces the barrier function of human skin. *Proc. Natl. Acad. Sci. USA* **2012**, *109*, 17111–17116.
4. Natarajan, V.T.; Ganju, P.; Ramkumar, A.; Grover, R.; Gokhale, R.S. Multifaceted pathways protect human skin from UV radiation. *Nat. Chem. Biol.* **2014**, *10*, 542–551.
5. Lee, C.-H.; Wu, S.-B.; Hong, C.-H.; Yu, H.-S.; Wei, Y.-H. Molecular mechanisms of UV-induced apoptosis and its effects on skin residential cells: The implication in UV-based phototherapy. *Int. J. Mol. Sci.* **2013**, *14*, 6414–6435.
6. Kunchana, K.; Jarisarapurin, W.; Chularojmontri, L.; Wattanapitayakul, S.K. Potential use of amla (*Phyllanthus emblica* L.) fruit extract to protect skin keratinocytes from inflammation and apoptosis after UVB irradiation. *Antioxidants* **2021**, *10*, 703.
7. Nichols, J.A.; Katiyar, S.K. Skin photoprotection by natural polyphenols: Anti-inflammatory, antioxidant and DNA repair mechanisms. *Arch. Dermatol. Res.* **2010**, *302*, 71–83.
8. Thongrakard, V.; Ruangrungsi, N.; Ekkapongpisit, M.; Isidoro, C.; Tencomnao, T. Protection from UVB toxicity in human keratinocytes by Thailand native herbs extracts. *Photochem. Photobiol.* **2014**, *90*, 214–224.
9. Wynberg, R. Making sense of access and benefit sharing in the rooibos industry: Towards a holistic, just and sustainable framing. *S. Afr. J. Bot.* **2017**, *110*, 39–51.
10. Chuarienthong, P.; Lourith, N.; Leelapornpisid, P. Clinical efficacy comparison of anti-wrinkle cosmetics containing herbal flavonoids. *Int. J. Cosmetic. Sci.* **2010**, *32*, 99–106.
11. Joubert, E.; De Beer, D.; Rooibos *(Aspalathus linearis)* beyond the farm gate: From herbal tea to potential phytopharmaceutical. *S. Afr. J. Bot.* **2011**, *77*, 869–886.
12. Pringle, N.A.; Koekemoer, T.C.; Holzer, A.; Young, C.; Venables, L.; Van De Venter, M. Potential therapeutic benefits of green and fermented Rooibos *(Aspalathus linearis)* in dermal wound healing. *Planta Med.* **2018**, *84*, 645–652.
13. Tiedtke, J.; Marks, O. Rooibos-The new" white tea" for hair and skin care. *Euro Cosmet.* **2002**, 10,16–19.
14. Walters, N.A.; Villiers, A.D.; Joubert, E.; Beer, D. Improved HPLC method for rooibos phenolics targeting changes due to fermentation. *J. Food Compos. Anal.* **2017**, *2017*, 20–29.
15. Beer, D.; Malherbe, C.J.; Beelders, T.; Willenburg, E.L.; Brand, D.J.; Joubert, E. Isolation of aspalathin and nothofagin from rooibos (*Aspalathus linearis*) using high-performance countercurrent chromatography: Sample loading and compound stability considerations. *J. Chromatogr. A.* **2015**, *1385*, 29–36.

16. Heinrich, T.; Willenberg, I.; Glomb, M.A. Chemistry of color formation during rooibos fermentation. *J. Agric. Food Chem*. **2012**, *60*, 5221–5228.
17. Zillich, V.; Eisner, P.; Kerscher, M. Polyphenols as active ingredients for cosmetic products. *Int. J. Cosmet. Sci.* **2015**, *2015*, 455–464.
18. Breiter, T.; Laue, C.; Kressel, G.; Gröll, S.; Engelhardt, U.H.; Hahn, A. Bioavailability and antioxidant potential of rooibos flavonoids in humans following the consumption of different rooibos formulations. *Food Chem.* **2011**, *128*, 338–347.
19. Baba, H.; Ohtsuka, Y.; Haruna, H.; Lee, T.; Nagata, S.; Maeda, M.; Yamashiro, Y.; Shimizu, T. Studies of anti-inflammatory effects of rooibos tea in rats. *Pediatrics Int.* **2009**, *51*, 700–704.
20. Marnewick, J.; Joubert, E.; Joseph, S.; Swanevelder, S.; Swart, P.; Gelderblom, W. Inhibition of tumour promotion in mouse skin by extracts of rooibos (*Aspalathus linearis*) and honeybush (*Cyclopia intermedia*), unique South African herbal teas. *Cancer Lett.* **2005**, *224*, 193–202.
21. Marnewick, J.L.; Rautenbach, F.; Venter, I.; Neethling, H.; Blackhurst, D.M.; Wolmarans, P.; Macharia, M. Effects of rooibos (*Aspalathus linearis*) on oxidative stress and biochemical parameters in adults at risk for cardiovascular disease. *J. Ethnopharmacol.* **2011**, *133*, 46–52.
22. Magcwebeba, T.U.; Riedel, S.; Swanevelder, S.; Swart, P.; De Beer, D.; Joubert, E.; Andreas Gelderblom, W.C. The potential role of polyphenols in the modulation of skin cell viability by *Aspalathus linearis and Cyclopia* spp. herbal tea extracts in vitro. *J. Pharm. Pharmacol.* **2016**, *68*, 1440–1453.
23. Krafczyk, N.; Woyand, F.; Glomb, M.A. Structure–antioxidant relationship of flavonoids from fermented rooibos. *Mol. Nutr. Food Res.* **2009**, *53*, 635–642.
24. Chaudhary, S.K.; Sandasi, M.; Makolo, F.; Van Heerden, F.R.; Viljoen, A.M. Aspalathin: A rare dietary dihydrochalcone from *Aspalathus linearis* (rooibos tea). *Phytochem. Rev.* **2021**, 1–32.
25. Erlwanger, K.; Ibrahim, K.; Aspalathin a unique phytochemical from the South African rooibos plant (*Aspalathus linearis*): A mini Review. *J. Afr. Assoc. Physiol. Sci.* **2017**, *5*, 1–6.
26. Johnson, R.; De Beer, D.; Dludla, P.V.; Ferreira, D.; Muller, C.J.; Joubert, E. Aspalathin from rooibos (*Aspalathus linearis): A* bioactive *C*-glucosyl dihydrochalcone with potential to target the metabolic syndrome. *Planta Med.* **2018**, *84*, 568–583.
27. Huang, M.; Du Plessis, J.; Du Preez, J.; Hamman, J.; Viljoen, A. Transport of aspalathin, a rooibos tea flavonoid, across the skin and intestinal epithelium. *Phytother. Res.* **2008**, *22*, 699–704.
28. Koeppen, B.H. Flavone c-glycosides-the periodic acid oxidation of orientin and homo-orientin tetramethyl ethers. *Chem. Ind.* **1962**, *52*, 2145–2145.
29. Hillis, W.E.; Inoue, T. The polyphenols of Nothofagus species—II.: The heartwood of *Nothofagus fusca*. *Phytochemistry* **1967**, *6*, 59–67.
30. Krafczyk, N.; Glomb, M.A. Characterization of phenolic compounds in rooibos tea. *J. Agric. Food Chem.* **2008**, *56*, 3368–3376.
31. Terra, V.A.; Souza-Neto, F.P.; Pereira, R.C.; Silva, T.N.X.; Costa, A.C.C.; Luiz, R.C.; Cecchini, R.; Cecchini, A.L. Time-dependent reactive species formation and oxidative stress damage in the skin after UVB irradiation. *J. Photochem. Photobiol. B Biol.* **2012**, *109*, 34–41.
32. Terra, V.A.; Souza-Neto, F.P.; Pereira, R.C.; Silva, T.N.X.; Costa, A.C.C.; Luiz, R.C.; Cecchini, R.; Cecchini, A.L. Time-dependent reactive species formation and oxidative stress damage in the skin after UVB irradiation. *J. Photochem. Photobiol. B Biol.* **2012**, *109*, 34–41.
33. Magcwebeba, T.U.; Swart, P.; Swanevelder, S.; Joubert, E.; Gelderblom, W.C. In vitro chemopreventive properties of green tea, rooibos and honeybush extracts in skin cells. *Molecules* **2016**, *21*, 1622.
34. Joubert, E.; Winterton, P.; Britz, T.J.; Gelderblom, W.C. Antioxidant and pro-oxidant activities of aqueous extracts and crude polyphenolic fractions of rooibos (*Aspalathus linearis*). *J. Agric. Food Chem.* **2005**, *53*, 10260–10267.
35. Kumar, P.; Nagarajan, A.; Uchil, P.D. Analysis of cell viability by the MTT assay. *Cold Spring Harb. Protoc.* **2018**, 2018, pdb-rot095505.
36. Humm, S. and Cole, S. Changes with time in Langerhans cell number, ATPase reactivity and morphology in murine epidermis after exposure to UVB. *Photodermatology* **1986**, *3*, 174–178.
37. Park, J.; Halliday, G.M.; Surjana, D.; Damian, D.L. Nicotinamide prevents ultraviolet radiation-induced cellular energy loss. *Photochem. Photobiol.* **2010**, *86*, 942–948.
38. Abdel-Malek, Z.A. Fueling melanocytes with ATP from keratinocytes accelerates melanin synthesis. *J. Investig. Dermatol.* **2019**, *139*, 1424–1426.
39. Magcwebeba, T.; Swart, P.; Swanevelder, S.; Joubert, E.; Gelderblom, W. Anti-inflammatory effects of *Aspalathus linearis* and *Cyclopia* spp. extracts in a UVB/keratinocyte (HaCaT) model utilising interleukin-1α accumulation as biomarker. *Molecules* **2016**, *21*, 1323.
40. Meloni, M.; Nicolay, J.F. Dynamic monitoring of glutathione redox status in UV-B irradiated reconstituted epidermis: Effect of antioxidant activity on skin homeostasis. *Toxicol. Vitr.* **2003**, *17*, 609–613.

41. Elmore, S. Apoptosis: A review of programmed cell death. *Toxicol. Pathol.* **2007**, *35*, 495–516.
42. Paz, M.L.; Ferrari, A.; Weill, F.S.; Leoni, J.; Maglio, D.H.G. Time-course evaluation and treatment of skin inflammatory immune response after ultraviolet B irradiation. *Cytokine* **2008**, *44*, 70–77.
43. Garrit, R.; Gonzalez, A.; Justiniano, J.; Wan, Y. Alteration of p-PKM2 by UV radiation and H_2O_2 in human keratinocytes. *FASEB J.* **2015**, *29*, 726–16.

44. Wang, Y.; Li, W.; Xu, S.; Hu, R.; Zeng, Q.; Liu, Q.; Li, S.; Lee, H.; Chang, M.; Guan, L. Protective skin-aging effects of cherry blossom extract (*Prunus yedoensis*) on oxidative stress and apoptosis in UVB-irradiated HaCaT cells. *Cytotechnology* **2019**, *71*, 475–487.
45. Horakova, L.; Licht, A.; Sandig, G.; Jakstadt, M.; Duracková, Z.; Grune, T. Standardized extracts of flavonoids increase the viability of PC12 cells treated with hydrogen peroxide: Effects on oxidative injury. *Arch. Toxicol.* **2003**, *77*, 22–29.
46. Abdul, N.S.; Nagiah, S.; Chuturgoon, A.A. Fusaric acid induces mitochondrial stress in human hepatocellular carcinoma (HepG2) cells. *Toxicon* **2016**, *119*, 336–344.
47. Koeppen, B.H. Flavone c-glycosides-the periodic acid oxidation of orientin and homo-orientin tetramethyl ethers. *Chem. Ind-London,* **1962**, (52), 2145-2145.

Chapter five

Cytotoxic effects of phytomediated silver and gold nanoparticles synthesised from rooibos *(Aspalathus linearis*), and aspalathin.

Akeem O. Akinfenwa [1], Naeem S. Abdul [2], Fathima T. Docrat [2], Jeanine L. Marnewick [2], Robbie C. Luckay [3], Ahmed A. Hussein [1]*

[1] Department of Chemistry, Cape Peninsula University of Technology, Symphony Rd. Bellville 7535, South Africa; oa.akeemlaja@gmail.com (A.O.A); mohammedam@cput.ac.za (A.A.H.)

[2] Applied Microbial and Health Biotechnology Institute, Cape Peninsula University of Technology, Symphony Rd. Bellville, 7535, South Africa; sheikabduln@cput.ac.za (A.N.S); docratt@cput.ac.za (D.T.F); marnewickj@cput.ac.za (J.L.M.).

[3] Chemistry & Polymer Science Department, Stellenbosch University, Matieland, Stellenbosch, 7602, South Africa

*Correspondence: mohammedam@cput.ac.za; Tel.: +27-21-959-6193; Fax: +27-21-959-3055

NOTE: the article has been accepted in Plants in 22/10/2021

Abstract

The green chemistry approach has continuously been applied for the synthesis of functional nanomaterials to reduce waste, environmental hazards, and the use of toxic chemicals among other reasons. Bioactive natural compounds have been found great potential in this regard and are used to improve the stability, activity and biodistribution of metal nanoparticles (MNPs). Aspalathin (ASP) from *Aspalathus linearis* (rooibos) has a well-defined pharmacological profile and functional groups capable of both reducing and capping agents in the synthesis of metallic nanoparticles (NP). This study provides the first report of the phyto-mediated synthesis of gold and silver nanoparticles (AuNPs/AgNPs) *via* ASP, and green rooibos (GR) extract. The study demonstrated a green chemistry approach to the biosynthesis of nanoparticles of GR-AuNPs, ASP-AuNPs, GR-AgNPs, and ASP-AgNPs. The results showed that GR and ASP could act both as reducing and stabilizing agents in the formation of crystalline, with different shapes and dispersity of NPs in the ranges of 1.6 – 6.7 nm for AgNPs and 7.5 – 12.5 nm for the AuNPs. However, ASP NPs was less stable in selected biogenic media compared to GR NPs and was later stabilized with polyethene glycol. The cytotoxicity studies showed that GR-AgNPs were most cytotoxic against the SH-SY5Y and HepG2 with IC_{50} 108.8 and 183.4 µg/mL, respectively. Cellular uptake analysis showed high uptake of AuNPs and indicated AgNPs of rooibos at a lower dose (1.3 – 1.5 µg/mL) is favourable for its anti-cancer potentials. This study is a contribution to plant-mediated metallic nanoparticles using a pure single compound which can be further developed for targeted drug delivery for cancer cells treatments in the coming years.

Keywords: Aspalathin, green rooibos, synthesis, gold, silver, nanoparticles, cancer, metal uptake.

6.1. Introduction

Cancer, a multistep disease involving rapid, and uncontrol cell multiplication are among the world-leading health challenges that have attracted global concern. Rapid division of cancer cells is often prompted by genetic impairment which leads to abnormal cell cytosis in different parts of the body such as in the brain, lungs, and liver, to name a few. The major cancer treatment is chemotherapy using a chemically synthesised drug from bulk platinum (II) complexes such as cisplatin, oxaliplatin and carboplatin. The potential anticancer activities of platinum complexes were attributed to a high affinity of the platinum for sulphur binding and the guanine bases of DNA [1]. Platinum-based drugs have recorded tremendous success by slowly inhibiting growth and blocking tumour cells. However, huge concerns have been raised about the serious side effects including kidney and liver toxicity, and hearing impairment associated with these drugs. Besides platinum, other biocompatible metals-based drugs such as gold and silver have been reported as promising anticancer agents [2], [3]. As a result,

strategies to reduce the side effects while improving the potencies of metal-based anticancer drugs has been ongoing. Among such strategies is the development of nanosystems for gold and silver as nanoparticles capped with antioxidant-rich plant sources for anticancer studies [4].

The plant-based synthesis method of metallic nanoparticles is considered less expensive and eco-friendly. The method involves bio-reduction and stabilization of metal NPs with phytochemical constituents of plants which act as reducing and capping agents. They are reportedly used as alternatives to synthetic drugs in the targeted delivery of metallic anticancer drugs due to their improved biodistribution and clearance in the body [5]–[7]. To expand the use of metals in nanomedicine, gold and silver functionalised with plant phytochemicals are commonly used for active drug delivery and diagnosis. The plant phytochemicals possess functional groups such hydroxyl, amide and sulphides which act as capping agents to enhance activities of a metal-based drug through size reduction and increase surface area [8]. Oyagi *et al.* (2014) previously reported the synthesis of non-toxic silver nanoparticles encapsulated by rooibos herbal tea components which can be used for targeted delivery of silver to cancer cells. In complementary research on rooibos, Diallo *et al*. (2016) demonstrated the biosynthesis of europium oxide nanocrystal from a rooibos extract showing a luminescent property for potential application in the photothermal treatment of cancer cells [9–10].

A. linearis extracts have been reported in the synthesis of different metal NPs [9–10], however, reports on the use of aspalathin (ASP) as a single stabilizing and reducing agent in the plant-mediated synthesis of MNPs is still lacking. The phytochemical studies of rooibos revealed different flavonoids such as rutin, orientin, quercetin, luteolin, ASP and many others to be present [11–12]. Aspalathin is a unique bio-antioxidant that has a *C*-glucoside dihydrochalcone skeleton and is found in high concentrations in green rooibos [13]. This compound is reported to play important roles in numerous health-promoting potentials of rooibos, including protection of DNA strands and suppression of induced cancer growth [14–16]. The chemistry of ASP presents electron-rich and multi-binding sites favourable as a reducing agent in the synthesis of metallic nanoparticles. This property of ASP and the high phenolic content of rooibos extract have been explored in different studies for biomedical applications. Still, limited information exists in the literature on the application of ASP for the synthesis of gold (Au) and silver (Ag) nanoparticles and the toxicity of the synthesised NPs on cancer cell lines. Although, the use of natural pure compounds such as hypoxoside, proanthocyanidin dimer and chalcones from different plant species in the preparation of Au- and AgNPs have been reported [17-19]. The current study presents a complimentary report on the synthesis of metal NPs using a single natural compound with a well-defined pharmacological profile such as ASP. Hence, ASP in addition to the total extract of *A. linearis* (GR) was used for the synthesis. Considering the importance of surface functionalisation with a well defined pharmacological natural compound

is crucial to bioactivity, biodistribution and biocompatibility of different MNPs in the medical field, thus, this study aims to biosynthesized Au- and AgNPs capped with rooibos extract and pure ASP compound using a green chemistry approach, to evaluate their cytotoxic activity against liver cancer and neuroblastoma human cell lines and determine the cellular uptake of the nanoparticles.

Materials and methods

6.2. General

Freshly dried and pulverized green Rooibos plant material was generously donated by the South African Rooibos Council, while pure aspalathin was isolated in-house. Liver and neuroblastoma cell culture reagents were purchased from ThermoFisher. All other consumables were purchased from Sigma Aldrich. Analytical grade metal salt and acid were used as precursors. Sodium tetrachloroaurate (III) dihydrate ($NaAuCl_4.2H_2O$, 99.99%), gold standard, silver nitrate salts, and silver standard solution were purchased from BDH Chemical Limited (England), polyethylene glycol was supplied by Sigma-Aldrich Chemie, Germany while Milli-Q de-ionized water used was produced in-house

6.2.1. Cell culture and cell conditioning

The HepG2 cells were cultured in minimum essential media (10% foetal calf serum, 1% penstrepfungizone, 1% L-glutamine) at 37 °C in a humidified incubator (5% CO_2). Cells were allowed to reach 80% confluency in culture flasks before treatment with the full rooibos extract and aspalathin nanoparticles. On the other hand, the neuroblastoma cells were cultured in Dulbeccos minimum essential media (10% foetal calf serum, 1% penstrepfungizone, 1% L-glutamine) at 37 °C in a humidified incubator (5% CO_2). Cells were allowed to reach 80% confluency in culture flasks before treatment with the total green rooibos extract and aspalathin nanoparticles. The two cell lines were then treated for 24 hours with a range of concentrations (0 - 500 ug/mL) of both Rooibos nanoparticles mentioned before experimental analysis was conducted.

6.3. Experimental

6.3.1. Preparation of plant extract and isolation of aspalathin

Five grams of freshly dried and pulverized green rooibos (GR) plant material (consisting mainly of leaves and stems) was extracted in 100 mL deionized water heated to 70 °C for 40 minutes resulting in a reddish-brown aqueous extract. The freshly prepared aqueous extract (5% GR) was centrifugated at 800 rpm for 20 minutes, filtered with a 0.45 µm syringe filter, stored at 4 °C and used within two days of preparation. Complimentary chromatography of acetonic extract of GR yielded the aspalathin.

6.3.2. Biogenic synthesis of Gold and silver nanoparticles

The synthesis of nanoparticles of the metals required six different set-ups. Hence, a two-batch experiment was carried out. The first batch (Batch A) involved stepwise addition of the aqueous extract of GR (acting as a reducing/capping agent) to solutions of each metal precursor separately, while in the second batch (Batch B), the purified compound, ASP was used in place of the GR. In a typical experiment, 10 mL of the aqueous GR extract (Batch A) was added separately and in a dropwise manner to a 90 mL heated (at 70 °C) solution of 0.001M of each of the metal nanoparticle precursors, stirring under reflux. The resultant mixtures were allowed to react until visible colour change was observed. The colour change is usually an indication of complete biosynthesis. A change to a ruby red colour (28 mins) for AuNPs from the initial pale-yellow colour, was noticed. Also noticed, was the appearance of a yellowish-brown colour (30 mins) for AgNPs from a colourless $AgNO_3$. These procedures were repeated for the batch B experiment in which 20 mg of ASP dissolved in 2 mL de-ionized water was added to each metal solution in place of the total green rooibos extract. A similar colour change observed in batch A was noticed with a time difference of ± 10 mins for the reaction times.

6.3.3. Characterisation of nanoparticles

The structural measurement of the nanoparticles was carried out using spectroscopic and imaging techniques including ultraviolet-visible light (UV/Vis), high-resolution transmission electron microscope (HR-TEM), x-ray diffraction (XRD), Fourier transform infrared (FTIR) and dynamic light scattering (DLS) measurements. The surface plasmon resonance absorption peak characteristic of metal nanoparticles was monitored by A polar star Omega microlitre plate UV/Vis reader (BMG Labtech, Ortenberg, BW, Germany). Characteristic functional groups involved in the synthesis were recorded on a PerkinElmer Fourier-Transform Infrared Spectrometer 2000, equipped with a universal ATR-FTIR (PerkinElmer Spectrum 100, Llantrisant, Wales, UK) in the range of 400 – 4000 cm^{-1}. The morphology of the biosynthesised AuNPs and AgNPs were studied with High-Resolution Transmission Electron Microscopy (FEI Tecnai G2 F20 S-Twin HRTEM, operated at 200 kV). For each NP, a few drops were placed on a carbon-coated copper grid and allowed to dry completely at room temperature. The crystal structures of the samples were then determined by X-ray diffraction (X-ray diffraction Model Bruker AXS D8 advance with radiation at $\lambda kCuk\alpha_1$ = 1.5406 Å). The sample was mounted in the centre of the sample holder on a glass slide and levelled to the correct height. The measurements were performed within a range in 2θ between 30°- 80° with a typical step size of 0.034° in 2θ. A position-sensitive detector, Lyn-Eye, was used to record diffraction data at a typical speed of 0.5 sec/step which is equivalent to an effective time of 92 sec/step for a scintillation counter. Analysis of HR-TEM and XRD images was carried out using ImageJ software, 1.50b version 1.8.0_60 (http://imagej.nih.gov/ij) and Origin pro-2019 (64 bits) software, respectively.

6.3.4. Stability study

The stability of the synthesised NPs in solution was studied using two techniques, the electrophoretic light scattering (ELS) based on Smoluchowski theory and, *in vitro* stability in biogenic media at a given time interval.

The ELS technique provides the zeta potential which indicates the potential stability of the particles in a colloidal system. This was done using a Malvern Zetasizer Instrument with Zetasizer software version 7.11 (Malvern Ltd., U.K) at 25° and a 90° angle. The *in vitro* stability test was carried out by mixing 200 µL of gold nanoparticles solution with 100 µL biogenic amino acids (such as 0.5% Glycine, 0.5% BSA), phosphate buffer saline (PBS at pH 7 and pH 9) and 1% NaCl solution in a 96-well plate and incubated (at 37 °C) for different periods. The stability of AgNPs and AuNPs in these media were monitored with UV-Vis based on retention of their absorbance maxima at an interval of 6 hours.

6.3.5. Cell viability

The MTT assay has been extensively used for determining the cytoprotective effects of several phytochemicals [45]. To monitor cell viability as a measure of metabolic activity, the MTT assay was performed. After the 24 hours exposure, the HepG2 and SH-SY5Y cells (15 000 cells per well in 96-well plates) were incubated for 2 hours with 100 µL MTT solution (5 mg/mL) after PBS washing. The MTT formazan crystals were then solubilised by DMSO resuspension. The optical density of the formazan product was read at 570 nm wavelength with a reference wavelength of 690 nm using a multi-plate reader (Multiska Thermo scientific, version 1.00.40). The half-maximal inhibitory concentration (IC_{50}) was determined. Results were analysed using GraphPad Prism5. The IC_{50} value defines the potency of a substance in inhibiting a specific biological or biochemical function. For the nanoparticles, it is the concentration at which 50% of the cells die.

6.3.6. In vitro cellular uptake of Au and Ag nanoparticles

Cellular uptake of AuNPs and AgNPs have been studied by different methods which can be classified as either qualitative and quantitative methods [46], [47]. Qualitative methods measure the response of treated cells MNPs by colourimetry, florescent changes, or by visualisation of the location of the metal in treated cells via transmission electron microscope or energy dispersive x-ray (EDX) analysis. Although there is yet a generally accepted standard for quantification of MNPs entry into living cells due to limitations posed by different physicochemical properties of particle and types, biological media etc. A quantitative method reportedly used to determine the concentration of MNPs taken up by physiological media involves the use of inductively coupled plasma-(mass spectroscopy/optical emission spectroscopy), ICP-MS or ICP-OES within a selected range of standard solutions of the metal solution [44]. For cellular uptake of our AuNPs and AgNPs, an in-house protocol was used.

Briefly, a $1*10^5$ of HePG2, and SH-SY5Y cells treated with (GR and ASP) AuNPs and AgNPs was seeded in 6 well plates and incubated for 24 hours. After incubation, the medium was discarded, and the cell was washed with PBS. The cells were trypsinized into 15 mL tubes, centrifugated at 3000 rpm, rewashed with PBS and again centrifugated. PBS was discarded and the MNPs were digested with aqua regia (1 mL) at 80°C for 2 hours to release the metal ions. The released metal ions from cells were then quantified with ICP-OES analysis. In the ICP-OES analysis, standard solutions each of gold and silver of 100 ppm was prepared and serial dilutions of these concentrations gave 50 ppm, 25 ppm, 12.5 ppm, and 6.25 ppm that were used for the standard calibration. The uptake of the MNPs by cells correspond to the concentrations of gold ions and silver ions in the cells.

6.4. Results

In continuation of the previous studies to probe the involvement of isolated compounds from plant extracts in the phyto-mediated synthesis of metallic nanoparticles, a green method was used to synthesise gold and silver nanoparticles using the total extract from green rooibos (GR) and its major phenolic compound, aspalathin (ASP). It is interesting to note that, the isolation procedures of the pure ASP (Figure 5.1) and its spectroscopic data which confirm the chemical structure of the ASP used in this study have been reported [20].

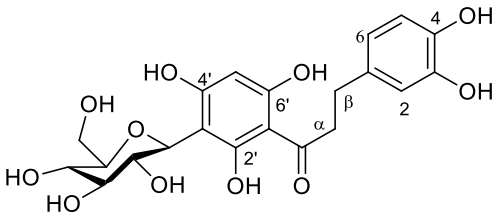

Figure 6.1: Structure of Aspalathin

The chemistry of GR and ASP are interwoven for GR being the only source of ASP till the time of this report. The chemical structure of ASP makes it prone to oxidation due to the high polyphenol content. This characteristic makes it suitable for use as a reducing agent that brings out the reduction of metals in solution to a stable zero valence state. Both GR and ASP demonstrated reducing and stabilizing properties in the synthesis of both Au and Ag metal nanoparticles. The successful synthesis of Au^0 and the Ag^0 via phytochemicals of rooibos and their cytotoxicity potentials on cancer cell lines were validated through different characterisation methods and bioassays as discussed in the subsection 5.4 below.

6.4.1. UV-Vis Spectrophotometry analysis

The visual observation of colour change was quantified by absorbance measurement for GR-AuNP and GR-AgNPs, and ASP-AuNP and ASP-Ag and presented in (Fig. 5.2) and (Fig. 3) respectively. Surface plasmon resonance (SPR) occurs due to absorption of incident UV-Vis

light by solutions of transition metals. This phenomenon causes the surface electrons to collectively oscillate at a specific frequency. Au and Ag NPs are known to show characteristic SPR in the UV-Vis range 500 – 600 (ruby red colour) nm and 400 – 500 nm (yellowish-brown), respectively. As noted in the experimental section the colour changes of the aqueous solutions of $NaAuCl_4.2H_2O$ and $AgNO_3$ at their corresponding absorption maxima served as the initial indication of complete biosynthesis of the NPs.

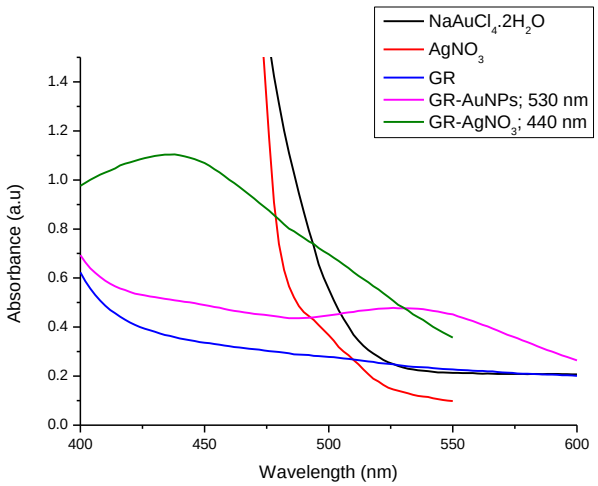

Figure 6.2: UV-Vis spectra for the synthesised Green Rooibos (GR) gold and silver nanoparticles

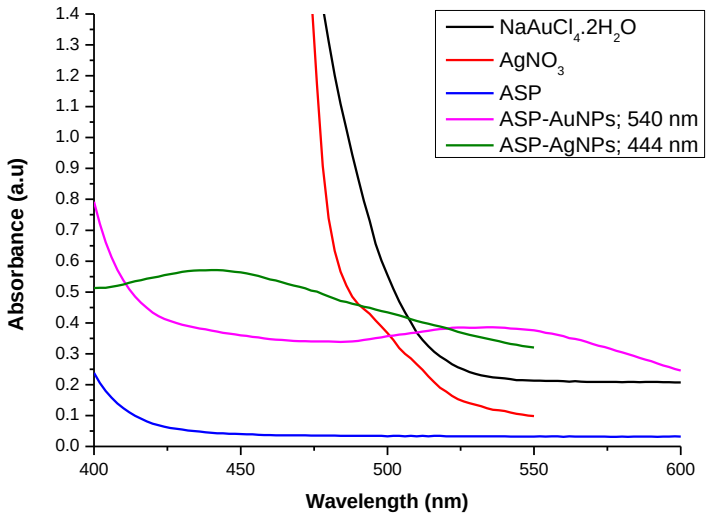

Figure 6.3: UV-Vis spectra for the synthesised aspalathin (ASP) gold and silver nanoparticles

6.4.2. High-Resolution Transmission electron microscope analysis

To confirm the morphology and size distribution of our NPs, TEM micrographs and selected area electron diffractions were recorded and elucidated. TEM images of all synthesised NPs revealed well-structured and non-agglomerated grains (Figure 5.4). GR-AgNPs and ASP-AgNPs images displayed uniform quasi-spherical shapes in the size range of 6.7 nm ± 0.39 and 1.6 nm ± 0.08 respectively. Several literature reports show that the size and, shape of metal nanoparticles are influenced by different factors [21-22]. The synthesis procedure resulted in spherical sizes of the AgNPs which are in accord with the report by Oyagi et al. (2014). However, this study reports a relatively bigger size of the AgNPs than was reported which could be due to the difference in the rooibos type used in the studies [9]. The report of Analike et al., (2021) demonstrated the synthesis of mostly spherical AuNPs stabilized with gum Arabic at 45 °C in the size ranges of 4.89 and 37.89 nm [23]. The AuNPs *via* GR and ASP show rarely occurring hydra-like shapes MNPs. The GR and ASP exhibited average size ranges of 7.5 nm ± 03.4 and 12.5 nm ± 0.04 respectively. It is interesting to note that the GR NPs showed smaller particle size by 2 to 3 folds than their corresponding ASP in each of AuNPs and AgNPs. This observation is complementary to the several reports of synergistic effects of the other compounds in GR during synthesis despite the ASP, being the major compound [17-19, 24]. Remarkably, smaller sizes of GR and ASP AgNPs were formed relative to the AuNPs counterpart even though both Au and Ag belong to the same family of *d*-block in the periodic table. These size distributions agree with the smaller ionic radii of silver when compared to gold.

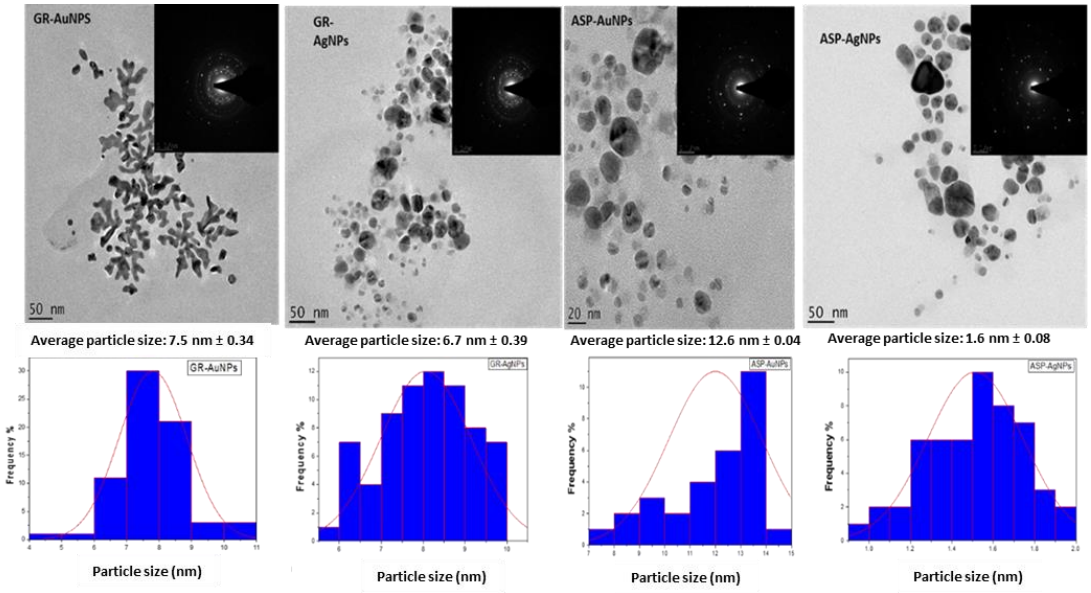

Figure 6.4: HRTEM images (left-right) for GR-AuNPs, GR-AgNPs, ASP-AuNPs, and ASP-AgNPs. The corresponding insets are the SAED of the respective TEM images.

6.4.3. Zeta potential and particle size distributions of gold and silver NPs

The DLS analysis of all NPs provided important information on stability, size distribution and the hydrodynamic diameters of nanoparticles as shown in Table 1. The zeta potential values (± mV) give the degree of interparticle repulsion in a dispersion. It is an important factor to be considered for the stability of metallic NP to be used as a drug. Higher negative values greater than -25 mV are usually considered more stable. The GR-AuNPs (-26.2 mV) and ASP-AgNPs (-26.7 mV) were most stable (Figure 5.5). The lower zeta potential value recorded of -15.0 mV (GR-AgNPs) and -19.2 mV (ASP-AgNPs) have been reported for biosynthesized AuNPs and AgNPs to fall in the typical range of stable and non-agglomerated nanomaterials [7], [25]. Furthermore, the polydispersity index (PDI) information obtained from the DLS represents the degree of homogeneity of different particles sizes to the total number of particles. Numerical values (no unit) for PDI ranges from 0.0 – 1.0. Generally, particles with a PDI value of 0.0 is considered perfectly monodispersed. Values lower than 0.5 are accepted and indicate a near homogeneous and monodisperse particles size distribution while values above 0.5 tend towards the polydisperse limits [26]. As shown in Table 1 and Figure 5.6, the range of values of the PDI for all the NPs is indicative of near-uniform particle sizes showing a polydispersity index of ASP-AgNPs (0.1), ASP-AuNPs (0.111), GR-AuNPs (0.128), and GR-AgNPs (0.274). The hydrodynamic size from DLS measurement is the particles sizes in the colloidal system and is often higher than the mean particle size from TEM due to the attraction of surface charges of ions of opposite charges in the dispersed medium [18]. Evidently, (Figure S2) the hydrodynamic sizes of all the NPs are higher than statistical calculations from TEM images which support the trend of size variation in NPs of gold and silver from GR and ASP.

Table 6.1: DLS analysis; Particle sizes, zeta potential and polydispersity index

Samples	Hydrodynamic sizes (nm)	Zeta potential (mV)	PDI
GR-AuNPS	107	-26.2	0.128
GR-AgNPs	109	-15.0	0.274
ASP-AgNPs	136.4	-26.7	0.100
ASP-AuNPS	104.7	-19.2	0.111

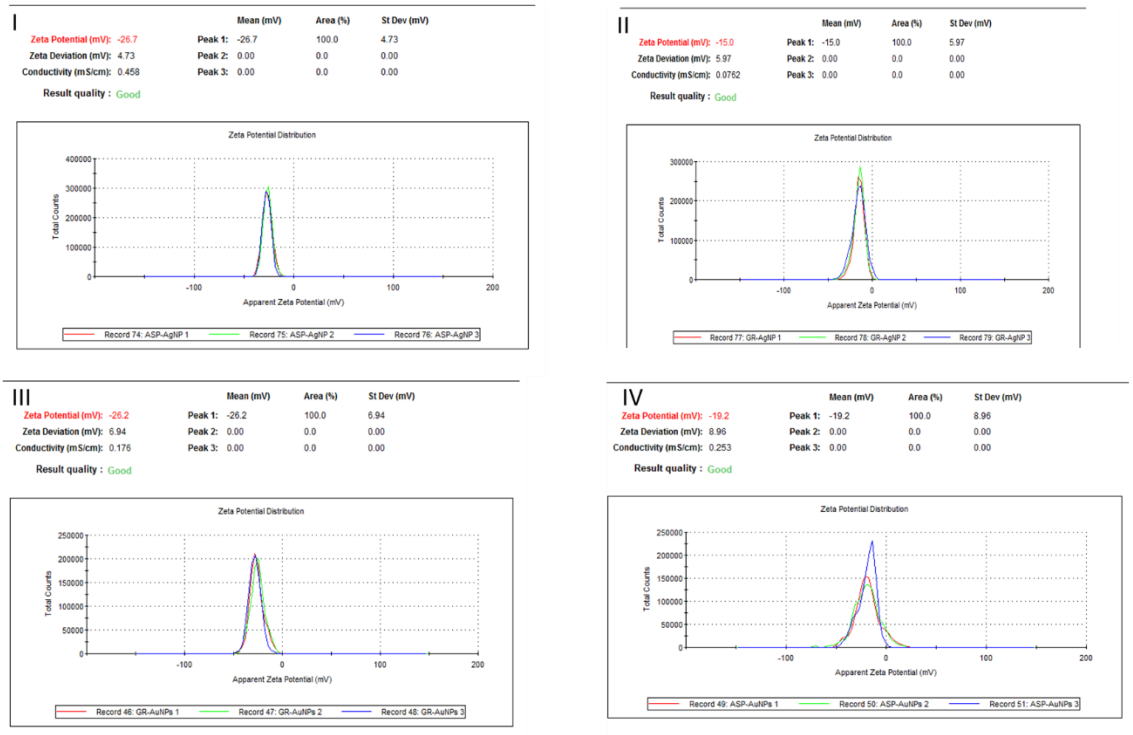

Figure 6.5: Zeta potential; ASP-AuNPs (I), GR-AgNPs (II), GR-AuNPs (III) and ASP-AuNPs (IV)

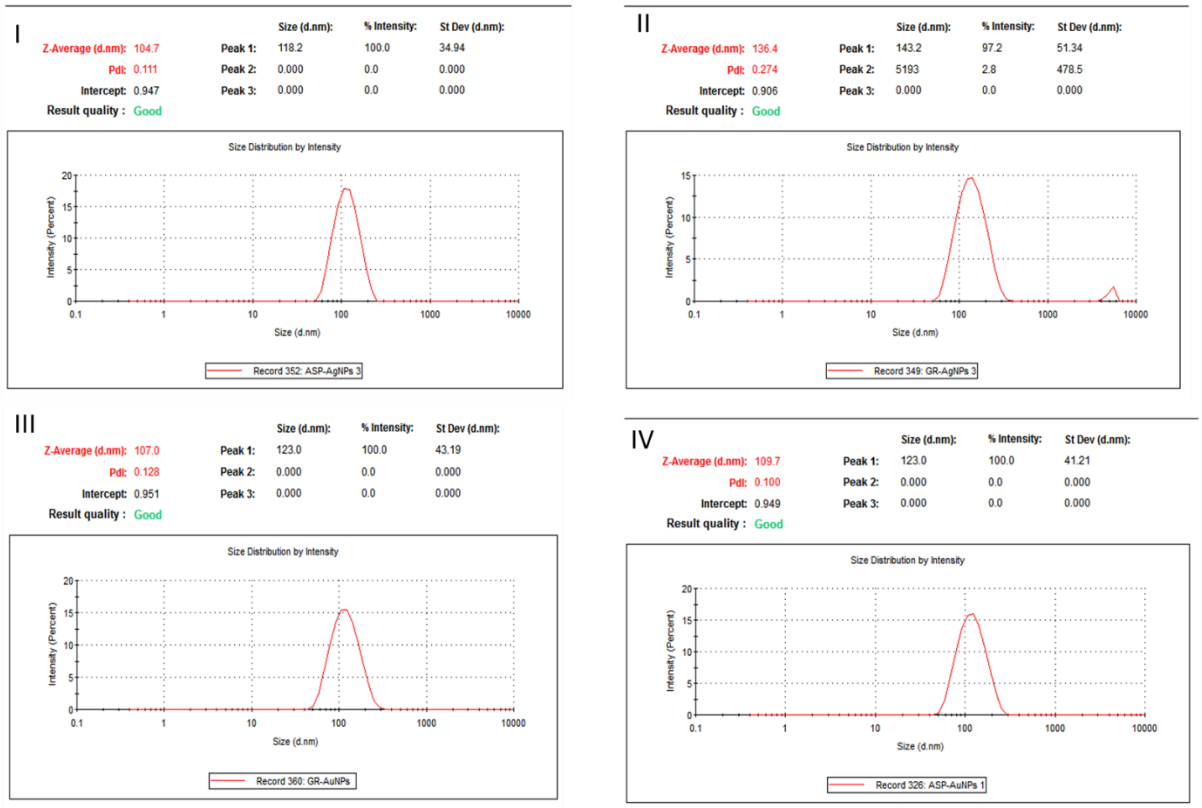

Figure 6.6: Hydrodynamic Average size; ASP-AuNPs (I), GR-AgNPs (II), GR-AuNPs (III) and ASP-AuNPs (IV)

6.4.4. X-Ray Diffraction (XRD) Analysis

We further confirm the crystalline structure of the Au and Ag NPs from GR and ASP using X-ray crystallography at room temperature. The AuNPs for both GR and ASP revealed four distinct Bragg peaks centred at 38.185, 44.393, 64.578 and 77.549 (2θ) corresponding to the crystallographic reflections (111), (200), (220), and (311) from the planes of crystalline gold (Figure 5.7). The silver NPs in fig. 7 also exhibited similar crystallographic reflections of Bragg's peaks centred at 38.117, 44.278, 64.427 and 77.475 (2θ). The peaks match for face-centred cubic crystalline metallic gold and silver phases as documented by the Joint Committee on Powder Diffraction Standards (JCP2 gold number 04-0784 and JCP2 silver number 04-0783 respectively). The results also corroborated the non-agglomerated nature of our NPs as seen on the TEM micrographs and the bright circular ring of the SAED (Figure 5.2). The extra peaks observed in the GR-AgNPs was presumably due to contamination by chlorargyrite (AgCl) when mounting the sample during preparation.

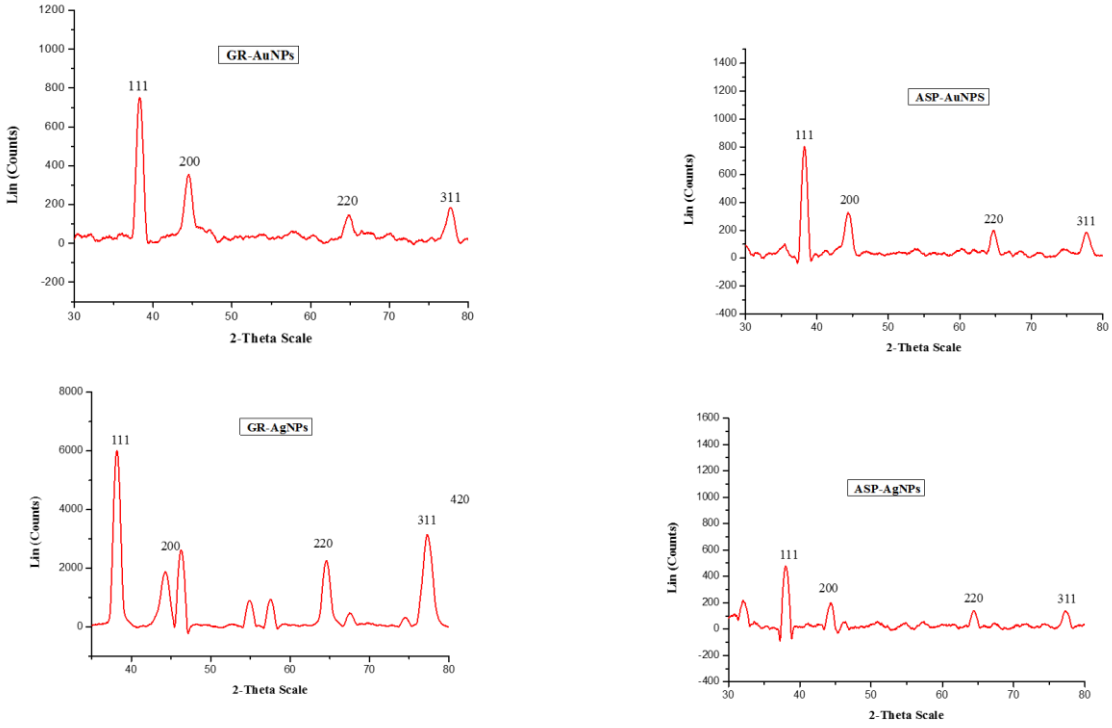

Figure 6.7: XRD patterns showing face-centred cubic phases of GR and ASP AuNPs and AgNPs

6.4.5. Attenuated total reflection Fourier transform infrared

A. linearis contains numerous polyphenols, with aspalathin having a structure in which aromatic ring is linked to O-H groups, C-O and α, β-unsaturated ketone C=O and C-H groups. These functional groups in many teas and herbal tea plants were reportedly involved in the

synthesis of gold nanoparticles using black tea, made from *Camellia sinensis* [27]. A comparison of the FTIR of the GR and ASP and their synthesised nanoparticles show that the major peaks located at 1050 – 1076 cm^{-1}, 1698 – 1715 cm^{-1}, 2950 - 3000 cm^{-1}, and 3300 - 3340 cm^{-1} correspond to the respective C-O (phenolic), C=O (α, β-unsaturated ketone), C-H (aromatics) and a broad O-H vibrational stretching bonds [23]. According to the IR spectra, the functional groups present in GR and ASP were also found in both AuNPs and AgNPs. The C-H vibrational frequencies of ASP in AuNPs and AgNPs was shifted from 2995 cm^{-1} to 3000 cm^{-1} in the two NPs. Also, the C-O bands of GR and the synthesised NPs were blue-shifted by approximately 3 cm^{-1} in the NPs. The spectra also show higher intensities of peaks of all NPs before synthesis (Figure 5.8 and Figure 5.9). These changes in absorptions before and after synthesis are indicative of their involvement in the bio-reduction process.

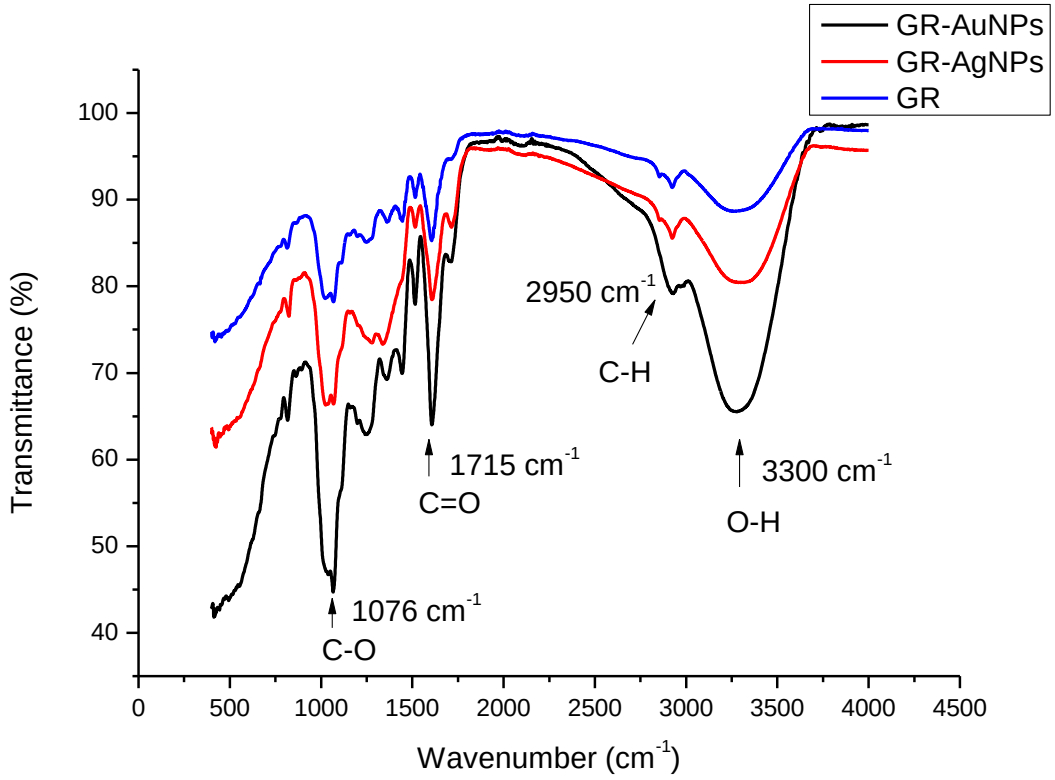

Figure 6.8: FTIR spectra of GR, GR-AuNPs, and GR-AgNPs

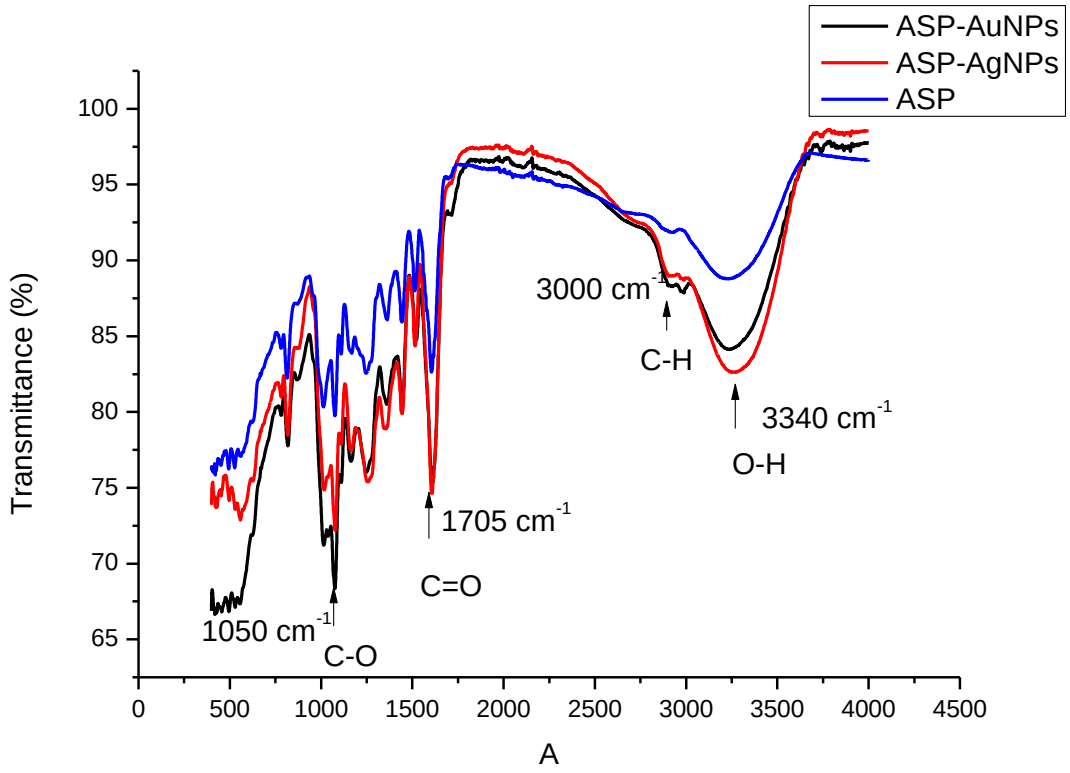

Figure 6.9: FTIR spectra of ASP, ASP-AuNPs, and ASP-AgNPs

6.4.6. *In vitro* stability study

The *in vitro* stability study was performed for the GR and ASP as well as their AuNPs and AgNPs in biogenic media. The synthesised metal NPs were mixed with (0.5%) BSA, glycine, and cysteine, (1%) NaCl solution, and 50 mM PBS at pH 7 and pH 9 in a 96-well plate in ratio 2:1, while metal NPs was used as the control. The mixtures and the controls samples were then incubated, and absorbance measurements were monitored on a UV-Vis spectrophotometer at 0 hr and 24 hours. The 24 hours interval was selected to reflect the approximate time required for complete biodistribution of drugs in physiological systems. Stable NPs are expected to maintain nearly the same wavelength as the control samples within a certain time interval before becoming unstable. Figures 5.10 and 5.11 revealed stable absorption bands for GR-AgNPs at 440 nm within the time interval. However, the ASP-AgNPs, ASP-AuNPs, and GR-AuNPs were unstable showing different absorption maxima within these time intervals. Interestingly, resynthesis of ASP NPs using 5% polyethylene glycol as stabilizer afforded stable ASP-AuNPs (530 nm), and ASP-AgNPs (440 nm) within 0 – 24 hours in all the tested media (Figure 5.12).

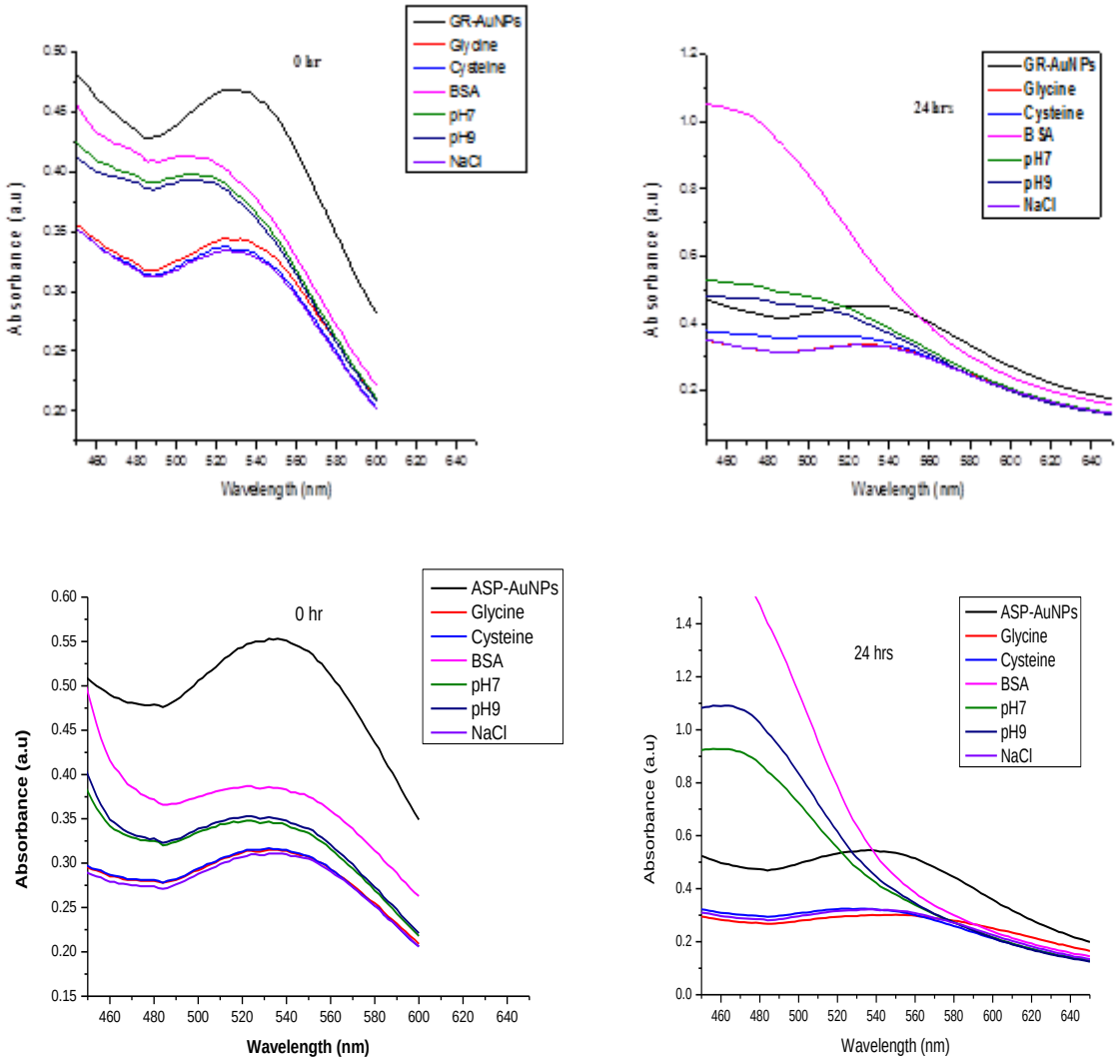

Figure 6.10: In vitro stability of GR and ASP AuNPs in biogenic media

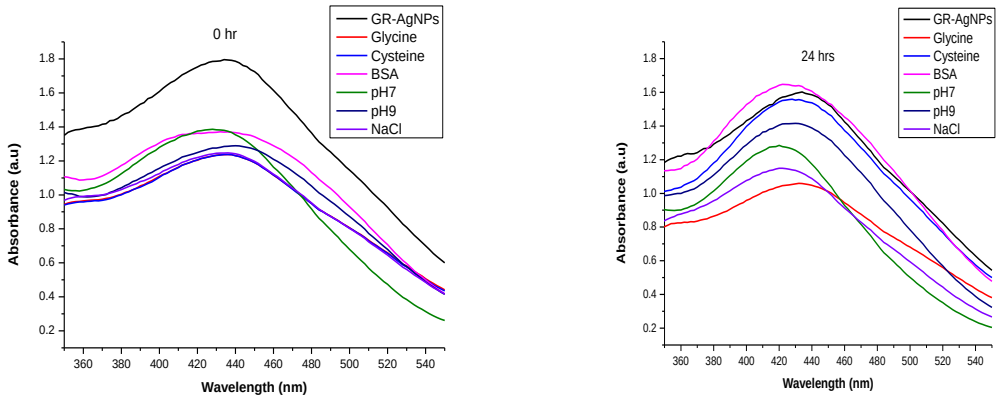

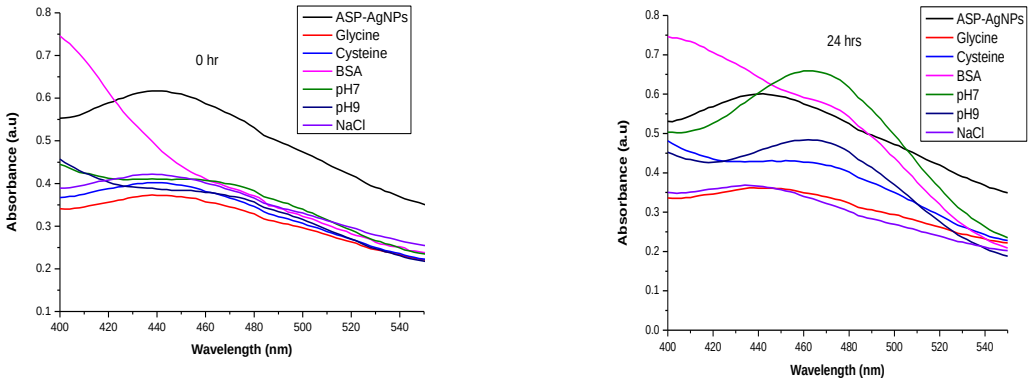

Figure 6.11: In vitro stability of GR and ASP AgNPs in biogenic media

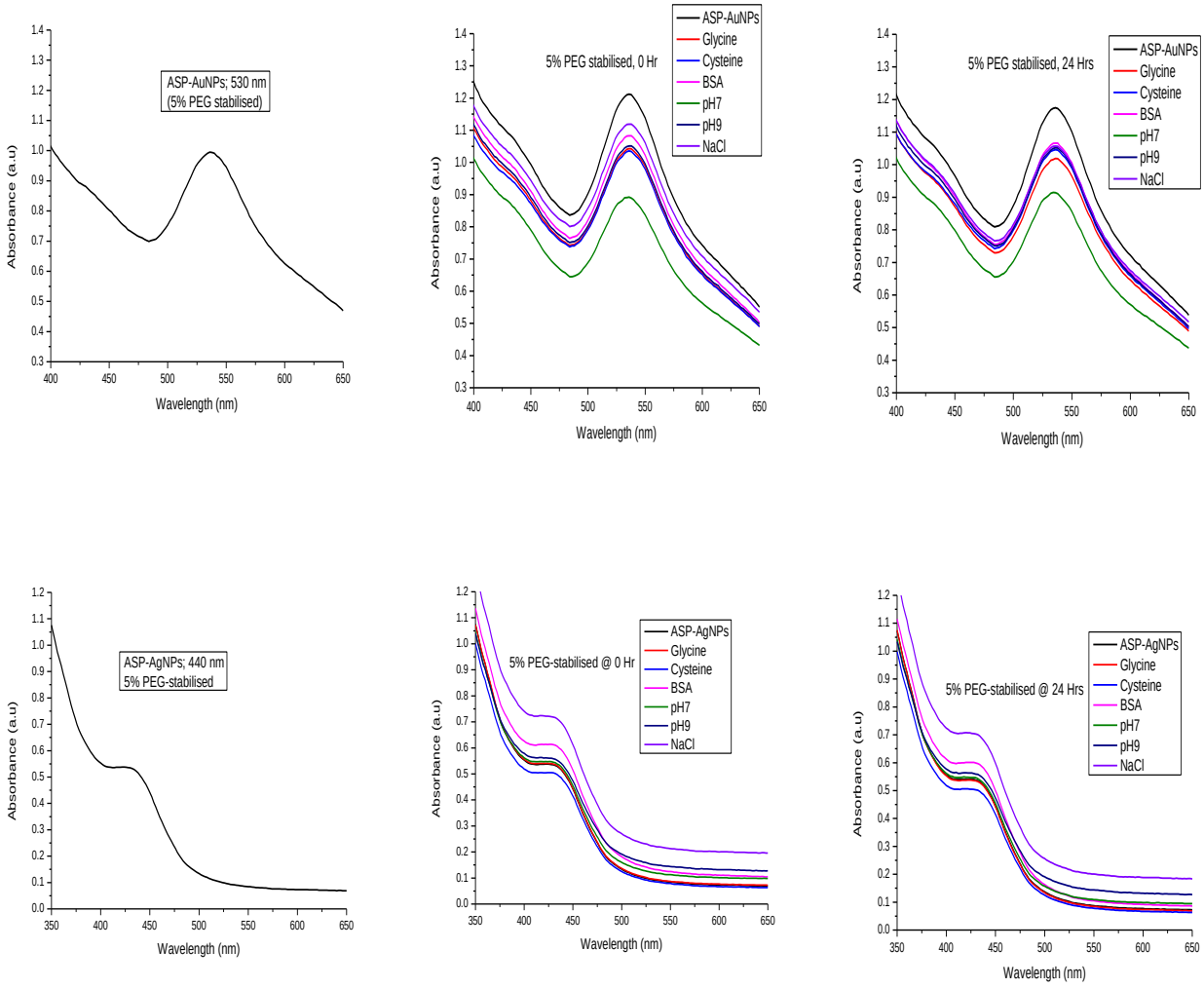

Figure 6.12: In-vitro stability of PEG- stabilised ASP-AuNPs and ASP-AgNPs AuNPs in biogenic media

6.4.7. Cell viability with biosynthesised AgNPs and AuNPs from GR and ASP

The 3-(4,5-dimethylthiazol-2-yl)-2,5-diphenyl-2H-tetrazolium bromide assay is a conventional method used to determine the viability of metabolic activity *in vitro*. Both the HepG2 and SH-

SY5Y cells were treated with 25, 50, 100, 200 and 500 µg/mL of synthesized GR and ASP nanoparticles for 24 h, respectively. The highest activity against HepG2 cells was observed at 500 µg/mL concentration for all tested treatments. However, the lowest concentration of 25 µg/mL showed the least anti-proliferation effect, which was comparable to the control group. From the result of cell viability (Figure 5.13) with synthesised MNPs, it is evident that the GR silver nanoparticles are the most effective against hepatocellular carcinoma as it is the only nanoparticle that was able to decrease cell viability to below 50% at concentrations higher than the determined IC_{50} (184.4 µg/mL). A similar trend was observed in the neuroblastoma cell line (Figure 5.14) as only the silver GR nanoparticles were able to induce a 50% loss of cell viability (IC_{50} = 108.8 µg/mL). However, this cell line was less sensitive to all other nanoparticles when compared to the HepG2 liver cells as cell viabilities remained comparable to untreated cells.

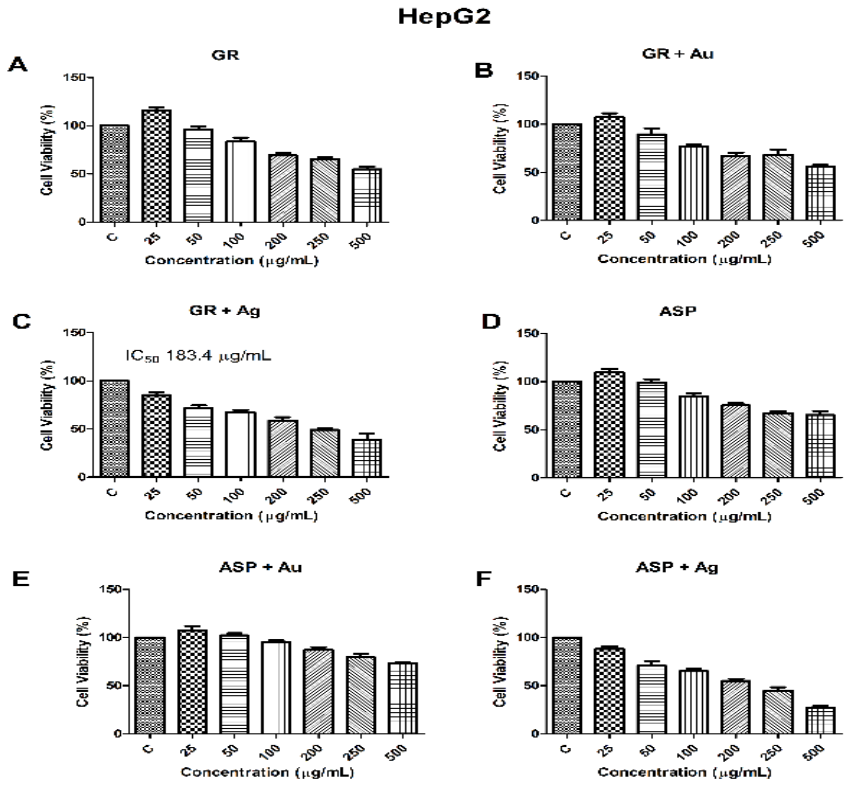

Figure 6.13: The results of MTT assay in HepG2 treated with GR and ASP nanoparticles after 24 h (results are reported as viability in comparison with control samples.

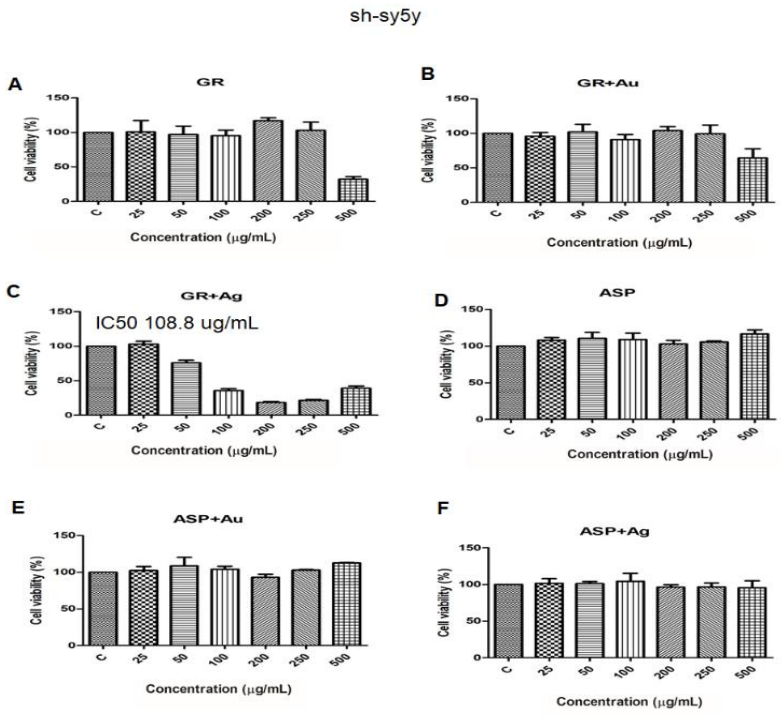

Figure 6.14: Figure 5.13: The results of the MTT assay in sh-sy5y treated with GR and ASP nanoparticles after 24 h (results are reported as viability in comparison with control samples.

6.4.8. Cellular uptake of AgNPs and AuNPs from GR and ASP

The cellular uptake of metallic nanoparticles used as drug carriers plays an important role in atom economy, dose loading and their interactions with physiological media. To confirm uptake of nanoparticles of both gold and silver, ICP-MS analysis on each cell treated with 100 µg/mL each of AuNPs and AgNPs were carried out using standard solutions of each metal for determination of standard curves for each metal. Fig. 5.15 shows the concentrations of AuNPs and AgNPs of rooibos assimilated in their respective cancer cells. The uptake of ASP-AuNPs (5.368 µg/mL) and GR-AuNPs (3.625 µg/mL) by SH-SY5Y and HepG2 cells were relatively higher than their corresponding AgNPs. However, the uptake of lower concentrations of GR-AgNP (1.549 µg/mL and 1.314 µg/mL) by HepG2 and SH-SY5Y respectively further support the observed anticancer activities in MTT assay at lower concentrations. It's well-known that AuNPs perfectly penetrate cells especially cancer cell lines [28], [29] and this may help in the treatment than using Ag. The high penetration of Au may represent another concern if we consider the neuroblastoma cells, however, further work is required in this regard. These results also suggest that a higher dose of the MNPs on cancer cells could lead to clogging of the interface between the cells and the reactive sites causing low permeation into the cells.

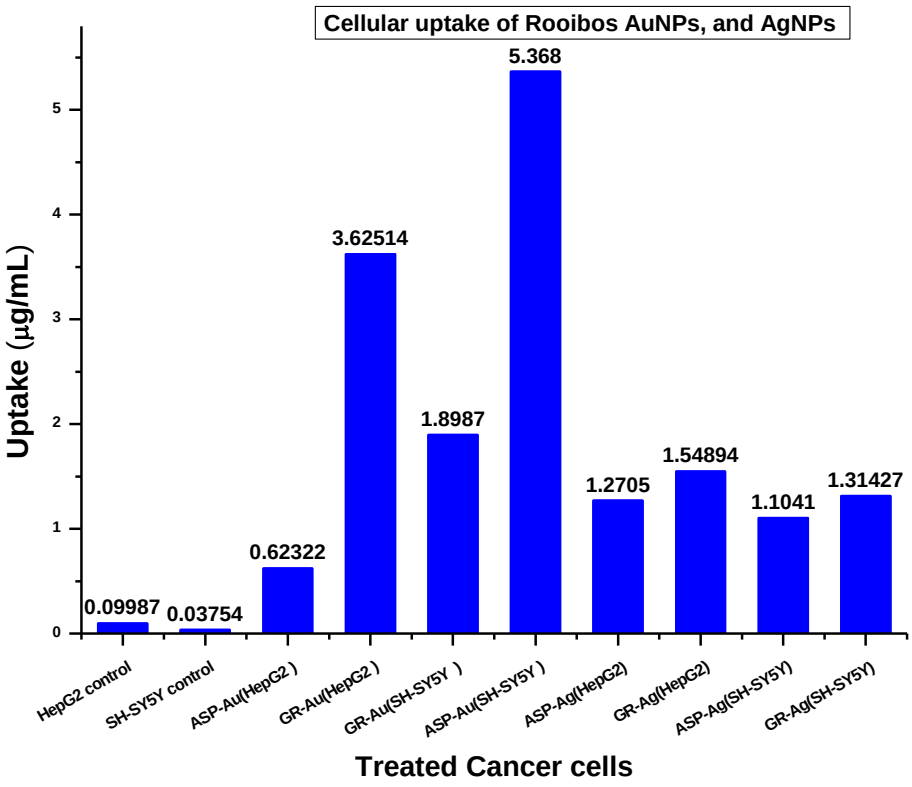

Figure 6.15: Cellular uptake of GR/ASP AuNPs and AgNPs

6.5. Discussion

The chemistry of GR and ASP are interwoven as GR remain the only source of ASP till the time of this report. Other phenolic constituents of interest in GR are orientin, iso-orientin and nothofagin [30]. The chemical structure of ASP (Figure 1) makes it prone to oxidation on incubation due to the high polyphenol content [11]. This characteristic makes it suitable for use as a reducing agent that could bring out the reduction of metals in solution to a stable zero valence state. The polyphenols provide electron donors for the reduction/scavenging of free radicals via the hydroxyl (2', 4', and 6') and carbonyl functional groups in the AC-ring (Figure 1). The 3,4 dihydroxyl phenols of the B-ring are relatively less active due to strongly bonded phenoxyl groups [31]. The 2', 4', 6'-trihydroxy and carbonyl groups present in ASP have also been attributed to the potent antioxidant activities of phloretin and 2,4,6-trihydroxy acetophenone which have similar dihydrochalcone skeletons [32]. Rezk et al. (2002) showed that the antioxidant/reducing ability of phloretin involves a keto-enol transformation of the carbonyl group, and the abstraction of the α-hydrogen atom of the carbonyl group to produce oxygen radicals (Figure 5.16).

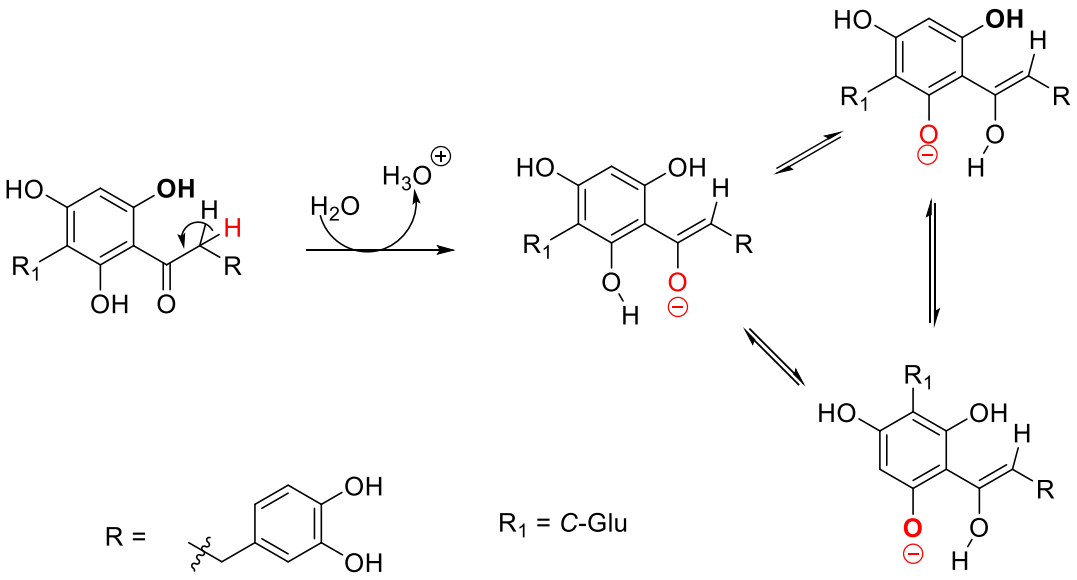

Figure 6.16: The proposed reduction mechanism of aspalathin

The IR data (Figure 5.8–5.9) suggest the presence of hydroxyl (3340 cm^{-1}), carbonyls (1710 cm^{-1}) and alcohols (1050 cm^{-1}) which undergoes a slight band shift and in intensities. Both GR and ASP demonstrated reducing properties in the synthesis of both Au and Ag metal nanoparticles. The successful synthesis of Au^0 and the Ag^0 via phytochemicals of rooibos and their anti-cancer potencies were validated with different characterisation methods and bioassays as discussed below. The effect of resonance and absorption of surface electrons of GR and ASP synthesised Au and Ag NPs showed characteristic absorption peaks at 530 nm (for AuNPs) and 440 nm (for AgNPs) respectively. The GR mediated AuNPs and AgNPs (Figure 5.2) agrees with reports of the literature for these metals [9], [21]. A similar result of AuNPs was obtained by reduction of $NaAuCl_4$ with black tea [27] and by the green synthesis of chalcone capped gold nanoparticles from *Helichrysum foetidum* [17]. In figure 5.3, the AgNPs of ASP exhibited similar absorption peaks at 540 nm (for AuNPs) and 444 nm (AgNPs). From the literature search and until this study, ASP mediated Au and Ag NPs was scarcely reported. However, the strong relationship observed between the UV absorption of ASP NPs and GR NPs for each metal further support our result as ASP represent the major compound found in GR. It is noteworthy to mention that the GR NPs of Au and Ag show absorptions at lower wavenumbers and at a faster reaction time compared to the NPs formed by ASP. This difference in absorption wavelengths and reaction time in the GR could be due to the synergies of reducing activities contributed by other phytochemicals.

The crystal structure and morphology of GR and ASP NPs support the feasibility of the biogenic synthesis of MNPs via bioactive compounds. Clear distinguishable particles for each GR and ASP that were mostly spherical were seen under HR-TEM (Figure 5.4) which is a common shape mostly reported for plant-based green synthesis of MNPs [8]. In addition to spherical

shapes, a rarely reported shape from plant-based MNPs was (hydra-like shape) observed for synthesised GR-AuNPs. The XRD pattern of NPs of GR and ASP samples further complement the observed shapes as non-amorphous and a crystalline signature for all samples. The four main rings for each GR and ASP MNPs were indexed as (111), (200), (220), and (311) reflections of face cubic centre matching for face-centred cubic crystalline metallic gold and silver phases as documented by the Joint Committee on Powder Diffraction Standards (JCP2 gold number 04-0784 and JCP2 silver number 04-0783 respectively).

The mean particle sizes and colloidal stability (zeta potentials) of metal nanoparticles for use as drug candidates are among essential considerations for efficient biodistribution and clearance in the cytosol [33]. The HR-TEM images of GR and ASP mediated AgNPs from statistical analysis exhibited a smaller size range (6.7 nm ± 0.39 and 1.6 nm ± 0.08 respectively) than it was reported for GR-AgNPs in the literature [9]. On the other hand, GR and ASP mediated AuNPs displayed mean particles sizes (7.5 nm ± 0.34 and 12.5 nm ± 0.04 respectively) that are very close to the value reported for GR-AuNPs [21]. As observed in figure 5.5 and figure 5.6, the zeta potential values of both GR and ASP MNPs indicated that interaction of the NPs and aqueous media led to high negative zeta potentials due to interparticle repulsion forces, such that they repel each other and no tendency for particle aggregation. However, *in vitro* stability studies of ASP NPs (without PEG) in biogenic media proves contrary to its hydrodynamic stability especially in neutral to alkaline pH (Figure 5.10). Notably is the instability of ASP NPs at pH ≥ 7 and in BSA. ASP is relatively acidic and was reported to be stable in PBS at pH 3 for up to 29 hours and less stable at pH 7 [34]. This agrees with the pH-dependent stability of aspalathin previously reported [34]. The authors showed that ASP was unstable at pH above 7.4 transforming to dihydro-iso-orientin and further to iso-orientin and orientin [30, 35]. The instability in BSA is presumably due to its complex mix of amino acids and forces interfacing with ASP which result in conformational changes of the BSA [36]. The stability of ASP in these media was improved by using 5% PEG as both stabilizer and surfactant during synthesis. We hypothesised that the 5% PEG elicit a lowering effect on surface tension between the suspension of ASP MNPs and solution of PBS ≥ 7, and BSA to stabilise ASP AuNPs and AgNPs (Figure 5.11).

The cytotoxic effects of various extracts from rooibos using several *in vivo* and *in vitro* cancer models have been reported [14], [37]–[40]. However, there are limited studies on the synthesis of nanoparticles using Green rooibos or its unique dihydrochalcone aspalathin and the evaluation of cytotoxic effects. The results of the MTT assay showed that the increase in the concentrations of GR and ASP Ag NPs enhanced the inhibitory effect on the cell proliferation

in HepG2 and SH-SY5Y cell lines. The IC_{50} value of the GR Ag nanoparticles (183 and 108 µg/mL, respectively) demonstrated that a lower concentration of Ag NPs was required to inhibit cell growth than the parent GR or ASP. A putative mechanism of action for the silver nanoparticles could be by an inducement of a state of oxidative stress on the cells by generating free radicals and reactive oxygen species (ROS) through disruption of mitochondrial function [41]. ROS have been associated with various processes such as DNA and cellular macromolecule damage, interference with cellular signalling cascades, and initiation of apoptotic processes. Although the exact mechanisms by which GR and ASP silver nanoparticles have not been elucidated, it is plausible that these pathways are activated.

Cellular identification of NPS for uptake is known to be influenced by physicochemical properties of the particle such as shape and size and the biological environment interacting it interact with [42]. Successful interaction of NPs with cell membrane could lead to penetration through any of the following mechanisms: phagocytosis, micropinocytosis, endocytosis, diffusion, or adhesion [42] According to Meiyu et al., smaller size AgNPs can permeate cell membrane relatively to bigger size NPs [43]. Analysis of ICP-OES quantification shows that membrane crossing of GR and ASP NPs was not size-dependent. Uptake was in decreasing order of ASP-AuNPs (SH-SY5Y) > GR-AuNPs (HepG2) > GR-AuNPs (SH-SY5Y) > GR-AgNPs (HepG2). Although the AgNPs of both samples were smaller in size when compared to AuNPs, a higher concentration of AuNPs were taken up by both neuroblastoma and hepatocellular cancer cells (Figure 5.15). The observed gold uptake can be attributed to its optical property, inertness, high biocompatibility and bioconjugation, and low toxicity on biomolecules [44].

6.6. Proposed mechanism of the metal nanoparticles formation

The chemical structures of aspalathin (ASP) show the properties of Lewis bases due to the availability of a divalent oxygen atom in the polyphenols which serves as an electron donor via the hydroxyl and carboxyl functional groups, as shown in fig. 7. The electron-deficient M^{n+} ions in solution could give stable complexes with organic molecules containing oxygen and hydroxyl donors/groups. Scheme 5.1 explains our proposed reaction mechanism in an aqueous mixture of both GR and ASP with Au^{3+}/Ag^{+} ions from sodium tetrachloroaurate (III) dihydrate ($NaAuCl_4.2H_2O$)/ silver nitrate ($AgNO_3$). We propose a four-step reaction involving; (i) ionization of the metal precursor (ii) reduction of Au^{3+}/Ag^{+} ions to their respective M^0 via metal-alkoxide formation with GR and ASP, (iii) NPs growth/stabilization by dative π-bonding of donated electrons and (iv)growth termination/capping. ASP represents GR, behaves as soft bases (ligands) and are oxidised while M^{n+} ions act as soft acid, due to incomplete outer filled d-orbital, hence reduced. Also, the reducing ability of ASP on M^{n+} is easily noticed as both are hexadentate ligands that can bind from seven different active sites; with O-H at positions 2', 3,

4', 4, and 6' and with O=C carbonyl (Figure 1, Scheme 1). This increases the tendencies for the Au^{3+}/Ag^{+} to be reduced to neutral Au^{0}/Ag^{0}. The stabilization of the zerovalent oxidation state of Au^{0}/ Ag^{0} by ASP can be attributed to available d-orbital electrons for dative π-bonding with lone pairs of electrons from O=C carbonyl and O-H groups. This proposed mechanism is further supported by the band maxima of GR-AuNPs, GR-AgNPs, ASP-AuNPs, and ASP-AgNPs at 530, 440, 540 and 44 nm respectively, which can be attributed to ligand-to-metal charge transfer.

Scheme 5.1: Proposed mechanism of synthesis of gold and silver nanoparticles with GR or ASP and gold precursor

6.7. Conclusion

This study contributes to the biosynthesis of metallic nanoparticles for biomedical applications. It shows that the use of the aqueous extract of *Aspalathus linearis* (green rooibos) and aspalathin are effective in the bio-reduction of gold and silver crystalline nanoparticles. Also, the study shows that the pure compound has a comparative advantage for smaller sizes of nanoparticles from plant phytochemicals. Furthermore, the use of silver nitrate precursors could elicit smaller sizes of both GR and ASP nanoparticles over the gold precursor. Based on the anticancer potency, the comparative analysis of the IC_{50} values of the parent GR, and ASP and the synthesized silver nanoparticles of GR, and ASP indicate that the synthesized silver nanoparticles are more efficacious in preventing cancer cell growth compared to the plant or pure compound alone. The combined results of this study and from our previous work

confirmed that the major pure compounds from plants are responsible for the reducing/capping ability during the synthesis of metallic nanoparticles.

Conflicts of interest

The authors declare no conflict of interest.

Acknowledgement

We wish to acknowledge the South African Rooibos Council (SARC) for the financial support towards the completion of this research. In addition, partial funding was provided by the South African Medical Research Council (SAMRC) through its Division of Research Capacity Development under funding received from the South African National Treasury. The content hereof is the sole responsibility of the authors and do not necessarily represent the official views of the SAMRC or the funders.

References

1. Zhao, J.; Gou, S.; Liu, F.; Sun, Y.; Gao, C. Anticancer Potency of Platinum (II) Complexes Containing Both Chloride Anion and Chelated Carboxylate as Leaving Groups. *Inorg. Chem*. **2013**, 52, 8163–8170.
2. Zhang, J.; Jiang, M.; Li, S.; Zhang, Z.; Sun, H.; Yang, F.; Liang, H. Developing a Novel Anticancer Gold (III) Agent to Integrate Chemotherapy and Immunotherapy. *J. Med Chem.*, **2021**, 64, 6777 – 6791.
3. Mohd Sofyan, N.R.F.; Nordin, F.J.; Mohd Abd Razak, M.R.; Abdul Halim, S.N.A.; Mohd Khir, N.A.F.; Muhammad, A.; Rajab, N.F.; Sarip, R. New silver complexes with mixed thiazolidine and phosphine ligands as highly potent antimalarial and anticancer agents. *J. Chem.,* **2018**, 2018, 1–10.
4. Ruiz, M. E.; Gantner, M. E.; Talevi, A. Applications of Nanosystems to Anticancer Drug Therapy (Part II. Dendrimers, Micelles, Lipid-based Nanosystems. *Recent Pat Anti-Canc*, **2014**, 9, 99–128.
5. Al-radadi, N. S. Green synthesis of platinum nanoparticles using Saudi's Dates extract and their usage on the cancer cell treatment. *Arab. J. Chem*., **2019**, 12, 330–349.
6. Jeyaraj, M.; Gurunathan, S.; Qasim, M.; Kang, M.; Kim, J. A Comprehensive Review on the Synthesis, Characterization, and Biomedical Application of Platinum Nanoparticles. *Nanomaterials*, **2019**, 9(12), 1719.
7. Patra, S.; Mukherjee, S.; Barui, A. K; Ganguly, A.; Sreedhar, B.; Patra, C. R. Green synthesis, characterization of gold and silver nanoparticles and their potential application for cancer therapeutics. *Mater. Sci. Eng. C*, **2015**, 53, 298–309.
8. Peralta-Videa, J.R.; Huang, Y.; Parsons, J.G.; Zhao, L.; Lopez-Moreno, L.; Hernandez-Viezcas, J.A.; Gardea-Torresdey, J.L. Plant-based green synthesis of metallic nanoparticles: scientific curiosity or a realistic alternative to chemical synthesis? *Nanotechnol. Environ. Eng.,* **2016**, 1(4), 1–29.
9. Oyagi, M. O.; Michira, I. N.; Guto, P.; Baker, P. G. L.; Kamau, G. Polydisperse Low Diameter 'Non-toxic' Silver Nanoparticles Encapsulated by Rooibos Tea Templates*. Nano Hybrids*, **2014**, 8(2014), 57–72.
10. Diallo, A.; Mothudi, B.M.; Manikandan, E.; Maaza, M. Luminescent Eu2O3 nanocrystals by *Aspalathus linearis*' extract: structural and optical properties. *J. Nanophotonics*, **2016**, *10*(2), p.026010.
11. Krafczyk, N.; Glomb, M.A. Characterization of phenolic compounds in rooibos tea. *J. Agr. Food Chem.* **2008**, *56*(9), 3368-3376.
12. Stander, M. A.; Van Wyk, B. E.; Taylor, M. J. C.; Long, H. S. Analysis of Phenolic Compounds in Rooibos Tea (*Aspalathus linearis*) with a Comparison of Flavonoid-Based Compounds in

Natural Populations of Plants from Different Regions. *J. Agric. Food Chem.,* **2017,** 65, (47), 10270–10281.
13. Koeppen, B. H.; Roux, D. Aspalathin: A novel C-glycosylfavonoid from *Aspalathus linearis. Tetrahedron Lett.*, **1965** (39), 3497–3503.
14. Marnewick, J. L.; Van Der Westhuizen, F. H.; Joubert, E.; Swanevelder, S.; Swart, P.; Gelderblom, W. C. A. Chemoprotective properties of rooibos (*Aspalathus linearis*), honeybush (*Cyclopia intermedia*) herbal and green and black (*Camellia sinensis*) teas against cancer promotion induced by fumonisin B_1 in rat liver. *Food Chem*. *Toxicol*., **2009**, 47(1) 220–229.
15. Lee, E.-J.; Jang, H.-D. Antioxidant activity and protective effect on DNA strand scission of Rooibos tea (*Aspalathus linearis*). *BioFactors*, **2004**, 21, 285–292.
16. Komatsu, K.; Kator, K.; Mitsuda, Y.; Mine, M.; Okumura, Y. Inhibitory effects of Rooibos tea, *Aspalathus linearis*, on X-ray-induced C3H 10T 1/2 cell transformation. *Cancer Lett*., **1994**, 77, 33–38.
17. Omolaja, A. A.; Brendon, P.; Omoruyia, S.I.; Badmus, J.A.; Ismail, E.; Marnewick, J.L.; Botha, S.; Benjeddou, M.; Ekpob, O.E.; Hussein, A.A. The potential of chalcone-capped gold nanoparticles for the management of diabetes mellitus. *Surfaces and Interfaces*. **2021**, 25, 101251.
18. Badeggi, U. M.; Ismail, E.; Adeloye, A. O.; Botha, S.; Hussein, A. A. Green Synthesis of Gold Nanoparticles Capped with Procyanidins from *Leucosidea sericea* as Potential Antidiabetic and Antioxidant Agents. *Biomolecules*, **2020**, 10 (452).
19. Badeggi, U.M.; Badmus, J.A; Botha, S.; Ismail, E.; Marnewick, J.L.; Charlene, W.J.A.; Hussein, A.A. Biosynthesis, Characterization, and Biological Activities of Procyanidin Capped Silver Nanoparticles. *Journal of Functional Biomaterials,* **2020**, 11(3), 66.
20. Akinfenwa, A.O.; Abdul, S. N.; Marnewick, J.L; Hussein, A. A. Protective Effects of Linearthin and Other Chalcone Derivatives from *Aspalathus linearis* (Rooibos) Against UVB Induced Oxidative Stress and Toxicity in Human Skin Cells*, Plants* **2021**,10, 1936.
21. Adewale, B.O.; Hajierah, D.; Lynn, C.; Saartjie, R. Toxicological Behavior of Gold Nanoparticles on Various Models: Influence of Physicochemical Properties and Other Factors. *Int. J. Toxicol.* **2019**, 38(5), 357-384
22. Phuoc Van, T.; Shinnosuke, A.; Kenichiro, K.; Nobuo, S.; Kazumasa, T.; Toru, S.; Takashi, K. Size/shape control of gold nanoparticles synthesized by alternating current glow discharge over liquid: the role of pH, *Mater. Res. Express*, **2019,** 6 (9), 095074.
23. Analike, B. S.; Daniela, K.; Giorgia, C.; Mauro, P.; Maribanyana, L.; Nonhlanhla, C; Suprakas, S.R.; L. Namrita. Synthesis and characterization of gold nanoparticles biosynthesised from *Aspalathus linearis* (Burm.f.) R. Dahlgren For progressive macular hypomelanosis. *J. Herb. Med.*, **2021**, 29, 100481.
24. Smith, C.; Swart, A. *Aspalathus linearis* (Rooibos) – a functional food targeting cardiovascular disease. *R. Soc. Chem. Food Funct.*, **2018**, 9(1).
25. Ali, Z. A.; Yahya, R.; Sekaran, S. D.; Puteh, R. Green synthesis of silver nanoparticles using apple extract and its antibacterial properties. *Adv. Mater. Sci. Eng.*, **2016**, 1 – 6.
26. Danaei, M.; Dehghankhold, M.; Ataei, S.; Hasanzadeh, D.F; Javanmard, R.; Dokhani, A.; Khorasani, S.; Mozafari, M.R. Impact of Particle Size and Polydispersity Index on the Clinical Applications of Lipidic Nanocarrier Systems. *Pharmaceutics*, **2018**, 10(2), 57, 1–17.
27. Nune, S. K.; Chanda, N.; Shukla, R.; Katti, K.; Kulkami, R.R.; Thilakayathy, S.; Mekapothula, S.; Katti, K.V. Green nanotechnology from tea: phytochemicals in tea as building blocks for production of biocompatible gold nanoparticles. *J. Mater. Chem.*, **2019**, 19, 2912–2920.
28. Dykman, L.A.; Khlebtsov, N. G. Uptake of Engineered Gold Nanoparticles into Mammalian Cell. *Chem. Rev.,* **2014**, 114, 1258−1288.
29. Malugin, A.; Ghandehari, H. Cellular uptake and toxicity of gold nanoparticles in prostate cancer cells: a comparative study of rods and spheres. *J. Appl. Toxicol*, **2010**, 30(3) 212-217.
30. Heinrich, T.; Willenberg, I.; Glomb, M.A. Chemistry of colour formation during rooibos fermentation. *J. Agr. Food Chem*. **2012**, *60*(20), 5221-5228.
31. Nakamura, Y.; Watanabe, S.; Miyake, N.; Kohno, H.; Osawa, T. Dihydrochalcones: evaluation as novel radical scavenging antioxidants. *J. Agr. Food Chem.*, **2003**, *51*(11), pp.3309-3312.

32. Rezk, B.M.; Haenen, G.R.; van der Vijgh, W.J.; Bast, A. The antioxidant activity of phloretin: the disclosure of a new antioxidant pharmacophore in flavonoids. *Biochemical and biophysical research communications*, **2002**, *295*(1), pp.9-13.
33. Honary, S.; Zahir, F. Effect of zeta potential on the properties of nano-drug delivery systems - A review (Part 1). *Trop. J. Pharm. Res*., **2013**, 12(2) 255 – 264.
34. De Beer, D.; Joubert, E.; Manley, M. Enhancing aspalathin stability in rooibos (*Aspalathus linearis*) ready-to-drink iced teas during storage: the role of nano-emulsification and beverage ingredients, citric and ascorbic acids. *J. Sci. Food Agric*., **2012**, 92(2011), 274–282.
35. Krafczyk, N.; Heinrich, T.; Porzel, A.; Glomb, M. Oxidation of the dihydrochalcone Aspalathin leads to dimerization. *J. Agric. Food Chem.*, **2009**, 57, 6838–6843.
36. Barbosa, L.R.S.; Ortore, M. G.; Spinozzi, F.; Mariani, P.; Bernstorff, S. The Importance of Protein-Protein Interactions on the pH-Induced Conformational Changes of Bovine Serum Albumin: A Small-Angle X-Ray Scattering Study. *Biophys. J.*, **2010**, 98(1), 147–157.
37. Marnewick, J.; Joubert, E.; Joseph, S.; Swanevelder, S.; Swart, P.; Gelderblom, W. Inhibition of tumour promotion in mouse skin by extracts of rooibos (*Aspalathus linearis*) and honeybush (*Cyclopia intermedia*), unique South African herbal teas. *Cancer Lett.* **2005**, 224(2), 193-202.
38. Marnewick, J.; Gelderblom, W.; Joubert, E. An investigation on the antimutagenic properties of South African herbal teas. *Mutat. Res.*, **2000**, 471, 157-166.
39. Pantsi, W. G; Marnewick, J. L.; Esterhuyse, A.J.; Rautenbach, F. J.; Van Rooyen, J. Rooibos (*Aspalathus linearis*) offers cardiac protection against ischaemia/reperfusion in the isolated perfused rat heart. *Phytomedicine*, **2011**, 18, 1220-1228.
40. Huang, S.-H.; Tseng, J.-C; Lin, C.-Y; Kuo, Y.-Y; Wang, B.-J; Kao, Y.-H; Muller, C. J; Joubert, E; Chuu, C.-P. Rooibos suppresses proliferation of castration-resistant prostate cancer cells via inhibition of Akt signaling. *Phytomedicine*, **2019**, 64 (153068).
41. Piao, M.J.; Kang, K.A.; Lee, I.K.; Kim, H.S.; Kim, S.; Choi, J.Y.; Choi, J.; Hyun, J.W. Silver nanoparticles induce oxidative cell damage in human liver cells through inhibition of reduced glutathione and induction of mitochondria-involved apoptosis. *Toxicol. Lett.*, **2011**, *201*(1), 92 – 100.
42. Behzadi, S.; Serpooshan, V.; Tao, W.; Hamaly, M.A.; Alkawareek, M.Y.; Dreaden, E.C.; Brown, D.; Alkilany, A.M.; Farokhzad, O.C.; Mahmoudi, M. Cellular Uptake of Nanoparticles: Journey Inside the Cell. *Chem Soc Rev.* **2017** 46(14), 4218 – 4244.
43. Foroozandeh, P; Aziz, A.A. Insight into Cellular Uptake and Intracellular Trafficking of Nanoparticles. *Nanoscale Research Letters* **2018**, 13(339) 1 – 12.
44. Meiyu, W.; Hongbo, G.; Lin, L.; Ying L.; Liming X. Size-dependent cellular uptake and localization profiles of silver nanoparticles. *International Journal of Nanomedicine* **2019**, 14, 4247 – 4259.
45. Alkilany, A.M.; Murphy, C.J. Toxicity and cellular uptake of gold nanoparticles: what we have learned so far?. *J. Nanopart. Res.*, **2010**,*12*(7), pp.2313-2333.
46. Amina, S.J.; Biu, G. A Review on the Synthesis and Functionalization of Gold Nanoparticles as a Drug Delivery Vehicle. *Int. J. Nanomedicine* **2020**, 15, 9823–9857.
47. Barbara, D.; Dimitri, V.; Laura, R.-L.; Alke, P.-F. Barbara Rothen-Rutishauser. Quantifying nanoparticle cellular uptake: which method is best? *Nanomedicine*, **2017**, 12(10), 1095 – 1099.

Supplementary data

Supplementary 6.1: DLS Measurements of GR-AgNPs

		Size (d.nm):	% Intensity:	St Dev (d.nm):
Z-Average (d.nm): 136.4	Peak 1:	143.2	97.2	51.34
PdI: 0.274	Peak 2:	5193	2.8	478.5
Intercept: 0.906	Peak 3:	0.000	0.0	0.000
Result quality : Good				

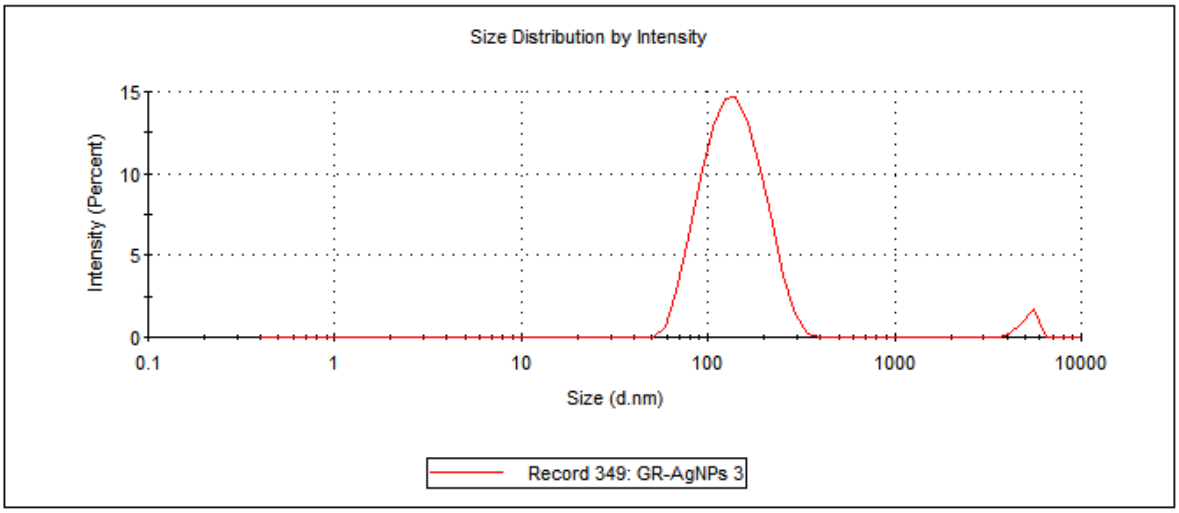

Supplementary 6.2: DLS measurements for ASP-AgNPs

		Size (d.nm):	% Intensity:	St Dev (d.nm):
Z-Average (d.nm): 104.7	Peak 1:	118.2	100.0	34.94
PdI: 0.111	Peak 2:	0.000	0.0	0.000
Intercept: 0.947	Peak 3:	0.000	0.0	0.000
Result quality : Good				

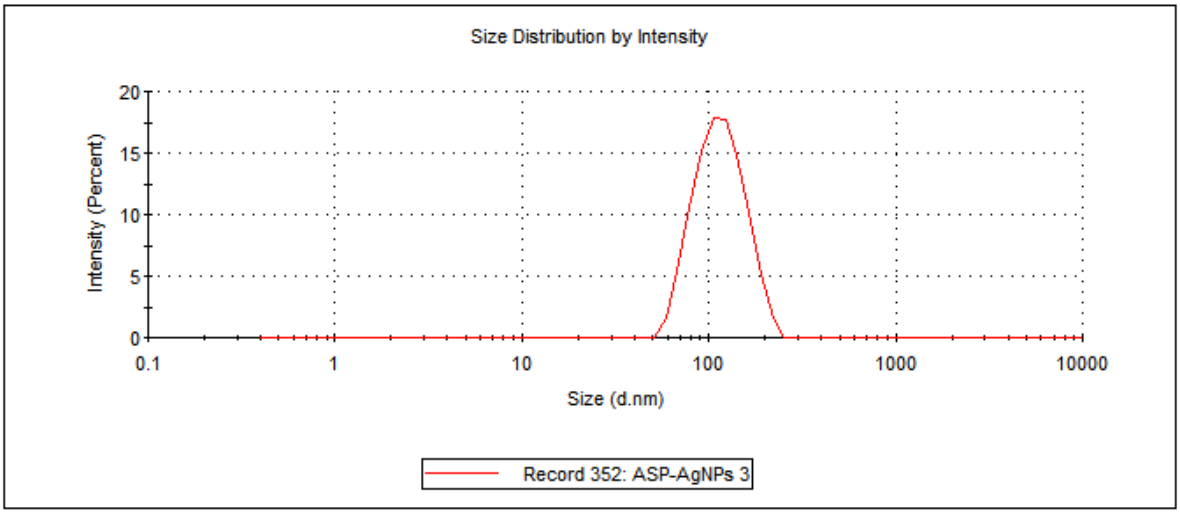

Supplementary 6.3: DLS measurements for GR-AuNPs

		Size (d.nm):	% Intensity:	St Dev (d.nm):
Z-Average (d.nm): 107.0	Peak 1:	123.0	100.0	43.19
PdI: 0.128	Peak 2:	0.000	0.0	0.000
Intercept: 0.951	Peak 3:	0.000	0.0	0.000
Result quality : Good				

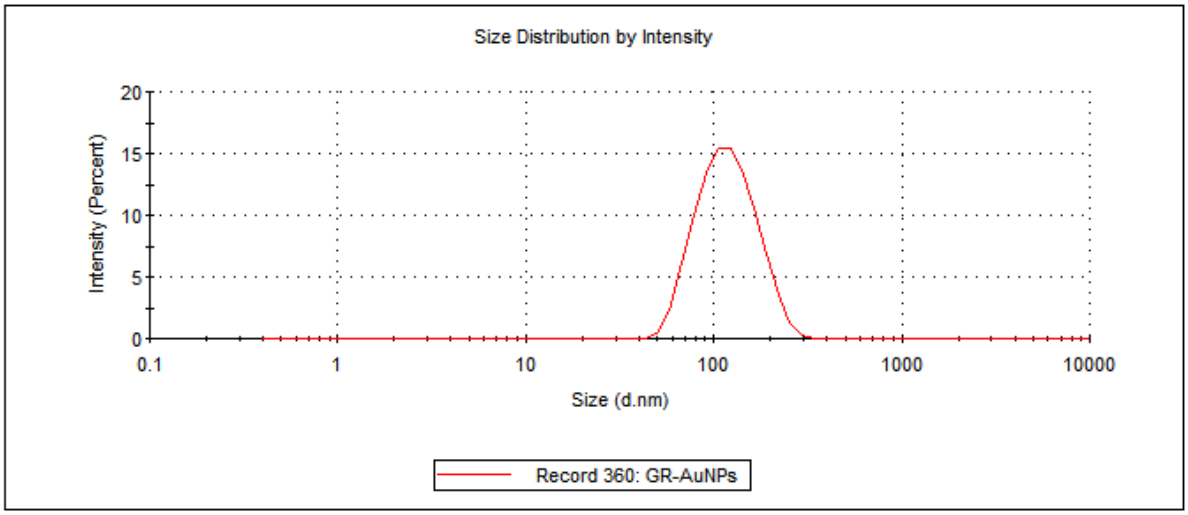

Supplementary 6.4: DLS measurements for ASP-AgNPs

		Size (d.nm):	% Intensity:	St Dev (d.nm):
Z-Average (d.nm): 109.7	Peak 1:	123.0	100.0	41.21
PdI: 0.100	Peak 2:	0.000	0.0	0.000
Intercept: 0.949	Peak 3:	0.000	0.0	0.000
Result quality : Good				

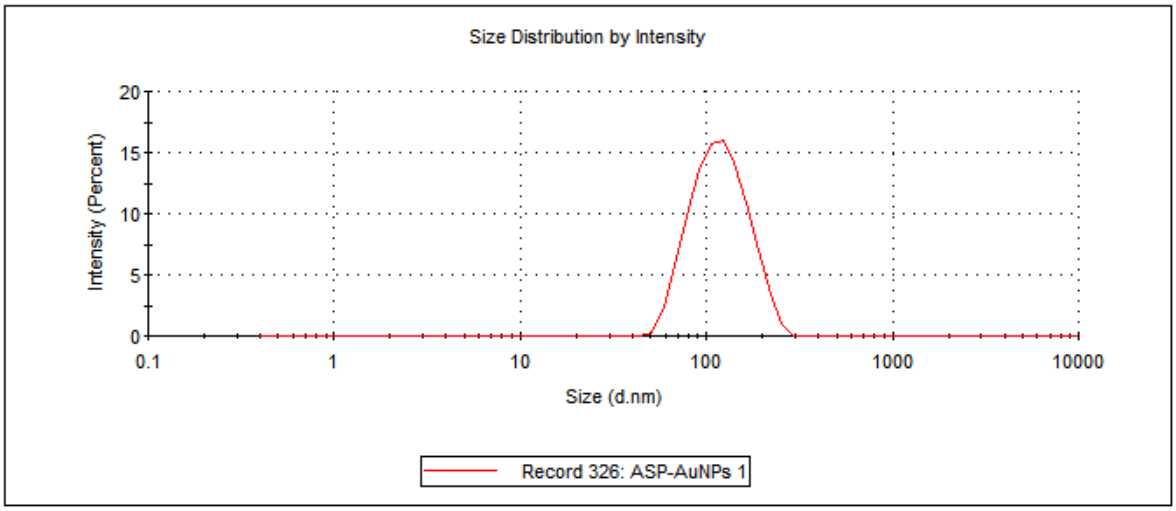

Chapter six

The potential of chalcone-capped gold nanoparticles for the management of diabetes mellitus

Akinfenwa A.O [a], Brendon Pearce [b], Sylvester I. Omoruyia [a], Jelili A. Badmus [c], Enas Ismail [a,f], Jeanine Marnewick [c], Subelia Botha [d], Mongi Benjeddou [b], Okobi E. Ekpob [e], Ahmed A. Hussein [a]*

[a] Department of Chemistry, Cape Peninsula University of Technology, Symphony Rd. Bellville 7535, South Africa; 217305296@mycput.ac.za (O.A.A); oa.akeemlaja@gmail.com (A.O.A); siomoruyi@gmail.com; ismailen@cput.ac.za (E.I.); mohammedam@cput.ac.za (A.A.H.)

[b] Precision Medicine Laboratory, Department of Biotechnology, 2nd Floor, Life Science Building, University of the Western Cape, Cape Town 7530, South Africa; brendon.biff@gmail.com (B.P.); mebenjeddou@uwc.ac.za (M.B.)

[c] Applied Microbial and Health Biotechnology Institute, Cape Peninsula University of Technology, Symphony Rd. Bellville, 7535, South Africa; jabadmus@lautech.edu.ng (J.A.B.); marnewickj@cput.ac.za (J.L.M.)

[d] Electron Microscope Unit, University of the Western Cape, Bellville, 7535, South Africa; subotha@uwc.ac.za (S.B.)

[e] Department of Medical Biosciences, University of the Western Cape, Cape Town, Robert Sobukwe Road, Bellville 7535, South Africa; oekpo@uwc.ac.za.

[f] Physics department, Faculty of Science (Girl's Branch), Al Azhar University, Cairo, Egypt; enas.ismail4@yahoo.com

*Correspondence: mohammedam@cput.ac.za; Tel.: +27-21-959-6193; Fax: +27-21-959-

Abstract

Searching for new natural bioactive capping agents represent an urgent priority in the green synthesis of metal nanoparticles. Additionally, the biosafety of metal nanoparticles is a major concern, especially in medical applications. Recently, the use of pharmacologically active natural products as capping agents has been deployed to avoid toxic effects during the preparation of the nanoparticles and to enhance their drugability compared with conventional drugs. Helichrysum foetidum is a South African medicinal plant used in folk medicine for the treatment of different human pathologies, and it is known to contain a variety of bioactive compounds. Herein, the total extract and two pure chalcones, helichrysetin and helichrysin, isolated from the same plant were successfully used to synthesize quasi-monodispersed gold

nanoparticles in the size range of 2–12 nm. The bio-evaluation of samples indicated that the AuNP/capping agent conjugates are biostable and have different biological profiles from the total extract/pure compounds. The enzymatic inhibition assays showed significant inhibition by the total extract, helichrysetin and their gold nanoparticles. Interestingly, a similar activity was observed for glucose uptake in HEK293 treated cells. On the other hand, all the tested samples relatively demonstrated no cytotoxicity when tested against the HaCaT keratinocytes. In conclusion, the study demonstrated potential enhancement of glucose uptake in mammalian kidney cells, and inhibition of carbohydrate-hydrolysing enzymes by green synthesized gold nanoparticles of H. foetidum. It also provides a therapeutic appraisal of AuNPs/chalcones conjugate towards the development of antidiabetic drugs derived from H. foetidum and its gold nanoparticles.

Keywords: *Helichrysum foetidum*; Chalcones, Gold nanoparticles; Bio-reduction, α-glucosidase; Toxicity; Glucose uptake

Highlights

I. Two flavonoid compounds, a chalcone and its glycoside were successfully isolated and chemically characterised from *Helichrysum foetidum.*
II. The activities of the total extract and the flavonoid compounds were explored for the bio-reduction of gold in green synthesis gold nanoparticles.
III. Physicochemical characterisation and stability time were performed for the green synthesised gold nanoparticles in different biogenic media.
IV. *In vitro* evaluation of all samples for the amelioration of diabetes was conducted.

7.1. Introduction

Polyphenols, aromaticity, and conjugated systems are characteristic of plant-based flavonoids which account for their numerous roles. These properties have been shown to exert influence on the interface between the flavonoids and cell membranes during bio evaluation as antioxidants, cytotoxicity, and stress-related diseases such as diabetes and overweight [29,35]. Carbohydrate metabolism requires α-glucosidase and α-amylase enzymes secreted in the small intestine to hydrolyse glycoside bonds from complex carbohydrate foods at different points to produce α-glucose as the product. Uncontrolled activities of these enzymes increase postprandial glucose that lead to an imbalance between glucose absorption in the bloodstream and insulin secretion for glucose uptake [21]. Inhibition of activities of α-glucosidase and α-amylase enzymes have been reported to reduce the risk of obesity, kidney failure and cardiovascular diseases during Type-2 diabetic (T2D) management [11]. Acarbose, voglibose, miglitol and metfomin are conventional antidiabetic drugs commonly prescribed to inhibit hepatic glucose production due to the breakdown of carbohydrates by α-glucosidase and α -amylase enzymes [2]. However, due to the potential side effect of increasing gas build up in the intestine and liver toxicity on prolonged usage [9], there is a need for the evaluation of alternative drugs in the nano range. Hence, it has become necessary to consider α-glucosidase and amylase inhibition drugs from natural products. *Helichrysum* species, also known as everlasting flowers, are widely distributed in the Southern hemisphere of Africa, Europe, and Australia [4]. They are valued as medicinal plants for the treatment of ailments such as influenza*,* eye infection, kidney stones, relief from gastrointestinal disorders, menstrual pain, headache, wound-healing, inflammation and to induce trance [22,32]. Previous studies of the phytochemicals from *H. foetidum* demonstrated antioxidants, antimicrobial, and protease-inhibiting activities [5,26,27,34]. Apart from kaur-16-en-18-oic, these phytochemicals were mostly chalcones and flavonoids (helichrysetin and its glycoside, helichrysin, apigenin and its glycoside and 7,4′ -dihydroxy-5-methoxy-flavanone), which are known to have antioxidant properties, and could counteract glucose-induced oxidative stress [18,19,26]. Furthermore, several studies have shown a dual role of flavonoids compounds with antidiabetic potential [30] and as reducing agents in the formation of gold nanoparticles [6,14,28]. Among other metal nanoparticles, gold nanoparticles are increasingly being used in biomedicine and therapeutics due to their large surface area, biocompatibility, and ease to be functionalized with biomolecules for active drug delivery [25,31]. This property of gold nanoparticles may help to overcome the possible removal of drugs from the systemic circulation by activities of the spleen and the liver. The synthesis of functionalized gold nanoparticles using total extracts of *Cassia auriculate* for the treatment of diabetes mellitus has been previously reported [36]. However, the use of pure compounds could give a better understanding of the mechanism of

formation and surface interface of flavonoid-mediated metallic nanoparticles [3,33,38]. Hence, in this report, the green synthesis of gold nanoparticles *via H. foetidum* total extract and its isolated pure compounds is presented. The total extract, the isolates and the biosynthesized gold nanoparticles were characterized and evaluated *in vitro* for glucose uptake and cytotoxicity. To the best of our knowledge, this is the first study to report the green synthesis of gold nanoparticles *via H. foetidum* constituents and to evaluate their potential use in the management of diabetes.

7.2. Materials and methods

7.2.1. Plant material

Helichrysum foetidum was collected from Worcester in November 2018 and identified by Professor Cupido, department of Botany, Fort Hare University, South Africa. The fresh plant materials were left to dry in shade for four weeks before extraction.

7.2.2. Chemicals and reagents

All chemicals were analytical grade. Methanol, hexane, dichloromethane, ethanol, acetone, ethyl acetate, sodium hydroxide and sodium chloride were purchased from Science World Chemicals, South Africa. Sodium tetrachloroaurate (III) dihydrate ($NaAuCl_4.2H_2O$, 99.99%) was purchased from BDH Chemical Limited England. Silica gel 60 (0.063-0.200 mm) and Sephadex (LH-20) were supplied by Merck (Darmstadt, Germany) and Sigma-Aldrich (Cape Town, WC, South Africa) respectively. Cysteine, glycine, bovine serum albumin (BSA), α-glucosidase (*Saccharomyces cerevisiae*), 4-nitrophenyl α-D-glucopyranoside (P-NPG), and 3,5-dinitro salicylic acid (DNS) were purchased from Sigma-Aldrich (St. Louis, MO United States). The NMR spectra were recorded on an Avance 400 MHz NMR spectrometer (Bruker, Rheinstetten, Germany) in deuterated acetone. Milli-Q de-ionized water was produced in-house (18.2 MΩ·cm at 25 °C), was used.

7.2.3. Cell culture and treatment

Renocytes (HEK293 kidney cells) were obtained from the American Type Culture Collection (Manassas, VA, USA), and were cultured in DMEM containing essential amino acids, sodium pyruvate and L-glutamine. Cell seeding was done on 24-well plates (50 000 cells/well) for the 2-deoxy-[^{3}H]-D-glucose assay (Promega, Madison, WI, USA). The HaCaT keratinocyte cell line from the human skin was a generous donation by the Mintek Laboratory, Department of Biotechnology, University of the Western Cape. Cells were cultured in monolayer using Dulbeco Modified Eagles Medium (DMEM, Lonza Group Ltd., Verviers, Belgium) supplemented with 10% foetal bovine serum (FBS, Gibco, Life Technologies Corporation, Paisley, UK) and 1% 100 U/mL penicillin and 100 µg/mL (Lonza Group Ltd. Verviers, Belgium). Cells were grown at 37°C, in a humidified atmosphere consisting of 5% CO2 and 95% air. All

cell culture media were routinely replaced every two to three days and were subcultured when they attained 80% confluency using a solution of 0.25 % trypsin EDTA (Lonza Group Ltd., Verviers, Belgium). Mycoplasma test was also conducted at intervals and only cells that were mycoplasma free were used for experiments.

For treatment, a 1 mg/mL stock solution of extract, compounds and nanoparticles was prepared in distilled water and further dilutions were made in cell growth medium to obtain final concentrations of 20, 40, 60 80 and 100 µg/mL used for the treatment.

7.3. Experimental

2.5.6 Extraction, isolation, and characterization of compounds

Air-dried leaves and flowers of *H. foetidum* weighing 620 g were chopped, coarsely powdered, and completely extracted with methanol (5 litres) for 48 hours at room temperature. The supernatant liquid was carefully decanted, filtered, and concentrated. A dried dark yellowish crude extract (79.87 g) was obtained. The crude extract was fractionated by silica gel column (40 x 8 cm) chromatography using a solvent gradient system in order of increasing polarity using hexane and ethyl acetate. Fractions of 500 mL each were collected, and similar fractions were further combined to 18 sub-fractions labelled F1 - F18 based on similarities of TLC profiles. Successive column chromatography of F9 and F16 lead to the isolation of two compounds; helichrysetin (compound B) and helichrysin (compound A) and their structures were characterized based on the analysis of their 1D and 2D NMR.

2.5.7 Spectroscopic data of Compound A and B

Compound B; Helichrysetin (6`-methoxy-2`,4, 4`-trihydroxy-chalcone): $^{1}$H NMR (400 MHz, acetone-$d_6$): $\delta_H$ 7.88 (1H, *d*, *J* = 15.6 Hz, Hα), 7.74 (1H, d, *J* = 15.6 Hz, Hβ), 7.61 (2H, d, *J* = 8.4 Hz, H-2`, -6`), 6.93 (2H, *d*, *J* = 8.0 Hz, H-3`,-5`), 6.09 (1H, s, H-5), 6.02 (1H, s, H-3), 3.98 (3H, s, OMe). $^{13}$C NMR and DEPT-135 (100 MHz, acetone-$d_6$): $\delta_C$ 193.2 (C=O), 168.5 (C-2), 165.7 (C-4), 164.3 (C-6), 143.3 (Cβ), 131.3 (C-6`), 128.0 (C-1`), 125.3 (Cα), 116.8 (C-3`), 106.3 (C-1), 96.9 (C-3), 92.2 (C-5), 56.41 (OMe).

Compound A; Helichrysin (6`-methoxy-2`,4-dihydroxy-chalcone-4`-*O*-β-D-glucopyranoside): $^{1}$H NMR (400 MHz, acetone-$d_6$): $\delta_H$ 7.88 (1H, d, *J* = 15.6 Hz, Hα), 7.77 (1H, d, *J* = 15.6 Hz, Hβ), 7.62 (2H ,d, *J* = 8.4 Hz, H2`), 6.93 (2H, d, *J* = 8.0 Hz, H3`), 6.30 (1H, d, *J* = 2.4 Hz, H3), 6.21 (1H, d, *J* = 2.0 Hz, H5), glucose moiety; 5.13 (1H, d, *J* = 7.6 Hz, H1``), complex signals from 3.49 – 3.98 for H-2``- H-6``, 4.02 (3H, s, OMe). $^{13}$C NMR (100 MHz, acetone-$d_6$) and DEPT-135: $\delta_C$ 193.7 (C=O), 168.3 (C4), 165.0 (C-2), 97.7 (C-3), 92.9 (C-5), 163.7 (C-6), 161 (C-4`), 144.1 (Cβ), 131.5 (C-2`), 127.8 (C-1`), 124.9 (Cα), 116.9 (C-3`), 107.8 (C-1), 56.64 (OMe), glucose moiety; 101.00 (C-1``), 78.1 (C-5``), 77.9 (C-3``), 74.5 (C-2``), 71.3 (C-4``),

62.6 (C-6``). Total extract and representative fractions were then screened for glucosidase and amylase enzymes inhibition and formation of AuNPs.

2.5.8 Synthesis of gold nanoparticles

The crude extract (HF) and isolated compounds A and B were screened for green synthesis of gold nanoparticles as reducing agents, at different concentrations in a 96-well microplate for determination of the optimum concentrations and the ratio of reducing agent to the gold precursor for further upscaling. 20 mg each of HF, compounds A and B were dissolved separately in 2 mL of de-ionized water, vortexed for 5 minutes to obtain homogeneous solutions and then added dropwise to 50 mL 1% w/w of sodium chloroaurate (III) solution at 90 ^{o}C for 40 minutes under continuous stirring. An instantaneous colour change was observed from pale yellow to ruby red for HF and compound A. The ruby red colour appeared after 25 minutes for compound B suggesting the formation of gold nanoparticles for all samples.

2.5.9 Characterization of gold nanoparticles

Different characterization techniques such as UV, HR-TEM, XRD, FTIR, and dynamic light scattering (DLS) were used to investigate the formation of gold nanoparticles and their various physicochemical properties. The absorption bands due to electrons confined on the nanogold particles surface were measured with SPECTROstar Nano (BMG LABTECH, Germany) 2450 UV-vis spectrophotometer.

The potential stability of the gold nanoparticles was determined through zeta potential measurement and the presence of inter-particle interaction from polydispersity indices (PDI), using a Zetasizer Nanoseries ZS90, model number ZEN3690 (Malvern Instruments Ltd, UK). To determine the hydrodynamic size, gold nanoparticles were diluted in de-ionized water in a volume ratio of 2:1. The zeta potential value gives an indication of the magnitude of repulsion between particles, which is suggestive of the stability of the colloidal system while the PDI gives the size distribution of the particles.

High-Resolution Scanning Electron Microscope (HR-TEM) micrographs were recorded on an FEI Tecnai G2 F20 S-Twin HRTEM, operated at 200 kV. A drop of the aqueous gold suspension was dropped on a carbon-coated copper grid and allowed to dry completely for an hour at room temperature. X-ray diffraction (Model Bruker AXS D8 advance with radiation at $\lambda kCuk\alpha_1$ = 1.5406 Å) was used to observe the crystallinity of the particles. Measurements were performed using a multipurpose X-ray diffractometer D8-Advance from Bruker operated in a continuous θ-θ scan in locked coupled mode with Cu-K_α radiation. The sample was mounted in the centre of the sample holder on a glass slide and levelled up to the correct height. The measurements were performed within a range in 2θ between 30°-80° with a typical step size

of 0.034° in 2θ. A position-sensitive detector, Lyn-Eye, was used to record diffraction data at a typical speed of 0.5 sec/step which is equivalent to an effective time of 92 sec/step for a scintillation counter. Analysis of HR-TEM and XRD images were carried out with ImageJ software, 1.50b version 1.8.0_60 (http://imagej.nih.gov/ij) and Origin pro-2019 (64 bits) software respectively. Vibrational bands of possible functional groups involved in the synthesis were recorded on a PerkinElmer Fourier-Transform Infrared Spectrometer 2000, equipped with a universal ATR-FTIR (PerkinElmer Spectrum 100, Llantrisant, Wales, UK) at transmission mode of 400 – 4000 cm^{-1}.

2.5.10 *In vitro* stability study

The in-vitro stability test was carried out by mixing 200 µL of gold nanoparticles solution with 100 µL biogenic amino acids (such as 0.5% Glycine, 0.5% BSA), phosphate buffer saline (PBS at pH 7 and pH 9) and 1% NaCl solution in a 96-well plate and incubated (at 37 °C) for different periods. The stability of HF-AuNPs, Compound A-AuNPs and Compound B-AuNPs in these media were monitored with UV-Vis at an interval of 24 hours for three days, for correlation of their respective maximum wavelengths with that of their synthesized gold nanoparticles.

2.5.11 Enzymatic inhibition bioassay

The inhibition potentials of α-glucosidase and α-amylase for HF, Compounds A, Compound B and their respective gold nanoparticles were carried out with slight modification of Badeggi *et al*. [3]. The samples were initially dissolved in methanol at 1 mg/mL as stock solution respectively. A 96-well plate was set up for the reaction followed by a step-by-step pipetting of samples, buffer solution, enzymes, and substrates. 50 µL phosphate buffer (100 mM, pH = 6. 8) was dispersed plus 10 µL α -glucosidase enzyme (1 U/mL) and 20 µL of varying concentrations of HF (0.0625, 0.125, 0.25, 0.5, and 1 mg/mL) were preincubated at 37◦C for 15 min. Following preincubation, 50 µL of 5 mM P-NPG was added as a substrate and incubated further at 37 °C for 20 mins. The reaction was brought to end by adding 50 µL Na2CO3 (0.1 M). The absorbance of the reaction mixture was measured at 405 nm using Multiplate Reader (Multiskan Thermo scientific, version 1.00.40, Vantaa, Finland) and correlated to α-glucosidase inhibition. For the α-amylase inhibition experiment, α-amylase enzyme replaced α-glucosidase enzyme, 1% starch solution was used in place of PNG and DNS in place of 0.1 M Na_2CO_3 in the mixtures. After the addition of 50 µL DNS, the reaction mixtures were boiled on a steam bath at 95 °C for 20 minutes for colour change. The same procedure was repeated for compounds A and B and their respective gold nanoparticles. Uninhibited solutions samples with AuNP were set up in parallel as control and each experiment was performed in triplicates. The results were expressed as percentage inhibition calculated according to the formula, *Inhibitory activity* (%) = (*A* - *B*)/*A* × 100.

Where A = absorbances of uninhibited control and B = absorbances of test samples with inhibition agent. GraphPad Prism 5 statistical package (GraphPad Software, USA) was used for statistical analysis for the concentration of sample resulting in 50% inhibition of the α-glucosidase and α- amylase activities (IC_{50}) respectively and results expressed in terms of mean ± standard deviation.

2.5.12 Glucose Uptake assay

The method for measuring glucose uptake in mammalian cells based on the detection of 2-deoxyglucose-6-phosphate was performed according to the manufacturer's guidelines. When cells are exposed to 2- deoxyglucose (2DG), there are transported across the membrane and rapidly phosphorylated in the same manner as glucose. However, enzymes that further modify glucose-6-phosphate (G6P) cannot modify 2DG6P, and thus a membrane-impermeable analyte accumulates in the cell. After a brief period of incubation, the acidic Stop Buffer is added to lyse cells, terminate uptake, and destroy any NADPH. A high-pH buffer solution (Neutralization Buffer) is then added to neutralize the acid. A Detection reagent is added to the sample wells. Glucose-6-Phosphate Dehydrogenase oxidizes the deoxyglucose to 6-phosphodeoxygluconate and simultaneously reduces NADP+ to NADPH. The reductase uses NADPH to convert the proluciferin to luciferin, which is then used by Ultra-Glo™ Recombinant Luciferase to produce a luminescent signal that is proportional to the concentration of 2DG6P. The reaction mixtures were incubated at room temperature for 1 hour. After 1 hour the cells were incubated with various concentrations of each compound, the cells were washed with 100µl PBS. A volume of 50 µL 1mM 2DG was added to each well and allowed to incubate for 10 minutes. A volume of 25 µL stop buffer was added to each well and shaken briefly. Thereafter, 25 µL of neutralization buffer was added to each well and shaken briefly. Finally, a volume of 100 µL of reductase substrate mix was added and the plate was shaken briefly. The plate was then incubated at room temperature for 30 minutes and read on a plate reader at 15 minutes intervals for 2 hours.

Figure 7 indicates the relative glucose uptake for a given compound, compared to the control. The p-values in these graphs were calculated using an independent two-tailed T-test where 0.05 is the threshold for significance.

2.5.13 Cytotoxicity assay

Cytotoxicity was assessed using the 3-[4,5-dimethylthiazol-2-yl]-2,5diphenyltetrazolium bromide colourimetric assay (MTT, Sigma). The MTT is a yellow tetrazolium salt that is reduced to purple formazan in living cells. Briefly, the HaCaT keratinocytes were plated in 96-well cell culture plates at a cell density of 5000 cells per well and incubated overnight to allow for attachment. The medium was thereafter replaced with a fresh medium containing increasing

concentrations (20, 40, 60 80 and 100 µg/mL) of HF, HA, HB, HF-AuNPs, HA-AuNPs and HB-AuNPs for 48 hours. Cells incubated with medium only served as control. After the 48 hours incubation, 10 µL of the MTT solution (5 mg/mL) was added to each well and the cells were incubated for an additional 4 hours at 37 °C. Thereafter, the resultant MTT crystals formed were solubilized in DMSO and the absorbance of each well was read at 570 nm using a BMG Labtech Omega® POLARStar multimodal plate reader. The percentage cell viability was calculated using the formula below:

$$\%\ \text{Cell Viability} = \frac{\text{Absorbance of treated well}}{\text{Absorbance of Untreated well}}\ \text{X}\ 100$$

The concentration required to kill 50% of the cells (IC_{50}) was determined via a survival curve using GraphPad Prism6 software (GraphPad Software, San Diego, CA, USA).

7.4. Results and discussion

7.4.1. Isolation and identification of compounds

Preliminary screening of *H. foetidum* extract for the synthesis of AuNPs [10], showed promising results, subsequently, it was subjected to purification steps to identify the compounds responsible for the reduction and stabilization of AuNPs. Chromatographic manipulation in parallel with NPs assay formation, two compounds were isolated. Structural elucidation of these compounds was completed by recording the ^{1}H and ^{13}C NMR data and compared with the literature [7, 19, 23, 26, 37]. The ^{1}H and ^{13}C NMR of compounds A and B discussed in the experimental session showed identical ^{1}H and ^{13}C NMR profiles with the same compounds reported previously. Compound B was identified as 6`-methoxy-2`,4,4`-trihydroxy-chalcone (helichrysetin), and compound A as 6`-methoxy-2`,4-dihydroxy-chalcone-4`-*O*-β-D-glucopyranoside (helichrysin) a glycosylated form of HB (Fig. 7.1). These compounds were previously reported by [19] and [26] from the same plant [19, 26]. However, the first record of these compounds from the *Helichrysum* genus shows that they were isolated from the flower extract of *Helichrysurn ps. aff. H. cooperi* Harv. and the aerial part of *H. heterolasium* respectively [7, 37]. Compound B was later isolated from a flower extract of *H. odoratissimum* [23] and was recently reported to induce apoptosis of cancer cells [16].

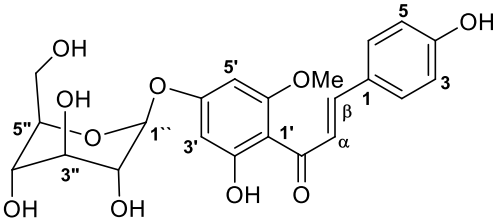

Compound A; Helichrysin

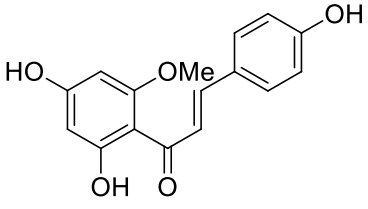

Compound B; Helichysetin

Figure 7.1: Compounds A and B isolated from polar fractions of *H. foetidum*

7.4.2. The interaction of the chalcones on the surface of gold nanoparticle

The chemical structures of helichrysin and helichrysetin show the properties of Lewis bases due to the availability of a divalent oxygen atom, which serves as an electron donor/proton acceptor *via* the hydroxyl and carboxyl functional groups, as well as the presence of conjugated double bonds system, as shown in scheme 6.1. The oxidation/reduction abilities of phenolic compounds are possible and depend on the reaction conditions [24]. In the case of chalcones, the extended chromophore supports the stability of the resulted –ve/+ve charges entity. From the practical point of view, the formation of the AuNPs is usually associated with the drop of the pH and the solution becomes acidic, under this condition and as given in scheme 6.1, the protonation of the oxygen atoms is very possible to form a positively charged stable system. The interaction of the positively charged with the negatively charged surface metal stabilizes the NPs. This proposed mechanism is supported by the highly negative potential of the NPs as indicated from Zeta potential and the drop of the pH of the NPs solution

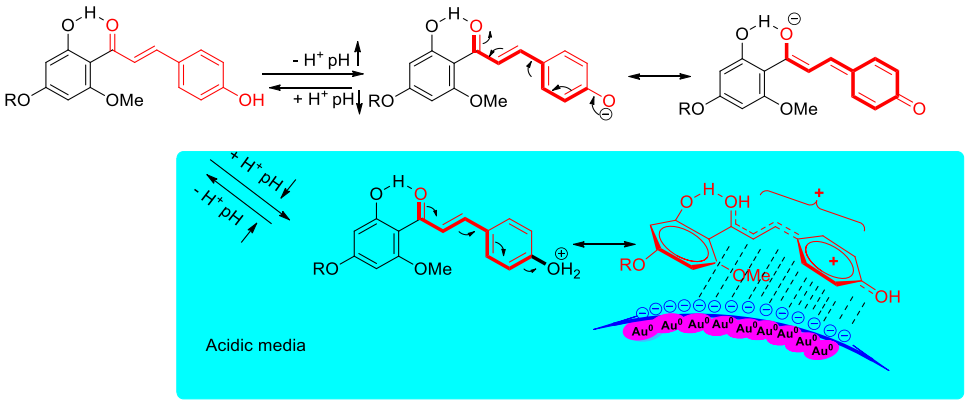

Scheme 6.1: Proposed mechanism of gold nanoparticle formation

7.4.3. Optical properties

UV-Vis spectroscopy was used to confirm the formation of AuNPs. The solution of auric chloride, the total extracts and the two compounds, all had yellowish colours before synthesis. A visual colour change from yellowish to ruby red was the initial confirmation of AuNPs formation. This was characterized by intensely ruby red colours observed at 536 nm, 540 and 546 nm bands for HF, compound A and compound B nanoparticles respectively (Fig. 3). These

band absorptions were within the range reported for green mediated gold nanoparticles synthesis [25]. The absorption bands of compound A-AuNPs and compound B-AuNPs were almost similar suggestive of symmetrical sizes and shapes of their nanoparticles compared to HF-AuNPs. Worthy of note is that the formation of the nanoparticles by the extract was instantaneous with higher intensity compared to the individual compounds. Abdel-Rauf *et al*. [1] reported a similar rapid formation of gold nanoparticles via an extract of *Galaxaura elongate* [1]. This could be due to the collective effect of more than one reducing agent present in HF which enhance the reducing ability of the total extract to yield a gold nanoparticle with a higher absorption peak compared to the others. Similar peaks for gold nanoparticles were reported by Thiphe *et al*. [33], which supports the phytochemical reduction of the auric chloride by the flavonoid constituents of *H. foetidum* [33].

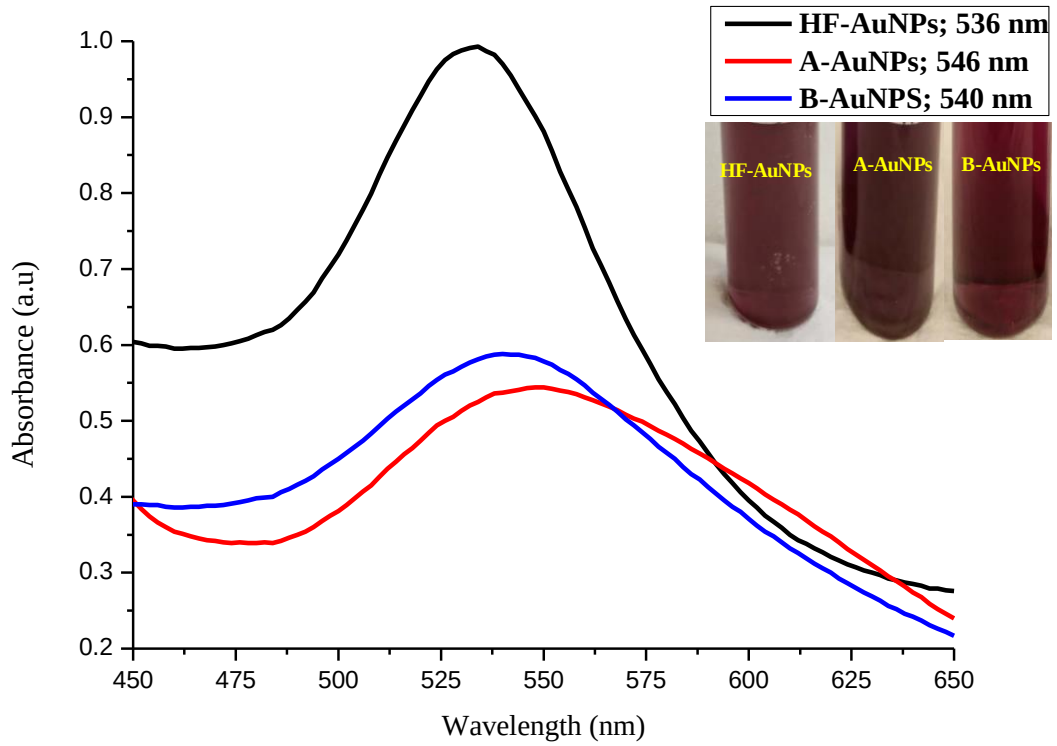

Figure 7.2: UV-Vis spectra for the synthesized HF, HA and HB gold nanoparticles

7.4.4. Morphology and size distribution

HR-TEM technique gives information on the size, shape, and crystallinity of synthesized nanoparticles. The HR-TEM micrographs recorded for the biosynthesized gold nanoparticles clearly show nanosized and non-agglomerated particles for compound B-AuNPs, A-AuNPs, and HF-AuNPs respectively (Fig. 6.4–6.6). Compound B-AuNPs and compound A-AuNPs images revealed quasi-monodisperse shapes mostly hexagonal with a few spherical and triangular shapes, while HF-AuNPs exhibited varieties of shapes including spherical, triangular hexagonal, and rod shapes. Mean particles sizes from the histograms showed sizes in the range of 12.5±04.3, 6.7±1.68 and 2.02±0.53 nm for HF-AuNPs, compound A-AuNPs and compound B-AuNPs respectively. It is interesting to note that the pure compounds enhanced the size reduction of the AuNPs formed when compared to the crude extract. The smaller sizes of compound A-AuNPs and compound B-AuNPs compared to HF-AuNPs can be attributed to the phenolic content of flavonoids that interface with the metal ions. Hence, it is suggestive that pure compounds could proffer a better size-control of nanoparticles than using total extract in the biosynthesis of gold nanoparticles. The SAED patterns (Fig. 6.4 – 6.6) indicated high crystallinity of all biosynthesized gold nanoparticles and it was in strong agreement with the XRD results.

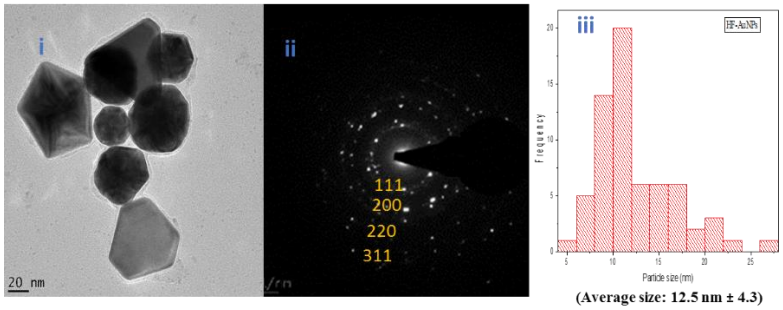

Figure 7.3: (i) HR-TEM (ii) SAED (iii) size distribution histogram of HF-AuNPs

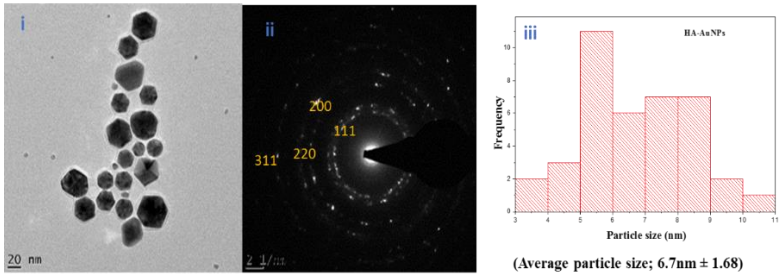

Figure 7.4: (i) HR-TEM (ii) SAED (iii) size distribution histogram of compound A-AuNPs

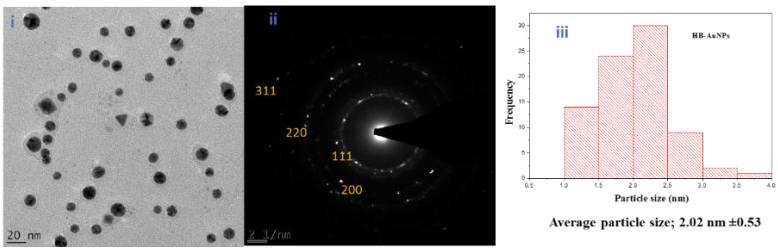

Figure 6.7.5: (i) HR-TEM (ii) SAED (iii) size distribution histogram of compound B-AuNPs

7.4.5. Dynamic light scattering by AuNPs

Determination of zeta potential (ZP) of nanoparticles is necessary for nano-bio materials as it gives valuable information on the degree of stability of the particles in the colloidal system [13]. The zeta potential values range between +100 mV to -100 mV, however, values greater than +25 mV or less than -25 mV is considered to have a high degree of stability for low molecular weight samples [17]. Similarly, PDI measured provides information on the size distribution of particles and the level of uniformity or heterogeneity of particles sizes. PDI values less than 0.05 show high homogeneity of particles, values between 0.5-0.7 are less uniform and above 0.7 is highly polydisperse [8]. To determine the stability of our nanoparticles between the interfacial double layers of particles surface charges, the dispersing medium and the PDI, a Zetasizer that measures ZP and PDI based on dynamic light scattering was used. All samples gave moderate zeta potentials of -27.1, -24.3 and -24.1 mV for the total extract compound A and B respectively (Fig. 6.7 and 6.8) These values indicate that formed AuNP were less prone to aggregation with a slightly higher stability of HF-AuNPs than that of the compounds. This can be attributed to the possible influence of the polyphenols found in the total extract. Relatively high PDI values of 0.440, 0.408 and 0.320 were obtained for HF-AuNPs, Compound A-AuNPs and Compound B-AuNPs respectively. This reflects the level of uniformity of sizes of nanoparticles as seen under HR-TEM.

Sample Name:	Cpd A-AuNPs 1		
SOP Name:	mansettings.nano		
File Name:	Akeem000.dts	**Dispersant Name:**	Water
Record Number:	8	**Dispersant RI:**	1.330
Date and Time:	28 November 2019 09:08:57 PM	**Viscosity (cP):**	0.8872
		Dispersant Dielectric Constant:	78.5

Temperature (°C):	25.0	**Zeta Runs:**	12
Count Rate (kcps):	99.8	**Measurement Position (mm):**	2.00
Cell Description:	Clear disposable zeta cell	**Attenuator:**	8

			Mean (mV)	Area (%)	St Dev (mV)
Zeta Potential (mV):	-24.3	**Peak 1:**	-24.3	100.0	8.11
Zeta Deviation (mV):	8.01	**Peak 2:**	0.00	0.0	0.00
Conductivity (mS/cm):	0.413	**Peak 3:**	0.00	0.0	0.00

Result quality : Good

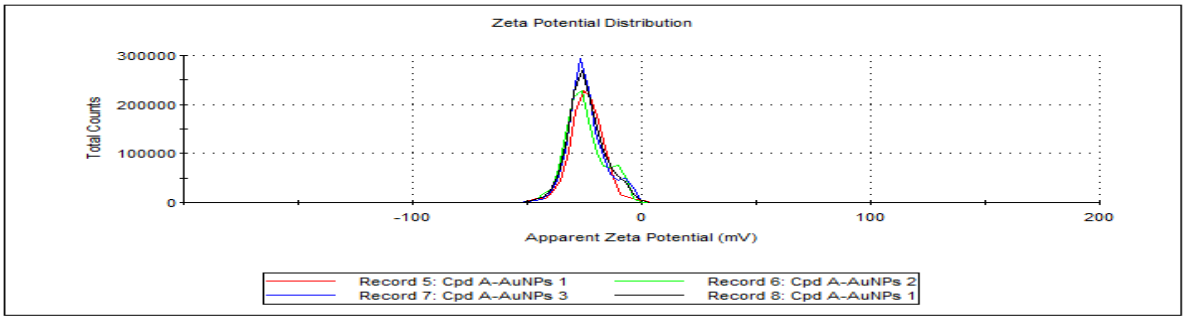

Figure 7.6.7: Representative Zeta potential of compound A-AuNPs

Sample Name:	CpdB AuNPs 3		
SOP Name:	mansettings.nano		
File Name:	Akeem.dts	**Dispersant Name:**	Water
Record Number:	283	**Dispersant RI:**	1.330
Date and Time:	13 November 2019 04:05:50 PM	**Viscosity (cP):**	0.8872
		Dispersant Dielectric Constant:	78.5

Temperature (°C):	25.0	**Zeta Runs:**	12
Count Rate (kcps):	89.0	**Measurement Position (mm):**	2.00
Cell Description:	Clear disposable zeta cell	**Attenuator:**	7

			Mean (mV)	Area (%)	St Dev (mV)
Zeta Potential (mV):	-24.1	**Peak 1:**	-24.3	99.8	8.37
Zeta Deviation (mV):	9.36	**Peak 2:**	72.8	0.2	0.00
Conductivity (mS/cm):	0.844	**Peak 3:**	0.00	0.0	0.00

Result quality : Good

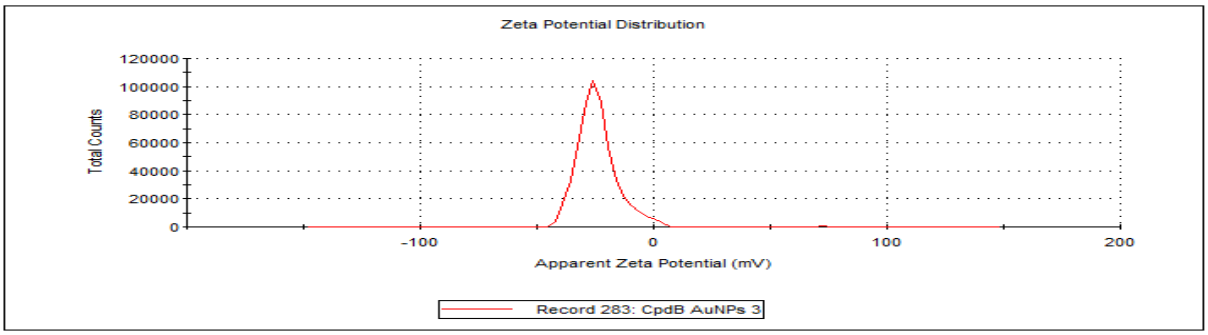

Figure Fig. 6.8: Representative Zeta potential of compound B-AuNPs

7.4.6. Crystallographic structure of green mediated nanoparticles

In addition to SAED patterns, we further confirmed the high crystallinity of all biosynthesized gold nanoparticles using X-ray diffraction measurement. Crystallographic reflection of all samples (Figure 6.9) exhibited four main peaks centred at 38°, 44°, 65° and 76° (2θ) for HF-AuNPs and 38°, 43°, 64° and 77° (2θ) for both compound A-AuNPs and compound B-AuNPs (supplementary data). The peaks matched with JCP2 gold number 04-0784 for 38.185, 44.393, 64.578 and 77.549, respectively. These values were attributed to crystallographic reflections that correspond to Miller indices of (111), (200), (220) and (311) planes of crystalline gold. Our result agrees with standard Bragg-Brentano geometry using Cu Kα radiation and corresponded to face-centred cubic metallic gold structure [12].

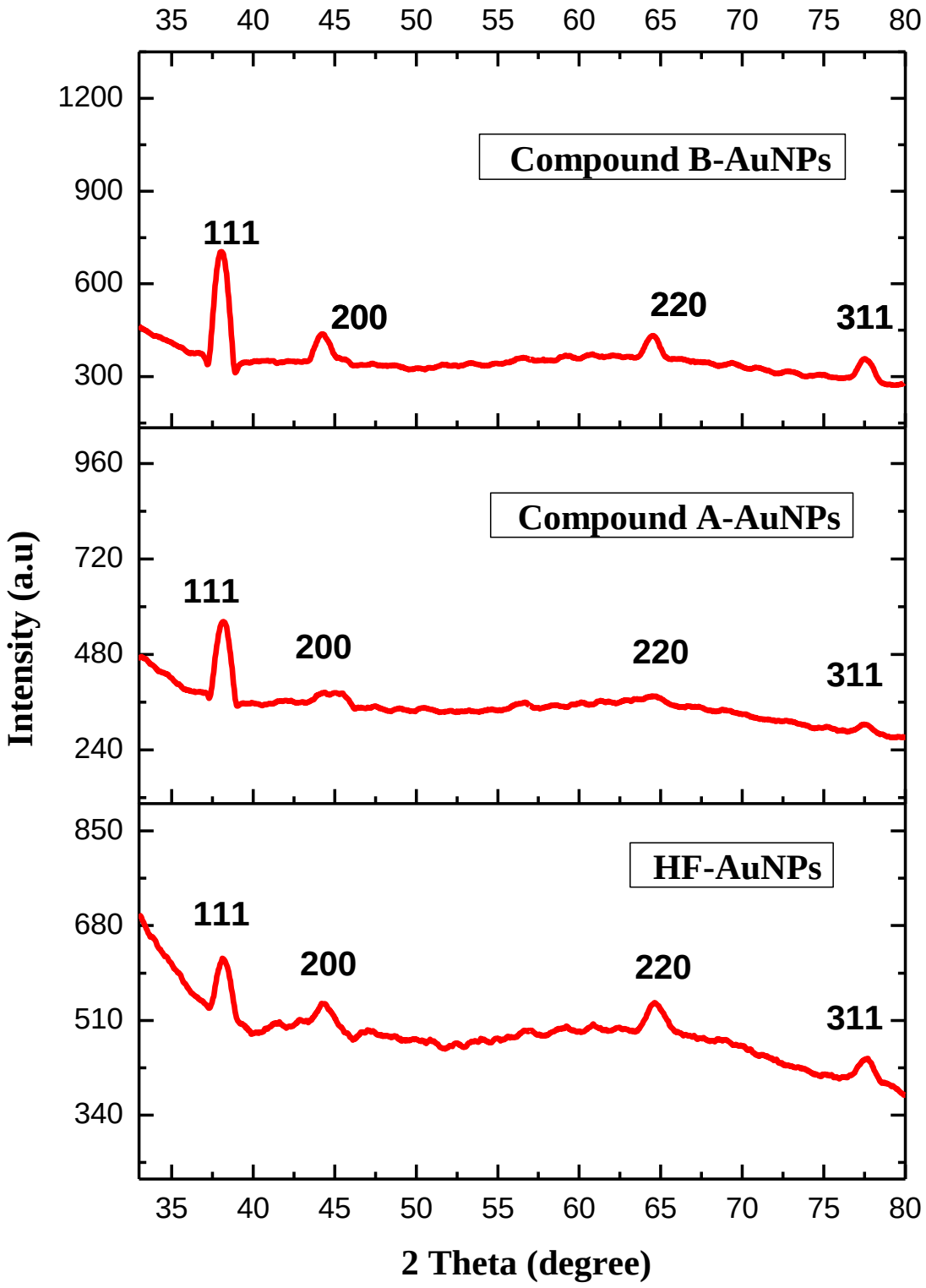

Figure 7.7: X-ray diffractograms (Scintage instrument) collected from a single crystal of compound B-AuNPs, Compound A-AuNPs and HFAuNPs

7.4.7. Vibrational spectroscopy

FTIR spectra measurement showed functional groups in the constituents of *H. foetidum* involved in the bioreduction of auric chloride. Functional groups of the extract and compounds matched with those of the nanoparticles indicating that the constituent of the plant capped the AuNPs (Figure 6.10 – 6.12). Peaks from HF, compound A, compound B and their gold nanoparticles were quite similar. However, a slight shift of some bands suggests the interaction of some functional groups with the surface of the AuNPs [23]. For example, and as indicated in the figures, the most effect was observed for hydroxyl group stretching (~3337 cm^{-1}) and C=O stretch (1690-1697 cm^{-1}) which slightly changed from the parent compound and the AuNPs conjugates. The presence of bands at 1600 cm^{-1} (HF), 1594 cm^{-1} (Compound A) and 1596 cm^{-1} (Compound B) can be attributed to the C-C stretch of the aromatic (in-ring), which were slightly shifted in the reduced gold nanoparticles. Additionally, there was an enhancement to the band at ~3000 cm^{-1}, for the aromatic C-H stretches, also, the phenolic C-O stretching vibration located at 1129 cm^{-1}, 1203 cm^{-1} and 1216 cm^{-1} in HF, compound A and B respectively. Bands were not shifted in the reduced AuNPs but appeared with different intensities. From the above discussion, the OH, C=O and aromatic rings could be the interaction points between the capping agents and the surface of Au NPs.

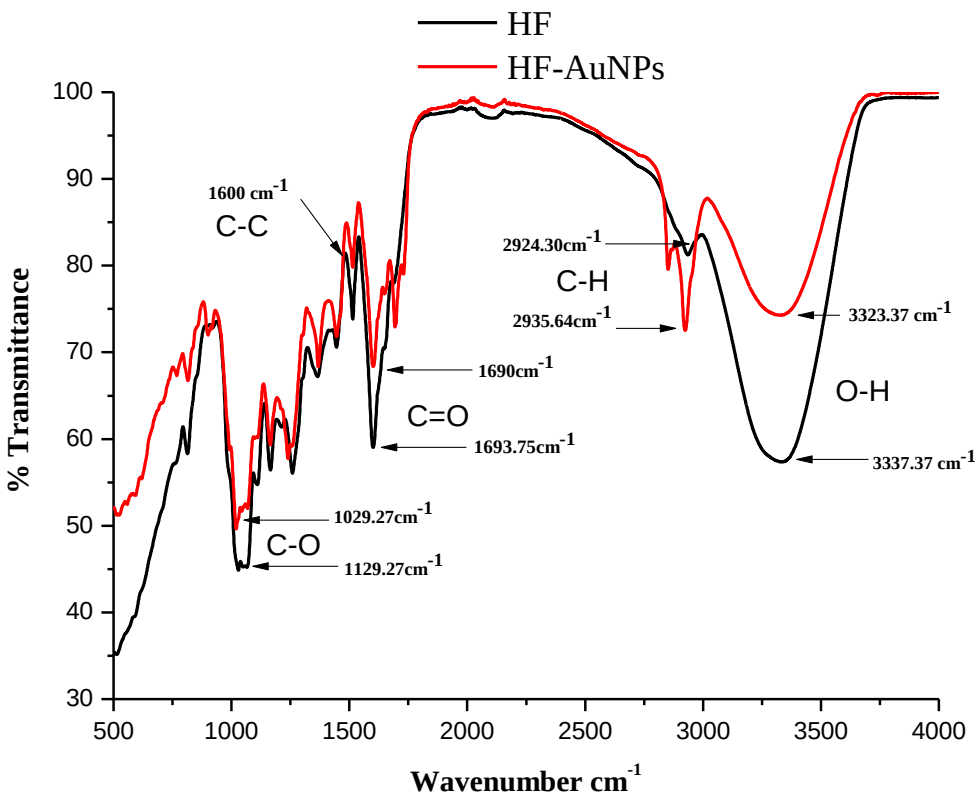

Figure 7.8: FTIR of HF and HF-AuNPs

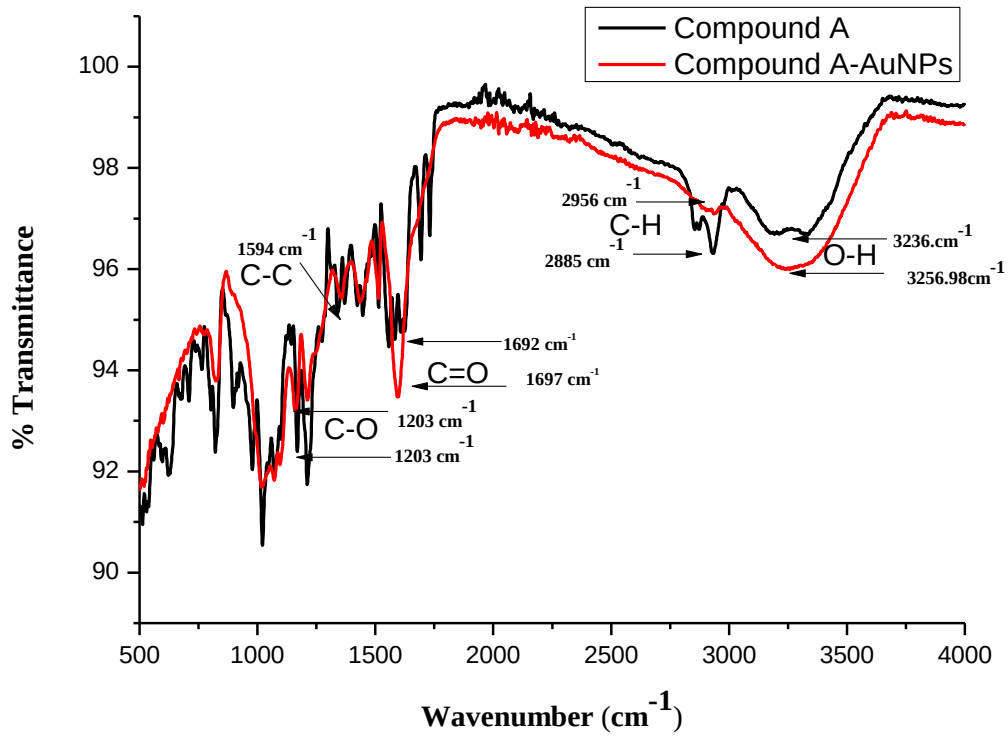

Figure 7.9: FTIR of Compound A and Compound A-AuNPs

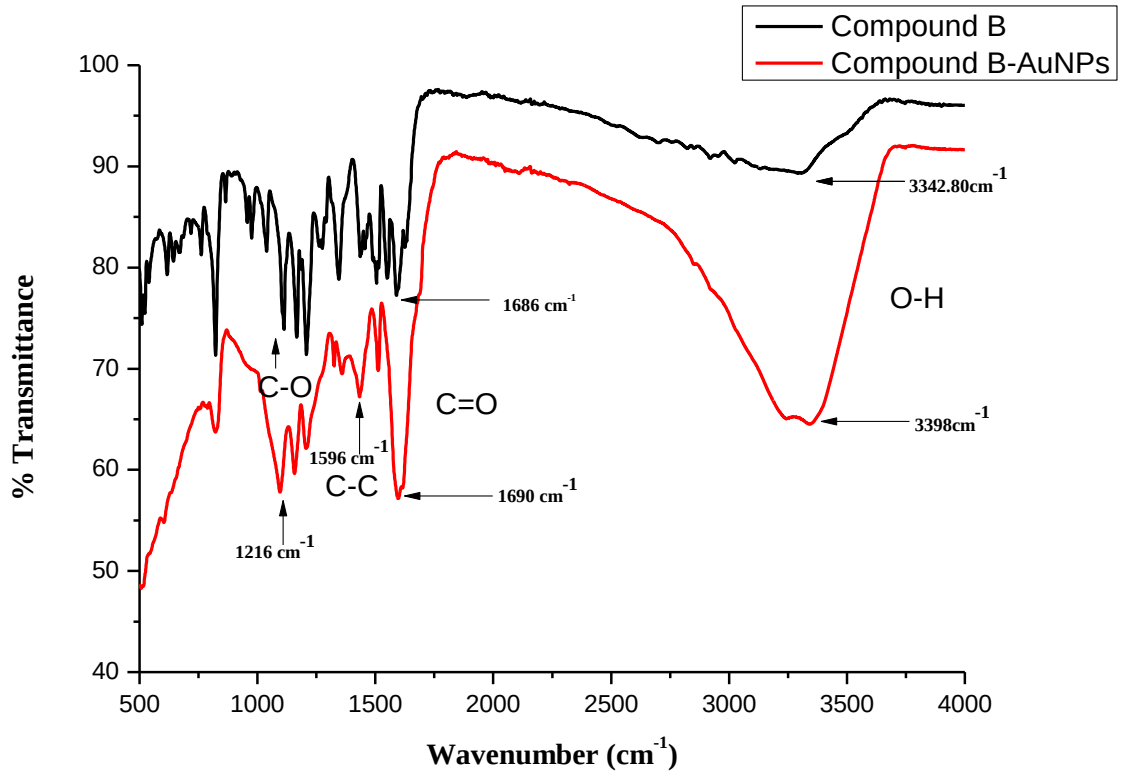

Figure 7.10: FTIR of Compound B and CompoundB-AuNPs

7.4.8. Stability of AuNPs

Figure 6.13 – 6.15 represent the in-vitro stability-time studies for biocompatibility of the gold nanoparticles in proteinogenic amino acids (BSA, glycine, cysteine), NaCl solution, PBS at pH 7 and pH 9. This is to check the time duration for nanoparticles to retain their properties without decomposition in physiological systems. Stable absorption bands of the particles were recorded at 0, 24 and 48 hrs in different biogenic media on UV-Vis spectrophotometer. Fig. 6i–6ii revealed that a stable absorption maximum at 536±3 and 546±3 nm for HF-AuNPs and compound B AuNPs respectively was maintained in all the media. However, compound A-AuNPs (Fig 6iii) was less stable after 24 hrs resulting in a broadening of bands in the media. This lower stability can be attributed to the availability of the glucose moiety in a metal-organic framework of compound A-AuNPs. It seems the glucose became unstable due to isomerization to fructose over gold nanoparticles in aqueous media of BSA, glycine and cysteine. A similar report was published for sodium titanate nanotubes where glucose in aqueous media rapidly isomerized to fructose [20]. Also, the lower stability of compound A-AuNPs can be attributed to the neutral to alkaline pH used, which facilitated possible isomerization and epimerization in a reversible reaction of glucose to fructose and mannose respectively [24].

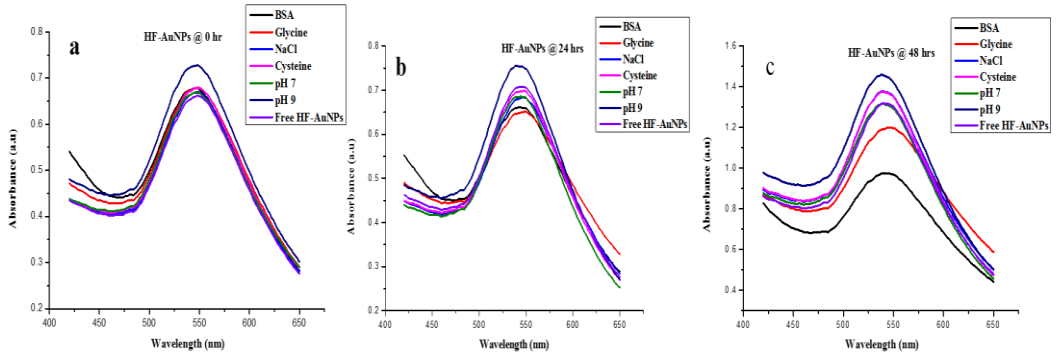

Figure 7.11: Stability-time studies of HF-AuNPs in different biogenic media

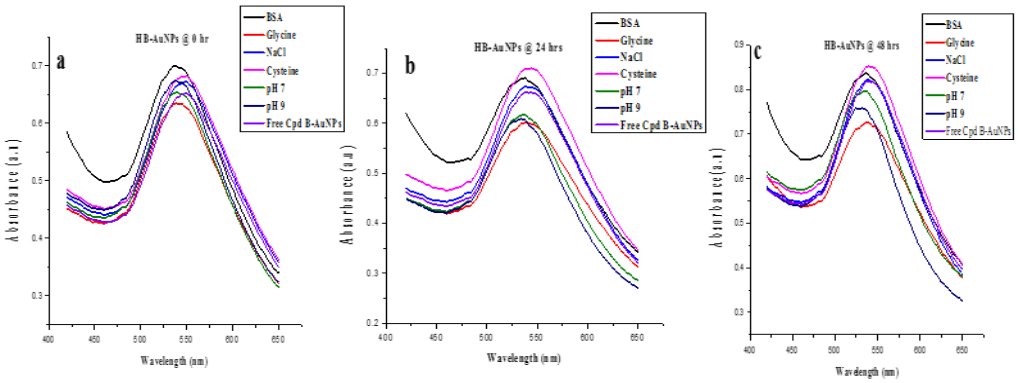

Figure 7.12: Stability-time studies of HB-AuNPs in different biogenic media

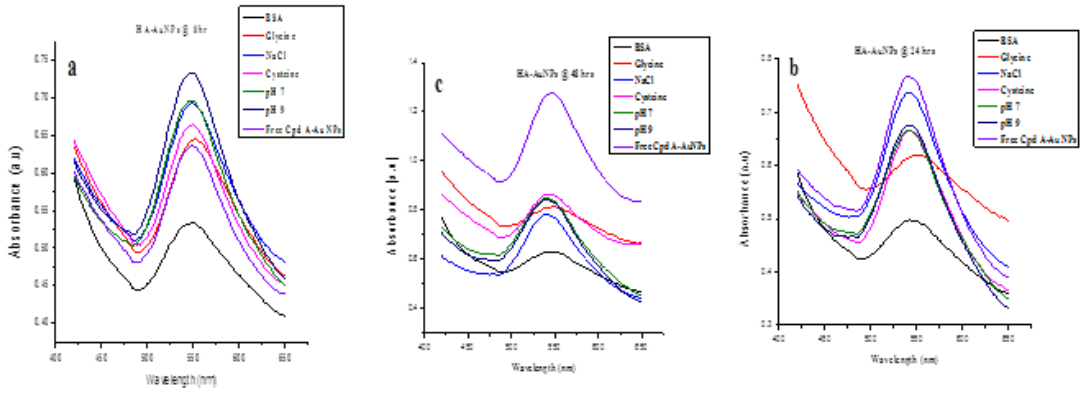

Figure 7.13: Stability-time studies of HA-AuNPs in different biogenic media

7.4.9. Inhibition of α-glucosidase and α-amylase enzymes

Enzymatic in vitro experiments for α-glucosidase and α-amylase inhibition at IC_{50} indicated higher activity for HF at 27.3 ± 0.3 µg/mL than HF-AuNPs at 391.5 ± 0.1 µg/mL, but no activity for α-amylase inhibition compared to HF-AuNPs (44.5 ± 0.1 µg/mL). Compound B and its AuNPs showed dual inhibitory potentials for both α-glucosidase and α-amylase enzymes, with HB (19.4 ± 0.3 µg/mL) slightly higher by two folds (40.0 ± 0.2 µg/mL) for α-glucosidase and nearly the same activity for α-amylase at 25.1± 0.3 µg/mL and 35.6 ± 0.1 µg/mL respectively, (Table 6.1). . The dual activity of compound B and its AuNPs could be attributed to the sp^2 hybridized carbons of the conjugated ring system and the hydroxyl groups of the chalcone structure, which facilitates the interaction with the enzymes. This is similar to the report of Hamid et al., [15] on the structure-activity-relationship of compounds from *Tinospora crispa* plant evaluated for α-glucosidase and α-amylase enzymes inhibition [15] However, compound A is the least active sample but displayed a higher activity for α-glucosidase than its nanoparticles. Both HA and its gold nanoparticles show no inhibition for α-amylase enzymes (Table 6.1). This may be attributed to the glycosidic bond attached to the chalcone structure that raised the inhibition threshold of the amylase enzyme. HF and HF-AuNPs displayed relatively strong activity probably because of synergy between chalcones present and their nanoparticles as demonstrated by compound B and its AuNPs. Despite the higher activities of HF constituents over their gold nanoparticles as drug candidates, the ability of the spleen and liver to recognize and remove drugs from systemic circulation may affect drug delivery. Badeggi et al. [3] reported gold nanoparticles capped by the total extract, fractions of procyanidins dimer and trimer isolated *Leucosidea sericea*. In comparison, the AuNPs of the dimer was noted with higher inhibitory activity for α-amylase while the AuNPs of the trimer showed higher inhibition for α-glucosidase. Functionalized gold nanoparticles from HF constituents may be considered as an option for active drug targeting due to the inert and biocompatibility properties of gold. Overall, α-glucosidase activities of samples were in the following order: compound B > HF > compound B-AuNPs > compound A > compound A-AuNPs > HF-AuNPs, while for α-amylase activities were compound B > compound B-AuNPs > HF-AuNPs.

Table 7.1: Inhibitory activities of HF, isolated compounds and biosynthesized nanoparticles on alpha-glucosidase and alpha-amylase

	IC_{50} (µg/mL)	
Sample	**α-Glucosidase**	**α-Amylase**
HF	27.3 ± 0.3	NA
HF-AuNPs	391.5 ± 0.1	44.46 ± 3.3
compound A	48.3 ± 0.1	NA
compound A-AuNPs	173.3 ± 0.1	NA

compound B	19.4 ± 0.3	25.13 ± 0.3
compound B-AuNPs	40.0 ± 0.2	35.6 ± 0.1
Acarbose	610.4 ± 1.0	10.2 ± 0.6

*NA = No activity

7.4.10. Glucose uptake activities of compounds and nanoparticles

High blood glucose is known to be among the high-risk factors for cardiovascular diseases (CVD). Given the side effect of the prolonged use of synthetic drugs for the control of blood glucose, this study aimed to assess the activity of the crude extract, pure compounds, and their nanoparticles on glucose uptake in mammalian cells. Figure 6.16 shows that all the compounds, except for HF Crude and HB, seem to decrease the relative glucose uptake with significant p-values. A similar report by Rajarajeshwari et. al., [39] show minimal glucose uptake by 3T3-Li adipocytes cells treated with gymnemic acid commonly found in *Gymnema sylvestre* and its synthesised gold nanoparticles [39]. HF Crude increased relative glucose uptake significantly. However, this action may be due to a combination of compounds working synergistically to activate glucose 'pick-up' by insulin instead of a single compound providing the action. This further confirms our result from carbohydrate enzyme inhibition and the potential of the total extract and the compound helichrysetin of *H. foetidum* as potential drug candidates for the management of diabetes conditions.

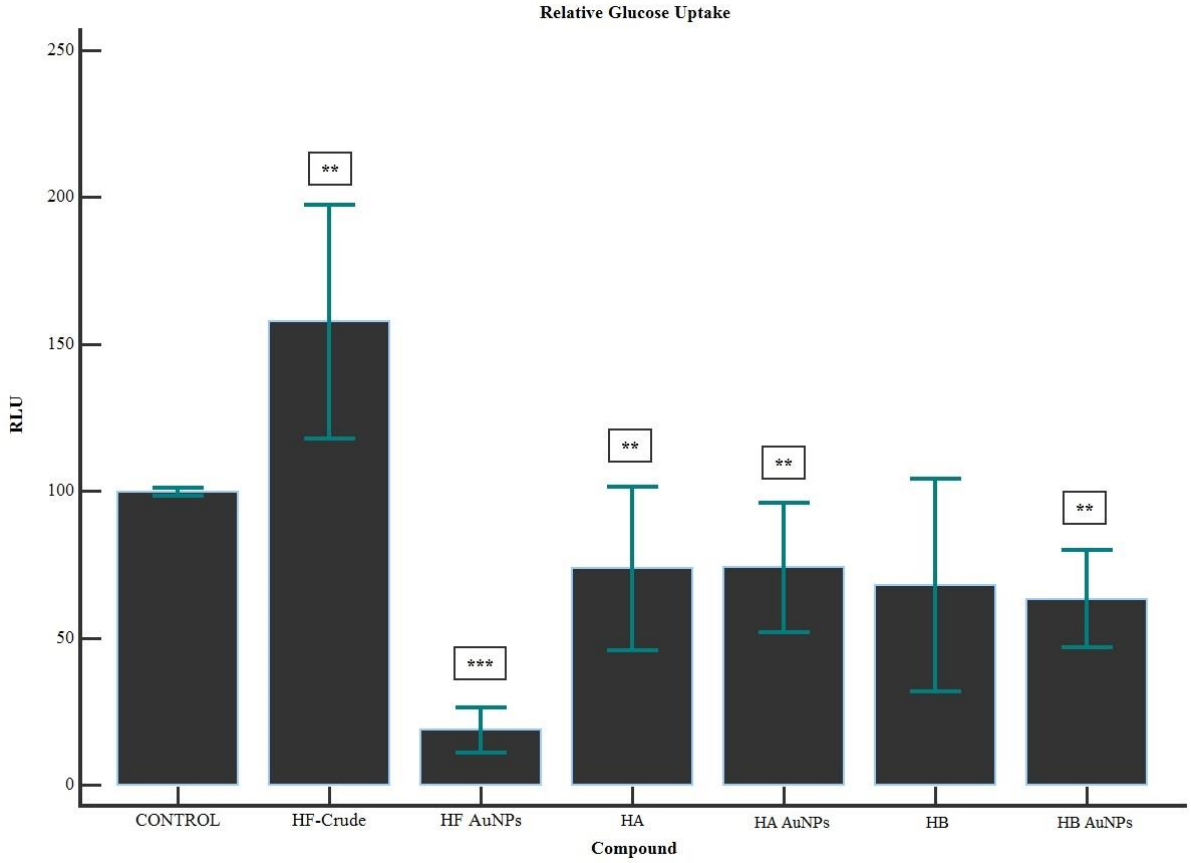

Figure 7.14: Relative glucose uptake of crude extract, compounds, and nanoparticles; where the p-value is indicative of the statistical significance versus the control, using an independent two-tailed T-test. * p = 0.05, ** p = 0.005, ***p = 0.001

7.4.11. Cytotoxicity results

To determine the cytotoxicity of the plant extract, compounds, and nanoparticles, the HaCaT keratinocytes from the human skin were used. This is a non-cancerous cell line and will be able to indicate the safety and toxicity of the extracts, compounds, and nanoparticles. Following treatments, the MTT assay was performed, and the results show that the plant extract, compounds, and nanoparticles differentially induced cytotoxicity on the HaCaT cells (Figure 6.17). In specifics, the IC_{50} obtained for HF and HF-AuNPs was 49.04 µg/mL and 29.87 µg/mL respectively making them the most cytotoxic to the cells (Fig. 6.16A). In addition, the HA-AuNPs also induced cytotoxicity in the cells with IC_{50} of 67.42 µg/mL while the compound HA showed slight toxicity to the cells (Figure 6.16B). However, the compound HB, as well as the HB-AuNPs, had IC_{50}s greater than 100 µg/mL (Fig. 6.16C). Taken together, findings from this study gave an indication of the cytotoxicity of the plant material and compounds as well as their various nanoparticles. The compound HA was least cytotoxic and could be explored further.

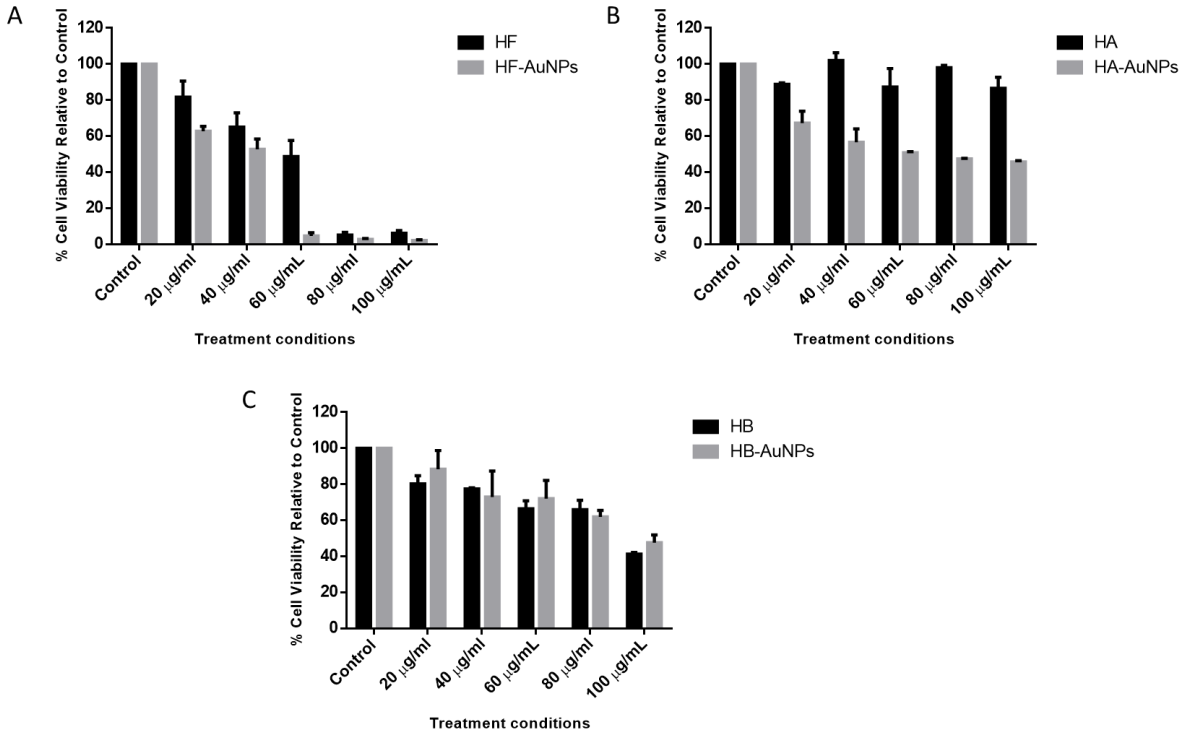

Figure 7.15: Evaluation of the cytotoxicity of HF, compounds, and nanoparticles on HaCaT cells. Cells were treated with HF and HF-AuNPs (A) HA and HA-AuNPs (B) HB and HB-AuNPs (C) at concentrations of 20 to 100 µg/mL and MTT assays were performed.

7.5. Conclusion

In this article, plant-mediated synthesis of gold nanoparticles with total extract and pure compounds from *H. foetidum* is reported for the first time. Through successive column chromatography, helichrysin and helichrysetin compounds were successfully isolated and characterized among other constituents. Extract and isolates showed promising application as both reducing and capping agents for the biosynthesis of gold nanoparticles through different physicochemical techniques. The pure compounds show a better effect in the size reduction of gold nanoparticles than the total extract and will be valuable in therapeutic and biomedical applications. In addition, the use of pure compounds isolated from the total extract allows for a better understanding of the mechanism of biosynthesis of gold nanoparticles and the systemic glucose utilization due to glucose phosphorylation and activities of glucose hydrolysing enzymes in the cells. This study contributes to a possible novel blood-glucose-lowering scaffold developed through the conjugation of metal NPs and natural chalcones. These conjugations have an inhibitory potential activity against α-amylase and α-glucosidase enzymes, and glucose uptake in vitro. It also paves way for further studies on animal studies to establish the use of *H. foetidum* and its gold nanoparticles against diabetes and glucose-induced oxidative stress.

Declaration of Competing Interest

The authors declare no conflict of interest.

Acknowledgement

We wish to acknowledge the South African Rooibos Council for the financial support towards the completion of this research. In addition, partial funding was provided by the South African Medical Research Council (SAMRC) through its Division of Research Capacity Development under funding received from the South African National Treasury. The content hereof is the sole responsibility of the authors and do not necessarily represent the official views of the SAMRC or the funders. Also, we acknowledge the NMR facility at the University of the Western Cape, Mr Hamza Alsayed of iThemba Labs for XRD and Dr Rajan Sharma for his contribution.

References

[1] N. Abdel-Raouf, N.M. Al-Enazi, I.B.M. Ibraheem, Green biosynthesis of gold nanoparticles using *Galaxaura elongata* and characterization of their antibacterial activity, Arab. J. Chem. 10 (2017) S3029–S3039, https://doi.org/10.1016/j. arabjc.2013.11.044.

[2] K. Aoki, H. Sato, Y. Terauchi, Usefulness of antidiabetic alpha-glucosidase inhibitors: a review on the timing of administration and effects on gut hormones, Endocr. J. 66 (5) (2019) 395–401.

[3] U.M. Badeggi, E. Ismail, A.O. Adeloye, S. Botha, A.A. Hussein, Green synthesis of gold nanoparticles capped with procyanidins from *Leucosidea sericea* as potential antidiabetic and antioxidant agents, Biomolecules 10 (452) (2020).

[4] L. Barcelos, G. Heiden, First record of *Helichrysum foetidum* (L.) Moench. (Asteraceae, Gnaphalieae) for South America, J. Biodiversity Data 13 (4) (2017) 331–334.

[5] A.F. Barrero, P. Arteaga, M.M. Herrador, ent-Kaurene diterpenoids from *Helichrysum foetidum*, Fitoterapia 69 (1) (1998) 83–84.

[6] M. Bhardwaj, P. Yadav, S. Dalal, S. Kumar, A review on ameliorative green nanotechnological approaches in diabetes management, Biomed. Pharmacother. 127 (April) (2020), https://doi.org/10.1016/j.biopha.2020.110198.

[7] F. Bohlmann, W.R Abraham., New diterpenes and other ingredients from *Helichrysum calliconum* and *Helichrysum heterolasium*, Phytochemistry 18 (5) (1979) 889–891.

[8] M. Danaei, M. Dehghankhold, S. Ataei, F.H. Davarani, R. Javanmard, A. Dokhani, S. Khorasani, M. Mozafari, Impact of particle size and polydispersity index on the clinical applications of lipidic nanocarrier systems, Pharmaceutics 10 (57) (2018) 1–17.

[9] Y. Dong, B. Zhang, W. Sun, Y. Xing, Intervention of Prediabetes by Flavonoids From *Oroxylum indicum*, 2nd ed., Elsevier Inc, 2019 https://doi.org/10.1016/B978-0- 12-813822-9.00036-9.

[10] A.M. Elbagory, C.N. Cupido, M. Meyer, A.A. Hussein, Large scale screening of southern african plant extracts for the green synthesis of gold nanoparticles using microtitre-plate method, Molecules 21 (1498) (2016) 1–20.

[11] N.G.E.R. Etsassala, Jelili A. Badmus, Tesfaye T. Waryo, Jeanine L. Marnewick, Christopher N. Cupido, Ahmed A. Hussein, Emmanuel I. Iwuoha, Alpha-glucosidase and alpha-amylase inhibitory activities of novel abietane diterpenes from *Salvia africana-lutea*, Antioxidants 8 (10) (2019) 1–12.

[12] V. Ganesh Kumar, S. Dinesh Gokavarapu, A. Rajeswari, T. Stalin Dhas, V. Karthick, Z. Kapadia, T. Shrestha, I.A. Barathy, A. Roy, S Sinha, Facile green synthesis of gold nanoparticles

using leaf extract of antidiabetic potent *Cassia auriculata*, Colloids Surf. B 87 (1) (2011) 159–163, https://doi.org/10.1016/j.colsurfb.2011.05.016.

[13] S. Gangadoo, A. Taylor-Robinson, J. Chapman, Nanoparticle and biomaterial characterisation techniques, Mater. Technol. 30 (B1) (2015) B44–B56.

[14] A. Ghorbani, Biomedicine & pharmacotherapy mechanisms of antidiabetic effects of flavonoid rutin, Biomed. Pharmacother. 96 (September) (2017) 305–312.

[15] H.A. Hamid, M.M. Yusoff, M. Liu, M.R. Karim, α-Glucosidase and α-amylase inhibitory constituents of *Tinospora crispa*: Isolation and chemical profile confirmation by ultra-high performance liquid chromatography-quadrupole time-of-flight/mass spectrometry, J. Funct. Foods 16 (2015) 74–80, https://doi.org/ 10.1016/j.jff.2015.04.011.

[16] F. Ho Yen, A.M. Sri Nurestri, H.S. Yee, K. Saiful Anuar, Helichrysetin induces DNA damage that triggers JKN-mediated apoptosis in Ca Ski cells, Pharmacognosy Mag. 13 (52) (2017) 607–612.

[17] S. Honary, F. Zahir, Effect of zeta potential on the properties of nano-drug delivery systems - a review (Part 2), Trop. J. Pharmaceut. Res. 12 (2) (2013) 265–273.

[18] N. Jaradat, M. Qneibi, M. Hawash, A. Sawalha, S. Qtaishat, F. Hussein, Chemical composition, antioxidant, antiobesity, and antidiabetic effects of *Helichrysum sanguineum* (L.) Kostel. from Palestine, Arab. J. Sci. Eng. (2020), https://doi.org/ 10.1007/s13369-020-04707-z.

[19] Z. Kakam, A. M., K. Franke, J.C. Ndom, E. Dongo, T.N. Mpondo, L.A Wessjohann, Secondary metabolites from *Helichrysum foetidum* and their chemotaxonomic significance, Biochem. Syst. Ecol. 39 (2) (2011) 166–167, https://doi.org/ 10.1016/j.bse.2011.02.005.

[20] S. Kumar, D. Nepak, K. Kansal, Expeditious isomerization of glucose to fructose in aqueous media over sodium titanate nanotubes, R. Soc. Chem. Adv. 8 (2018) 30106–30114.

[21] K.Y. Loo, K.H. Leong, Y. Sivasothy, H. Ibrahim, K. Awang, Molecular insight and mode of inhibition of α-glucosidase and α-amylase by pahangensin A from *Alpinia pahangensis* RIDL, Chem. Biodivers. 16 (6) (2019).

[22] A.C.U. Lourens, A.M. Viljoen, F.R van Heerden, South African *Helichrysum* species: a review of the traditional uses, biological activity and phytochemistry, J. Ethnopharmacol. 119 (3) (2008) 630–652.

[23] P. Luc Van, D.K. Norbert, C. Jean, M. Viateur, N. Speciosa, H. Etienne, S Niceas, Isolation of flavonoids and a chalcone from *Helicrysum odoratissimum*, J. Nat. Prod. 52 (3) (1989) 629–633.

[24] Q. Luo, Y. Zhang, L. Qi, S.L. Scott, Glucose isomerization and epimerization over metal-organic frameworks with single-site active centers, ChemCatChem (11) (2019) 1903–1909, 2019. [25] O. Lushchak, A. Zayachkivska, A. Vaiserman, Review article metallic nanoantioxidants as potential therapeutics for type 2 diabetes: a hypothetical background and translational perspectives, Oxidat. Med. Cell. Longevity (3407375) (2018) 1–9, 2018.

[26] F.A.E. Malolo, A.B. Nouga, A. Kakam, K. Franke, L. Ngah, O. Flausino, E. M. Mpondo, F. Ntie-Kang, J.C. Ndom, V. Bolzani, L Wessjohann, Protease-inhibiting, molecular modeling and antimicrobial activities of extracts and constituents from *Helichrysum foetidum* and *Helichrysum mechowianum* (compositae), Chem. Cent. J. 9 (1) (2015), https://doi.org/10.1186/s13065-015- 0108-1.

[27] A. Maroyi, Medicinal uses, biological and phytochemical properties of *Helichrysum foetidum* (L.), Moench. (Asteraceae) 12 (7) (2019) 63–68.

[28] R. Mata, J.R. Nakkala, S.R. Sadras, Polyphenol stabilized colloidal gold nanoparticles from *Abutilon indicum* leaf extract induce apoptosis in HT-29 colon cancer cells, Colloids Surf. B 143 (2016) 499–510, https://doi.org/10.1016/j. colsurfb.2016.03.069.

[29] P.I. Oteiza, A.G. Erlejman, S.V Verstraeten, C.L Keen, Flavonoid-membrane interactions: a protective role of flavonoids at the membrane surface? Clin. Dev. Immunol. 12 (1) (2005) 19–25.

[30] M.N. Sarian, Q.U. Ahmed, S. Zaiton, M. So, A.M. Alhassan, S. Murugesu, V. Perumal, S. Nurul, A. Syed, A. Khatib, J. Latip, Antioxidant and antidiabetic effects of flavonoids: a structure-activity relationship-based study, BioMed. Res. Int. Volume 2017 (2017) 1–14.

[31] M. Sengani, A.M. Grumezescu, V.D. Rajeswari, Recent trends and methodologies in gold nanoparticle synthesis—a prospective review on drug delivery aspect, OpenNano 2 (July) (2017) 37–46, https://doi.org/10.1016/j.onano.2017.07.001.

[32] S. Süzgeç-Selçuk, A.S. Birteks¨oz, Flavonoids of *Helichrysum chasmolycicum* and its antioxidant and antimicrobial activities, S. Afr. J. Bot. 77 (1) (2011) 170–174, https://doi.org/10.1016/j.sajb.2010.07.017.

[33] V. Thipe, K. Panjtan Amiri, P. Bloebaum, A.R. Karikachery, M. Khoobchandani, K. K. Katti, S.S. Jurisson, K.V. Katti, Development of resveratrol-conjugated gold nanoparticles: interrelationship of increased resveratrol corona on anti-tumor efficacy against breast, pancreatic and prostate cancers, Int. J. Nanomed. 14 (2019) 4413–4428.

[34] B. Tirillini, L. Menghini, L. Leporini, N. Scanu, S. Marino, G. Pintore, V.A. Saffi, U. Pu, Antioxidant activity of methanol extract of *Helichrysum foetidum* Moench, Nat. Prod. Res. 27 (16) (2012) 14.

[35] H. Tsuchiya, Structure-dependent membrane interaction of flavonoids associated with their bioactivity, Food Chem. 120 (4) (2010) 1089–1096, https://doi.org/ 10.1016/j.foodchem.2009.11.057.

[36] M. Venkatachalam, K. Govindaraju, A. Mohamed Sadiq, S. Tamilselvan, V. Ganesh Kumar, G. Singaravelu, Functionalization of gold nanoparticles as antidiabetic nanomaterial, Spectrochimica Acta - Part A: Mol. Biomol. Spectrosc. 116 (2013) 331–338, https://doi.org/10.1016/j.saa.2013.07.038.

[37] W.G. Wright, South African plant extractives. Part 11 Helichrysin, a new chalcone glucoside from a *Helichrysum* species, J. Chem. Soc., Perkin Trans. 1 (1) (1976) 1819–1820.

[38] G. Zhan, J. Huang, L. Lin, W. Lin, K. Emmanuel, Q. Li, Synthesis of gold nanoparticles by *Cacumen Platycladi* leaf extract and its simulated solution: toward the plant-mediated biosynthetic mechanism, J. Nanopart. Res. 13 (10) (2011) 4957–4968.

[39] T. Rajarajeshwari, C. Shivashri, P. Rajasekar, Synthesis and characterization of biocompatible gymnemic acid – gold nanoparticles: a study on glucose uptake stimulatory e ff ect in 3T3-L1 adipocytes, RSC Advances 4 (2014) 63285-63295.

Chapter seven

Antidiabetic potential of *Helichrysum foetidum* chemical constituents

Akinfenwa O. Akeem [a], Brendon Pearce [b], Mongi Benjeddou [b], Ahmed A. Hussein [a*]

[a] Department of Chemistry, Cape Peninsula University of Technology, Symphony Rd. Bellville 7535, South Africa; oa.akeemlaja@gmail.com (A.O.A); mohammedam@cput.ac.za (A.A.H.).

[b] Precision Medicine Laboratory, Department of Biotechnology, 2nd Floor, Life Science Building, University of the Western Cape, Cape Town 7530, South Africa; brendon.biff@gmail.com (B.P.); mebenjeddou@uwc.ac.za (M.B.)

Corresponding author: mohammedam@cput.ac.za; Tel.: +27-21-959-6193; Fax: +27-21-959-3055

Abstract

The *Helichrysum* genus of the Asteraceae family is known with varieties of phytochemicals including phloroglucinol, flavonoids, pyrones, terpenoids and polyacetylenes. A mixture of 3-methoxyquercetin and luteolin was isolated in addition to five known compounds namely, luteolin, quercetin, helichrysin, helichrysetin, and kaur-16-en-19-oic acid, 15 methoxylate diterpene from South African *Helichrysum foetidum*. The structure of the mixed flavonoid was elucidated using 1D and 2D NMR spectroscopic data. The total extract and compounds were evaluated for antidiabetic potentials *via* glucose uptake activities *in vitro*. The results showed a shift in ^{13}C NMR signals of the 3-methoxyquercetin while the ^{13}C NMR of luteolin remain unchanged when compared to the C-13 of the single unit of each compound isolated. The kaurene type diterpene (IC_{50} 16.3± 0.1 µg/mL) and quercetin (IC_{50} 8.9± 0.3 µg/mL) were most potent for inhibition of α-glucosidase and α-amylase respectively. In decreasing order, the kaurene type diterpene (p = 0.001), the total extract (p = 0.005), and quercetin significantly improve glucose uptake *in vitro* over the other flavonoids constituent.

Keywords: Asteraceae, *Helichrysum foetidum*, mixed-flavone, glucose uptake, NMR

8.1. Introduction

Dietary intake, digestion of carbohydrate foods, and an inactive lifestyle are common precursors to the onset of Type-2 diabetes mellitus which is becoming a common disease. Digestion of carbohydrate foods in two sequences ends up in monosaccharides which are absorbed into the bloodstream for metabolic activities. In the first sequence, amylase enzymes break down carbohydrates into oligosaccharides which in turn are broken down into monosaccharide units by glucosidase enzymes [1]. Excess blood glucose (hyperglycaemia) results from defects in pancreatic β-beta cells to produce enough insulin or the produced insulin is resistant to glucose uptake and clearance [2]. Therapeutic measures taken to maintain the blood glucose level at a normal level include administration of chemically synthesised antidiabetic drugs which sometimes pose serious side effects. Recent discoveries show that plant-derived flavonoids and terpenoids which are also present in HF are good sources for developing antidiabetic drugs [3]. For instance, the flavonoid apigenin and its glycoside isolated from the ethanol extract of *Cephalotaxus sinensis* leaves were reported with antihyperglycemic activities and increased glucose transporter (GLU-4 effect) when treated with mice adipocytes [4].

Helichrysum foetidum (L.) Moench (HF) species native to Cape Provinces of South Africa is known for its strong aromatic smell which attracts traditional healers to use them in folk medicine [5]. The species was reportedly used for the treatment of wounds, respiratory and ailments related to metabolic disorder and cell inflammation [6]. Scientific investigations of HF showed different bioactivities including antioxidants, antimicrobial, antifungal, antiviral, and protease enzyme inhibition [7-10]. These bioactivities are attributed to the phytochemical constituents of HF. Flavonoids and diterpenoids such as kaur-16-en-18-oic acid, 6’-methoxy-2’,4,4’-trihydroxychalcone and its glycoside, apigenin and its glycoside and 7,4'-dihydroxy-5-methoxy-flavanone [9, 11-13] are major phytochemical constituents reported from HF. However, many interesting spots of developed TLC of eluted polar fractions from the main column which represents polar compounds were noted. The chemistry of these polar fractions from HF which include flavonoids is yet to be fully reported. Also, scientific investigations of many species of South African *Helichrysum* showed their antidiabetic potentials, still, the hypoglycaemic activities of HF have not been evaluated.

The identification of an additional compound and the antihyperglycemics effects of HF triggered our study to investigate the methanolic extract and compounds of *Helichrysum foetidum* for stimulation of glucose uptake. This work aims to expand the knowledge base on constituents of *Helichrysum foetidum* and its indication as a route to antidiabetic drugs.

8.2. Materials and methods

8.2.1. Plant

Fresh plant *Helichrysum foetidum* (1kg) was purchased from Kirstenbosch National Botanical Gardens, Cape Town, South Africa in January 2019.

8.2.2. Chemicals

Analytical grade chemicals: methanol, hexane, dichloromethane, ethanol, acetone, and ethyl acetate were purchased from Science World Chemicals, South Africa. Silica gel 60 pre-coated aluminium plates (0.063-0.200 mm) and Sephadex (LH-20) supplied by Merck KGaA (64271 Darmstadt Germany) and Sigma-Aldrich.

8.2.3. Extraction, isolation, and characterization of compounds

The dried whole plant was ground to a fine powder. 620 grams of the fine powder was exhaustively extracted with 5 litres of methanol twice as previously described (Akinfenwa et al., 2021) to yield 79.87 g (13% as calculated) dry dark extract. The extract was fractionated on silica gel column chromatography using gradient elution with hexane - dichloromethane - methanol (90:10:0 → 0:0:100, v/v) in increasing polarity and yielded 18 main fractions. The main fractions F1 – F5 were identified to contain mainly chlorophyll and are not interesting. Phytochemical investigation of fraction F8 (DCM extract, 300 mg) on Sephadex column chromatography using 10% aqueous ethanol acidified with 0.5% acetic acid in isocratic mode yielded compound **7.1** (42 mg). The solvent system was maintained for other Sephadex CC. **7.2** (45 mg) was obtained from a silica gel column of fraction F9 (1 g). The 1 g starting material of fraction (F11) chromatographed on silica gel CC and subsequent purification by Sephadex column yielded **7.3** (46 mg). The main fraction F12 (300 mg) applied to Sephadex CC yielded **7.4** (30 mg). Fraction F13 (320 mg) yielded **7.5** (25 mg). Elution from Sephadex column of a mixture of the fractions F6 and F7 (600 mg) afforded in **7.6** (54 mg).

8.2.4. Spectra data of compounds

Spectroscopic data from 1D NMR recorded on an Avance 400 MHz NMR spectrometer (Bruker, Rheinstetten, Germany) in deuterated acetone were analysed.

Compound 7.1:

(Quercetin): ^{1}H-NMR (400 MHz, Acetone-d_6, ppm): *δ* 7.8 (1H, *s*, H-2’), *δ* 7.71 (1H, *d*, *J* = 8.1 Hz, H-6’), *δ* 7.01 (1H, *d*, *J* = 8.5 Hz, H-3’), *δ* 6.60 (1H, *s*, *H*-3), *δ* 6.54 (1H, *s*, H-8), *δ* 6.28 (1H, *s*, H-6). ^{13}C-NMR (100 MHz, Acetone-d_6, ppm): *δ* 175.6 (C-4), *δ* 164.0 (C-7), *δ* 161.2 (C-5), *δ* 156.9 (C-9), *δ* 147.3 (C-2), *δ* 145.9 (C-4’), *δ* 144.8 (C-3’), *δ* 135.8 (C-3), *δ* 122.8 (C-1’), *δ* 120.5 (C-6’), *δ* 115.3 (C-2’), *δ* 114.8 (C-5’), *δ* 103.2 (C-10), *δ* 98.1 (C-6), *δ* 93.5 (C-8).

Compound 7.2:

(Helichysetin): ^{1}H NMR (400 MHz, acetone--d_6): δH 7.88 (1H, d, J = 15.6 Hz, Hα), 7.74 (1H, d, J = 15.6 Hz, Hβ), 7.61 (2H, d, J = 8.4 Hz, H-2`, -6`), 6.93 (2H, d, J = 8.0 Hz, H-3`, -5`), 6.09 (1H, s, H-5), 6.02 (1H, s, H-3), 3.98 (3H, s, OMe). 13C NMR (100 MHz, acetone--d_6): δC 193.2 (C=O), 168.5 (C-2), 165.7 (C-4), 164.3 (C-6), 143.3 (Cβ), 131.3 (C-6`), 128.0 (C- 1`), 125.3 (Cα), 116.8 (C-3`), 106.3 (C-1), 96.9 (C-3), 92.2 (C-5), 56.41 (OMe).

Compound 7.3:

(Mixture of 3-methoxyquercetin and luteolin):^{1}H-NMR (400 MHz, Acetone-d_6, ppm): *δ* 7.70 (1H, *s*, H-2"'), *δ* 7.58 (1H, *d*, *J* = 7.9 Hz, H-6"') *δ* 7.51 (1H, *d*, *J* = 1.8 Hz, H-2'), *δ* 7.47 (1H, *d*, *J* = 8.0 Hz, H-6'), *δ* 7.01 (2H, *d*, *J* = 8.1 Hz, H-5'/5"'), *δ* 6.58 (1H, *s*, *H*-3), *δ* 6.53 (1H, *s*, H-8), *δ* 6.49 (1H, *s*, H-8"), *δ* 6.26 (2H, *s*, H-6/H-6"), *δ* 3.87 (3H, *s*, OCH_3). ^{13}C-NMR (100 MHz, Acetone, ppm): *δ* 182.1 (C-4), 175.6 (C-4"), *δ* 164.3 (C-2), *δ* 164.0 (C-5"/C-7"), *δ* 162.1 (C-7), *δ* 161.9 (C-5), *δ* 157.9 (C-9), *δ* 156.9 (C-9"), *δ* 155.9 (C-2"), *δ* 149.2 (C-4'), *δ* 148.2 (C-4'"), *δ* 145.6 (C-3'), *δ* 144.9 (C-3'"), *δ* 138.3 (C-3"), *δ* 122.8 (C-1'), *δ* 122.1 (C-1'"), *δ* 121.2 (C-6'"), *δ* 119.2 (C-6'), *δ* 115.7 (C-2'), *δ* 115.3 (C-2"'), *δ* 115.3 (C-5'"), *δ* 113.1 (C-5'), *δ* 104.9 (C-10"), *δ* 104.4 (C-10), *δ* 103.3 (C-3) *δ* 98.7 (C-6), *δ* 98.4 (C-6"), *δ* 93.8 (C-8), *δ* 93.6 (C-8").

Compound 7.4:

(Helichrysin): ^{1}H NMR (400 MHz, acetone-d_6): δH 7.88 (1H, d, J = 15.6 Hz, Hα), 7.77 (1H, d, J = 15.6 Hz, Hβ), 7.62 (2H,d, J = 8.4 Hz, H2`), 6.93 (2H, d, J = 8.0 Hz, H3`), 6.30 (1H, d, J = 2.4 Hz, H3), 6.21 (1H, d, J = 2.0 Hz, H5), glucose moiety; 5.13 (1H, d, J = 7.6 Hz, H1``), complex signals from 3.49 – 3.98 for H-2``- H-6``, 4.02 (3H, s, OMe). 13C NMR (100 MHz, acetone-$d_6$): δC 193.7 (C=O), 168.3 (C4), 165.0 (C-2), 97.7 (C-3), 92.9 (C-5), 163.7 (C-6), 161 (C-4`), 144.1 (Cβ), 131.5 (C-2`), 127.8 (C-1`), 124.9 (Cα), 116.9 (C-3`), 107.8 (C-1), 56.64 (OMe), glucose moiety; 101.00 (C-1``), 78.1 (C-5``), 77.9 (C-3``), 74.5 (C-2``), 71.3 (C-4``), 62.6 (C-6``).

Compound 7.5:

(Luteolin): ^{1}H-NMR (400 MHz, Acetone-d_6, ppm): *δ* 7.51 (1H, *d*, *J* = 1.8 Hz, H-2'), *δ* 7.48 (1H, *dd*, *J* = 8.3, 2.1 Hz, H-6'), *δ* 7.01 (1H, *d*, *J* = 8.0 Hz, H-3'), *δ* 6.60 (1H, *s*, *H*-3), *δ* 6.54 (1H, *d*, *J* = 2.0 Hz, H-8), *δ* 6.27 (1H, *d*, *J* = 2.0 Hz, H-6),. ^{13}C-NMR (100 MHz, Acetone-d_6, ppm): *δ* 182.1 (C-4), *δ* 164.2 (C-6), *δ* 164.0 (C-2), *δ* 162.1 (C-5), *δ* 157.9 (C-9), *δ* 149.2 (C-4'), *δ* 145.6 (C-3'), *δ* 122.8 (C-1'), *δ* 119.2 (C-6'), *δ* 115.7 (C-2'), *δ* 113.1 (C-5'), *δ* 104.4 (C-10), *δ* 103.3 (C-3) *δ* 98.3 (C-6), *δ* 93.8 (C-8).

Compound 7.6:

(Kaur-16-en-19-oic acid, 15 methoxylate) ^{1}H-NMR (400 MHz, Acetone-d_6, ppm): *δ* 5.21 (1H, *s*, H-15), *δ* 5.09 (2H, *s*, H-17), *δ* 2.78 (2H, *m*, H-13), *δ* 2.03 (3H, *s*, *H*-22), *δ* 1.22 (3H, *s*, H-18), *δ* 1.00 (3H, *s*, H-20). ^{13}C-NMR (100 MHz, Acetone-d_6, ppm): *δ* 40.8 (C-1), *δ* 19.1 (C-2), *δ* 38.5 (C-3), *δ* 44.0 (C-4), *δ* 56.4 (C-5), *δ* 20.3 (C-6), *δ* 43.1 (C-7), *δ* 47.3 (C-8), *δ* 53.1 (C-9), *δ* 39.7 (C-10), *δ* 18.3 (C-11), *δ* 32.5 (C-12), *δ* 42.5 (C-13), *δ* 36.9 (C-14), *δ* 82.5 (C-15), *δ* 155.8 (C-16), *δ* 109.3 (C-17), *δ* 20.9 (C-18), *δ* 178.5 (H<u>C</u>OO; C-19), *δ* 15.5 (C-20), *δ* 170.1 (Me<u>C</u>OO; C-21), *δ* 28.3 (C-22).

8.2.5. Glucose Uptake assay and α-Glucosidase inhibition assay

To evaluate the potentials of isolated compounds to mitigate against the onset of hyperglycemia due to activities of carbohydrate hydrolyzing enzymes, the methods reported in chapter 7 for glucose uptake assay, α-glucosidase, and α-amylase inhibition was adopted to include the compounds **6**, **10**, and **11**.

8.3. Result and discussion

8.3.1. Chemical constituents:

The compounds **7.1**, **7.2**, **7.4**, **7.5** and **7.6** were identified by comparing their NMR spectra data with those reported in the literature [9, 11, 13] namely: quercetin, luteolin helichrysin, helichrysetin, and Kaur-16-en-19-oic acid, 15-acetate respectively. Compounds **7.1** and **7.5** were isolated as yellow crystalline powders. The ^{1}H and ^{13}C NMR data revealed both compounds consist of flavonoids skeletons with slight variation due to the presence and absence of hydroxyl proton at position C-3 in **7.1** and **7.5** respectively. This was confirmed by *δ* 135.8 (C-3, –OH) for substituted benzene and *δ* 103.3 (C-3, –H) for unsubstituted benzene in **7.1** and **7.5** respectively. This effect is also noticeable in chemical shifts of the adjacent carbons, hence the C-2 (*δ* 164.0) and C-4 (*δ* 182.1) of **7.2** are further downfield than in **7.1**. The compounds **7.2**, and **7.4** were reported in the published article of chapter 6 of this thesis.

Compound **7.6** was isolated as white needle-like crystals. The ^{13}C-NMR data of compound **7.6** match closely with a 15α-hydroxy-16-kauren-19-oic acid skeleton that was reportedly isolated from the same plant [11], with kaur-16-en-19-oic acid isolated from *Aralia cordata* [16], *Aralia continentalis* [17], and *Xylopia laevigata* [18]. However, in addition to the carboxylic carbon (C-19), it presents a methoxylate group attached to C-15. The observed higher chemical shifts for C-19 (*δ* 178.5) than for C-21 (*δ* 170.1) could be due to the higher deshielding effect of low electron density by the hydroxyl group when compared to the methoxyl group. Similarly, the two methyl carbons C-20 (*δ* 15.5) and C-22 (*δ* 28.3) displayed different chemical shifts upfield, because different electron densities caused the deshielding effect of oxygen and hydrogen on each carbon.

Compound **7.3** was isolated as a yellow amorphous powder containing a mixture of luteolin (**I**) and 3-methoxyquercetin (**II**) units which were inseparable from available chromatographic methods including UHPLC. $UV_{\lambda max}$: 356 and 278 nm characteristic of absorption bands for flavonoids. The IR data suggest the presence of carbonyls (1670 cm^{-1}) and alcohols (1310 cm^{-1}). The molecular formula ($C_{30}H_{20}O_{12}$) was proposed from ^{1}H, ^{13}C, DEPT-135, ^{1}H-^{1}H COSY, HSQC, and HMBC spectra (Supplementary data). The ^{1}H-NMR spectrum indicated eleven signals in the aromatic regions, four of these signals are doublets at *δ* 7.58 (1H, *d*, *J* = 7.9 Hz, H-6"') *δ* 7.51 (1H, *d*, *J* = 1.8 Hz, H-2'), *δ* 7.47 (1H, *d*, *J* = 8.0 Hz, H-6'), and *δ* 7.01 (2H, *d*, *J* = 8.1 Hz, H-5'/5"'). ^{1}H- ^{1}H COSY correlation of these signals indicated two AA 'XX' spin-systems for two *para*-substituted phenyl moieties in present in **7.3** (Figure 7.1). The chemical shifts of other aromatic singlet protons are similar to their corresponding units except for an additional 3-*O*-methyl proton, *δ* 3.87 (3H, *s*, OCH_3) recorded for **II**. The ^{13}C-NMR and DEPT-135 showed the presence of signals for 30 carbons which includes two carbonyl carbons at *δ* 182.1 and 175.6, and one sp^3 carbon (OCH_3). A shift in ^{13}C NMR signals of the 3-methoxyquercetin was observed while the ^{13}C NMR of luteolin remained unchanged when compared to the C-13 of the single unit of quercetin and luteolin isolated. These signals thus confirm the presence of a mixed flavonoid of luteolin and 3-methoxyquercetin units. The combined analysis of spectra from ^{1}H and ^{13}C experiments revealed that signals at *δ* 7.51, 7.01, and 7.47 could be assigned to protons of C-2`, C-5`, and C-6` of the luteolin unit. Similarly, the signals at *δ* 7.70, 7.01, and 7.58 belong to C-2```, C-5```, and C-6``` of the 3-methoxyquercetin unit of the mixture.

8.3.2. Glucose uptake and enzymes inhibition assay:

Several scientific investigations gave credence to the diterpene class of compounds for improving glucose uptake/metabolism and inhibiting the activities of starch digestive enzymes such as α-glucosidase and α-amylase and in the body [19-20, 22]. Hamid et al. (2015) reported the diterpene borapetoside C among other classes of compounds isolated from *Tinospora crispa* with the most potent high inhibitory activities against α-glucosidase and α-amylase enzymes [21]. From the result of glucose uptake by constituents of HF, the crude methanolic extract (HF) and compound **7.6** showed significant activity in HEK293 treated cells for glucose uptake. Also, compound **7.1** showed a marginal activity while the other compounds decreased the glucose uptake (Fig. 7.2). Similarly, the inhibitory activities against α-glucosidase (Table 7.2) corroborate the observed trend in glucose uptake with compound **7.6** showing the strongest inhibition against α-glucosidase but no activity against α-amylase. The compound **7.4** displayed the least inhibition against α-glucosidase probably due to the glucose moiety which is lacking in other flavonoids. Among the tested compounds, compound **7.1** was potent against α-amylase enzymes (8.9± 0.3) while other compounds were either not active or only active at higher concentrations than tested (1 mg/mL). Activities of **7.6** and **7.1** collectively

demonstrated amelioration of hyperglycaemia, a condition that can lead to Type-2 diabetes mellitus if not well-managed [22]. Although the mechanism of action of these compounds is yet to be studied, the significant increase in glucose uptake by compound **7.6** can be attributed to the -COOH and the -$COOCH_3$ groups of the diterpene which are lacking in the flavonoid compounds. This agrees with the report of improved glucose uptake by diterpenes, 19-acetoxy-12-methoxycarnosic acid and clinopodiolides B containing these groups from *Salvia africana-lutea* by Etsassala et al. (2019;,2020) [22, 23]. Overall, isolated compound 15-acetoxykaur-16-en-19-oic acid, , and quercetin demonstrated potency for glucose uptake assay over the other compounds. In addition to the total extract, all compounds tested displayed higher inhibitory activities on the α-glucosidase than acarbose standard with compound **7.6**, compound **7.1** and compound **7.2** most potent (Table 7.2). On the other hand, inhibition of the α-amylase enzyme showed no activity except for compounds **7.1**, **7.2**, and **7.5** with compound **7.1** having slightly higher inhibition than the standard. This selective activity could be attributed to their polyphenolic structure in the compounds. Natural polyphenols have been reported to be effective inhibitors of mammalian α-amylase with IC_{50}s in the order of micromolar concentration due to multiple reactive sites that counteract α-amylase [25].

Table 7.1: ^{1}H and ^{13}C chemical shifts, and HMBC correlations of Compound 7.3

	(Luteolin)		**(3-methoxy quercetin)**		
Position	**δ_C**	**δ_H**	**Position**	**δ_C**	**δ_H**
C-2	164.3		C-2	115.9	
C-3	103.3	6.58, *s*	C-3	138.3	
C-4	182.1		C-4	175.6	
C-5	161.9		C-5	164.0	
C-6	98.7	6.26, *s*	C-6	98.4	6.26, *s*
C-7	162.1		C-7	164.0	
C-8	93.8	6.53, *s*	C-8	93.6	6.49, *s*
C-9	157.9		C-9	156.9	
C-10	104.4		C-10	104.9	
C-1`	122.8		C-1`	122.1	
C-2`	115.7	7.51, *s*	C-2`	115.3	7.70, *s*
C-3`	145.6		C-3`	144.9	
C-4`	149.2		C-4`	148.2	
C-5`	113.1	7.01, *d*	C-5`	115.3	7.01, *d*
C-6`	119.2	7.47, *d*	C-6`	121.2	7.58, *d*
			OCH_3		3.87

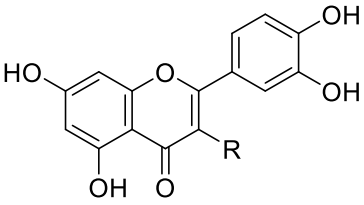

7.1: Quercetin; R = OH
7.5: Luteolin; R = H

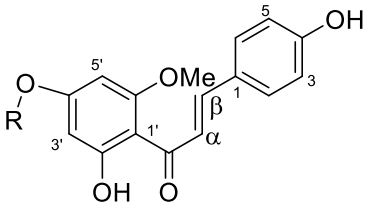

7.2: Helichysetin; R = H
7.4: Helichrysin; R = Glu

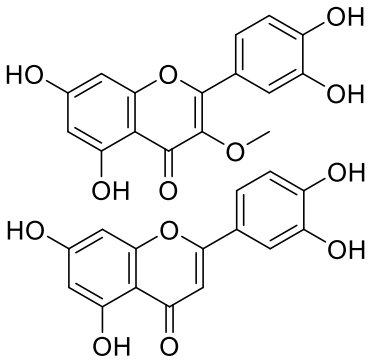

7.3: 3-methoxyquercetin + luteolin (1:1)

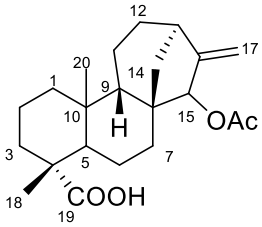

7.6: 15-acetoxykaur-16-en-19-oic

Figure 7.1: Isolated compounds from *Helichrysum foetidum*

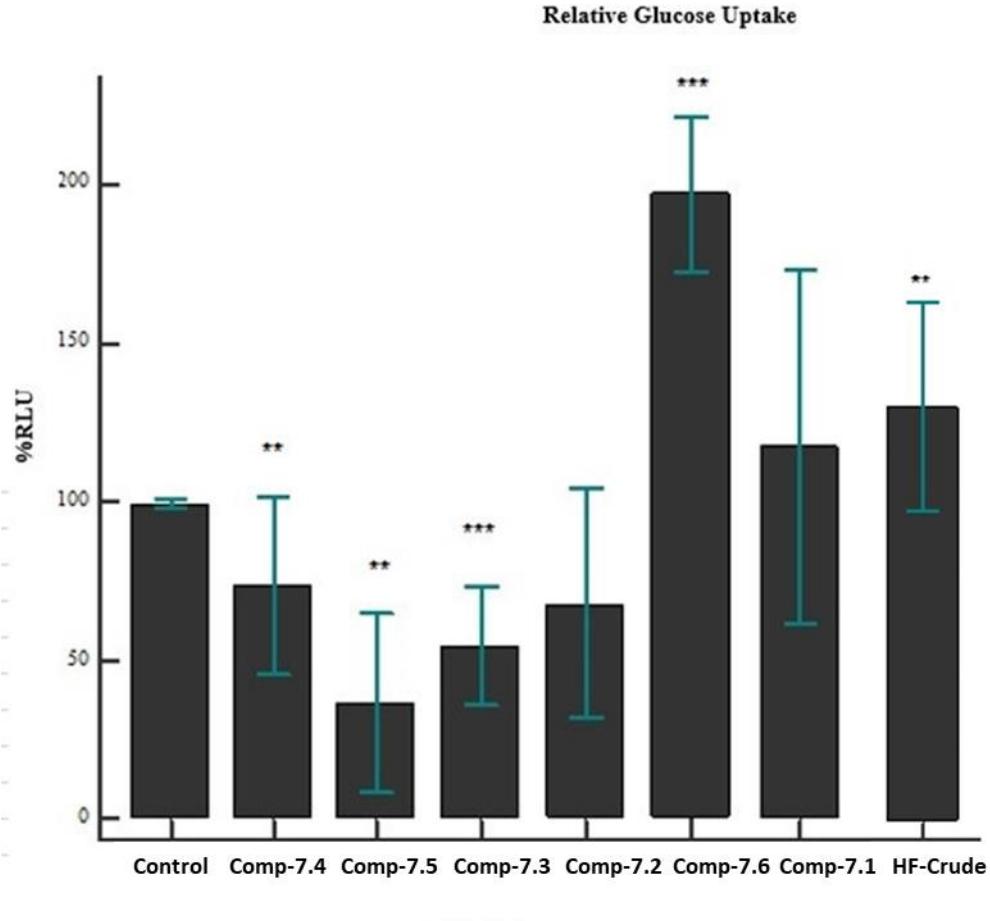

Figure 7.2: Glucose uptake activities of phytochemicals from *Helichrysum foetidum* (Note: HF = Total extract)

Table 7.2: α-Glucosidase and α-Amylase inhibitory activities of compounds

Sample	α-Glucosidase IC_{50} (µg/mL)	α-Amylase IC_{50} (µg/mL)
HF	27.3 ± 0.1	NA
Comp 7.1	24.0 ± 0.1	8.9± 0.3
Comp. 7.2	19.4 ± 0.3	25.13 ± 0.3
Comp. 7.3	37.3 ± 0.1	NA
Comp. 7.4	48.3 ± 0.1	NA
Comp. 7.5	32.9 ± 0.2	55.0 ± 0.1
Comp. 7.6	16.3± 0.1	NA
Acarbose	610.4 ± 1.0	10.2 ± 0.6

Note: HF = Total extract, NA = Not active)

8.4. . Conclusion

The phytochemical studies on H. foetidum resulted in the islaotion of 5 known compounds and a mixture. It also elaborates on the medicinal and in vitro biological activities of the plant as a drug candidate for hyperglycaemia. Overall, the phytochemical constituents of *Helichrysum foetidum* can be formulated for potential use in the management of DM.

Acknowledgement

We wish to acknowledge the Centre for Postgraduate Studies of Cape Peninsula University of Technology, South Africa, the South African Rooibos Council (SARC) for the financial support towards the completion of this research. In addition, partial funding was provided by the South African Medical Research Council (SAMRC) through its Division of Research Capacity Development under funding received from the South African National Treasury. The content hereof is the sole responsibility of the authors and do not necessarily represent the official views of the SAMRC or the funders.

References

1. Elizabeth, B.; Michael, J. H.; Gary, W. Flavonoids as Human Intestinal α-Glucosidase Inhibitors. *Foods*, **2021**, 10, 1939.
2. Rudrapal, M.; Hussain, N.; Egbuna, C. Diabetes Mellitus and its Management with Plant-Based Therapy. In: Egbuna C., Hassan S. (eds) *Dietary Phytochemicals. Springer, Cham.* **2021**.

3. Hung, H.; Qian, K.; Morris-natschke, S. L.; Hsu, C.; Lee, K. Recent discovery of plant-derived anti-diabetic natural products. *Natural Product Reports*, **2012**, 29, 580 – 606.
4. Wei, L.; Rong-Ji, D.; Yu-Hong, Y.; Liang, L.; Chong-Ming, W.; Wei-Wei, L.; Wei-Wei, M.; Xin-Sheng, Z.; Yu-Lin, D. Antihyperglycemic Effect of Cephalotaxus sinensis Leaves and GLUT-4 Translocation Facilitating Activity of Its Flavonoid Constituents. *Biol. Pharm. Bull*. **2007**, 30(6), 1123—1129.
5. Lourens, A.C.U.; Viljoen, A.M.; Van Heerden, F.R. South African *Helichrysum* species: a review of the traditional uses, biological activity and phytochemistry. *Journal of Ethnopharmacology*, **2008**,119(3), 630 – 652.
6. Akaberia, M.; Sahebkar, A.; Azizi, N.; Ahmad S.E. Everlasting flowers: Phytochemistry and pharmacology of the genus *Helichrysum. Industrial Crops & Products*, **2019**, 138 (2019) 111471, 1 – 21.
7. Sindambiwe, J.B.; Calomme, M.; Cos, P.; Totte, J.; Pieters, L.; Vlietinck, A.; Berghe, D.V. Screening of seven selected Rwandan medicinal plants for antimicrobial and antiviral activities. *Journal of Ethnopharmacology*. **1999**, 65, 71-77.
8. Lourens, A. C.U.; Van Vuuren, S. F.; Viljoen, A. M.; Davids, H.; Van Heerden, F. R. Antimicrobial activity and in vitro cytotoxicity of selected South African *Helichrysum* species. *S. Afr*. J. *Bot*. **2011**, 77(1), 229 – 235.
9. Malolo, F.A.E.; Nouga, A.B.; Kakam, A.; Franke, K.; Ngah, L.; Flausino, O.; Mpondo, E. M.; Ntie-Kang, F.; Ndom, J.C.; Bolzani, V.; Wessjohann, L. Protease-inhibiting, molecular modeling and antimicrobial activities of extracts and constituents from *Helichrysum foetidum* and *Helichrysum mechowianum* (Compositae), *Chem. Cent. J.* **2015**, 9 (1).
10. Maroyi. Medicinal uses, biological and phytochemical properties of *Helichrysum foetidum* (L.), Moench. (Asteraceae). *Asian Journal of Pharmaceutical and Clinical Research*, **2019**,12 (7), 63–68.
11. Barrero, A. F.; Arteaga, P.; Herrador; M. M. ent-Kaurene diterpenoids from *Helichrysum foetidum*. *Fitoterapia*, **1998**, 68(1), 83 – 84.
12. Akinfenwa, O.A.; Pearce, B.; Omoruiya, S.I.; Badmus, J.A; Ismail, E.; Marnewick, J.L.; Mongi, B.; Ekpob, O.E; Hussein A.A. The potential of chalcone-capped gold nanoparticles for the management of diabetes mellitus. *Surfaces and Interfaces*, **2021**, 5 (2021), 101251.
13. Kakam, Z.; Antoine, M.; Franke, K.; Ndom, J.C.; Dongo, E.; Mpondo, T. N.; Wessjohann, L. A. Secondary metabolites from *Helichrysum foetidum* and their chemotaxonomic significance. *Biochemical Systematics and Ecology*, **2011**, 39(2), 166 – 167.
14. Lourens, A. C.U.; Van Vuuren, S. F.; Viljoen, A. M.; Davids, H.; Van Heerden, F. R. Antimicrobial activity and in vitro cytotoxicity of selected South African *Helichrysum* species. *South African Journal of Botany*, **2011**, 77(1), 229 – 235.
15. Iwona, W.; Agnieszka, Z. C CP/MAS NMR studies of flavonoids. *Magn. Reson. Chem*. **2001**; 39, 374–380.
16. Dang, N.H; Zhang, X.; Zheng, M.; Son, K.H.; Chang, H.W.; Kim, H.P.; Bae, K.; Kang, S.S. Inhibitory constituents against cyclooxygenases from *Aralia cordata* Thunb. *Archives of Pharmacological Research*, **2005**, 28, 28–33.
17. Ji Hyo Lyu; Geum San Lee; Kyun Ha Kim; Hyung-Woo Kim; Su-In Cho; Seung-Il Jeong; Hong-Jun Kim; Young-Seung Ju; Ho-Kyoung Kim; Ruxana T. Sadikot; John W. Christman; Sei-Ryang Oh; Hyeong-Kyu Lee; Kyung-Seop Ahn; Myungsoo Joo. ent-kaur-16-en-19-oic acid, isolated from the roots of *Aralia continentalis*, induces activation of Nrf2. *Journal of Ethnopharmacology*, **2011**,137, 1442–1449.
18. Dayanne, M.S.; Emmanoel, V.C.; Paulo Cesar, L.N.V.; Sócrates, C.H.C; Marcos, J.S.; Luis Henrique, G.R.G.; Andersson, B.; Antonio G.F. ent-Kaurane diterpenoids and other constituents from the stem of *Xylopia laevigata*. (Annonaceae). *Quim. Nova*, **2012**, 35(8), 1570-1576.
19. Şen, A.; Ayar, B.; Yilmaz, A.; Acar, O.O; Turgut, G.Ç.; Topçu, G. Natural diterpenoid alysine A isolated from *Teucrium alyssifolium* exerts antidiabetic effect via enhanced glucose uptake and suppressed glucose absorption. *Turk J Chem*, **2019**, 43, 1350 – 1364.
20. Duarte, A.M.; Guarino, M.P.; Barroso, S.; Gil, M.M. Phytopharmacological Strategies in the Management of Type 2 Diabetes Mellitus. *Foods*, **2020**, 9, 271, 1 – 31.
21. Hamid, H.A; Yusoff, M.M; Liu, M.; Karim, M.R. α-Glucosidase and α-amylase inhibitory constituents of *Tinospora crispa*: Isolation and chemical profile confirmation by ultra-high performance liquid chromatography-quadrupole time-of-flight/mass spectrometry. *Journal of Functional Foods*, **2015**, 16, 74-80.

22. Etsassala, N.G.; Cupido, C.N.; Iwuoha, E.; Hussein, A.A. Review: Abietane diterpenes as potential candidates for the management of type 2 diabetes. Curr. Pharm. Des. **2020**, 26, 1–13.
23. Etsassala, N.G.E.R.; Badmus, K.A.; Tesfaye, T.J.W; Marnewick, J.L.; Cupido, C.N.; Hussein, A.A.; Iwuoha, E.I. Alpha-Glucosidase and Alpha-Amylase Inhibitory Activities of Novel Abietane Diterpenes from *Salvia africana-lutea*. *Antioxidants*, **2019**, 8, 10, 11 – 12.
24. Etsassala, N.G.E.R.; Ndjoubi, K.O.; Mbira, T.J.; Pearce, B.; Pearce, K.; Iwuoha, E.I.; Hussein, A.A.; Benjeddou, M. Glucose-Uptake Activity and Cytotoxicity of Diterpenes and Triterpenes Isolated from Lamiaceae Plant Species. *Molecules*, **2020**, 18, 1-10.
25. Mahmood, N. A review of α -amylase inhibitors on weight loss and glycemic control in pathological state such as obesity and diabetes. *Comparative Clinical Pathology*, **2016**, 25, 1253 – 1264.

CHAPTER EIGHT

9.1. General discussion, conclusions and recommendations

This study interfaced between phytochemistry and nanostructure materials from plant phytochemicals. It investigated the phytochemical constituents of two plants; *Aspalathus linearis* (Rooibos) and *Helichrysum foetidum*, and the ability of each plant and their respective major compounds to act as both reducing and capping agents in the green synthesis of gold and silver nanoparticles. The study was divided into five projects to cover; selection between unfermented and fermented *Aspalathus linearis* based on their total phenolic and antioxidant capacity, chemical elucidation of a novel compound isolated from *Aspalathus linearis* and the evaluation of isolated compounds for protection against UV-induced skin disorder and synthesis of aspalathin-mediated gold and silver nanoparticles from *Aspalathus linearis* for potency against cancer cells *in vitro*. The other two projects were focused on *H. foetidum*. The isolation of five known compounds and inseparable mixture from *H. foetidum* and the bio-evaluation of the compounds for glucose uptake and inhibitions of carbohydrate hydrolysing enzymes for antidiabetic potentials was carried out. In a similar approach to *Aspalathus linearis*, the potentials of the total extract and the major compounds of *Helichrysum foetidum* for the biosynthesis of gold nanoparticles for the potential management of diabetes mellitus were demonstrated.

In the first project of this study, the total phenolic and antioxidant capacity of unfermented (green) and fermented (red) rooibos obtained from different solvent extraction methods were compared using Folin & Ciocalteu's phenol reagent and ferric reducing ability of plasma (FRAP) and 2,2' -azino-bis-3-ethylbenzothiazolin-6-sulphonic acid assays (ABTS). The green rooibos displayed relatively higher total phenol and antioxidant capacity than the red rooibos. Also, antioxidant capacity by FRAP and ABTS assays confirmed a higher potency for ethanol and hydro ethanol extracts over acetone extracts for green and red rooibos. This result agrees with the result from Damiani et al., 2019 which proved that cold and hot brewed green rooibos has higher phenolic and antioxidant content than the red counterpart. This result generated a short communication article that informs the selection of green rooibos for further study.

The second project of this study focussed on aspalathin, the major compound and its derivatives since other compounds have been reported from many other plants. Isolation of the novel compound from rooibos was quite challenging given the complex matrix of its polyphenols and hundreds of studies on the plant in the literature. However, detailed

chromatographic and chemical analyses of strongly polar fractions from the total extract resulted in the isolation of linearthin (**4.1**) which is being reported for the first time by this study in addition to the known aspalathin and nothofagin. The compound was identified as a derivative of aspalathin with a similar skeleton of the A and B ring separated by three carbons in a typical dihydrochalcone. Unlike aspalathin and nothofagin that were reported with a *C*-sugar moiety (Krafczyk et al., 2008), it presented a dioxygenated carbon (δ_C 117.8) which indicated a deoxy monosaccharide. The molecular formula $C_{21}H_{22}O_{10}$ best fits according to the HRMS determination. When compared the molecular formula to aspalathin ($C_{21}H_{23}O_{11}$), it indicated the presence of extra unsaturation of a CH_2 group (δ_C 33.3), which should be cyclic ether. Linearthin and other chalcone derivatives from rooibos have not been reported for protective effects on skin damages from excessive ROS generated by UVB exposure in vitro. The isolates used in this study showed the capacity to improve cell viability and inhibit apoptosis induced by UVB exposure by likely exploiting pathways associated with the established antioxidant properties of rooibos. Isolates reduced biomarkers associated with lipid oxidative damage and improved the oxidative status of the cell. Thus, linearthin and other chalcone derivatives can be beneficial as a therapeutic agent to alleviate the effects of extreme sun exposure and subsequent oxidative stress.

Project three explored green chemistry in the synthesis of gold and silver metal nanoparticles via aspalathin and rooibos natural extract for applications in delivery to cancer cells. The antioxidant properties of rooibos and being a unique source of dihydrochalcone compound with reports of different bioremediations is a motivation for this study. The aspalathin and the total extract successfully reduced the respective solutions of gold and silver salts forming crystalline nanoparticles. The physicochemical characterisations confirmed SPR at 530 nm and mean particle sizes of 7.5 – 12.5 nm for the AuNPs. The AgNPs SPR was also found at 440 nm with the mean particles sizes of 1.6 nm – 6.7 nm which are within the literature reports for rooibos (Oyagi et al., 2014; Analike et al., 2021). The cytotoxicity studies showed that GR-AgNPs were most toxic against the SH-SY5Y and HepG2 cells at IC_{50} 108.8 µg/mL and 183.4 µg/mL, respectively. Cellular uptake analysis of all NPs indicated AgNPs of rooibos at a lower dose (1.3 – 1.5 µg/mL) is favourable for its anti-cancer potentials.

In project four, five known compounds and a mixture were isolated from the *Helichrysum foetidum* plant As expected, the presence of terpenes and flavonoids in the *Helichrysum* genus was established from this study. However, acylphloroglucinols that were reported from other South African species (Jakupovic et al., 1998; Lourens et al., 2008) was not identified in *H. foetidum* in this study. The activities of the total extract (HF) and Compound **7.1**, and **7.6** on glucose uptake on Renocytes (HEK293 kidney cells) suggest the antidiabetic potential of the

plant. In addition, all tested samples for α-glucosidase inhibition complement the antidiabetic potential of the plant by delaying the release of glucose sugar when compared to the acarbose standard which is helpful in the management of insulin-dependent diabetes. α-amylase inhibition experiments may require further studies due to the inactivity of most compounds.

In project five, the total extract (HF) and the two main compounds isolated from *Helichrysum foetidum* were screened for reducing potentials of sodium tetrachloroaurate (III) dihydrate ($NaAuCl_4.2H_2O$) for optimum concentration. Interestingly, compounds **7.2** and **7.4** in addition to HF were most effective as both reducing and capping agents and were upscaled based on the stoichiometric relationship during synthesis. The result from synthesis showed quasi-monodispersed gold nanoparticles in the size range of 2–12 nm. The bio-evaluation of samples indicated that the AuNP/capping agent conjugates are biostable and have different biological profiles from the total extract/pure compounds. The enzymatic inhibition assays showed significant inhibition by the total extract, helichrysetin and their gold nanoparticles similar to the observed activity for glucose uptake in HEK293 treated cells. All the tested samples relatively demonstrated no cytotoxicity against normal HaCaT keratinocytes which also support their application as drug candidates.

In conclusion, this study presents the first report of the compound linearthin from rooibos. The green synthesis of aspalathin mediated gold and silver nanoparticles, as well as *H. foetidum*, helichrysetin, and helichrysin gold nanoparticles. The study demonstrated the richness of rooibos in dihydrochalcones, its protection of skin cells against UVB-induced damages, and the anticancer potentials of its green synthesised silver nanoparticle. It also showed that phytochemicals of *H. foetidum* and its green synthesized gold nanoparticles potentially enhanced glucose uptake in mammalian kidney cells, and inhibited carbohydrate-hydrolysing enzymes.

Recommendation

Based on the promising results generated from this study, it is recommended that:

i. in addition to the published work from this study, other drafted manuscripts from this study should be published.
ii. other fractions collected from extractions may be bio-evaluated for further studies of the *Helichrysum foetidum*
iii. other sophisticated equipment such as high-resolution electron ionisation mass spectrometry (HREIMS) and energy-dispersive X-ray spectroscopy (EDS) be used to complement spectra of compounds and particles with complicated signals.

References

Damiani, E.; Carloni, P.; Rocchetti, G.; Senizza, B.; Tiano, L.; Joubert, E.; de Beer, D.; Lucini, L. Impact of Cold versus Hot Brewing on the Phenolic Profile and Antioxidant Capacity of Rooibos (Aspalathus linearis) Herbal Tea. *Antioxidants*, **2019**, 8, 499, 1 – 19.

Krafczyk, N.; Glomb, M.A. Characterization of phenolic compounds in rooibos tea. *J. Agr. Food Chem.* **2008**, *56*(9), 3368-3376.

Jakupovic, J.; Zdero, C.; Grenz, M.; Tsichritzis, F.; Lehmann, L.; Hashemi-Nejad, S.M.; Bohlmann, F. Twenty-one acylphloroglucinol derivatives and further Constituents from South African *helichrysum* species. *Phytochemrstry*, **1989**, 28(4), 1119 – 1131.

Lourens, A.C.U.; Viljoen, A.M.; van Heerden, F.R. South African *Helichrysum* species: a review of the traditional uses, biological activity and phytochemistry, *J. Ethnopharmacol*. **2008**, 119(3), 630–652.

Oyagi, M. O.; Michira, I. N.; Guto, P.; Baker, P. G. L.; Kamau, G. Polydisperse Low Diameter 'Non-toxic' Silver Nanoparticles Encapsulated by Rooibos Tea Templates. *Nano Hybrids*, **2014**, 8(2014), 57–72.

Analike, B. S.; Daniela, K.; Giorgia, C.; Mauro, P.; Maribanyana, L.; Nonhlanhla, C; Suprakas, S.R.; L. Namrita. Synthesis and characterization of gold nanoparticles biosynthesised from *Aspalathus linearis* (Burm.f.) R. Dahlgren For progressive macular hypomelanosis. *J. Herb. Med.*, **2021**, 29, 100481.

9.2. APPENDICES

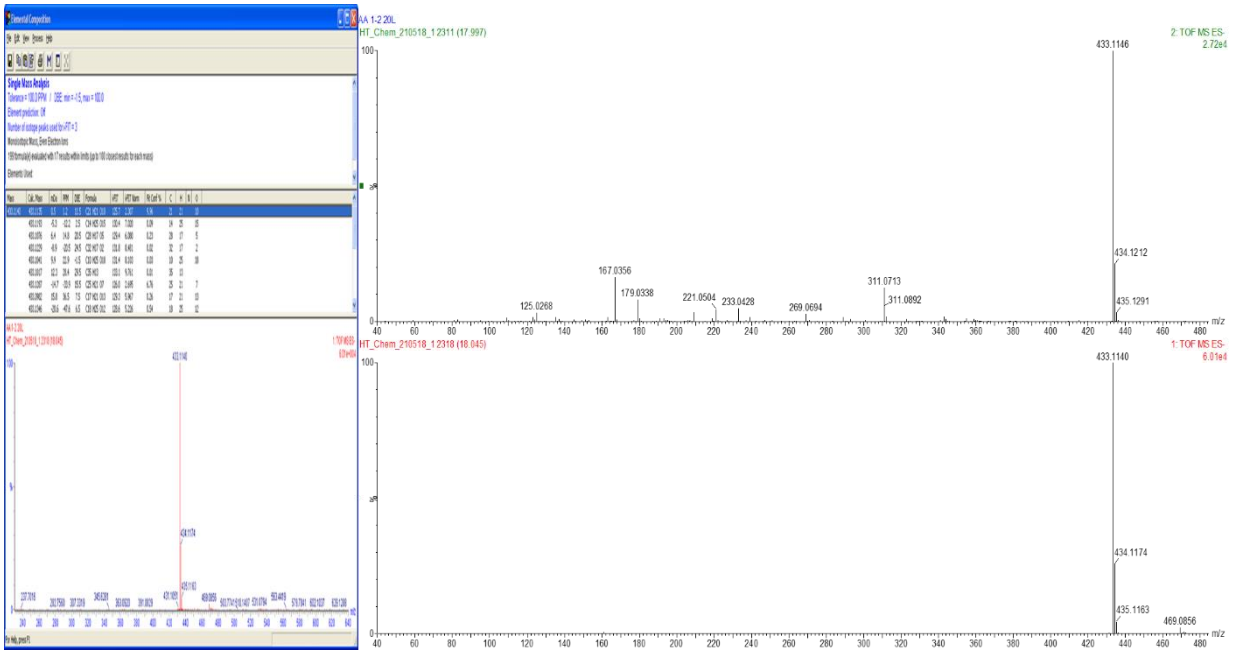

APPENDIX 1: High-Resolution Mass spectrometry of compound 4.1

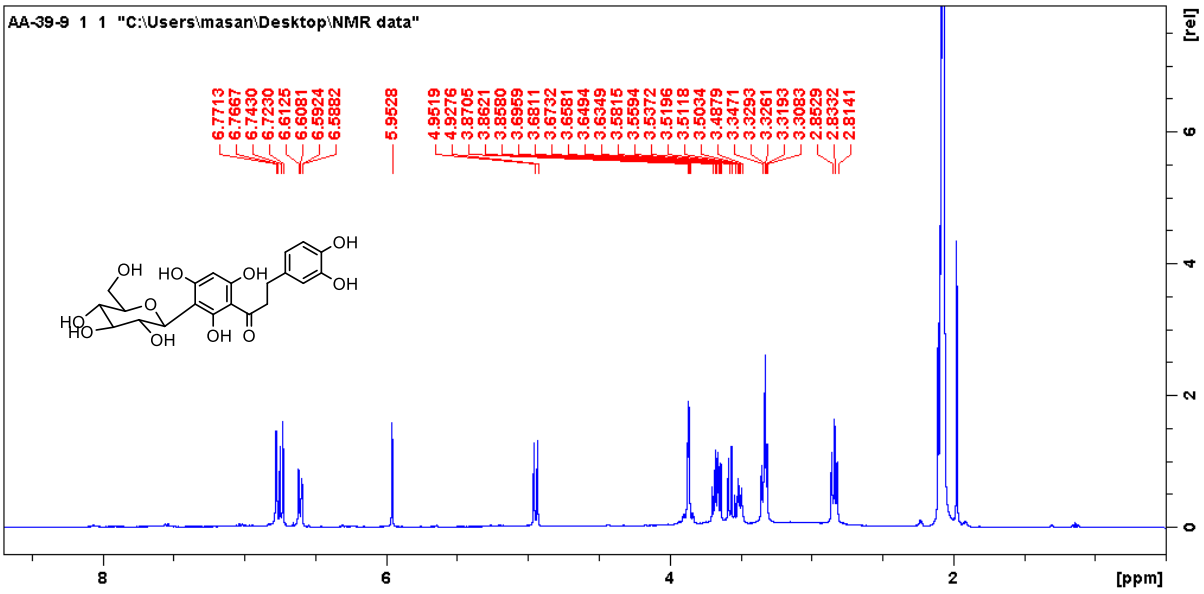

APPENDIX 2: ^{1}H NMR (400 MHz, Acetone$_{-d6}$) spectrum of compound 4.2

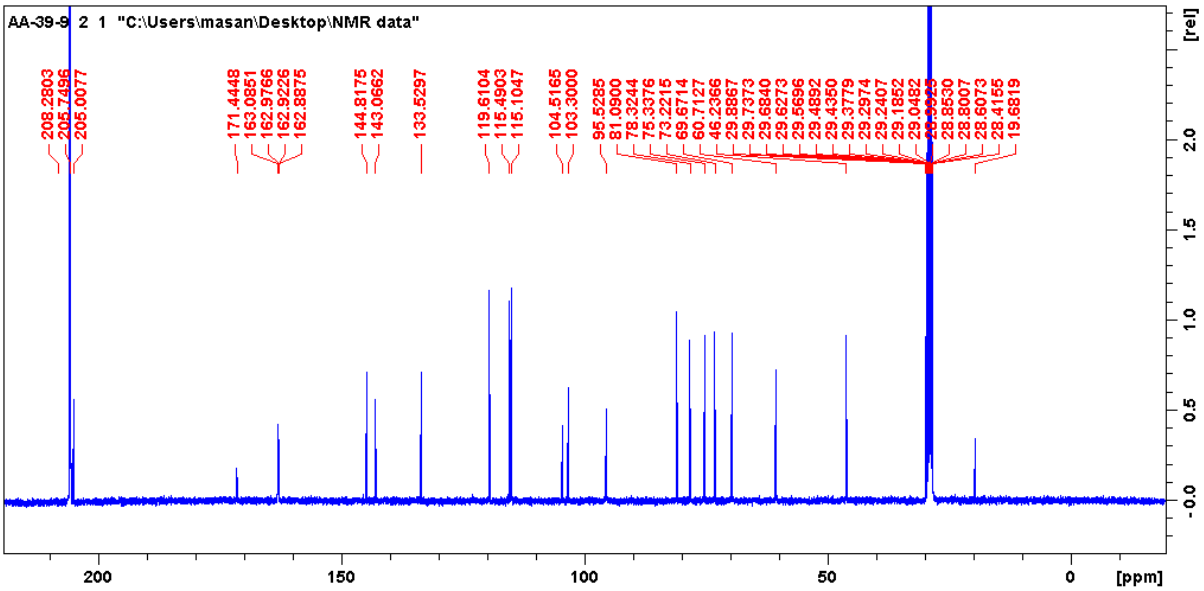

APPENDIX 3: ^{13}C NMR (400MHz, Acetone$_{-d6}$) spectrum of compound 4.2

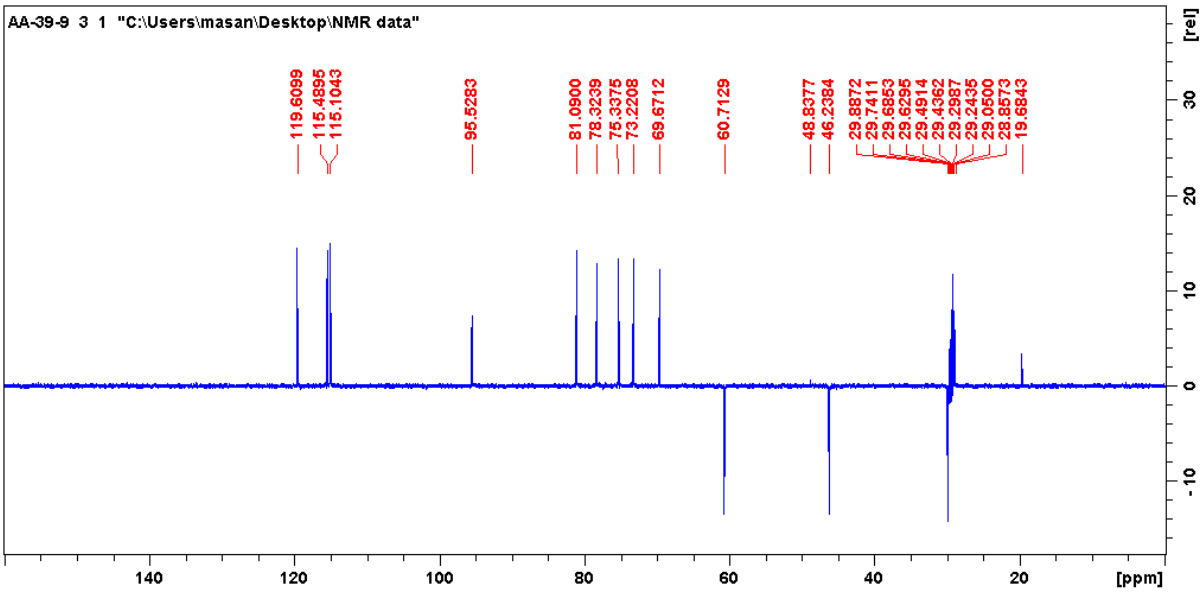

APPENDIX 4: DEPT-135 NMR (400MHz, Acetone$_{-d6}$) spectrum of compound 4.2

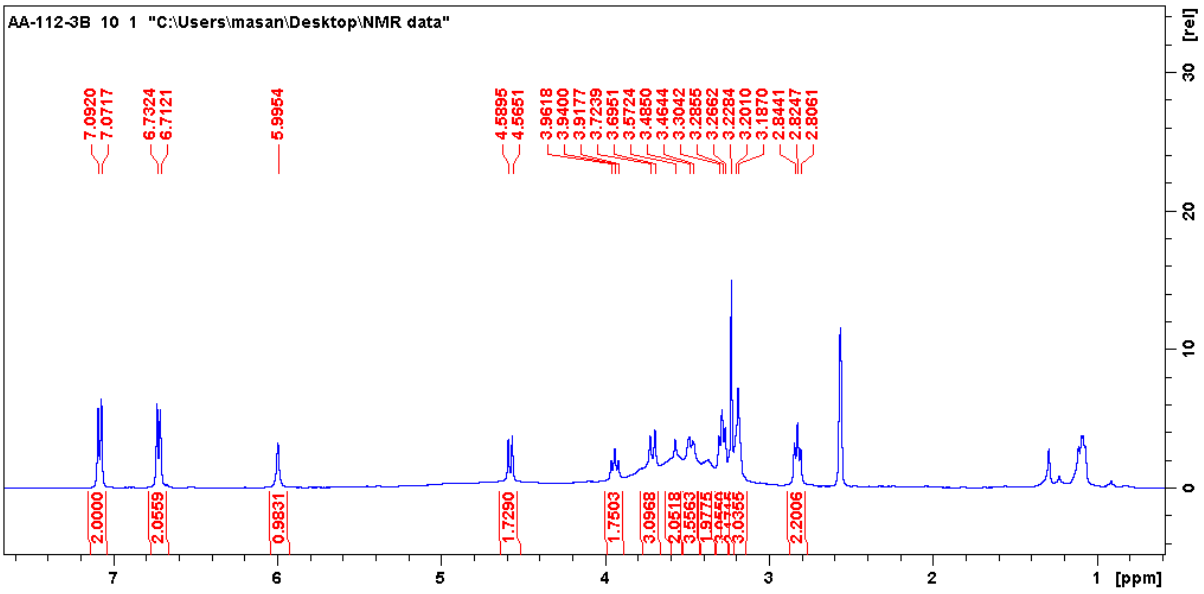

APPENDIX 5: ^{1}H NMR (400MHz, DMSO$_{-d6}$) spectrum of compound 4.3

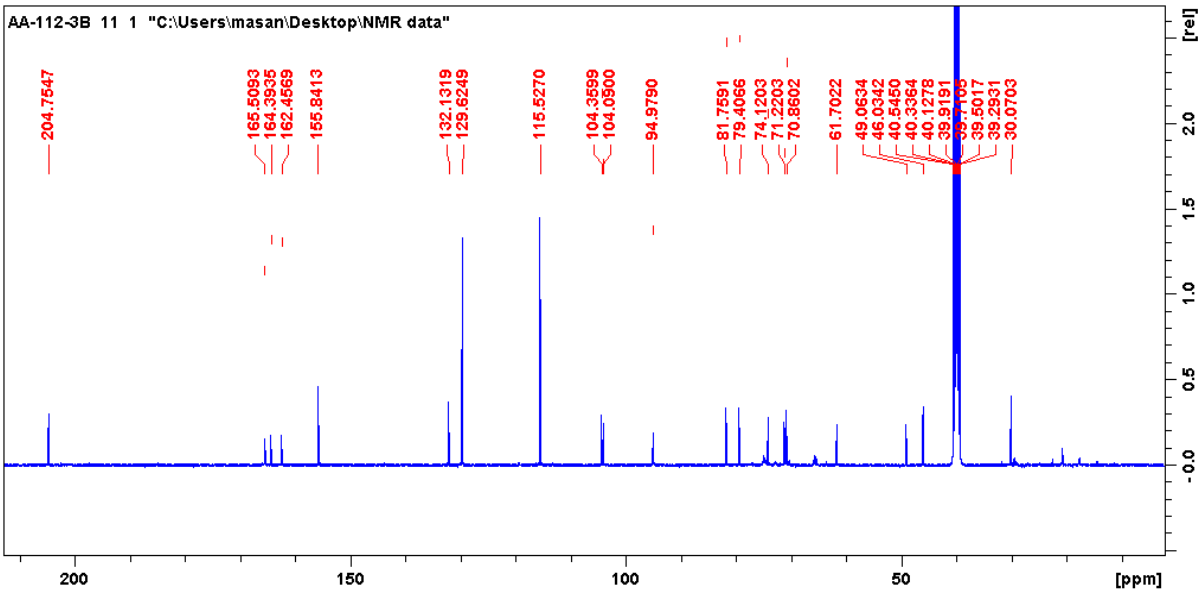

APPENDIX 6: ^{13}C NMR (400 MHz, DMSO$_{-d6}$) spectrum for 4.3

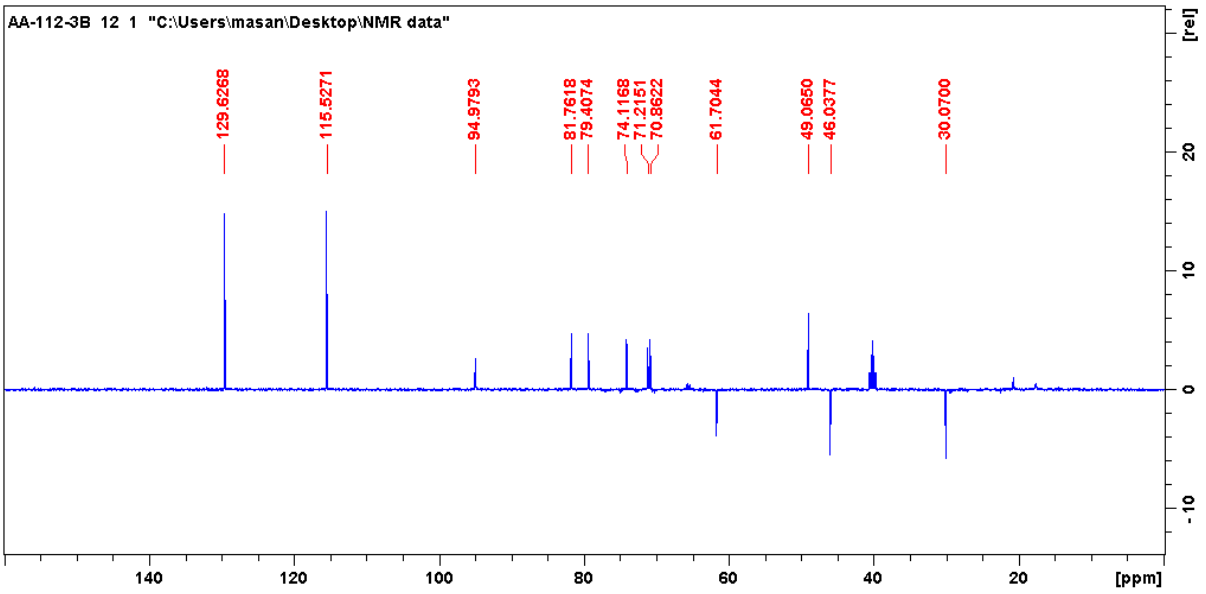

APPENDIX 7: DEPT-135 NMR (400MHz, Acetone$_{-d6}$) spectrum of compound 4.3

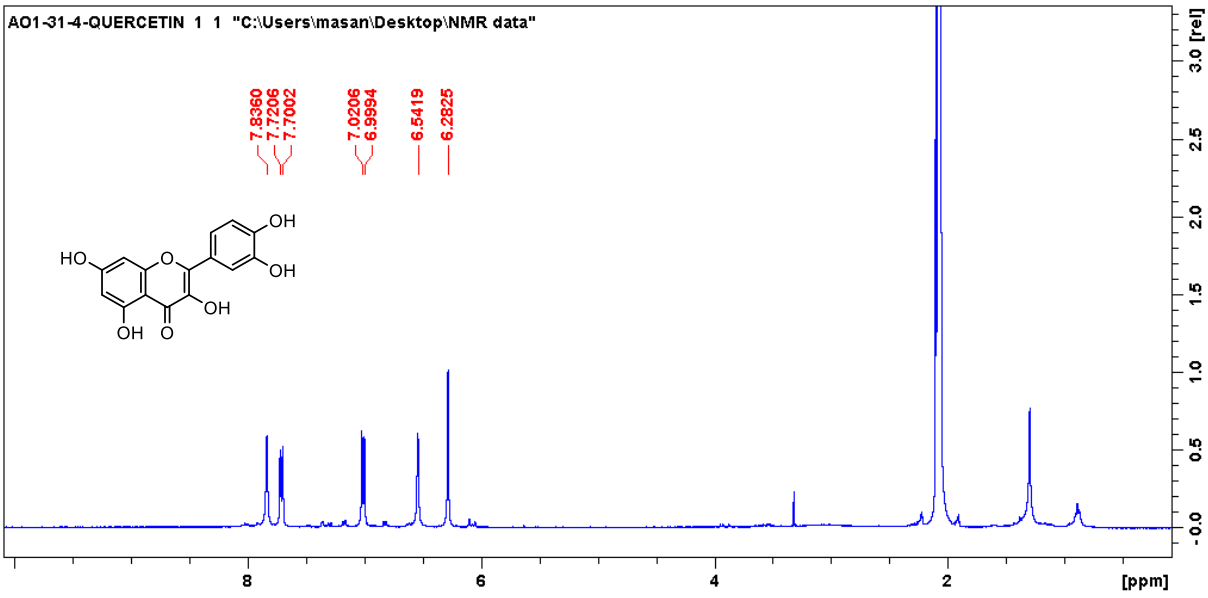

APPENDIX 8: ^{1}H NMR (400 MHz, Acetone$_{-d6}$) spectrum of compound 7.1

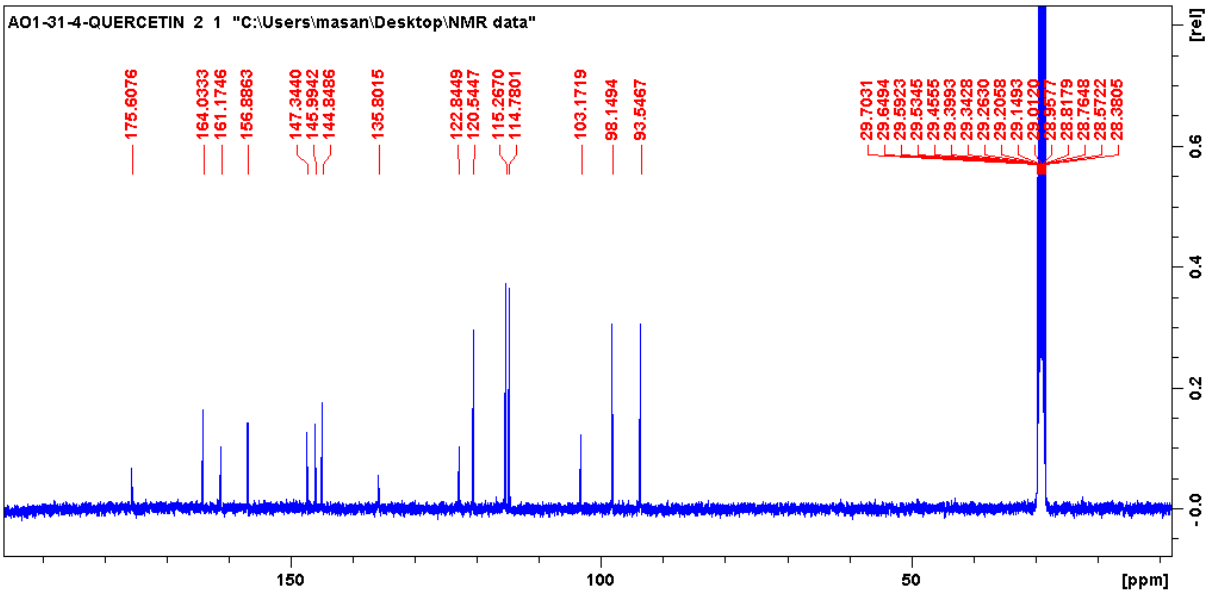

APPENDIX 9: ^{13}C NMR (400MHz, Acetone$_{-d6}$) spectrum of compound 7.1

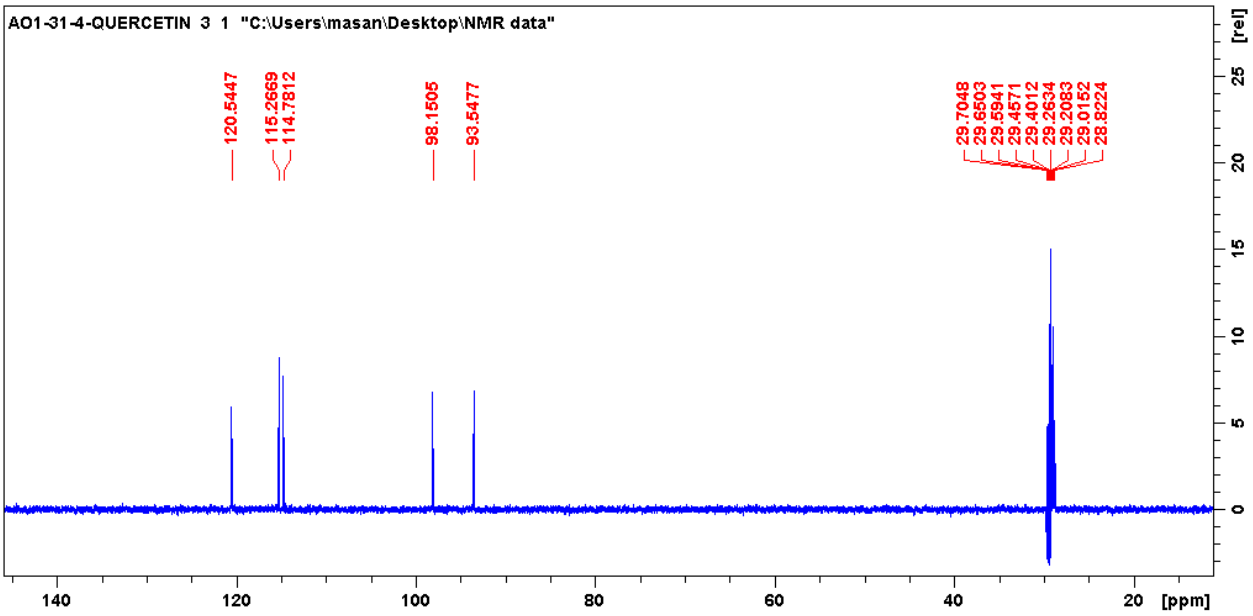

APPENDIX 10: DEPT 135 NMR (400MHz, Acetone$_{-d6}$) spectrum of compound 7.1

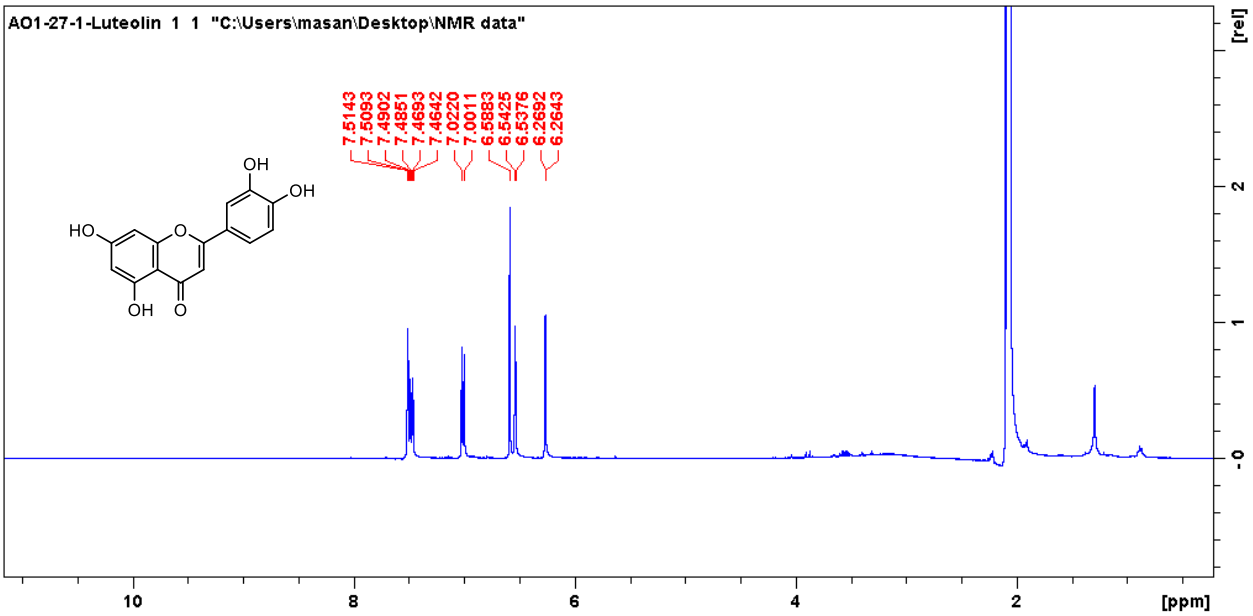

APPENDIX 11: ^{1}H-NMR (400MHz, Acetone$_{-d6}$) spectrum of compound 7.5

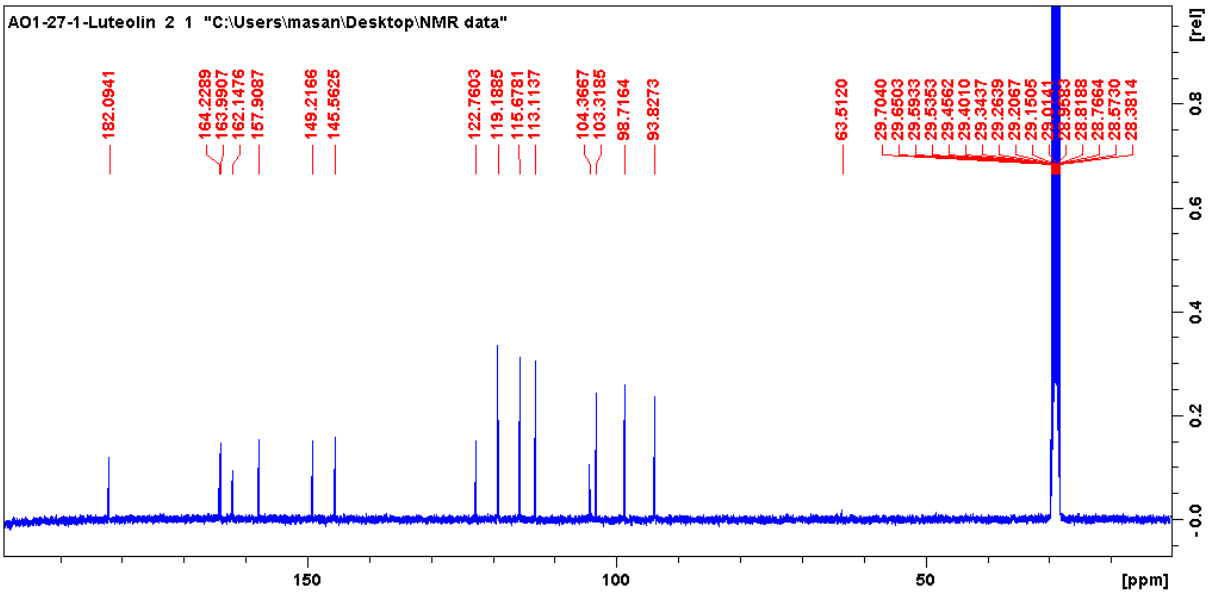

APPENDIX 12: ^{13}C-NMR (400MHz, Acetone$_{-d6}$) spectrum of compound 7.5

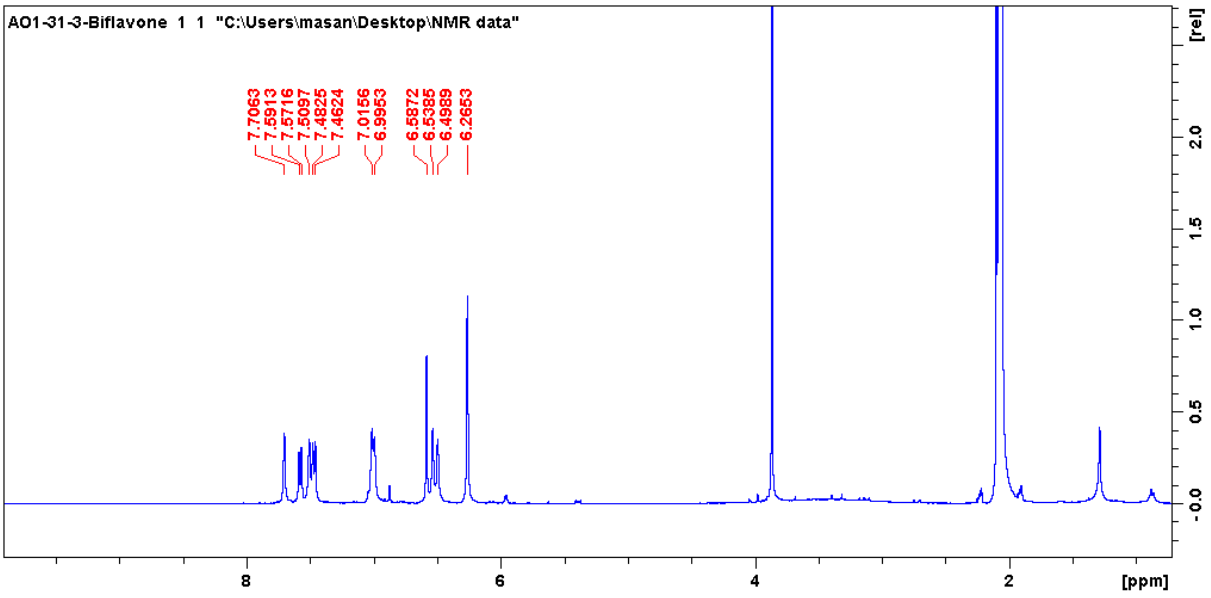

APPENDIX 13: ^{1}H NMR (400 MHz, Acetone$_{-d6}$) spectrum of 7.3

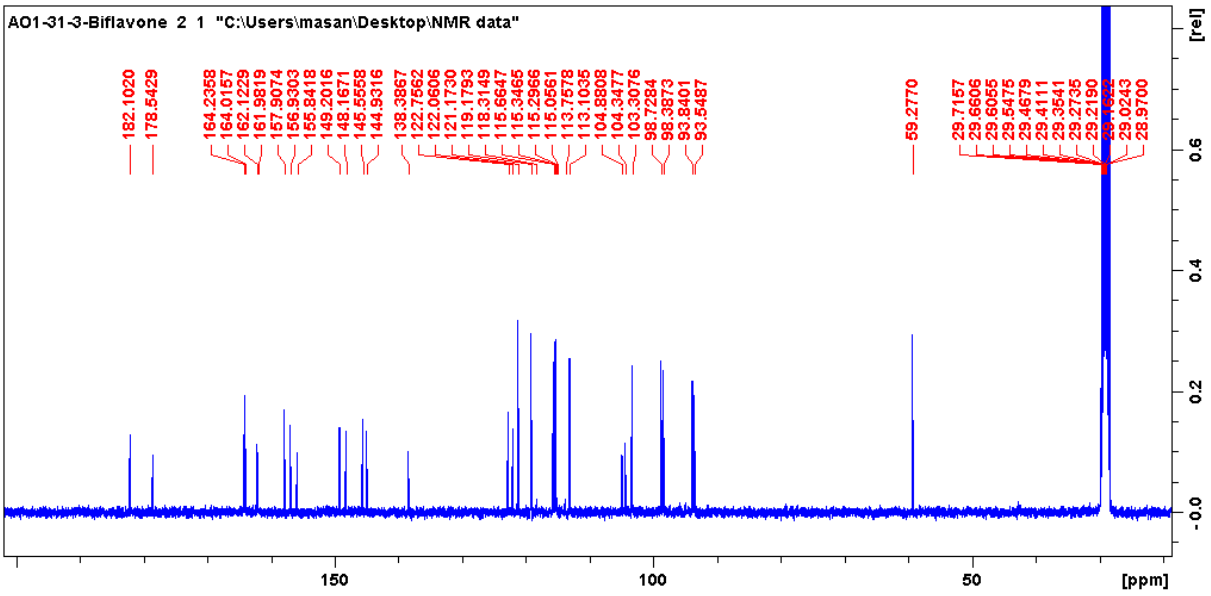

APPENDIX 14: ^{13}C-NMR (400 MHz, Acetone$_{-d6}$) spectrum of Compound 7.3

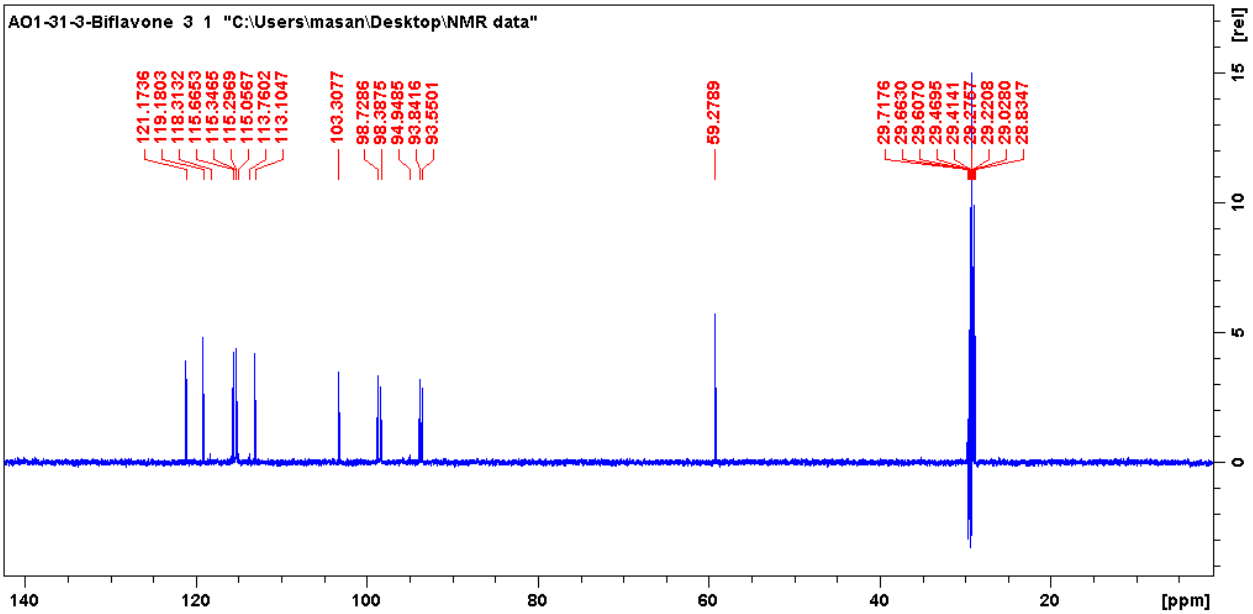

APPENDIX 15: DEPT-135 NMR (400MHz, Acetone$_{-d6}$) spectrum of compound 7.3

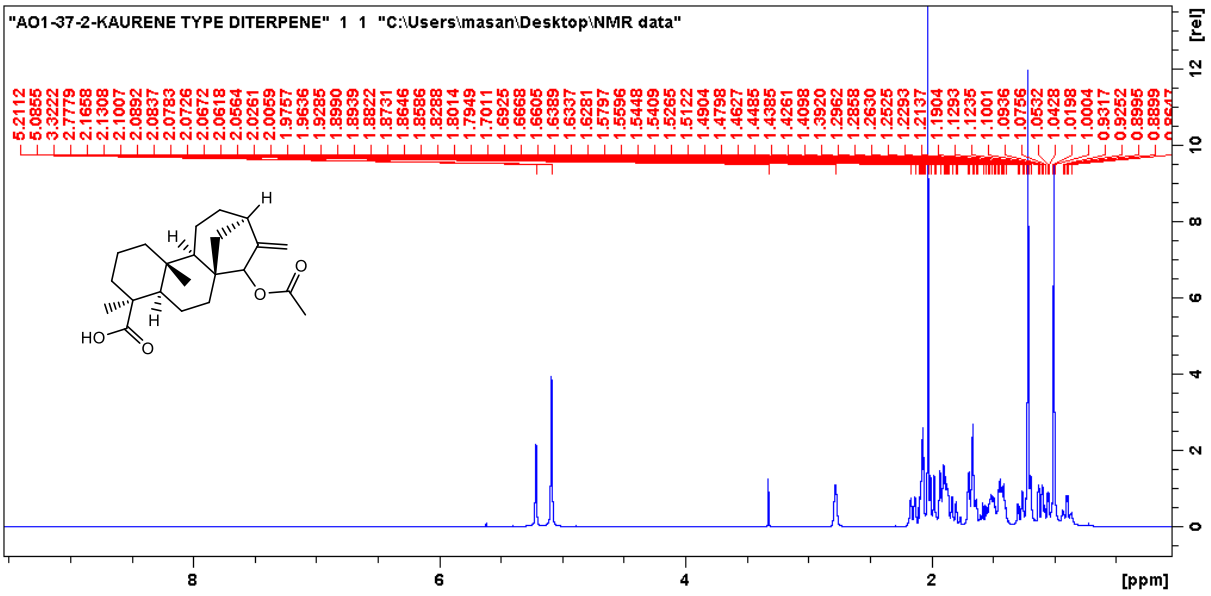

APPENDIX 16: ^{1}H NMR (400 MHz, Acetone$_{-d6}$) spectrum of compound 7.6

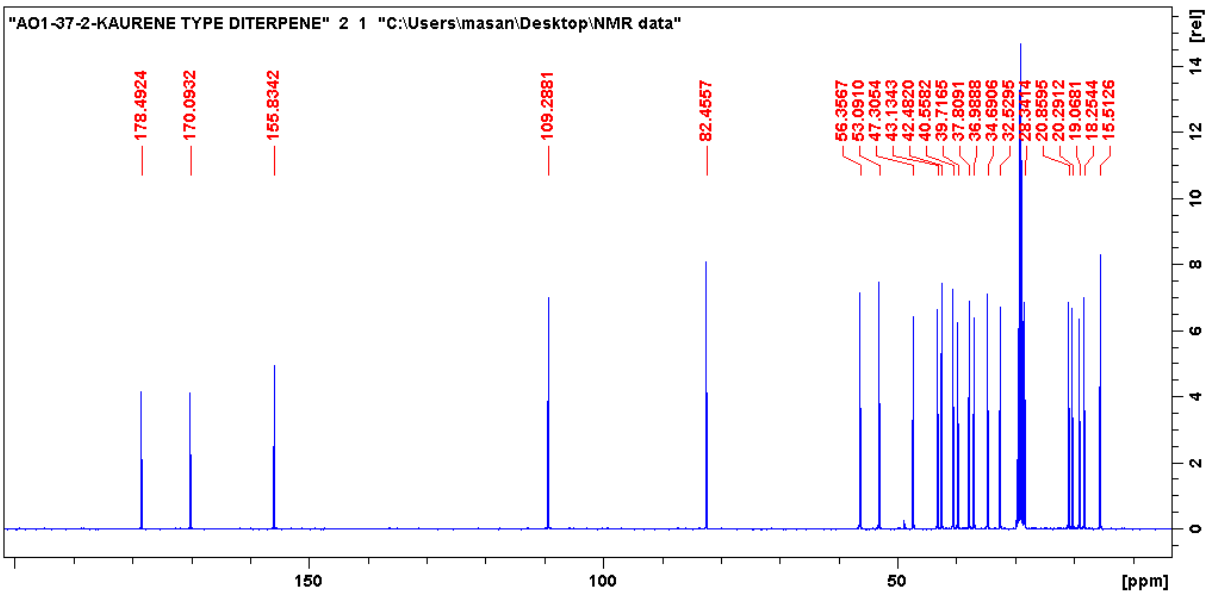

APPENDIX 17: ^{13}C NMR (400MHz, Acetone$_{-d6}$) spectrum of compound 7.6

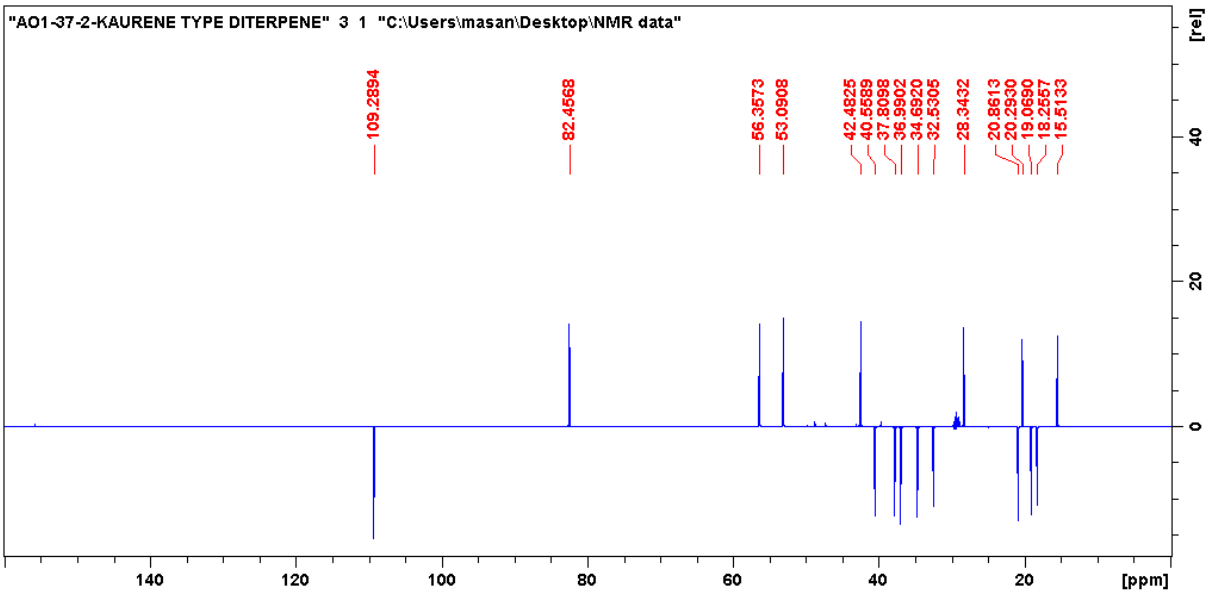

APPENDIX 18: DEPT-135 NMR (400MHz, Acetone$_{-d6}$) spectrum of compound 7.3

9.3. Appendix I (Addendum)

Addendum I: Research outputs

Akinfenwa O. Akeem, Abdul N. Sheik, Jeanine Marnewick, Ahmed A. Hussein. "Protective Effects of Linearthin and Other Chalcone Derivatives from *Aspalathus linearis* (Rooibos) Against UVB Induced Oxidative Stress and Toxicity in Human Skin Cells", ***Plants* 2021,10, 1936. https://doi.org/10.3390/plants10091936** (**Published**).

Akinfenwa O.Akeem, Brendon Pearce, Sylvester I. Omoruyia, Jelili A. Badmus, Enas Ismail, Jeanine Marnewick, Subelia Both, Mongi Benjeddou, Okobi E. Ekpob, Ahmed A. Hussein. "The potential of chalcone-capped gold nanoparticles for the management of diabetes mellitus", 2021. ***Interfaces and surfaces,* 25, 101251** (**Published**).

Akinfenwa O. Akeem, Abdul N. Sheik, Docrat T. Fathima, Robbie C. Luckay, Jeanine Marnewick, Ahmed A. Hussein. "Cytotoxic effects of phytomediated silver and gold nanoparticles synthesised from rooibos *(Aspalathus linearis*), and aspalathin". (**Accepted for publication** by the journal of ***Plants***, under **Phytochemistry section**. Manuscript ID: **Plants-14337**).

Akinfenwa, O. Akeem, Brendon, Pearce, Ahmed A.Hussein. Antidiabetic potential of Helichrysum foetidum chemical constituents" (**draft article**)

Akinfenwa O. Akeem, Abdul N. Sheik, Jeanine Marnewick, Ahmed H. Hussein. "Effect of sequential and non-sequential solvent extraction on the total polyphenol content and antioxidants capacity of green and fermented rooibos tea (*Aspalathus linearis*)" (**draft article**).

Addendum II: Award, conferences, and symposium

- South African Chemical Institute (SACI) Post-Graduate Awardee, 2021.
- Oral Presentation at the Cape Peninsula University of Technology, South Africa 2020 Postgraduate Conference on 23rd February 2021.
- Poster Presentation at the 2020 Young STEM Symposium organised by South Africa Chemical Institute/Young Chemist Central on 17th-18th November 2020, by the University of Johannesburg's Department of Chemistry.
- Enabling the commercialisation of nanotechnological innovation (NANOAFRICA, 2020). "Alpha-amylase and alpha-glucosidase inhibition potentials of total extract of *Helichrysum* foetidum" **Akinfenwa O.A**, Subelia Botha, Enas Ismail, Ahmed

Mohammed (Abstract accepted for oral presentation).